Application of Inverse Modeling to Partitioning Interwell Tracer Tests for Estimating Oil Saturation

by

Elif Ilke Altinay, BSc.

Thesis

Presented to the Faculty of the Graduate School of
The University of Texas at Austin
in Partial Fulfillment
of the Requirements
for the Degree of

Master of Science in Engineering

The University of Texas at Austin
May 2005

Application of Inverse Modeling to Partitioning Interwell Tracer Tests for Estimating Oil Saturation

Approved by
Supervising Committee:

Gary Pope

Kamy Sepehrnoori

Acknowledgements

During my master program at the University of Texas at Austin, I gained a lot of valuable knowledge and experience in my field of study. I had a chance to meet wonderful people from all over the world and make unique friends during my stay in Austin. There are many people I would like to thank.

First of all, I would like to thank my supervisor Dr. Gary A Pope for giving me the opportunity to contribute to his research program, his guidance and encouragement throughout my research. I would also like to thank Dr. Kamy Sepehrnoori for accepting to be my thesis reader.

I would like to thank Dr. Akhil Datta-Gupta for giving us the opportunity to work with inverse model. I appreciate the assistance he provided when we needed. Special thanks goes to Hao Cheng and Adedayo Oyerinde for answering our technical questions regarding the inverse model.

I would like to express my appreciation to Kazuhiro Asakawa for answering my endless questions, helping me through my research and giving me his valuable advices.

I have also been very fortunate to have the opportunity to learn from Rohit Sinha. He provided the help I needed in getting started on my research.

I would like to thank Esther Barrientes for her administrative help whenever I needed. I also appreciate the assistance Joanna Castillo provided with all the software and hardware problems that I encountered.

I would also like to thank Jesus, Jitendra, Kaz, Robin, Rohit, Vishal and Waleed for their friendship.

Finally, I would like to thank to my family and Paul for their love, support, patience and encouragement throughout my study.

Abstract

Application of Inverse Modeling to Partitioning Interwell Tracer Tests for Estimating Oil Saturation

by

Elif Ilke Altinay, M.S.E

The University of Texas at Austin, 2005

SUPERVISOR: Gary A. Pope

The objectives of this thesis are learning and combining inverse model with method of moments (MOM) for obtaining accurate and realistic oil saturation estimates. The streamline-based inverse model developed in Texas A&M University coupled with the finite-difference ECLIPSE simulator was used to calculate the oil saturation distribution from partitioning interwell tracer test (PITT) data. Inverse model was tested for both single-phase at residual oil saturation and then for two-phase flow simulations during a waterflood. First sensitivity tests were performed. Then, the MOM and inverse modeling techniques were applied to PITTs at various tracer detection limits and their accuracy compared. Furthermore, these methods are used in a complementary way by using the saturation from the MOM as the initial guess for the inverse model calculation. In two-phase flow simulations, the sensitivity of inverse modeling to relative permeability, injection rate, cross-flow and to different partition coefficients was investigated.

Table of Contents

Acknowledgements iv

Abstract v

Table of Contents vi

List of Tables ix

List of Figures xiii

List of Figures xiii

CHAPTER 1: Introduction 1

CHAPTER 2: Literature Review 4

2.1. Method of Moments Analysis of Partitioning Interwell Tracer Tests 4

2.2. Inverse Model of Partitioning Interwell Tracer Tests 7

CHAPTER 3: Use of Inverse Model in Single Phase Flow 15

3.1 Simulation of a Reservoir Model with Uniform Layered Permeability 15

3.1.1 Reservoir Description 15

3.1.2 Forward Model Simulation 16

3.1.3 Application of Inverse Model to PITT data 16

3.1.4 Sensitivity Analysis of Inverse Model 18

3.1.4.1 Sensitivity of Inverse Model to Partition Coefficient 18

.3.1.4.2 Sensitivity to Initial Guess 19

.3.1.4.3 Sensitivity to Tracer Concentration Detection Limit 22

.3.1.4.4 Sensitivity to Permeability Distribution Order 23

3.1.5 Application of Method of Moments and Inverse Model to the Reservoir Model with the Uniform Layered Permeability 24

3.1.5.1 Method of Moments and Extrapolation of Tracer Data 24

3.1.5.2 Comparison of Inverse Model with Method of Moments 27

3.2 Simulation of a Reservoir Model with Stochastic Permeability Field. 28

3.2.1 Reservoir Description 28

3.2.2 Forward Model Run 29
3.2.3 Application of Method of Moments and Inverse Model to the Reservoir Model with the Stochastic Permeability Field 29
3.2.3.1 Reservoir study with kv/kh ratio 0.1 29
3.2.3.2 Reservoir study with kv/kh ratio 0.01 32
3.2.3.3 Reservoir study with kv/kh ratio 0.001 35
3.3 Conclusions 39
CHAPTER 4: Use of Inverse Modeling in Two Phase Flow 153
4.1 Reservoir Description 153
4.2 Run Description 153
4.2 Sensitivity Analysis 153
4.3 Application of Inverse Model 155
4.3 Conclusions 159
CHAPTER 5: Conclusions and Recommendations for Future Work 192
5.1 Inverse Model in Single-Phase Flow 192
5.2 Inverse Model in Two-Phase Flow 194
5.3 Recommendations for the Future Work 194
Appendix A: Fundamentals of Streamline Simulation for Obtaining Analytical Sensitivities 196
A.1 Convective tracer transport 196
A.2. Computation of Sensitivity of Tracer Response to Reservoir Parameters 197
A.3. Accounting for Mobile Oil Saturations 201
Appendix B: Sample Input Files 204
B.1 Inverse Model Forward Run ECLIPSE Input File For Single Phase Flow 204
B.2 Inverse Model Forward Run ECLIPSE Input File For Two Phase Flow 210

Nomenclature.....213

References.....215

VITA.....219

List of Tables

Table.3.1: Description of the layered permeability reservoir 41

Table 3.2: Comparison of inverse model oil saturation estimate errors with partitioning coefficients 1, 2, 3 4, and 5 at initial oil saturation estimate 0.26.....41

Table 3.3: Comparison of inverse model oil saturation estimate errors at partitioning coefficients 6, 7, 8, 9 and 10 with initial oil saturation estimate 0.2642

Table 3.4: Comparison of inverse model oil saturation estimate errors at initial oil saturation guesses 0.21, 0.22, 0.23, 0.24 and 0.25 with partitioning coefficient 2 42

Table 3.5: Comparison of inverse model oil saturation estimate errors at initial oil saturation guesses 0.26, 0.27, 0.28, 0.29 and 0.30 with partitioning coefficient 2 43

Table 3.6: Comparison of inverse model oil saturation estimate errors at initial oil saturation guesses 0.14, 0.26, and 0.38 with partitioning coefficient 243

Table 3.7: Comparison of inverse model oil saturation estimate errors at tracer concentration detection limits (TDL) 0.0001, 0.001 and 0.01 with partitioning coefficient 2 at initial oil saturation guess 0.26.....44

Table 3.8: Comparison of inverse model oil saturation estimate errors at tracer concentration detection limits (TDL) 0.0001, 0.001 and 0.01 with partitioning coefficient 2 at initial oil saturation guess 0.26.....44

Table 3.9: Inverse model oil saturation estimate error in the reservoir model with the rearranged permeability distribution.....45

Table 3.10. MOM swept pore volume estimate with and without extrapolation for the reservoir model with the uniform layered permeability 45
Table 3.11: MOM oil saturation estimate errors at tracer concentration detection limits (TDL) 0.0001, 0.001 and 0.01. 46
Table 3.12: Comparison of inverse model oil saturation estimate errors with MOM. 46
Table 3.13. Description of the reservoir model with the stochastic permeability field 47
Table 3.14. Description of the stochastically generated permeability field.....47
Table 3.15. Swept pore volume estimate with and without extrapolation for the reservoir model with the stochastic permeability field for TDL= 0.0001 at kv/kh=0.1. 47
Table 3.16. MOM So estimate with and without extrapolation for the reservoir model with the stochastic permeability field for TDL= 0.0001 at kv/kh=0.1.48
Table 3.17. MOM oil saturation estimate errors in each layer in each quadrant for TDL=0.0001 at kv/kh=0.1. 48
Table 3.18. Inverse model oil saturation estimate errors in each layer in each quadrant for TDL=0.0001 at kv/kh=0.1.....49
Table 3.19. Swept pore volume estimate with and without extrapolation for the reservoir model with the stochastic permeability field for TDL= 0.0001 at kv/kh=0.01. 49
Table 3.20. MOM So estimate with and without extrapolation for the reservoir model with the stochastic permeability field for TDL= 0.0001 at kv/kh=0.01. 50

Table 3.21. MOM oil saturation estimate errors in each layer in each quadrant for TDL=0.0001 at kv/kh=0.01. 50
Table 3.22. Inverse model oil saturation estimate errors in each layer in each quadrant for TDL=0.0001 at kv/kh=0.01.....51
Table 3.23. Swept pore volume estimate with and without extrapolation for the reservoir model with the stochastic permeability field for TDL= 0.0001 at kv/kh=0.001. 51
Table 3.24. MOM So estimate with and without extrapolation for the reservoir model with the stochastic permeability field for TDL= 0.0001 at kv/kh=0.001. 52
Table 3.25. Inverse model oil saturation estimate errors in each layer in each quadrant for TDL=0.0001 at kv/kh=0.001.....52
Table 3.26. Inverse model oil saturation estimate errors in each layer in each quadrant for TDL=0.0001 at kv/kh=0.001.....53
Table 3.27. Swept pore volume estimate with and without extrapolation for the reservoir model with the stochastic permeability field for TDL= 0.001 at kv/kh=0.001. 53
Table 3.28. MOM So estimate with and without extrapolation for the reservoir model with the stochastic permeability field for TDL= 0.001 at kv/kh=0.001. 54
Table 3.29. Inverse model oil saturation estimate errors in each layer in each quadrant for TDL= 0.001 at kv/kh=0.001.....54
Table 3.30. Inverse model oil saturation estimate errors in each layer in each quadrant for TDL=0.001 at kv/kh=0.001.....55
Table 4.1 Description of the two dimensional reservoir model.....160

Table 4.2. Relative permeability parameters and viscosities. 160

Table 4.3. Run summary of oil saturation estimate 160

Table 4.4. Run summary of oil saturation estimate 161

List of Figures

Figure 2.1. Flowchart for history matching finite-difference models using streamline derived sensitivities (Chent *et al.*, 2004). 12

Figure 2.2. Minimization of travel time match - $\min \sum (t_{obs} - t_{cal})^2$ - of the observed and the calculated tracer concentration curves (Cheng *et al.*, 2004) 13

Figure 2.3. Minimization of the amplitude match - $\min \sum (C_{obs} - C_{cal})^2$ - of the observed and the calculated tracer concentration curves (Cheng *et al.*, 2004). 13

Figure 2.4. Minimization of the shift time - $\min \sum (\Delta\tau)^2$ - by shifting the model response towards the observed data at each well (Cheng *et al.*, 2004)14

Figure 2.5. Maximized coefficient of determination by the optimal shift time (Cheng *et al.*, 2004). 14

Figure 3.1 Vertical permeability distribution of the three-dimensional layered reservoir 56

Figure 3.2 Permeability distribution of the uniform layered permeability reservoir56

Figure 3.3 Correlation between the permeability and the oil saturation for the layered reservoir 57

Figure 3.4 Vertical oil saturation distribution of the three-dimensional layered reservoir 57

Figure 3.5. Forward model normalized tracer concentration response from the production well 58

Figure 3.6 Forward model normalized tracer concentration response from the least permeable layer 5 58

Figure 3.7 Forward model normalized tracer concentration response from the most permeable layer 8 59
Figure 3.8 Streamline distribution after inverse modeling 59
Figure 3.9 Root Mean Square error (RMS) change on travel time and amplitude during inversion 60
Figure 3.10 Match of the forward model tracer response from all layers by iterations 1 and 5 of the inverse model 60
Figure 3.11 Match of the forward model tracer response from layer 5 by iterations 1 and 5 of the inverse model 61
Figure 3.12 Match of the forward model tracer response from layer 8 by iterations 1 and 5 of the inverse model 61
Figure 3.13 Vertical oil saturation distribution for the first and the fifth iteration of the inverse model compared to the forward model..... 62
Figure 3.14. Inverse model oil saturation estimate change with the number of iterations..... 62
Figure 3.15 Comparison of forward model oil saturation distribution (top image) with inverse model oil saturation distribution (bottom image) at the fifth iteration 63
Figure 3.16 Inverse model vertical oil saturation distribution with partition coefficients K= 1, 2, 3, 4, and 5. 64
Figure 3.17. Inverse model vertical oil saturation distribution with partition coefficients K=6, 7, 8, 9 and 10. 64
Figure 3.18. RMS error change on travel time and amplitude at partition coefficient K=1. 65

Figure 3.19. Match of the forward model tracer response from all layers with inverse model at tracer partition coefficient K=1.....65
Figure 3.20. Match of the forward model tracer response from layer 5 with inverse model at tracer partition coefficient K=1.....66
Figure 3.21. Match of the forward model tracer response from layer 8 with inverse model at tracer partition coefficient K=1.....66
Figure 3.22. RMS error change on travel time and amplitude at partition coefficient 3. 67
Figure 3.23. Match of the forward model tracer response from the all layers by iteration 3 of the inverse model at tracer partition coefficient K=3..67
Figure 3.24. Match of the forward model tracer response from layer 5 by iteration 3 of the inverse model at tracer partition coefficient K=3.....68
Figure 3.25. Match of the forward model tracer response from layer 8 by iteration 3 of the inverse model at tracer partition coefficient K=3.....68
Figure 3.26. RMS error change on travel time and amplitude at partition coefficient 5. 69
Figure 3.27. Match of the forward model tracer response from all layers by iteration 1 of the inverse model at tracer partition coefficient K=5.....69
Figure 3.28. Match of the forward model tracer response from layer 5 by iteration 1 of the inverse model at tracer partition coefficient K=5.....70
Figure 3.29. Match of the forward model tracer response from layer 8 by iteration 1 of the inverse model at tracer partition coefficient K=5.....70
Figure 3.30. RMS error change on travel time and amplitude at partition coefficient 10.....71

Figure 3.31. Match of the forward model tracer response from all layers by iteration 2 of the inverse model at tracer partition coefficient K=10.....71
Figure 3.32.Match of the forward model tracer response from layer 5 by iteration 2 of the inverse model at tracer partition coefficient K=10. 72
Figure 3.33. Match of the forward model tracer response from layer 8 by iteration 2 of the inverse model at tracer partition coefficient K=10.....72
Figure 3.34. Inverse model vertical oil saturation estimates at initial oil saturations guesses 0.21, 0.22, 0.23, 0.24 and 0.25.....73
Figure 3.35. Inverse model vertical oil saturation estimates at initial oil saturations guesses 0.26, 0.27, 0.28, 0.29 and 0.30.....73
Figure 3.36. RMS error change on travel time and amplitude at initial oil saturation guess 0.21.....74
Figure 3.37. Match of the forward model tracer response from all layers by iteration 4 of the inverse model at the initial oil saturation guess 0.21.....74
Figure 3.38. Match of the forward model tracer response from layer 5 by iteration 4 of the inverse model at the initial oil saturation guess 0.21.....75
Figure 3.39. Match of the forward model tracer response from layer 8 by iteration 4 of the inverse model at the initial oil saturation guess 0.21.....75
Figure 3.40. RMS error change on travel time and amplitude at initial oil saturation guess 0.28.....76
Figure 3.41. Match of the forward model tracer response from all layers by iteration 10 of the inverse model at the initial oil saturation guess 0.28.....76
Figure 3.42. Match of the forward model tracer response from layer 5 by iteration 10 of the inverse model at the initial oil saturation guess 0.28.....77

Figure 3.43. Match of the forward model tracer response from layer 8 by iteration 10 of the inverse model at the initial oil saturation guess 0.28.....77
Figure 3.44. RMS error change on travel time and amplitude at initial oil saturation guess 0.30.....78
Figure 3.45. Match of the forward model tracer response from all layers by iteration 1 of the inverse model at the initial oil saturation guess 0.30.....78
Figure 3.46. Match of the forward model tracer response from layer 5 by iteration 1 of the inverse model at the initial oil saturation guess 0.30.....79
Figure 3.47. Match of the forward model tracer response from layer 8 by iteration 1 of the inverse model at the initial oil saturation guess 0.30.....79
Figure 3.48. Inverse model vertical oil saturation estimates at initial oil saturations guesses 0.38, 0.26, and 0.14.....80
Figure 3.49. RMS error change on travel time and amplitude at initial oil saturation guess 0.14.....80
Figure 3.50. Match of the forward model tracer response from all layers by iteration 4 of the inverse model at the initial oil saturation guess 0.14.....81
Figure 3.51. Match of the forward model tracer response from layer 5 by iteration 4 of the inverse model at the initial oil saturation guess 0.14.....81
Figure 3.52. Match of the forward model tracer response from layer 8 by iteration 4 of the inverse model at the initial oil saturation guess 0.14.....82
Figure 3.53. RMS error change on travel time and amplitude and at initial oil saturation guess 0.38.....82
Figure 3.54. Match of the forward model tracer response from all layers by iteration 10 of the inverse model at the initial oil saturation guess 0.38.....83

Figure 3.55. Match of the forward model tracer response from layer 5 by iteration 10 of the inverse model at the initial oil saturation guess 0.38.....83
Figure 3.56. Match of the forward model tracer response from layer 8 by iteration 10 of the inverse model at the initial oil saturation guess 0.38.....84
Figure 3.57. Inverse model vertical oil saturation distribution estimates for TDLs 0.0001, 0.001 and 0.01 at initial oil saturation guess 0.26.....84
Figure 3.58. RMS error change on travel time and amplitude for TDL 0.001 at initial oil saturation guess 0.26.....85
Figure 3.59. RMS error change on travel time and amplitude for TDL 0.01 at initial oil saturation guess 0.26.....85
Figure 3.60. Match of the forward model tracer response from all layers with the inverse model for TDLs 0.0001, 0.001 and 0.01 at initial oil saturation guess 0.26.....86
Figure 3.61. Match of the forward model tracer response from layer 5 with the inverse model for TDLs 0.0001, 0.001 and 0.01 at initial oil saturation guess 0.26.....86
Figure 3.62. Match of the forward model tracer response from layer 8 with the inverse model for TDLs 0.0001, 0.001 and 0.01 at initial oil saturation guess 0.26.....87
Figure 3.63. Inverse model vertical oil saturation distribution estimates for TDLs 0.0001, 0.001 and 0.01at initial oil saturations guess 0.30. 87
Figure 3.64. RMS error change on travel time and amplitude for TDL 0.001 and initial oil saturation guess 0.30. 88
Figure 3.65. RMS error change on travel time and amplitude for tracer concentration detection limit 0.01 at initial oil saturation guess 0.30. 88

Figure 3.66. Match of the forward model tracer response from all layers with the inverse model for TDLs 0.0001, 0.001 and 0.01 at initial oil saturation guess 0.30.....89
Figure 3.67. Match of the forward model tracer response from layer 5 with the inverse model for TDLs 0.0001, 0.001 and 0.01 at initial oil saturation guess 0.30.....89
Figure 3.68. Match of the forward model tracer response from layer 8 with the inverse model for TDLs 0.0001, 0.001 and 0.01 at initial oil saturation guess 0.30.....90
Figure 3.69 Rearranged vertical permeability distribution of the three-dimensional uniform layered permeability reservoir model 90
Figure 3.70 Rearranged vertical permeability distribution of the three-dimensional uniform layered permeability reservoir model 91
Figure 3.71 Inverse model vertical oil saturation distribution estimates in the reservoir model with the rearranged permeability field.....91
Figure 3.72. Comparison of forward model oil saturation distribution (top image) with inverse model oil saturation distribution (bottom image) in the rearranged permeability field.....92
Figure 3.73. RMS error change on travel time and amplitude at in the rearranged permeability field.....93
Figure 3.74. Match of the forward model tracer response from all layers by iteration 5 of the inverse model at the reservoir model with the rearranged permeability field.....93

Figure 3.75. Match of the forward model tracer response from layer 5 by iteration 5 of the inverse model at the reservoir model with the rearranged permeability field. 94
Figure 3.76. Match of the forward model tracer response from all layers by iteration 8 of the inverse model at the reservoir model with the rearranged permeability field. 94
Figure 3.77. Extrapolation of tracer response from all layers for TDL =0.0001 ...95
Figure 3.78. Extrapolation of tracer response from layer 5 for TDL =0.0001. 95
Figure 3.79. Extrapolation of tracer response from layer 8 for TDL =0.0001. 96
Figure 3.80. MOM swept pore volume estimate of the reservoir after extrapolation for TDL =0.0001 96
Figure 3.81. MOM oil saturation estimate with and without extrapolation for TDL 0.0001....97
Figure 3.82. Extrapolation of tracer response from all layers for TDL =0.01 97
Figure 3.83. Extrapolation of tracer response from layer 5 for TDL =0.01. 98
Figure 3.84.Extrapolation of tracer response from layer 8 for TDL =0.01. 98
Figure 3.85. MOM swept pore volume estimate of the reservoir for TDL =0.01 after extrapolation 99
Figure 3.86. MOM oil saturation estimate with and without extrapolation for TDL 0.01....99
Figure 3.87. MOM oil saturation estimate with and with extrapolation at various TDLs. 100
Figure 3.88. RMS error change on travel time and amplitude during the inverse model run at initial oil saturation guess 0.241 (average MOM estimate)..100
Figure 3.89. Comparison of MOM and inverse model oil saturation estimates. .101

Figure 3.90. Stochastic permeability distribution at the vertical layer Z=7.....101
Figure 3.91. Stochastic permeability distribution at the vertical layer Z=3.....102
Figure 3.92. Stochastic permeability distribution in horizontal layer, Y=1.....102
Figure 3.93. Stochastic permeability distribution in horizontal layer, Y=16.....103
Figure 3.94. Vertical permeability distribution of the three-dimensional layered reservoir with the stochastic permeability field. 103
Figure 3.95. Correlation between the permeability and the oil saturation for the model with the stochastic permeability field. 104
Figure 3.96. Vertical oil saturation distribution of the three-dimensional layered reservoir with the stochastic permeability field. 104
Figure 3.97. Extrapolation of tracer response in the first quadrant for TDL =0.0001 at kv/kh=0.1 105
Figure 3.98. MOM swept pore volume estimate in the first quadrant after the extrapolation for TDL =0.0001 at kv/kh=0.1. 105
Figure 3.99. MOM oil saturation estimate with and without extrapolation in the first quadrant for TDL=0.0001 at kv/kh=0.1.....106
Figure 3.100. Extrapolation of tracer response in the second quadrant for TDL =0.0001 at kv/kh=0.1 106
Figure 3.101. MOM swept pore volume estimate in the second quadrant after the extrapolation for TDL =0.0001 at kv/kh=0.1. 107
Figure 3.102. MOM oil saturation estimate with and without extrapolation in the second quadrant for TDL=0.0001 at kv/kh=0.1. 107
Figure 3.103. Extrapolation of tracer response in the third quadrant for TDL =0.0001 at kv/kh=0.1 108

Figure 104. MOM swept pore volume estimate in the third quadrant after the extrapolation for TDL =0.0001 at kv/kh=0.1. 108
Figure 3.105. MOM oil saturation estimate with and without extrapolation in the third quadrant, for TDL=0.0001 at kv/kh=0.1.....109
Figure 3.106. Extrapolation of tracer response in the fourth quadrant for TDL =0.0001 at at kv/kh=0.1 109
Figure 107. MOM swept pore volume estimate at the fourth quadrant after the extrapolation for TDL =0.0001 at kv/kh=0.1. 110
Figure 3.108. MOM oil saturation estimate with and without extrapolation in the fourth quadrant for TDL 0.0001 at kv/kh=0.1. 110
Figure 3.109. Streamline distribution after inverse modeling in the reservoir model with the stochastic permeability field at kv/kh=0.1. 111
Figure 3.110. RMS error change on travel time and amplitude at the reservoir model with the stochastic permeability field at kv/kh=0.1. 112
Figure 3.111. Match of the forward model tracer response from the first quadrant with the inverse model for TDL=0.0001 at kv/kh=0.1. 112
Figure 3.112. Comparison of MOM and inverse model oil saturation estimates in the first quadrant for TDL=0.0001 at kv/kh=0.1. 113
Figure 3.113. Match of the forward model tracer response from the second quadrant with the inverse model for TDL=0.0001 at kv/kh=0.1. 113
Figure 3.114. Comparison of MOM and inverse model oil saturation estimates in the second quadrant for TDL=0.0001 at kv/kh=0.1. 114
Figure 3.115. Match of the forward model tracer response from the third quadrant with the inverse model for TDL=0.0001 at kv/kh=0.1. 114

Figure 3.116. Comparison of MOM and inverse model oil saturation estimates in the third quadrant for TDL=0.0001 at kv/kh=0.1. 115
Figure 3.117. Match of the forward model tracer response from the fourth quadrant with the inverse model for TDL=0.0001 at kv/kh=0.1. 115
Figure 3.118. Comparison of MOM and inverse model oil saturation estimates in the fourth quadrant for TDL=0.0001 at kv/kh=0.1. 116
Figure 3.119 Comparison of forward model oil saturation distribution (top image) with inverse model oil saturation distribution (bottom image) in layer Z=7. 117
Figure 3.120 Comparison of forward model oil saturation distribution (top image) with inverse model oil saturation distribution (bottom image) in layer Y=16. 118
Figure 3.121. Extrapolation of tracer response from the first quadrant for TDL =0.0001 at kv/kh=0.01 119
Figure 3.122. MOM swept pore volume estimate in the first quadrant after the extrapolation for TDL =0.0001 at kv/kh=0.01. 119
Figure 3.123. MOM oil saturation estimate with and without extrapolation in the first quadrant for TDL=0.0001 at kv/kh=0.01.....120
Figure 3.124. Extrapolation of tracer response from the second quadrant for TDL =0.0001 at kv/kh=0.01 120
Figure 3.125. MOM swept pore volume estimate in the second quadrant after the extrapolation for TDL =0.0001 at kv/kh=0.01. 121
Figure 3.126. MOM oil saturation estimate with and without extrapolation in the second quadrant for TDL=0.0001 at kv/kh=0.01. 121

Figure 3.127. Extrapolation of tracer response from the third quadrant for TDL =0.0001 at kv/kh=0.01 122
Figure 3.128. MOM swept pore volume estimate in the third quadrant after the extrapolation for TDL =0.0001 at kv/kh=0.01. 122
Figure 3.129. MOM oil saturation estimate with and without extrapolation in the third quadrant for TDL=0.0001 at kv/kh=0.01.....123
Figure 3.130. Extrapolation of tracer response from the fourth quadrant for TDL =0.0001 at kv/kh=0.01 123
Figure 3.131. MOM swept pore volume estimate in the fourth quadrant after the extrapolation fourth TDL =0.0001 at kv/kh=0.01. 124
Figure 3.132. MOM oil saturation estimate with and without extrapolation in the fourth quadrant for TDL=0.0001 at kv/kh=0.01.....124
Figure 3.133. Streamline distribution after inverse modeling in the reservoir model with the stochastic permeability field at kv/kh=0.01.....125
Figure 3.134. RMS error change on travel time and amplitude in the reservoir model with the stochastic permeability field at kv/kh=0.01.....126
Figure 3.135. Match of the forward model tracer response from the first quadrant with the inverse model for TDL=0.0001 at kv/kh=0.01. 126
Figure 3.136. Comparison of MOM and inverse model oil saturation estimates in the first quadrant for TDL=0.0001 at kv/kh=0.01. 127
Figure 3.137. Match of the forward model tracer response from the second quadrant with the inverse model for TDL=0.0001 atkv/kh=0.01.....127
Figure 3.138. Comparison of MOM and inverse model oil saturation estimates in the second quadrant for TDL=0.0001 at kv/kh=0.01. 128

Figure 3.139. Match of the forward model tracer response from the third quadrant with the inverse model for TDL=0.0001 at kv/kh=0.01. 128
Figure 3.140. Comparison of MOM and inverse model oil saturation estimates in the third quadrant for TDL=0.0001 at kv/kh=0.01. 129
Figure 3.141. Match of the forward model tracer response from the fourth quadrant with the inverse model for TDL=0.0001 at kv/kh=0.01. 129
Figure 3.142. Comparison of MOM and inverse model oil saturation estimates in the fourth quadrant for TDL=0.0001 at kv/kh=0.01. 130
Figure 3.143. Extrapolation of tracer response in the first quadrant for TDL =0.0001 at kv/kh=0.001 130
Figure 3.144. MOM swept pore volume estimate in the first quadrant after the extrapolation for TDL =0.0001 at kv/kh=0.001. 131
Figure 3.145. MOM oil saturation estimate with and without extrapolation in the first quadrant for TDL=0.0001 at kv/kh=0.001.....131
Figure 3.146. Extrapolation of tracer response in the second quadrant for TDL =0.0001 at kv/kh=0.001 132
Figure 3.147. MOM swept pore volume estimate in the second quadrant for TDL =0.0001 at kv/kh=0.001. 132
Figure 3.148. MOM oil saturation estimate with and without extrapolation in the second quadrant for TDL =0.0001 at kv/kh=0.001. 133
Figure 3.149. Extrapolation of tracer response in the second quadrant for TDL =0.0001 at kv/kh=0.001 133
Figure 3.150. MOM swept pore volume estimate in the third quadrant after the extrapolation for TDL =0.0001 at kv/kh=0.001. 134

Figure 3.151. MOM oil saturation estimate with and without extrapolation in the third quadrant, for TDL=0.0001 at kv/kh=0.001.....134
Figure 3.152. Extrapolation of tracer response in the fourth quadrant for TDL =0.0001 at at kv/kh=0.001 135
Figure 3.153. MOM swept pore volume estimate in the fourth quadrant after the extrapolation for TDL =0.0001 at kv/kh=0.001. 135
Figure 3.154. MOM oil saturation estimate with and without extrapolation in the fourth quadrant for TDL=0.0001 at kv/kh=0.001.....136
Figure 3.155. Streamline distribution after inverse modeling in the reservoir model with the stochastic permeability field at kv/kh=0.001.....137
Figure 3.156. RMS error change on travel time and amplitude at the reservoir model with the stochastic permeability field at kv/kh=0.001.....138
Figure 3.157. Match of the forward model tracer response from the first quadrant with the inverse model for TDL=0.0001 at kv/kh=0.001. 138
Figure 3.158. Comparison of MOM and inverse model oil saturation estimates in the first quadrant for TDL=0.0001 at kv/kh=0.001. 139
Figure 3.159. Match of the forward model tracer response from the second quadrant with the inverse model for TDL=0.0001 at kv/kh=0.001.....139
Figure 3.160. Comparison of MOM and inverse model oil saturation estimates in the second quadrant for TDL=0.0001 at kv/kh=0.001. 140
Figure 161. Match of the forward model tracer response from the third quadrant with the inverse model for TDL=0.0001 at kv/kh=0.001.....140
Figure 3.162. Comparison of MOM and inverse model oil saturation estimates in the third quadrant for TDL=0.0001 at kv/kh=0.001.....141

Figure 3.163. Match of the forward model tracer response from the fourth quadrant with the inverse model for TDL=0.0001 at kv/kh=0.001. 141
Figure 3.164. Comparison of MOM and inverse model oil saturation estimates in the fourth quadrant for TDL=0.0001 at kv/kh=0.001. 142
Figure 3.165. Extrapolation of tracer response from the first quadrant for TDL =0.001 at kv/kh=0.001 142
Figure 3.166. MOM swept pore volume estimate in the first quadrant after the extrapolation for TDL =0.001 at kv/kh=0.001. 143
Figure 3.167. MOM oil saturation estimate with and without extrapolation in the first quadrant for TDL=0.001 at kv/kh=0.001.....143
Figure 3.168.Extrapolation of tracer response from the second quadrant for TDL =0.001 at kv/kh=0.001 144
Figure 3.169. MOM swept pore volume estimate in the second quadrant after the extrapolation for TDL =0.001 at kv/kh=0.001. 144
Figure 3.170. MOM oil saturation estimate with and without extrapolation in the second quadrant for TDL=0.001 at kv/kh=0.001. 145
Figure 3.171. Extrapolation of tracer response from the third quadrant for TDL =0.001 at kv/kh=0.001 145
Figure 3.172. MOM swept pore volume estimate in the third quadrant after the extrapolation for TDL =0.001 at kv/kh=0.001. 146
Figure 3.173. MOM oil saturation estimate with and without extrapolation in the third quadrant for TDL=0.001 at kv/kh=0.001.....146
Figure 3.174. Extrapolation of tracer response from the fourth quadrant for TDL =0.001 at kv/kh=0.001 147

Figure 3.175. MOM swept pore volume estimate in the fourth quadrant after the extrapolation for TDL =0.001 at kv/kh=0.001. 147
Figure 3.176. MOM oil saturation estimate with and without extrapolation in the fourth quadrant for TDL=0.001 at kv/kh=0.001. 148
Figure 3.177. RMS error change on travel time and amplitude at the reservoir model with the stochastic permeability field for TDL=0.001 at kv/kh=0.001. 148
Figure 3.178.Extrapolation of tracer response from the second quadrant for TDL =0.001 at kv/kh=0.001 149
Figure 3.179. Comparison of MOM and inverse model oil saturation estimates in the first quadrant for TDL=0.001 at kv/kh=0.001. 149
Figure 3.180.Extrapolation of tracer response from the second quadrant for TDL =0.001 at kv/kh=0.001 150
Figure 3.181. Comparison of MOM and inverse model oil saturation estimates in the second quadrant for TDL=0.001 at kv/kh=0.001. 150
Figure 3.182.Extrapolation of tracer response from the third quadrant for TDL =0.001 at kv/kh=0.001 151
Figure 3.183. Comparison of MOM and inverse model oil saturation estimates in the third quadrant for TDL=0.001 at kv/kh=0.001. 151
Figure 3.184.Extrapolation of tracer response from the fourth quadrant for TDL =0.001 at kv/kh=0.001 152
Figure 3.185. Comparison of MOM and inverse model oil saturation estimates in the fourth quadrant for TDL=0.001 at kv/kh=0.001. 152
Figure 4.1. Relative permeability curves in Runs 000 and 600 161
Figure 4.2. Relative permeability curves in Runs 200, 100, and 500. 162

Figure 4.3. Fractional flow of water in Run 000.....162
Figure 4.44. Fractional flow of water in Run 600 and Run 700.....163
Figure 4.5. Fractional flow of water in Run 200.....163
Figure 4.6. Fractional flow of water in Run 100.....164
Figure 4.7. Fractional flow of water in Run 500.....164
Figure 4.8. Mean residence time sensitivity to the oil saturation in Run000 at partition coefficient 10.....165
Figure 4.9. Mean residence time sensitivity to the oil saturation in Run600 at partition coefficient 10.....165
Figure 4.10. Mean residence time sensitivity to the oil saturation in Run200 at partition coefficient 10.....166
Figure 4.11. Mean residence time sensitivity to the oil saturation in Run100 at partition coefficient 10.....166
Figure 4.12. Mean residence time sensitivity to the oil saturation in Run500 at partition coefficient 10.....167
Figure 4.13. The effect of the initial water saturation on the tracer response in Run 000.....167
Figure 4.14. The effect of the initial water saturation on the tracer response in Run 600.....168
Figure 4.15. The effect of the initial water saturation on the tracer response in Run 200.....168
Figure 4.16. The effect of the initial water saturation on the tracer response in Run 100.....169
Figure 4.17. The effect of the initial water saturation on the tracer response in Run 500.....169

Figure 4.18. Root Mean Square error (RMS) change on travel time and amplitude during inversion in Run 511 170
Figure 4.19. Match of the forward model tracer response from layer 1 by iteration 1 and 6 of inverse model in Run 511 170
Figure 4.20. Match of the forward model tracer response from layer 2 by iteration 1 and 6 of inverse model in Run 511 171
Figure 4.21. Inverse model oil saturation estimate in layer 1 in Run 511 171
Figure 4.22. Inverse model oil saturation estimate in layer 2 in Run 511 172
Figure 4.23. Root Mean Square error (RMS) change on travel time and amplitude during inversion in Run 512 172
Figure 4.24. Match of the forward model tracer response from layer 1 by iteration 1 and 4 of inverse model in Run 512 173
Figure 4.25. Match of the forward model tracer response from layer 2 by iteration 1 and 4 of inverse model in Run 512 173
Figure 4.26. Inverse model oil saturation estimate in layer 1 in Run 512. 174
Figure 4.27. Inverse model oil saturation estimate in layer 2 in Run 512. 174
Figure 4.28. Root Mean Square error (RMS) change on travel time and amplitude during inversion in Run 513 175
Figure 4.29. Match of the forward model tracer response from layer 1 by iteration 1 and 6 of inverse model in Run 513 175
Figure 4.30. Match of the forward model tracer response from layer 1 by iteration 1 and 6 of inverse model in Run 513 176
Figure 4.31. Inverse model oil saturation estimate in layer 1 in Run 513 176
Figure 4.32. Inverse model oil saturation estimate in layer 2 in Run 513 177

Figure 4.33. Root Mean Square error (RMS) change on travel time and amplitude during inversion in Run 514 177
Figure 4.34. Match of the forward model tracer response from layer 1 by iteration 1 and 6 of inverse model in Run 514 178
Figure 4.35. Match of the forward model tracer response from layer 2 by iteration 1 and 6 of inverse model in Run 514 178
Figure 4.36. Inverse model oil saturation estimate in layer 1 in Run 514 179
Figure 4.37. Inverse model oil saturation estimate in layer 2 in Run 514 179
Figure 4.38. Injection rate change in Run 513-b 180
Figure 4.39. Root Mean Square error (RMS) change on travel time and amplitude during inversion in Run 513-b with changing flow rate in each layer180
Figure 4.40. Match of the forward model tracer response from layer 1 by iteration 1 and 3 of inverse model in Run 513-b with changing flow rate in each layer.....181
Figure 4.41. Match of the forward model tracer response from layer 2 by iteration 1 and 3 of inverse model in Run 513-b with changing flow rate in each layer.....181
Figure 4.42. Inverse model oil saturation estimate in layer 1 in Run 513-b with changing flow rate in each layer 182
Figure 4.43. Inverse model oil saturation estimate in layer 2 in Run 513-b with changing flow rate in each layer 182
Figure 4.44. Root Mean Square error (RMS) change on travel time and amplitude during inversion in Run 613 183
Figure 4.45. Match of the forward model tracer response from layer 1 by iteration 1 and 7 of inverse model in Run 613 183

Figure 4.46. Match of the forward model tracer response from layer 2 by iteration 1 and 7 of inverse model in Run 613 184
Figure 4.47. Inverse model oil saturation estimate in layer 1 in Run 613 184
Figure 4.48. Inverse model oil saturation estimate in layer 2 in Run 613 185
Figure 4.49. The effect of the initial water saturation on the tracer response in Run 713.....185
Figure 4.50. Root Mean Square error (RMS) change on travel time and amplitude during inversion in Run 713 186
Figure 4.51. Match of the forward model tracer response from layer 1 by iteration 1 and 10 of inverse model in Run 713 186
Figure 4.52. Match of the forward model tracer response from layer 2 by iteration 1 and 10 of inverse model in Run 713 187
Figure 4.53. Inverse model oil saturation estimate in layer 1 in Run 713 187
Figure 4.54. Inverse model oil saturation estimate in layer 2 in Run 713 188
Figure 4.55. Mean residence time sensitivity to the oil saturation in Run723.....188
Figure 4.56. The effect of the initial water saturation on the tracer response in Run 723.....189
Figure 4.57. Root Mean Square error (RMS) change on travel time and amplitude during inversion in Run 723 189
Figure 4.58. Match of the forward model tracer response from layer 1 by iteration 1 and 6 of inverse model in Run 723 190
Figure 4.59. Match of the forward model tracer response from layer 2 by iteration 1 and 6 of inverse model in Run 723 190
Figure 4.60. Inverse model oil saturation estimate in layer 1 in Run 723 191
Figure 4.61. Inverse model oil saturation estimate in layer 2 in Run 723 191

CHAPTER 1: Introduction

At the end of the primary and secondary oil recovery methods, the total oil recovered is most of the time in the range of 5 to 40 percent of the initial oil volume in the reservoir. With most of the oil left in the reservoir after the primary and secondary recovery methods, enhanced oil recovery methods (EOR) have very high potential for additional oil recovery. However, since EOR methods are costly, identifying the amount and the place of the remaining oil volume in the reservoir before starting enhanced oil recovery is very important.

Partitioning interwell tracer tests (PITT) is a useful technique for estimating the remaining oil saturation in the reservoir before the EOR applications (Sinha *et al*., 2004; Allison, 1998; Allison *et al.*, 1991; Tang *et al*., 1991a;b Tang *et al*., 1995; Zemel, 1995). Tracer tests have been used to estimate the heterogeneity (Badessich *et al*., 2005, Cheng *et al*., 2004, Lliassov 2001, Mercado *et al*., 2003, Wagner 1977), well communication and flow barriers (Wagner 1977, Badessich *et al*., 2005) sweep efficiencies (Sinha *et al*., 2004, Mercado, 2003, Allison *et al*., 1991), reservoir layering (Abbaszadeh *et al*., 1984) and in for many other purposes. Furthermore, PITTs have also been used extensively to measure the amount of non-aqueous phase liquid contamination such as chlorinated solvents in aquifers (Jin 1995; Dwarakanath *et al*., 1999; Yoon *et al.*, 1999).

Various analytical methods are presented in the literature for the analysis of tracer tests (Brigham 1965; Tang 1995, 2001; Jin, 1995; Jin *et al*., 1995). Among the analytical techniques used to analyze PITT data, the method of moments (MOM) has many advantages because it is easy; fast and robust in estimating the oil saturation and the swept pore volume by simply calculating the first temporal moment of the tracer data. Inverse modeling is a rigorous way of analyzing tracer data and has the advantage that it

can be used to find the distribution of permeability and saturations that satisfy the tracer responses (Datta-Gupta 2000, Yoon *et al*.1999, Lliassov 2001, Oyerinde 2004).

In this thesis, the streamline-based inverse model, which is developed at Texas A&M University, coupled with the finite-difference ECLIPSE simulator from Schlumberger, is used to calculate the oil saturation distribution from partitioning interwell tracer data. Inverse modeling is tested both in single-phase and in two-phase flow simulations.

In single-phase flow simulations, first sensitivity tests are performed on inverse model to understand the way it works. Then, MOM and inverse model techniques are applied to the reservoir models at various tracer detection limits for comparing the estimations of both methods. Furthermore, MOM oil saturation estimates are useful as initial guesses for inverse modeling. Although both the MOM and inverse methods are useful ways of analyzing tracer data, both have weak points. MOM analysis requires either the tracer tail be measured accurately, which can take a long time, or the tracer curve must be extrapolated, which introduces uncertainty. Long simulation times can be done as shown in this research, but in PITTs in fields with large well spacing or low permeability, operators are reluctant to collect data for long time periods due to both the cost and the need to know the saturation in a reasonable time frame. On the other hand, since inverse model is an ill-posed problem, its solution is highly non-unique. Thus, a proper initial guess is very important for accurate estimates. The main purpose of this study is analyzing inverse modeling and method of moments together to observe if they can assist each other.

First, sensitivity of oil saturation to tracer partition coefficient is analyzed. In addition to the sensitivity of oil saturation to the tracer partition coefficient, the effect of the initial oil saturation in the reservoir to the produced tracer concentration is studied.

Then, the sensitivity of inverse modeling to two different relative permeability curves, changing injection rate, cross-flow and to two different partition coefficients were studied.

CHAPTER 2: Literature Review

The previous work done on method of moments and inverse modeling are reviewed below.

2.1. METHOD OF MOMENTS ANALYSIS OF PARTITIONING INTERWELL TRACER TESTS

The method of moments has been used for many years for the analysis of both swept pore volume and the average oil saturation within swept pore volumes from PITT data in both oil reservoirs and contaminated aquifers (Zemel, 1995; Jin *et al*., 1995). Himmelblau and Bischoff (1968) presented a classical derivation of the method of moments theory for single-phase non-reactive flow in packed bed reactors. Deans and Majoros (1980) used the method of moments to estimate the residual oil saturation from single well tracer tests. Maroongroge (1994) developed the method of moments for the calculation of residual oil saturation by using the streamline theory to extend the classical derivation from 1D to 2D. Jin *et al*. (1995) presented the use of the method of moments to calculate NAPL saturations during a PITT by using the difference in the mean residence times between two tracers. Dwarakanath *et al*. (1999) estimated the uncertainty in the oil saturation calculated by the method of moments caused by errors in experimental data. Deeds (1999) derived the first temporal moment in one dimension and applied the method of moments to the analysis of partitioning gas tracers in unsaturated soils contaminated with NAPL. Jayanti (2003) studied the impact of heterogeneity on the accuracy of the oil saturation derived from tracer data.

Asakawa (2005) extended the first temporal moment derivations to calculate oil saturation and swept pore volume from tracer concentration data to 3D heterogeneous reservoir models. With Asakawa's derivations, oil saturations above the residual oil saturations can be calculated from tracers. Asakawa's extended derivations also include oil saturation calculations in naturally fractured reservoirs. Sinha (2003) applied Asakawa's equations to various PITT cases including 3D heterogeneous reservoirs with spatially variable residual and mobile oil saturations. Sinha estimated the average vertical oil saturation distribution in the reservoir as well as the oil saturation in a fractured media. Furthermore, Sinha tested the use of low-cost alternative natural organic tracers in both single and dual porosity reservoirs. The method of moments equations used in this thesis are summarized below.

Swept pore volume V_s, from the produced tracer concentration is

$$V_s = \frac{\overline{V}_2(K_1 - 1) - \overline{V}_1(K_2 - 1)}{K_1 - K_2} \tag{2.1}$$

In Equation 2.1, $\overline{V}_1$ and $\overline{V}_2$ are mean residence volume of the first and second tracers injected. K_1 and K_2 are the partition coefficients of the injected tracers. The average oil saturation, $\bar{\bar{S}}_o$, in the swept pore volume is given by Equation 2.2

$$\bar{\bar{S}}_o = \frac{\overline{V}_1 - \overline{V}_2}{\overline{V}_2(K_1 - 1) - \overline{V}_1(K_2 - 1)} \tag{2.2}$$

The partition coefficient of tracer i is K_i and defined by Equation 2.3

$$K_i = \frac{C_{io}}{C_{iw}} \tag{2.3}$$

C_{io} is the concentration of tracer i in oil phase, C_{iw} is the concentration of tracer i in

water phase. For a tracer slug during two-phase flow of oil and water, mean residence volume of tracer i is as follows:

$$\overline{V}_i = \frac{\int_0^\infty qC_{it}\,tdt}{\int_0^\infty C_{iw}\,dt} - \frac{V_{slug}}{2} \tag{2.4}$$

Where q is liquid flow rate, C_{it} is the total concentration of tracer i in both phases and V_{slug} is the volume of the tracer slug. Total tracer concentration C_{it} is defined as:

$$C_{it} = f_w C_{iw} + f_o C_{io} \tag{2.5}$$

f_w is the fractional flow of water and f_o is the fractional flow of oil.

The method of moments is a fast and easy way of estimating oil saturation and swept pore volume in the reservoirs, but its accuracy depends on the detection limit of the tracer data since a complete and accurate tracer tail is needed. The lower the detection limit, the better the estimation. In highly heterogeneous reservoirs long times are required to recover the tracer tail (the low concentrations at the end of the tracer response data). Some tracers can be detected to very low concentrations (ppb), but the best available analytical methods are not always applied or not always applicable to all tracers and they can be expensive too. However, the biggest limitation is that oil field operators are often just willing to wait a long time for the answer. In groundwater applications, the well spacing is very close and the time short, so this is not usually a problem.

2.2. INVERSE MODEL OF PARTITIONING INTERWELL TRACER TESTS

PITTs are also analyzed by inverse modeling to be able to get the fluid saturation distributions in oil reservoirs. A computationally efficient approach to solving the inverse problem is streamline-based inverse model developed at Texas A&M University (Vasco *et al.,* 1999, Yoon *et al.,* 1999, Datta Gupta *et al,* 2002). Streamline-based inverse modeling uses well production data to estimate the spatial distribution of the reservoir parameters such as permeability and fluid saturation. Inverse modeling involves sensitivity computations to give the correlation of the change in the production data, caused by the small changes in the reservoir parameters like porosity, permeability and fluid saturation (Datta Gupta *et al.,* 2000).

Vasco *et al.,* (1999) introduced the streamline-based production data integration approach, which takes the advantage of the ideas used in seismic ray tracing. Later, Yoon *et al.* (1999) applied the streamline-based inversion model to interwell partitioning tracers in aquifers. Lliasov *et al.* (2001) used the TAMU inverse model to estimate the spatial distribution of residual oil saturation in the Ranger field from the PITT data. Cheng *et al* (2004) coupled the TAMU inverse model with a finite-difference simulator (ECLIPSE). Since, finite-difference simulators included detailed physics such as compressibility; gravity, viscous and capillary cross flow and cross-streamline mechanisms in general, they are more complete than streamline simulators. Cheng *et al.* applied the inverse model coupled to ECLIPSE to water cut data to predict permeability distribution. Oyerinde (2004) extended Lliasov's derivations to mobile oil saturations and applied the TAMU inverse model coupled with ECLIPSE to the multi-well PITT data from the Ranger field.

Inverse modeling is summarized in an understandable way in Cheng *et al*. (2004). First, the velocity field derived by the finite-difference simulator is used to compute

streamline trajectories, time of flight and parameter sensitivities about a known initial model based on static data. Then, these sensitivities are used to update the reservoir model in an inversion algorithm. The updated model is used in the finite difference simulation for reservoir parameter estimation to match the data. For history matching, a generalized travel time inversion is used, which is a minimization of a least squares functional representing the difference between the observed data and the calculated response from the finite difference simulator. Figure 2.1 shows the algorithm used by this inverse modeling approach. Below are steps of computation of inversion model algorithm.

1. Flow simulation using finite difference simulator: The finite-difference simulator ECLIPSE is used as the forward model. Fluxes obtained from the forward model are used to trace the streamlines.

2. Generalized travel-time computations: Generalized travel time match is the production data misfit in each production well. He *et al.* (2001) introduced the generalized travel time concept, which is efficient for large-scale field applications with changing conditions. Generalized travel time inversion reduces two minimization techniques, which are known as travel time and amplitude inversion, into a single step. Travel time inversion technique tries to minimize the misfit of the peak arrival times as shown in Figure 2.2 while amplitude inversion tries to minimize the misfit between the amplitudes in Figure 2.3 (Cheng *et al.*, 2003). To be precise, amplitude inversion tries to match tracer concentration values one by one directly as in conventional history matching. Generalized travel time combines these two minimizations by systematically shifting the computed production response towards the observed data till the cross-

correlation between the two is maximized at the best shift-time. This is shown in Figure 2.4 and 2.5. Generalized travel time is a robust and computationally efficient method, which converges fast.

The minimization given by the production data misfit function in Equation 2.6 is called amplitude matching.

$$J_p = \sum_{j=1}^{N_w} \sum_{i=1}^{N_{dj}} w_{ij} \left(y_j^{cal}(ti) - y_j^{obs}(t_i) \right)^2 \tag{2.6}$$

for i =1, …, N_{dj}, j = 1, …, N_w

$y_j(t_i)$ represents the production data for well j at time t_i, N_W and N_{dj} shows for the number of production wells and the number of observed data at each well, respectively. w_{ij} represents the data weights (Chent *et al.*, 2004).

For a well j, the optimal shift or generalized travel time will be given by the Δt_j that minimizes the misfit function Equation (2.7)

$$J_p = \sum_{i=1}^{N_{dj}} \left[y_j^{obs}(t_i + \Delta t_j) - y_j^{cal}(t_i) \right]^2 = f(\Delta t_j) \tag{2.7}$$

or maximizes the coefficient of determination which is given by Equation 2.8.

$$R^2(\Delta t_j) = 1 - \frac{\sum_{i=1}^{N_{dj}} \left[y_j^{obs}(t_i + \Delta t_j) - y_j^{cal}(t_i) \right]^2}{\sum_{i=1}^{N_{dj}} \left[y_j^{obs}(t_i) - \overline{y_j^{obs}}(t_i) \right]^2} \tag{2.8}$$

Generalized travel time computation is illustrated in Figures 2.3 and 2.4.

The generalized travel time inversion of PITT data is a two-step procedure, which is made in a single simulation run (Oyerinde, 2004). First, the inversion model is applied

to the conservative tracer for estimating the permeability distribution based on an initial permeability guess. Later, the estimated permeability field is used for estimating the water saturation distribution by partitioning tracer inversion based on a initial water saturation guess. Finally, the saturation distribution is used for checking the conservative tracer match. If the match is not satisfactory, an inversion on permeability is made again. This iteration process continues until the obtained match is satisfactory. In this study the permeability distribution of the reservoir model is assumed to be known. Thus, only partitioning tracer is used for the estimation of the saturation.

3. Streamline-based sensitivity computations: The time of flight is used to compute sensitivity of the generalized travel-time with respect to reservoir parameters along the streamlines that are traced by the fluid fluxes obtained from the finite-difference simulator. Here, sensitivity is the partial derivative of the production response, with respect to reservoir parameters such as phase saturations, permeability and porosity and the time of flight is the travel time of a neutral tracer along streamlines (Datta-Gupta 2000). In this thesis work, the tracer concentration is taken as the production response and the oil saturation in the reservoir is estimated. Detailed information on the computation of sensitivity of tracer response to reservoir parameters is given in Appendix A. The information given in Appendix A is taken from Oyerinde's master thesis.

4. Model updating via generalized travel-time: The changes in the model parameters are computed by the least squared minimization technique that uses the streamline derived sensitivity coefficients which is shown by Equation 2.10 (Oyerinde, 2004).

$$J = \left\|\varepsilon - G\delta m\right\|^2 + \gamma_1^2 \left\|\delta m\right\|^2 + \gamma_2^2 \left\|L\delta m\right\|^2 \qquad (2.10)$$

ε is the generalized travel time shift vector at all wells, G is the sensitivity matrix containing the sensitivities of the generalized travel time with respect to the reservoir parameters, respectively. Also, δm corresponds to the change in reservoir property and L

is the second spatial difference operator. Finally, γ_1 and γ_2 are the weighting factors. The first term guarantees that the difference between the observed data and the calculated data are minimized. The second term penalizes deviations from the initial model so that the geologic realism is preserved. Third term is the roughness penalty, which recognizes that production data are an integrated response; therefore it suits large-scale structures rather than small-scale property changes.

A shortcoming of the inverse modeling is that it is ill posed, which means the solution to the problem is not unique. In other words, an arbitrary small perturbation of the data can cause an arbitrarily large perturbation of the solution.

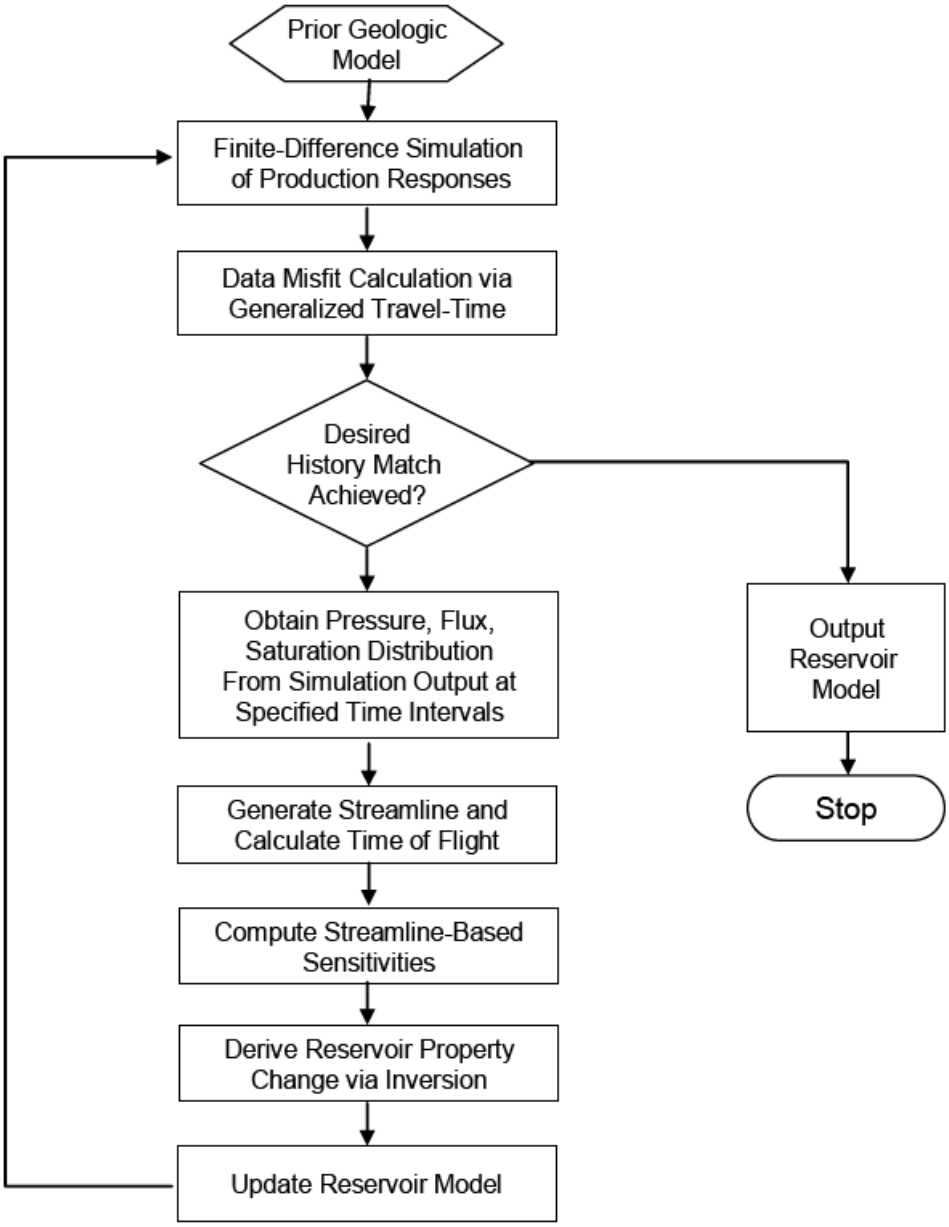

Figure 2.1. Flowchart for history matching finite-difference models using streamline derived sensitivities (Chent *et al.*, 2004).

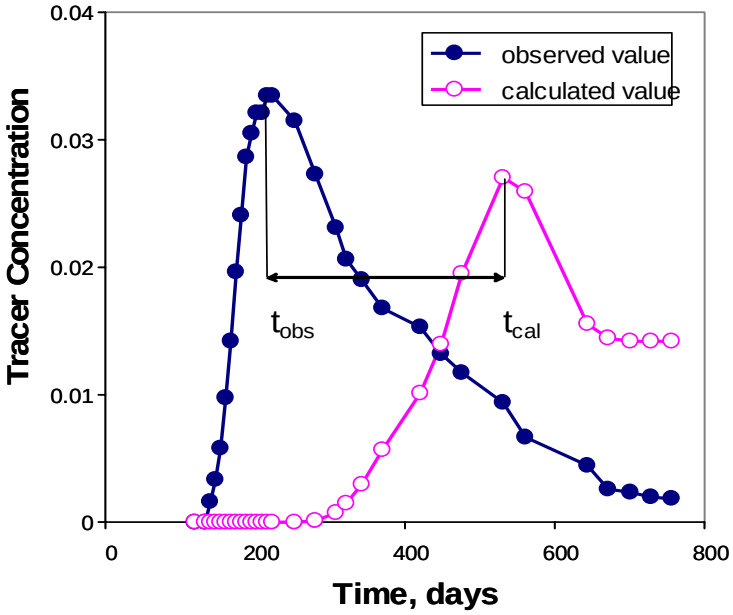

Figure 2.2. Minimization of travel time match - $\min \sum (t_{obs} - t_{cal})^2$ - of the observed and the calculated tracer concentration curves (Cheng *et al.*, 2004)

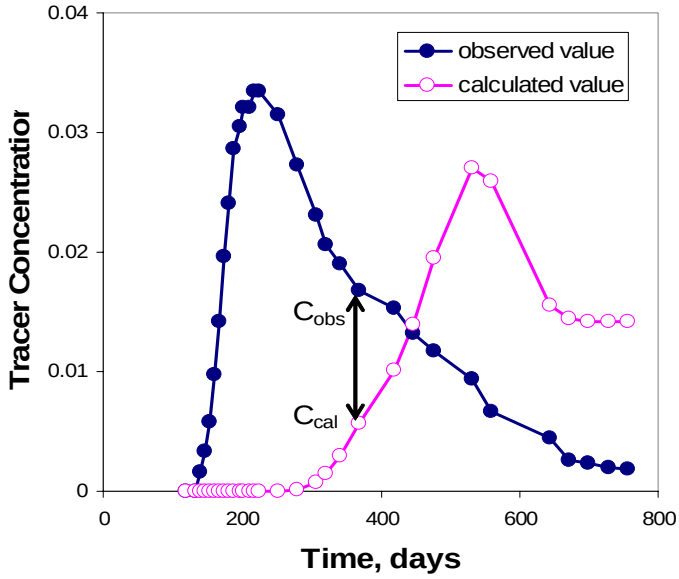

Figure 2.3. Minimization of the amplitude match - $\min \sum (C_{obs} - C_{cal})^2$ - of the observed and the calculated tracer concentration curves (Cheng *et al.*, 2004).

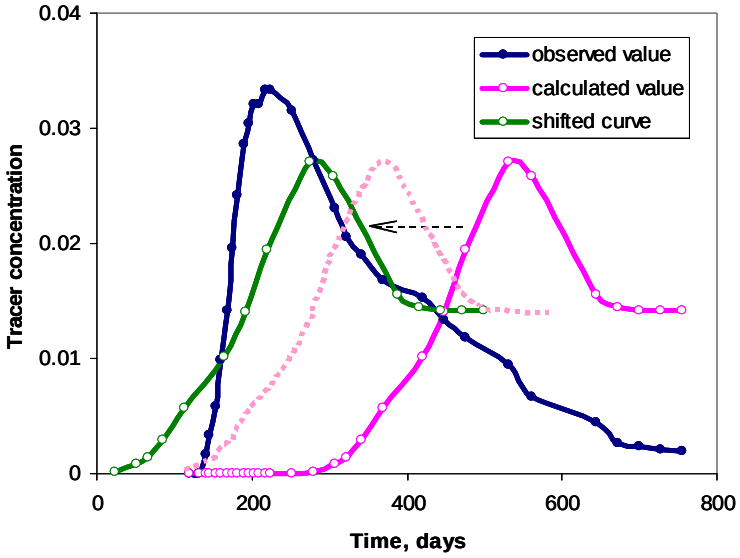

Figure 2.4. Minimization of the shift time - $\min \sum (\Delta\tau)^2$ - by shifting the model response towards the observed data at each well (Cheng *et al.*, 2004)

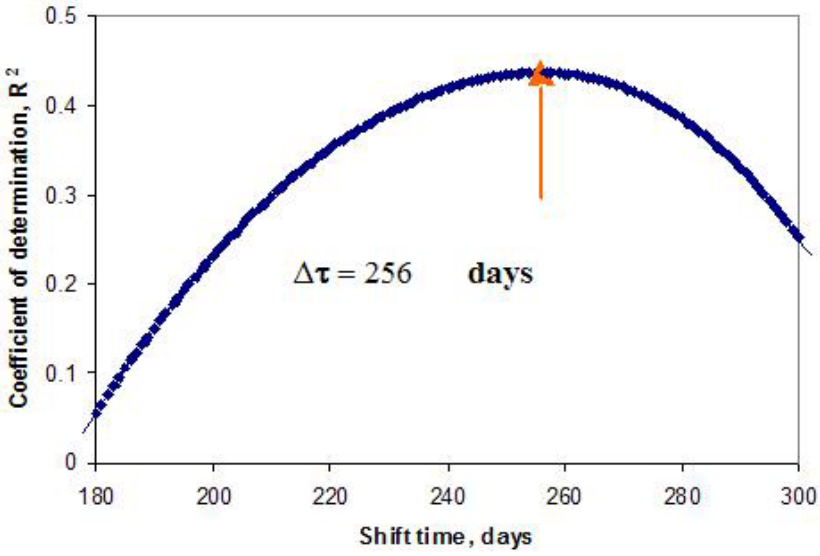

Figure 2.5. Maximized coefficient of determination by the optimal shift time (Cheng *et al.*, 2004).

CHAPTER 3: Use of Inverse Model in Single Phase Flow

In this chapter, the results using the TAMU inverse model are presented for a 3D synthetic reservoir model with permeability layers and later to a reservoir modeled with a stochastic permeability field. An initial analysis was done to get familiar with the inverse model and to find and understand its limitations. The number of iterations, partition coefficient, initial saturation guess and tracer response cut off were investigated. In the later sections, a comparison is made between the MOM and the inverse method for different tracer concentration detection limits. Next the methods are used in a complementary way by using the saturation from the MOM as the initial guess for the inverse calculation.

3.1 SIMULATION OF A RESERVOIR MODEL WITH UNIFORM LAYERED PERMEABILITY

3.1.1 Reservoir Description

The synthetic oil reservoir used for the forward model is a three-dimensional, layered permeability reservoir with a quarter of a five spot well pattern as summarized in Table 3.1. The reservoir well pattern modeled is 660 ft on each side and 50 ft thick. Porosity is 0.2 and uniform. Figure 3.1 shows the vertical permeability distribution in the reservoir. The permeability distribution has a log mean permeability of 256 md and Dykstra Parson's coefficient of 0.50. Figure 3.2 shows the permeability field. A residual oil saturation distribution is generated in the reservoir using the same exponential relation with permeability as used by Sinha (2004) and is given by Equation 3.1.

$$S_{or} = e^{-0.8k_x^{0.1}} \quad (3.1)$$

The relationship between the permeability and oil saturation is shown in Figure 3.3. Figure 3.4 illustrates the vertical oil saturation distribution. Low permeability layers have high oil saturation and vice versa.

3.1.2 Forward Model Simulation

In the forward model simulation, an aqueous 0.1 PV slug of tracer solution with one conservative tracer and one partitioning tracer with a partition coefficient of 2.0 was injected followed by water injection. Total simulation time is 2000 days corresponding to 15 PV. The reservoir is at a non-uniform residual oil saturation with an average value of 0.259. The injector is rate constraint while the producer is pressure constraint. The input file is given in Appendix B.

It is assumed that the tracer concentration can be measured in each layer by some means such as a downhole sensor or sampling device (Sinha, 2004). The tracer concentration response curve (normalized by the injected concentration) from all layers in the production well is shown in Figure 3.5. Figures 3.6 and 3.7 show the tracer concentration response curves of the least and most permeable geological layers. As it is expected, the tracer breakthrough from the most permeable layer is very fast compared to the least permeable layer.

3.1.3 Application of Inverse Model to PITT data

Inverse model was run with an initial guess of 0.26 for the oil saturation in all layers. Since the average oil saturation in the reservoir is 0.259, the initial guess given to the inverse model is very close to the values in each layer for this case. The partitioning tracer used has a partition coefficient of 2. And the normalized tracer concentration

detection limit is taken as 0.0001. The oil saturation for the iteration with the smallest RMS error is taken as the best estimate from the inverse model. The streamline distribution after inverse modeling is shown in Figure 3.8. Injected tracers follow these paths to the producer. Figure 3.9 shows the RMS (root mean square) error, which is the overall misfit reduction as a function of the number of iterations. The errors for both travel time and amplitude decrease as the number of iterations increase. Figure 3.10 shows the tracer concentration response curves after the inversion at the first and the fifth iterations using data from all layers in the reservoir. Although there is only a very small difference between the concentration response curves at different iterations, the iteration improves the estimate of the oil saturation. The tracer concentration response curves match with the forward model very well even after the first iteration. This can be explained by the initial oil saturation guess, which is very close to the reservoir average saturation. Figures 3.11 and 3.12 are the tracer concentration curve matches for the least and most permeable layers. The vertical oil saturation distribution (the average in each layer) is shown in Figure 3.13. Improvement with the number of iterations is noticeable. Figure 3.14 shows how the average oil saturation changes with the number of iterations. Inverse model oil saturation distribution is compared with forward model oil saturation distribution in Figure 3.15. Although the inverse model estimate is poor, it catches the high and low saturation areas. Probably, if there were more wells in the reservoir, the inverse model could predict the oil saturation distribution in the reservoir more accurately.

3.1.4 Sensitivity Analysis of Inverse Model

3.1.4.1 Sensitivity of Inverse Model to Partition Coefficient

In this section, results for various tracer partition coefficients are used to test the inverse model. In all the sensitivity analysis, 0.26 is used as the initial oil saturation guess. And, the iterations with the smallest RMS error both on travel time and amplitude match are chosen as the inverse model oil saturation estimate.

Figures 3.16 and Figure 3.17 show the estimates of the oil saturation for different partition coefficients. Figure 3.16 shows that inverse model is not sensitive to partition coefficient 1. Partition coefficients 2 and 3 give the closest estimate to forward model while partition coefficients 4 and 5 give the poorest estimates. In Figure 3.17, partition coefficients 6 to 10 give very close estimates to each other and unexpectedly the estimates with them are better than the estimates with partition coefficients 4 and 5.

Table 3.2 and Table 3.3 show the inverse model oil saturation estimate errors with various partition coefficients. RSM error plot for partition coefficient 1 is shown in Figure 3.18. As the Figure shows, satisfactory tracer concentration curve match is obtained without any iteration at partition coefficient 1. The tracer response match of the forward model from all layers with inverse model is displayed in Figure 3.19. And, the tracer response match from the least and most permeable layers are shown in Figures 3.20 and 3.21 respectively. The figures show the perfect tracer response match of the models. However at this partition coefficient, inverse model is not sensitive to oil saturation estimate. What we can conclude here is that perfect tracer curve match does not guarantee accurate oil saturation estimate. Figure 3.22 demonstrates the RSM error change of inverse modeling with partition coefficient 3 over the number of iterations. At the first two iterations, both travel time and amplitude errors decrease but they do not

keep this trend in the rest of the iterations. Tracer response match curve from all layers with this partition coefficient, at the 3rd iteration are illustrated in Figures 3.23. Figures 3.24 and 3.25 are the tracer concentration curve matches for the least and most permeable layers. The curve matches are satisfactory although there is a little separation among the tails in Figure 3.24. Figure 3.26 show that RSM error change of the inversion with partition coefficient 5 doesn't show any convergence. The tracer concentration match curves at the first iteration, which has the smallest RMS errors, are shown in Figures 3.27 to 3.29. The PITT simulation with partition coefficient 5 takes longer simulation time than the partition coefficient 2 and 3 due to the high retardation. Late tracer recovery can be observed in the concentration curves. There is not a perfect match between the forward and the inverse models in these figures. These poor matches increase the error in the oil saturation estimate as it is observed in the earlier Figure 3.16. Lastly, RSM error change for inverse modeling with partition coefficient 10 is shown in Figure 3.30. The error does not converge with this partition coefficient either. Tracer response match curve from all layers at the 2nd iteration is illustrated in Figures 3.31. Figures 3.32 and 3.33 are the tracer concentration curve matches for the least and most permeable layers. Especially in the least permeable layer, it takes almost 5000 days to recover the tracer with the partition coefficient 10. It is observed that tracer curve matches show the same behavior as the curve matches do with partition coefficient 5 although the error in oil saturation estimate with partition coefficient 5 is larger. This can be attributed to the nonuniqueness of inverse model.

.3.1.4.2 Sensitivity to Initial Guess

Inverse model is tested with various initial oil saturation guesses in this part. In all the sensitivity analysis, partitioning coefficient 2 is used. Figure 3.34 and Figure 3.35

demonstrate vertical oil saturation estimate of inverse model at various initial oil saturation guesses from 0.21 to 0.30. Figures show that various initial guesses, which are in the close range of the average oil saturation of the reservoir model, give pretty good estimates. Table 3.4 and Table 3.5 show the oil saturation estimate errors of inverse model at these initial guesses. As it may be observed from the tables, largest estimate error is at initial oil saturation guess 0.30 and the minimum is at initial oil saturation guess 0.26. These average oil saturation estimates errors are in acceptable limits. RMS error change at initial oil saturation guess 0.21 is given in figure 3.36. RMS error converges satisfactorily. 4^{th} iteration is taken as the inverse model oil saturation estimate at this initial oil saturation guess. Tracer response match curve from all layers is illustrated in Figures 3.37. Figures 3.38 and 3.39 are the tracer concentration curve matches for the least and most permeable layers. There is a little separation in the tails in the Figures 3.37 and 3.38. However, in real reservoirs tracer production concentration data is not in the form of a perfect curve as it is shown in the synthetic case here (Vasco et al 1999, Oyerinde, 2004). Thus, this kind of small differences in the concentration curve matches shouldn't effect inverse model estimates. The converging RMS error change at initial oil saturation guess 0.28 is demonstrated in Figure 3.40. Tracer response curves show prefect match at this initial guess in Figures 3.41 through 3.43. Thus, at this initial guess oil saturation root mean square error is 1.72%, which is very reasonable. Figure 3.44 shows the RMS error variation at the initial oil saturation guess 0.30. It seems like RMS starts to flatten out after the 8^{th} iteration but convergence is not clear. In this kind of situation, oil saturation estimates at the iterations, which seem to have the smallest RMS error, are compared. And, the iteration with the smallest error in the oil saturation estimate is taken as the inverse model result. In this case, a comparison between the 1^{st} and the 9^{th} iterations are made and the 1^{st} iteration is selected. Tracer

response match curve from all layers at the 1st iteration is illustrated in Figures 3.42. Figures 3.43 and 3.44 are the tracer concentration curve matches for the least and most permeable layers is given in Figures 3.45 though 3.47 from all, the least and the most permeable layer respectively. Sensitivity of inverse model to initial oil saturation guess was also tested with two values, which are further away from the average oil saturation of the reservoir model. Figure 3.48 shows the vertical oil saturation distribution estimate at initial guess 0.38, 0.26 and 0.14. Oil saturation estimate errors tabulated in Table 3.6. Although the estimate RMS error passes 4% (Table 3.6), the estimated vertical oil saturation curves catch the trend of the forward model. The RMS error convergence on travel time and amplitude match at initial oil saturation guess 0.14 is displayed in Figure 3.49. Tracer concentration curves at 4th iteration are illustrated in Figures 3.50 through 3.52. The poor tracer concentration match at the 5th layer in Figure 3.51 is noticeable. Lastly, Figure 3.53 shows the RMS error change at initial oil saturation guess 0.38. The smallest RMS error is viewed at iteration 10. Figures 3.54 through 3.56 illustrate the tracer concentration curve matches at initial guess 0.38. Again poor curve match is noticeable in the least permeable layer 5 in Figure 3.55.

Importance of a reasonable initial oil saturation guess for the inverse model is shown with the use of many different values as initial guesses above. Initial oil saturation guess, which is in the close range of the average oil saturation of the reservoir give pretty good estimates of the vertical oil saturation distribution of the reservoir. However, oil saturation estimate gets further away from the forward model as the initial guess moves away from the average oil saturation of the forward model. Additionally, a satisfactory tracer concentration match does not always guarantee accurate oil saturation estimate while a poor tracer concentration match increases the error in the estimate.

.3.1.4.3 Sensitivity to Tracer Concentration Detection Limit

With the current technology, small tracer concentrations in the produced fluid can not be detected in the oil fields and in addition, long PITTs are not economical. Thus, inverse model or analytical methods should be able to estimate oil saturations in the reservoirs accurately even at high tracer concentration detection limits (TDL). Sensitivity of inverse model to various TDLs is tested for this reason.

Figure 3. 57 shows inverse model vertical oil saturation distribution estimates at normalized tracer concentration detection limits 0.0001, 0.001 and 0.01 at initial oil saturations guess 0.26 and with partition coefficient 2. Oil saturation estimates overlap for detection limits 0.0001 and 0.001. However, error in the oil saturation estimate increases when the detection limit increases to 0.01. Table 3.7 displays the inverse model the oil saturation estimate errors. RMS error on travel time and amplitude for TDL 0.0001 converges in 5 iterations as it is shown earlier in Figure 3.9. For TDL 0.001, RMS error converges in six iterations in Figure 3.58. But, in Figure 3.59 for TDL 0.01, RMS error doesn't show a convergence as good as the other detection limits. For TDL 0.01 iteration 4 was taken as the inverse model oil saturation estimate. Tracer response match curve from all layers at various detection limits is illustrated in Figures 3.60. Figures 3.61 and 3.62 are the tracer concentration curve matches for the least and most permeable layers. There is perfect match between the forward and the inverse model. The inverse model extrapolates the tracer concentration data very well even at the high detection limit 0.01. This means long simulation times are not necessary for recovering the entire tracer injected to get accurate oil saturation estimate.

Inverse model at various TDLs is also tested with initial oil saturation guess 0.30. Figure 3.63 shows the inverse model vertical oil saturation distribution estimates for TDLs 0.0001, 0.001 and 0.01 at initial oil saturations guess 0.30 and with partition

coefficient 2. Again, oil saturation estimates for TDL 0.0001 and 0.001 overlap while saturation estimate for TDL 0.001 is a bit different than the other detection limits. Table 3.8 displays the inverse model oil saturation estimate errors at the studied TDLs. RMS error change for TDL 0.001 in Figure 3.64 shows the same behavior it shows for TDL 0.0001 which is shown earlier in Figure 3.44. Figure 3.65 shows the RMS error variation over the number of iterations for TDL 0.01. The error increases with more iteration at this TDL. At initial oil saturation guess 0.30, the saturation estimates at the first iteration are taken as the inverse model result. Tracer response match curve from all layers at various detection limits are illustrated in Figures 3.66. Figures 3.67 and 3.68 are the tracer concentration curve matches for the least and most permeable layers. At this initial oil saturation guess, inverse model extrapolates the tracer concentration data very well like it does with the initial oil saturation guess 0.26. There is a good match between the forward and the inverse model in all the detection limits.

Inverse model gives satisfactory results at tracer detection limits 0.0001, 0.001 and 0.01 in this synthetic problem with uniform permeability in every layer. Accurate oil saturation estimates at high detection limits are very valuable especially in field applications. However, in more complex reservoir models, the results may not be very reasonable. Sensitivity of inverse model to various detection limits at a reservoir with a stochastic permeability field is discussed in section 3.2.

.3.1.4.4 Sensitivity to Permeability Distribution Order

For testing the inverse model, vertical permeability distribution in the synthetic reservoir model is rearranged. Permeabilities are sorted in a descending order from the top to the bottom of the reservoir with the corresponding oil saturation values. Rearranged vertical permeability and oil saturation distribution are demonstrated in

Figures 3.69 and 3.70. In the simulations TDL is taken as 0.0001. Partition coefficient of the tracer used is 2 and the initial oil saturation guess given to the inverse model is 0.26. Figure 3.71 shows the inverse model vertical oil saturation distribution estimates in the reservoir model. Table 3.9 gives the saturation estimate errors of inverse model in every layer. Root mean square error is 1.43%, which is a little higher than the estimate error obtained with the base case permeability field. But, the error is still small and reasonable. Figure 3.72 shows the comparison of inverse model vertical oil saturation distribution estimate with the forward model. Figure 3.73 shows the RMS error variation. It converges in five iterations as it does in the base case. Tracer concentration match curves, which are shown in figures 3.74 through 3.76, are good as expected.

3.1.5 Application of Method of Moments and Inverse Model to the Reservoir Model with the Uniform Layered Permeability

3.1.5.1 Method of Moments and Extrapolation of Tracer Data

In the method of moments (MOM) calculations applied to this reservoir model, equations given in section 2.1 are used. Tracer concentration detection limit is taken as 0.0001 in MOM calculations. However, for accurate estimate of oil volume, completeness of the tracer response curves is significant because of the information contained in the tails of the tracer concentration response curves. Thus, tracer response curves are extrapolated with an exponential function (Jin, 1995). The tracer response curve is divided into two parts to obtain the first moments of the tracer response curves. The first part is from time zero to the time t_b, where the time becomes exponential and the second part is exponential part where time goes to infinity from t_b. It is assumed that

after time t_b, the tracer response follows an exponential decline, which is given by Equation 3.2.

$$C = C_b e^{-\left(\frac{t-t_b}{a}\right)} \tag{3.2}$$

In Equation 3.2, 1/a is the slope of the straight line when the tracer response curve is plotted on a semi log scale. And, C_b is the tracer concentration at time t_b. Equation 3.3 and 3.4 show the integration as,

$$\int_{t_b}^{\infty} C_b e^{-\left(\frac{t-t_b}{a}\right)} dt = aC_b \tag{3.3}$$

and

$$\int_{t_b}^{\infty} C_b e^{-\left(\frac{t-t_b}{a}\right)} t dt = a(a+t_b)C_b \tag{3.4}$$

Consequently, the first moment, $\bar{t}$, of the tracer response curve is calculated as

$$\bar{t} = \frac{\int_0^{t_b} tCdt + a(a+t_b)C_b}{\int_0^{t_b} Cdt + aC_b} - \frac{t_s}{2} \tag{3.5}$$

Extrapolation of the tracer concentration curves all layers for TDL=0.0001 is illustrated in Figures 3.77. Figures 3.78 and 3.79 are the tracer concentration extrapolations for the least and most permeable layers. The trend line equations given in these Figures are in the form of

$$y = \alpha e^{-\beta x} \tag{3.6}$$

And that is different than the form of Equation 3.2. In equation 3.6 a equals to $\frac{1}{\beta}$. C_b is the last tracer concentration response value detected and t_b is the corresponding breakthrough time. Figures show that exponential extrapolation is successful since the trend lines match with the forward model. Figure 3.80 demonstrates the swept pore volume estimate of MOM. Table 3.10 shows that 97% of the reservoir is swept. Oil saturation with and without extrapolation at this TDL is illustrated in Figure 3.81. Since the reservoir is almost all swept for TDL 0.0001, extrapolation doesn't improve the estimate more and the estimate curves overlap. Extrapolation of tracer response curves might not be satisfactory if the shape of the concentration curve changes after the detection limit. Extrapolation of tracer response curves for TDL =0.01 is a good example to this. Extrapolation of the tracer concentration curves all layers for TDL=0.0001 is illustrated in Figures 3.82. Figures 3.83 and 3.84 are the tracer concentration extrapolations for the least and most permeable layers. Because the slope of the forward model changes after the detection limit 0.01, exponential extrapolation doesn't match the forward model response. Figure 3.85 show that the extrapolation improves the swept pore volume estimate. In Table 3.10, swept pore volume estimate for TDL=0.01 is 0.75 while it increases to 0.80 with extrapolation. MOM oil saturation estimate comparison with and without extrapolation is demonstrated in Figure 3.86. Oil saturation estimate is improved in every layer. MOM oil saturation estimates at various detection limits are compared in Figure 3.87 and Table 3.11. Estimates for TDLs 0.0001 and 0.001 give the same estimates whereas estimates for TDL 0.01 are less accurate because of the extrapolation error.

3.1.5.2 Comparison of Inverse Model with Method of Moments

It is shown earlier that inverse model give accurate oil saturation estimates with initial guesses close to the average oil saturation value of the reservoir model. The forward model average oil saturation is 0.259, while the average MOM estimate in the reservoir with extrapolation for TDL=0.0001 is 0.241. This is a close estimate and a good initial guess for the inverse model. At this initial guess, RMS error change by the number of iterations during the inverse model run is given in Figure 3.88. Oil saturation estimate at the 6^{th} iteration, is taken as the inverse model estimate. Figure 3.89 shows the inverse model oil saturation estimate at this iteration. For comparison purposes, average MOM estimate in every layer and inverse model estimate at initial guess 0.26 are presented in the same graph too. The estimates given by MOM and inverse model with initial guess 0.26 look better than the inverse model estimate, which has the average MOM estimate as an initial guess. However, Table 3.12 shows that average estimate error is very low and within the acceptable limits.

Till here, a simple quarter of a five spot, 3D reservoir model with layered uniform permeability is used and the oil saturation estimates are very good with estimate errors below 4%. At more complex reservoirs, estimate errors may increase. In the next section, MOM and inverse model techniques are applied to a 3D five spot reservoir model.

3.2 SIMULATION OF A RESERVOIR MODEL WITH STOCHASTIC PERMEABILITY FIELD

3.2.1 Reservoir Description

The reservoir used here is a three dimensional, inverted five spot model with a stochastic permeability field. The reservoir is 930 ft in horizontal directions and 50 ft in vertical direction. The model is divided into 31 grid blocks in x and y directions while there are 10 grids in z direction. The porosity is 0.2 and uniform in the reservoir. Reservoir description is given in Table 3.13. The simulated permeability field was stochastically generated using geostatistical software FFT (Sinha, 2004; Jayanti 2003).

The generated permeability field has a log mean permeability of 227 md and Dykstra Parson's coefficient of 0.80. The correlation length is 300 ft in x and y directions and 10 ft in z direction. Table 3.14 shows the detailed description of the permeability field. Figure 3.90 and 3.91 show the permeability distribution in the most and least permeable vertical layers respectively. Figure 3.90 also shows the four quadrants of the reservoir model, which are referred to frequently in the later sections. Figures 3.92 and 3.93 show the permeability distributions of two layers Y=1 and Y=16. As the images show reservoir is highly heterogeneous. Especially between the vertical layers, there is high permeability contrast. Figure 3.94, which shows the vertical average permeability distribution, shows this contrast well. The exponential correlation between the permeability and the residual oil saturation given in Equation 3.1 is used to generate the residual oil saturation distribution. The correlation between the two reservoir parameters is shown in Figure 3.95. As the figure shows the oil saturation values have been limited to 0.1 by cutting off the extreme values. The average residual oil saturation is 0.27. Figure 3.96 illustrates the average residual oil saturation in each layer.

3.2.2 Forward Model Run

In the forward model simulation, a slug of tracer, which consists of one conservative and one partitioning tracer, is used. Tracer slug is injected for 0.1 PV and the partition coefficient of the tracer used is 2. The injector is rate constraint while the producer is pressure constraint. And like in the previous case, there are sensors in every layer.

Forward model is run three times for various vertical permeabilities. And, MOM calculations are performed for each case. Inverse model is applied to the model with initial guess of MOM oil saturation estimates and the results are interpreted.

3.2.3 Application of Method of Moments and Inverse Model to the Reservoir Model with the Stochastic Permeability Field

Below, MOM and inverse model are applied to various vertical permeabilites. In addition, the effect of heterogeneity and cross flow both on MOM and inverse model is discussed.

Sinha (2004) shows the dependence of MOM oil saturation estimates to vertical permeability. As he implies, MOM oil saturation estimate error increases with increasing kv/kh ratios. Next to heterogeneity, this can also affect inverse model results since MOM estimate is used as an initial guess for inverse model.

Here, tracer detection limit (TDL) is taken as 0.0001 but TDL 0.001 is also used where, MOM oil saturation estimate error is relatively small.

3.2.3.1 Reservoir study with kv/kh ratio 0.1

MOM calculation is first performed between the injector and the production well 1. Figure 3.97 shows the extrapolation applied to the tracer response curves.

Extrapolation increases the swept pore volume from 325, 000 bbl to 350,000 bbl (Figure 3.98) or increases the swept pore volume/reservoir volume ratio from 0.20 to 0.21 (Table 3.15). Figure 3.99 shows the vertical oil saturation distribution, which is calculated by the tracer concentration detected by sensors in each layer. Vertical saturation estimate of MOM is poor and extrapolation does not improve estimate of much. Average MOM oil saturation estimates in each quadrant with and without extrapolation are shown in Table 3.16. In the Table, average MOM estimate in quadrant one is 0.27 with extrapolation while the actual reservoir saturation in this quadrant is 0.28. This is a very good estimate.

Figure 3.100 shows the extrapolation of the tracer response curves in quadrant two. Extrapolation doesn't seem perfectly well for TDL 0.0001 since the added trend lines do not match with the forward model curves after the detection limit. In Figure 3.101, MOM swept pore volume estimate is around 340, 000 bbl. And it goes up to 350,000 bbl with extrapolation, which is 21% of the reservoir volume. Vertical saturation distribution estimate shown in Figure 3.102 has the largest estimate error in layers 3 and 4 that is about 14%.

In Figure 3.103, in quadrant three, after the TDL 0.0001, shape of the tracer response curves change after the detection limit and this change leads to error in the extrapolation. Figure 3.104 shows the swept pore volume in quadrant 2. Extrapolation does not increase the swept pore volume estimate much. Figure 3.105 illustrates the vertical oil saturation estimates. Average saturation estimate in this quadrant is 0.21 and that is 2% lower than the average oil saturation in this quadrant.

Figure 3.106 shows a perfect extrapolation of the tracer concentration response in quadrant four. Extrapolation increases the swept pore volume estimate around 1% and that is shown in Figure 3.107. MOM vertical oil saturation distribution estimate is shown in Figure 3.108. The estimate errors in each layer are less than the other quadrants due

high swept pore volume. Average oil saturation estimate in this quadrant is same as the reservoir average saturation value, which is 0.34.

With the extrapolated MOM estimates given as initial guesses for each quadrant, inverse model is run. Figure 3.109 shows the streamline distribution after the inverse model run. Streamlines are more complex than they are in section 3.1 because of high heterogeneity and cross flow. Figure 3.110 shows the RMS error change on travel time and amplitude. The 1st iteration is taken as the inverse model estimate. At this iteration, forward and the inverse model tracer concentration match very well for the first quadrant in Figure 3.111. Figure 3.112 shows the poor vertical saturation estimate of inverse model. Inverse model is not very successful at estimating the vertical oil saturation distribution. Estimate errors of MOM and inverse model at each quadrant and the root mean square errors of estimates are tabulated in Tables 3.17 and 3.18 respectively.

Again there is perfect tracer concentration match between the forward and the inverse models in quadrant two in Figure 3.113. Although inverse model catches the trend of oil saturation distribution in Figure 3.114, the vertical saturation distribution estimate is not as good as MOM's. Moreover, Tables 3.18 and 3.19 show the root mean square (RMS) error of inverse model is higher than the RMS error on MOM estimate in this quadrant.

Figure 3.115 and 3.116 show the tracer response match curves and the oil saturation estimate in the third quadrant respectively. Tables 3.18 and 3.19 show that RMS errors on inverse model and MOM oil saturation estimate are lower than they are in the first two quadrants and probably it is because of the lower heterogeneity in this quadrant.

Figures 3.117 and 3.118 show the tracer response match curves and the oil saturation estimate in the fourth quadrant respectively. In this quadrant, there is a little

separation in the tails of the tracer concentration curves. In this quadrant like in quadrant three, RMS errors on saturation estimate for both MOM and inverse model are small. But in Figure 3.118, inverse model vertical saturation distribution estimate is not as good as the MOM estimate.

Lastly Figures 3.119 and 3.120 show the inverse model oils saturation distribution estimate in Z=7 and Y=16 respectively. When the estimates are compared with the forward model, they are not satisfactory.

3.2.3.2 Reservoir study with kv/kh ratio 0.01

In the above example, due to the high cross flow between the layers, MOM estimates have high errors. And inverse model does not improve the average MOM estimates as desired. In this section, vertical permeability is decreased to observe its effect on MOM and inverse model estimates.

Figure 3.121 shows the extrapolation of the tracer response obtained from production well 1. Compared to Figure 3.97, separation between the forward model and the trend line is larger at this kv/kh ratio. Figure 3.122 shows the swept pore volume estimate that is 21 % of the reservoir volume. Table 3.19 shows the tabulated swept pore volume estimates in all quadrants. Figure 3.123 shows the oil saturation distribution estimate of the MOM. Estimate catches the trend of the forward model much better as expected compared to the estimate at a higher kv/kh ratio.

Figures 3.124 and 3.125 show the tracer concentration curve extrapolation and the swept pore volume estimate in quadrant two respectively. Swept pore volume in this quadrant is 22% of the reservoir volume. Figure 3.126 gives an oil saturation estimate of MOM with RMS error 3.80 %. However, the average oil saturation estimate obtained in this quadrant is 0.20 and that is 0.04 lower than the actual value in thus quadrant.

Figures 3.127 through 3.129 show the tracer response in quadrant three, swept pore volume and the oil saturation estimate. Swept pore volume in this quadrant is high compared to the other quadrants. Average oil saturation in this region is 0.22 while the actual value is 0.23. Also estimates in each layer are close to the forward model.

Finally, Figures 3.130 through 3.132 show the tracer response in quadrant four, swept pore volume and the oil saturation estimate. MOM estimates the average oil saturation in this quadrant accurately. And the vertical distribution of oil saturation is estimated close to the actual values with and RMS error of 0.27.

The results show that vertical oil saturation distribution of MOM becomes more accurate when the cross flow is decreased. However, average oil saturation estimates of MOM in each quadrant only improved in quadrant three when the kv/kh ratio is decreased. Obtaining the average oil saturations for each quadrant, MOM estimates are given as initial guesses to inverse model. Figure 3.133 shows the streamline distribution of inverse model. Streamlines seem more separate than each other at this kv/kh ratio. Figure 3.134 shows the RMS error variation over number of iterations. Fifth iteration is taken as the inverse model result.

Figure 3.135 shows the tracer concentration match of inverse and forward models. Decrease in kv/kh ratio does not change the tracer concentration match curve in this quadrant since Figure 3.135 is same as Figure 3.111. Figure 3.136 shows the oil saturation estimate of inverse model. Vertical oil saturation distribution of inverse model approaches the forward model curve more than it does at kv/kh ratio 0.01. This difference in the estimate can be attributed to the decrease in vertical permeability since the given initial oil saturation guess for this quadrant is same and 0.27 at kv/kh ratios 0.1 and 0.01.

Figure 3.137 shows the tracer concentration match curves of inverse and forward models in quadrant two. Again the graph is same as Figure 3.113. Figure 3.138 shows the vertical oil saturation estimate in this quadrant. Inverse model estimates in layers 6 to 10 get closer to the forward model but still the estimates in the first five layers are very poor. For this quadrant initial oil saturation is also same for both inverse model runs at kv/kh ratio 0.1 and 0.001. The initial saturation guess is 0.20 while the actual reservoir average saturation is 0.24.

Figure 3.140 shows the tracer concentration match of inverse and forward models in quadrant three. There is some separation in the tails just like in Figure 3.115. Figure 3.140 shows the oil saturation estimate of inverse model. There isn't much change in the vertical saturation estimate compared to the previous section although the initial oil saturation guess 1% closer to the actual value compared to the initial guess obtained in kv/kh ratio 0.1.

Figure 3.141 shows the tracer concentration match of inverse and the forward models. And also in this quadrant, concentration curve match has the same shape of Figure 3.117. Figure 3.141 shows the oil saturation distribution estimate of inverse model. Inverse model estimate does not improve with the decreasing vertical permeability in this region.

When the MOM estimates in kv/kh ratios 0.1 and 0.01 compared, at lower vertical permeability, MOM oil saturation estimates in each layer in each quadrant improve. But the average estimates in each quadrant do not change except one (quadrant 3).

When the tracer concentration match curves are compared in kv/kh ratios 0.1 and 0.01, it is observed that tracer concentration match curves do not change. It maybe be because of the same initial guesses used in each quadrant except one.

At low vertical permeability, inverse model oil saturation estimates approach the forward model values in some layers in different quadrants. But, overall, RMS error on saturation estimate of inverse model is higher at kv/kh ratio 0.01 then it is in kv/kh ratio 0.1 for all quadrants (Tables 3.19 and 3.22). This is not expected since initial oil saturation guesses used for three quadrants are same as the initial guesses used at kv/kh ratio 0.1. In addition, the initial guess in one quadrant is 1% closer to the actual value then the one used at kv/kh ratio 0.1.

3.2.3.3 Reservoir study with kv/kh ratio 0.001

At this kv/kh ratio, inverse model is tested for TDL=0.0001 and TDL=0.001.

TDL=0.0001

Vertical permeability is decreased to reduce the cross flow and the error in MOM estimate and to see if inverse model estimate is getting better.

Figures 3.143 to 3.145 show the tracer concentration curve extrapolation, swept pore volume and the saturation estimate of MOM in quadrant one respectively. Table 3.23 shows that swept pore volume estimate/reservoir volume ratio goes up from 0.24 to 0.25 with extrapolation. In Figure 3.145, MOM oil saturation estimates are more accurate in all layers compared to the previous kv/kh ratios. Average MOM oil saturation estimate in every layer and the improvement with extrapolation is shown in Table 3.24.

Figures 3.146 to 3.148 show the tracer concentration curve extrapolation, swept pore volume and the saturation estimate of the MOM in quadrant two in the written order.

The least sweep is in this quadrant with 21%. That's why average MOM estimate in this quadrant does not go above 0.21 with extrapolation.

Figures 3.149 to 3.151 show the tracer concentration curve extrapolation, swept pore volume and the saturation estimate of the MOM in quadrant three in the written order. In this quadrant extrapolation improves the MOM estimate. And the average estimate reaches to the forward model value.

Figures 3.152 to 3.154 show the tracer concentration curves and their extrapolations; swept pore volume and MOM estimates in the fourth quadrant. Average oil saturation estimate in this quadrant is same as the forward model value like in the other quadrants.

Overall, MOM and extrapolations worked well for this kv/kh ratio. The average oil saturation estimates in each quadrant are given as an initial guess to inverse model and the inverse simulation is performed. Figure 3.155 shows the streamline distribution performed by inverse model. Streamlines are covering most of the reservoir and that is very good, since inversion calculations are made along the streamlines. Figure 3.156 shows the RMS error change. RMS error on travel time is quite high and the error does not decrease much. The fifth iteration is taken as the inverse model result. Figure 3.157 shows the perfect match between the tracer concentration curves of the inverse and the forward models. Oil saturation estimate of inverse model is demonstrated in Figure 3.158. At this kv/kh ratio, inverse model approaches the forward model more in the vertical saturation estimate graph. And the RMS error on saturation estimate decreases 0.56 in this quadrant. Tables 3.21 and 3.22 show the errors in the estimates with both methods. However, still RMS error on MOM estimate in Table 3.21 is smaller than the RMS error of inverse model estimate is in Table 3.22.

Figure 3.159 shows the tracer concentration match of forward and the inverse model in the second quadrant. Figure 3.160 shows the inverse model oil saturation estimate. In this quadrant, inverse model has the higher error in vertical estimate compared to the error it has in quadrant two at kv/kh ratio 0.01.

Tracer concentration match of inverse and the forward model in quadrant three is shown in Figure 3.161. Figure 3.162 shows the oil saturation estimate of inverse model. In this quadrant, MOM average oil saturation estimate is improved to 0.23, which is also the actual average oil saturation of this quadrant. But average RMS error on vertical saturation estimate is higher than the RMS error in this quadrant at kv/kh ratio 0.01. And also, vertical MOM estimate is better than inverse model's.

Tracer concentration match of inverse and the forward model in quadrant four is shown in Figure 3.163. Figure 3.164 shows the oil saturation estimate of inverse model. Even though inverse model catches the trend of the forward model. Its RMS error on saturation is higher than the RMS error of MOM.

TDL=0.001

Figure 3.165 shows the tracer concentration match of inverse and the forward model for TDL=0.001. Separation between the response curves and the trend lines is large since the shape of the curves change a lot after the TDL=0.001. Figure 3.166 shows the swept pore volume estimate. Table. 3.27 shows the swept pore volumes/reservoir volume ratios for all quadrants with and without extrapolation. Table shows that extrapolation increases the swept pore volume estimate from 0.18 to 0.20 in the first quadrant. Figure 3.167 shows the oil saturation estimate of MOM in each vertical layer. From the Figure, it can be concluded that the error in estimate increases with the increasing detection limit. But, extrapolation improves the result and increases the

average estimate in this quadrant from 0.23 to 0.26 as Table 3.28 shows. It is a pretty good estimate since average oil saturation in this quadrant is 0.28.

Figures 3.168 to 3.170 show the tracer concentration match, swept pore volume and the oil saturation estimates in quadrant two respectively. RMS error on vertical saturation is higher than the RMS error obtained in this quadrant at kv/kh ratio 0.01.

Figures 3.171 to 3.173 show the tracer concentration match, swept pore volume and MOM estimates for the third quadrant. Swept pore volume estimate is 24% of the reservoir. Average oil saturation estimate in this quadrant is 0.20 while the actual value is 0.23. It is a good estimate with 3% error.

Figures 3.174 to 3.176 show the tracer concentration match, swept pore volume and MOM saturation estimate for the third quadrant. Oil saturation estimates are pretty good for each layer except the ninth layer. Average oil saturation in this quadrant is same as the actual forward model value.

For TDL=0.001, average MOM estimates in each quadrant is within the range of 3% of the actual values except quadrant two. Average estimates in every quadrant are given to inverse model as initial oil saturation guess values.

In Figure 3.177, RMS variation over travel time and amplitude is given. Travel time error at this TDL higher compared to the error for TDL=0.0001 which is the lower detection limit. And the amplitude error is in the same range with the error at the detection limit 0.0001.

Figure 3.178 show the tracer concentration match between inverse and the forward models. As the figure shows, tracer concentration is extrapolated very well even after TDL=0.001. Figure 3.179 shows the inverse model oil saturation estimate. Inverse model saturation estimate catches the trend of the forward model but it is not better than MOM. Table 3.29 shows the estimate errors of MOM in each layer while Table 3.30

show the estimate errors of inverse model. Tables 3.29 and Table 3.30 show that RMS error on inverse model saturation estimates is higher than the RMS error on MOM saturation estimates.

Figure 3.180 shows the tracer concentration match between the inverse and the forward models in quadrant two. The graph is very similar to the concentration match graph obtained for TDL=0.0001 at quadrant two. Figure 3.181 shows the oil saturation estimate of inverse model. The estimate is very poor mostly because of the bad initial guess.

Figure 3.181 shows the tracer concentration match between inverse model and MOM in quadrant three. Again graph is same as the graph obtained in quadrant three for TDL=0.0001. In Figure 3.183, oil saturation estimate of MOM overlaps with the forward model at a few layers and catches the trend of forward model better than inverse model. But the RMS error on saturation estimate of inverse model is smaller than the RMS error on MOM because of the high estimate of MOM in the first two layers.

Figure 3.184 shows the perfect match of tracer concentration between the inverse model and MOM. Figure 3.185 shows the oil saturation estimate of inverse model. Inverse model has the least RMS error on saturation estimate in this quadrant but still higher than the RMS error on MOM estimate.

3.3 CONCLUSIONS

In chapter 3, inverse model is first applied to a layered permeability reservoir model and later to a model with a stochastically generated permeability field. Sensitivity of inverse model to number of iterations, partition coefficient, initial guess, detection limit and to the order of vertical permeability are studied. It is concluded that inverse model is sensitive to the number of iterations, initial guess, partition coefficient and

detection limit. Afterwards, MOM oil saturation estimates are compared with inverse model estimates in both cases studied. Next the MOM and inverse model methods are used in a complementary way by using the saturation from the MOM as the initial guess for the inverse calculation. Although inverse model gives close estimates to the forward model in the uniform layered case, results are not very successful in the reservoir model with the stochastically generated permeability field. There may be many reasons for it. One particular reason found is the non-uniqueness of the result obtained from the tracer concentration match between the inverse and the forward model. Although poor tracer concentration match between the inverse and the forward models increase the error in oil saturation estimate, a perfect tracer concentration match does not guarantee accurate oil saturation estimate. One solution may be matching the concentration response of the conservative tracer with inverse model next to partitioning tracer.

Table.3.1: Description of the layered permeability reservoir

Well Pattern	**Quarter of a five spot**
Reservoir dimensions	**660x660x50 ft**
Number of grid blocks	**22x22x10**
Grid dimensions	**30x30x5 ft**
Simulated area	**10 acres**
Porosity	**0.2**
Dykstra Parson's coefficient of the permeability field	**0.5**
Kv/Kh	**0.1**
Maximum permeability,	**650 md**
Minimum permeability	**90 md**
Injection rate	**6000 bbl/day**
Slug time	**0.1 PV**

Table 3.2: Comparison of inverse model oil saturation estimate errors with partitioning coefficients 1, 2, 3 4, and 5 at initial oil saturation estimate 0.26

Depth, ft	**Inverse model oil saturation estimate error Initial Oil Saturation Guess=0.26**				
	K: 1	**K: 2**	**K: 3**	**K: 4**	**K: 5**
5	0.012	0.014	0.013	0.001	0.000
10	0.001	0.001	0.001	-0.001	-0.004
15	-0.032	-0.008	-0.008	-0.018	-0.020
20	-0.058	-0.014	-0.018	-0.031	-0.036
25	-0.065	-0.016	-0.018	-0.035	-0.040
30	-0.013	-0.004	-0.005	-0.009	-0.008
35	0.044	0.017	0.012	0.017	0.026
40	0.059	0.000	-0.002	0.034	0.030
45	0.054	0.022	0.006	0.031	0.028
50	0.012	0.018	0.012	0.000	-0.001
Root Mean Square Error, %	4.17%	1.36%	1.13%	2.23%	2.38%

Table 3.3: Comparison of inverse model oil saturation estimate errors at partitioning coefficients 6, 7, 8, 9 and 10 with initial oil saturation estimate 0.26

Depth, ft	Inverse model oil saturation estimate error Initial Oil Saturation Guess=0.26				
	K: 6	K: 7	K: 8	K: 9	K: 10
5	0.006	0.001	0.000	0.000	0.001
10	0.004	0.001	0.000	-0.003	-0.002
15	-0.011	-0.012	-0.012	-0.008	-0.008
20	-0.022	-0.022	-0.022	-0.022	-0.022
25	-0.024	-0.024	-0.024	-0.024	-0.024
30	0.000	0.000	-0.002	-0.003	-0.005
35	0.016	0.015	0.014	0.016	0.015
40	0.018	0.017	0.020	0.019	0.019
45	0.017	0.016	0.019	0.018	0.018
50	0.005	0.001	-0.001	0.000	0.001
Root Mean Square Error, %	1.45%	1.41%	1.47%	1.45%	1.45%

Table 3.4: Comparison of inverse model oil saturation estimate errors at initial oil saturation guesses 0.21, 0.22, 0.23, 0.24 and 0.25 with partitioning coefficient 2

Depth, ft	Inverse model oil saturation estimate error				
	Initial oil saturation guess: 0.21	Initial oil saturation guess: 0.22	Initial oil saturation guess: 0.23	Initial oil saturation guess: 0.24	Initial oil saturation guess: 0.25
5	-0.009	-0.014	0.001	0.015	0.019
10	-0.013	-0.006	-0.009	-0.003	-0.001
15	-0.029	-0.013	-0.014	-0.006	-0.008
20	-0.039	-0.030	-0.021	-0.015	-0.017
25	-0.040	-0.035	-0.021	-0.019	-0.016
30	-0.015	-0.008	-0.008	0.003	-0.004
35	-0.006	0.028	0.023	0.037	0.013
40	0.009	0.007	0.016	0.015	0.015
45	0.004	0.004	0.013	0.013	0.014
50	-0.008	-0.013	0.006	0.020	0.028
Root Mean Square Error, %	2.14%	1.89%	1.50%	1.75%	1.54%

Table 3.5: Comparison of inverse model oil saturation estimate errors at initial oil saturation guesses 0.26, 0.27, 0.28, 0.29 and 0.30 with partitioning coefficient 2

Depth, ft	Inverse model oil saturation estimate error				
	Initial oil saturation guess: 0.26	Initial oil saturation guess: 0.27	Initial oil saturation guess: 0.28	Initial oil saturation guess: 0.29	Initial oil saturation guess: 0.30
5	0.014	0.019	0.029	0.024	0.0302
10	0.000	0.007	0.009	0.015	0.0209
15	-0.009	0.000	0.000	-0.002	0.0036
20	-0.015	-0.008	-0.005	-0.014	-0.0103
25	-0.016	-0.011	-0.008	-0.018	-0.0137
30	-0.004	0.003	0.000	0.007	0.0141
35	0.017	0.045	-0.019	0.030	0.0399
40	0.000	0.002	-0.019	0.017	0.0060
45	0.021	0.022	0.011	0.041	0.0408
50	0.017	0.023	0.033	0.023	0.0287
Root Mean Square Error, %	1.34%	1.90%	1.72%	2.20%	2.44%

Table 3.6: Comparison of inverse model oil saturation estimate errors at initial oil saturation guesses 0.14, 0.26, and 0.38 with partitioning coefficient 2

Depth, ft	Inverse model oil saturation estimate error		
	Initial oil saturation guess: 0.14	Initial oil saturation guess: 0.26	Initial oil saturation guess: 0.38
5	-0.035	0.014	0.013
10	-0.037	0.000	0.045
15	-0.049	-0.009	0.043
20	-0.060	-0.015	0.028
25	-0.065	-0.016	0.030
30	-0.049	-0.004	0.046
35	-0.050	0.017	0.061
40	-0.024	0.000	0.016
45	-0.022	0.021	0.058
50	-0.035	0.017	0.058
Root Mean Square Error, %	4.48%	1.34%	4.30%

Table 3.7: Comparison of inverse model oil saturation estimate errors at tracer concentration detection limits (TDL) 0.0001, 0.001 and 0.01 with partitioning coefficient 2 at initial oil saturation guess 0.26

Depth, ft	Inverse model oil saturation estimate error		
	TDL 0.0001	TDL 0.001	TDL 0.01
5	0.014	0.014	0.011
10	0.000	0.001	-0.002
15	-0.009	-0.008	-0.009
20	-0.015	-0.014	-0.018
25	-0.016	-0.016	-0.027
30	-0.004	-0.004	0.004
35	0.017	0.017	0.076
40	0.000	0.000	0.015
45	0.021	0.022	0.013
50	0.017	0.018	0.017
Root Mean Square Error, %	1.34%	1.35%	2.78%

Table 3.8: Comparison of inverse model oil saturation estimate errors at tracer concentration detection limits (TDL) 0.0001, 0.001 and 0.01 with partitioning coefficient 2 at initial oil saturation guess 0.26

Depth, ft	Inverse model oil saturation estimate error		
	TDL 0.0001	TDL 0.001	TDL 0.01
5	0.030	0.030	0.025
10	0.021	0.021	0.016
15	0.004	0.004	0.001
20	-0.010	-0.010	-0.016
25	-0.014	-0.014	-0.021
30	0.014	0.014	0.011
35	0.040	0.040	0.040
40	0.006	0.006	0.006
45	0.041	0.041	0.041
50	0.029	0.029	0.023
Root Mean Square Error, %	2.44%	2.44%	2.35%

Table 3.9: Inverse model oil saturation estimate error in the reservoir model with the rearranged permeability distribution

Depth, ft	Inverse model oil saturation estimate error
5	0.000
10	0.022
15	0.018
20	0.018
25	0.018
30	0.001
35	-0.004
40	-0.008
45	-0.015
50	-0.017
Root Mean Square Error, %	1.43%

Table 3.10. MOM swept pore volume estimate with and without extrapolation for the reservoir model with the uniform layered permeability .

TDL	MOM swept pore volume estimate	
	swept pore volume/reservoir volume	
	Without extrapolation	With extrapolation
0.0001	0.97	0.98
0.001	0.93	0.95
0.01	0.75	0.80

Table 3.11: MOM oil saturation estimate errors at tracer concentration detection limits (TDL) 0.0001, 0.001 and 0.01.

Depth, ft	MOM So estimate error		
	TDL 0.0001	**TDL 0.001**	**TDL 0.01**
5	-0.011	-0.011	-0.014
10	-0.010	-0.010	-0.014
15	-0.007	-0.008	-0.014
20	-0.006	-0.006	-0.016
25	-0.005	-0.006	-0.015
30	-0.009	-0.009	-0.013
35	-0.014	-0.014	-0.017
40	-0.015	-0.015	-0.016
45	-0.015	-0.014	-0.017
50	-0.011	-0.012	-0.014
Root Mean Square Error, %	1.09%	1.09%	1.50%

Table 3.12: Comparison of inverse model oil saturation estimate errors with MOM.

Depth, ft	Oil Saturation Estimate Error		
	Inverse Model Initial So guess: 0.26	**Inverse Model** Initial So guess: average MOM estimate	**MOM Estimate**
5	0.014	0.015	-0.011
10	0.000	-0.003	-0.010
15	-0.009	-0.007	-0.007
20	-0.015	-0.016	-0.006
25	-0.016	-0.020	-0.005
30	-0.004	0.003	-0.009
35	0.017	0.037	-0.014
40	0.000	0.014	-0.015
45	0.021	0.013	-0.015
50	0.017	0.020	-0.011
Root Mean Square Error, %	1.34%	1.75%	1.09%

Table 3.13. Description of the reservoir model with the stochastic permeability field

Well Pattern	**Inverted five spot**
Reservoir dimensions	**930x930x50 ft**
Number of grid blocks	**31x31x10**
Grid dimensions	**30x30x5 ft**
Simulated area	**20 acres**
Porosity	**0.2**
Injection rate	**6000 bbl/day**
Slug time	**0.1 PV**

Table 3.14. Description of the stochastically generated permeability field

Random seed number	**800**
Correlation length in the x and y directions	**300 ft**
Correlation length in the z direction	**10 ft**
Dykstra Parson's coefficient of the permeability field	**0.80**
Log mean permeability	**227 md**
Standard deviation of log permeability	**1.61**
Maximum permeability in the simulation domain	**68,000 md**
Minimum permeability in the simulation domain	**0.48 md**

Table 3.15. Swept pore volume estimate with and without extrapolation for the reservoir model with the stochastic permeability field for TDL= 0.0001 at kv/kh=0.1.

Quadrant	**MOM swept pore volume estimate**	
	swept pore volume/reservoir volume	
	Without extrapolation	**With extrapolation**
I	0.20	0.21
II	0.20	0.21
III	0.24	0.24
IV	0.23	0.24
Sum	0.87	0.90

Table 3.16. MOM So estimate with and without extrapolation for the reservoir model with the stochastic permeability field for TDL= 0.0001 at kv/kh=0.1.

Quadrant	Forward Model	MOM Average So Estimate	
		Without extrapolation	With extrapolation
I	0.28	0.25	0.27
II	0.24	0.19	0.20
III	0.23	0.21	0.21
IV	0.34	0.33	0.34
Average	0.27	0.25	0.26

Table 3.17. MOM oil saturation estimate errors in each layer in each quadrant for TDL=0.0001 at kv/kh=0.1.

Depth, ft	MOM So estimate error			
	Quadrant I	Quadrant II	Quadrant III	Quadrant IV
5	-0.074	0.014	0.029	0.007
10	-0.070	-0.068	-0.032	0.006
15	-0.122	-0.138	-0.034	-0.031
20	-0.085	-0.136	-0.061	-0.063
25	0.029	-0.047	-0.072	-0.001
30	0.046	0.041	-0.007	0.001
35	0.025	0.004	0.023	0.033
40	-0.018	0.016	0.018	-0.012
45	0.002	0.003	-0.021	-0.031
50	-0.001	-0.002	-0.005	-0.006
Root Mean Square Error, %	6.03%	6.81%	3.64%	2.70%

Table 3.18. Inverse model oil saturation estimate errors in each layer in each quadrant for TDL=0.0001 at kv/kh=0.1.

Depth, ft	Inverse Model So estimate Error			
	Initial So guess: Average MOM So estimate in every quadrant			
	Quadrant I	Quadrant II	Quadrant III	Quadrant IV
5	-0.148	-0.062	-0.055	-0.049
10	-0.136	-0.155	-0.084	-0.036
15	-0.124	-0.216	-0.057	-0.064
20	-0.057	-0.130	-0.058	-0.068
25	0.018	0.002	-0.051	-0.021
30	0.052	0.038	0.001	0.025
35	0.022	0.014	0.020	0.039
40	-0.014	0.033	0.008	0.018
45	0.003	0.015	-0.020	0.014
50	0.004	0.023	-0.003	0.045
Root Mean Square Error, %	7.92%	9.74%	4.50%	4.20%

Table 3.19. Swept pore volume estimate with and without extrapolation for the reservoir model with the stochastic permeability field for TDL= 0.0001 at kv/kh=0.01.

Quadrant	MOM swept pore volume estimate	
	swept pore volume/reservoir volume	
	Without extrapolation	With extrapolation
I	0.20	0.21
II	0.21	0.22
III	0.24	0.25
IV	0.24	0.24
Sum	0.89	0.92

Table 3.20. MOM So estimate with and without extrapolation for the reservoir model with the stochastic permeability field for TDL= 0.0001 at kv/kh=0.01.

Quadrant	Forward Model	MOM Average So Estimate	
		Without extrapolation	With extrapolation
I	0.28	0.25	0.27
II	0.24	0.19	0.20
III	0.23	0.21	0.22
IV	0.34	0.33	0.34
Average	0.27	0.25	0.26

Table 3.21. MOM oil saturation estimate errors in each layer in each quadrant for TDL=0.0001 at kv/kh=0.01.

Depth, ft	MOM So estimate error			
	Quadrant I	Quadrant II	Quadrant III	Quadrant IV
5	0.004	-0.006	-0.033	-0.006
10	-0.062	-0.069	-0.027	0.014
15	-0.062	-0.081	-0.014	-0.014
20	-0.069	-0.033	-0.045	-0.054
25	0.017	-0.021	-0.070	-0.003
30	0.033	0.040	-0.016	0.013
35	0.017	-0.002	0.012	0.037
40	-0.020	0.007	0.005	-0.022
45	0.006	-0.005	-0.030	-0.040
50	0.001	-0.010	-0.007	-0.005
Root Mean Square Error, %	3.83%	3.84%	3.22%	2.66%

Table 3.22. Inverse model oil saturation estimate errors in each layer in each quadrant for TDL=0.0001 at kv/kh=0.01.

Depth, ft	Inverse model So estimate error			
	Initial So guess: average MOM So estimate in every quadrant			
	Quadrant I	Quadrant II	Quadrant III	Quadrant IV
5	-0.13	-0.06	-0.05	-0.02
10	-0.12	-0.16	-0.08	-0.04
15	-0.09	-0.22	-0.05	-0.06
20	-0.03	-0.15	-0.05	-0.08
25	0.02	-0.06	-0.04	-0.02
30	0.04	0.01	0.01	0.01
35	0.00	0.01	0.02	0.05
40	-0.02	0.02	0.01	0.02
45	0.00	-0.02	-0.01	-0.03
50	0.00	0.00	0.00	0.03
Root Mean Square Error, %	6.70%	10.27%	4.17%	4.05%

Table 3.23. Swept pore volume estimate with and without extrapolation for the reservoir model with the stochastic permeability field for TDL= 0.0001 at kv/kh=0.001.

Quadrant	MOM swept pore volume estimate	
	swept pore volume/reservoir volume	
	Without extrapolation	With extrapolation
I	0.24	0.25
II	0.20	0.21
III	0.25	0.25
IV	0.24	0.24
Sum	0.93	0.95

Table 3.24. MOM So estimate with and without extrapolation for the reservoir model with the stochastic permeability field for TDL= 0.0001 at kv/kh=0.001.

Quadrant	Forward Model	MOM Average So Estimate	
		Without extrapolation	With extrapolation
I	0.28	0.25	0.26
II	0.24	0.19	0.20
III	0.23	0.21	0.23
IV	0.34	0.33	0.34
Average	0.27	0.25	0.26

Table 3.25. Inverse model oil saturation estimate errors in each layer in each quadrant for TDL=0.0001 at kv/kh=0.001.

Depth, ft	MOM So estimate error			
	Quadrant I	Quadrant II	Quadrant III	Quadrant IV
5	0.014	0.013	-0.015	0.003
10	-0.035	-0.072	-0.021	0.011
15	-0.030	0.080	0.001	0.008
20	-0.011	0.035	-0.017	-0.022
25	0.003	0.004	-0.035	-0.002
30	0.018	0.011	-0.016	0.011
35	0.001	-0.006	0.000	0.033
40	-0.009	-0.001	-0.007	-0.010
45	0.011	-0.006	-0.027	-0.036
50	0.007	-0.005	-0.010	-0.007
Root Mean Square Error, %	1.76%	3.63%	1.82%	1.81%

Table 3.26. Inverse model oil saturation estimate errors in each layer in each quadrant for TDL=0.0001 at kv/kh=0.001

Depth, ft	Inverse model So estimate error			
	Initial So guess: average MOM So estimate in every quadrant			
	Quadrant I	Quadrant II	Quadrant III	Quadrant IV
5	-0.073	-0.070	-0.064	-0.015
10	-0.118	-0.160	-0.077	-0.034
15	-0.071	-0.222	-0.042	-0.057
20	-0.055	-0.145	-0.043	-0.131
25	0.036	-0.030	-0.026	-0.028
30	0.031	0.065	-0.057	0.007
35	0.027	-0.013	0.026	0.023
40	-0.030	0.042	0.009	-0.051
45	-0.009	0.006	-0.011	-0.033
50	-0.014	0.007	-0.026	0.001
Root Mean Square Error, %	5.62%	10.39%	4.37%	5.19%

Table 3.27. Swept pore volume estimate with and without extrapolation for the reservoir model with the stochastic permeability field for TDL= 0.001 at kv/kh=0.001.

Quadrant	MOM swept pore volume estimate	
	swept pore volume/reservoir volume	
	Without extrapolation	With extrapolation
I	0.18	0.20
II	0.18	0.20
III	0.23	0.24
IV	0.22	0.24
Sum	0.81	0.88

Table 3.28. MOM So estimate with and without extrapolation for the reservoir model with the stochastic permeability field for TDL= 0.001 at kv/kh=0.001.

Quadrant	Forward Model	MOM Average So Estimate	
		Without extrapolation	With extrapolation
I	0.28	0.23	0.26
II	0.24	0.15	0.15
III	0.23	0.19	0.20
IV	0.34	0.30	0.34
Average	0.27	0.22	0.24

Table 3.29. Inverse model oil saturation estimate errors in each layer in each quadrant for TDL= 0.001 at kv/kh=0.001.

Depth, ft	MOM So estimate error			
	Quadrant I	Quadrant II	Quadrant III	Quadrant IV
5	-0.10	0.030	-0.083	0.012
10	-0.08	-0.060	-0.136	0.014
15	-0.05	-0.215	0.008	0.004
20	-0.03	-0.049	-0.012	-0.037
25	0.00	-0.035	-0.017	-0.013
30	0.01	0.001	0.010	0.006
35	0.00	-0.009	0.006	0.022
40	-0.02	-0.006	-0.003	-0.039
45	0.00	-0.008	-0.044	-0.057
50	0.01	-0.014	-0.017	-0.021
Root Mean Square Error, %	4.65%	7.39%	5.31%	2.76%

Table 3.30. Inverse model oil saturation estimate errors in each layer in each quadrant for TDL=0.001 at kv/kh=0.001

Depth, ft	Inverse model So estimate error			
	Initial So guess: average MOM So estimate in every quadrant			
	Quadrant I	Quadrant II	Quadrant III	Quadrant IV
5	-0.067	-0.088	-0.049	-0.012
10	-0.109	-0.191	-0.106	-0.036
15	-0.058	-0.270	-0.042	-0.059
20	-0.071	-0.194	-0.057	-0.055
25	0.008	-0.081	-0.061	0.051
30	0.004	0.005	-0.032	0.037
35	-0.013	-0.026	0.015	0.030
40	0.034	0.001	0.002	-0.055
45	0.010	-0.023	-0.026	0.065
50	-0.008	-0.028	-0.012	0.007
Root Mean Square Error, %	5.11%	12.77%	4.94%	4.48%

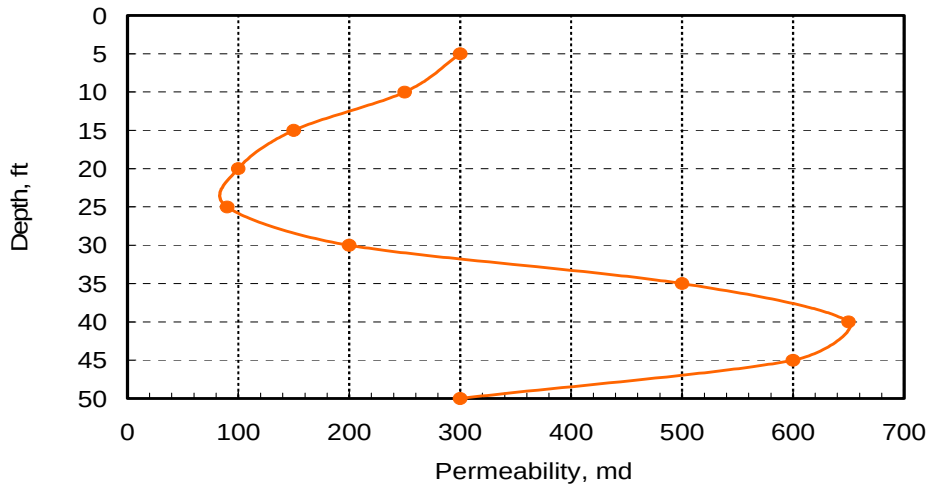

Figure 3.1 Vertical permeability distribution of the three-dimensional layered reservoir

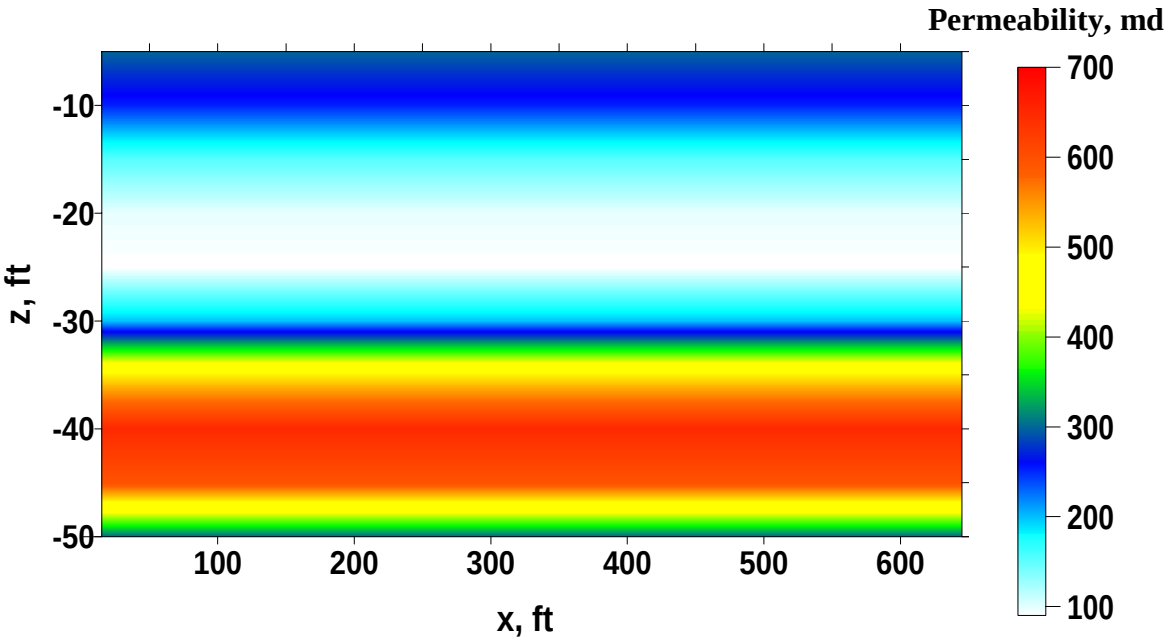

Figure 3.2 Permeability distribution of the uniform layered permeability reservoir

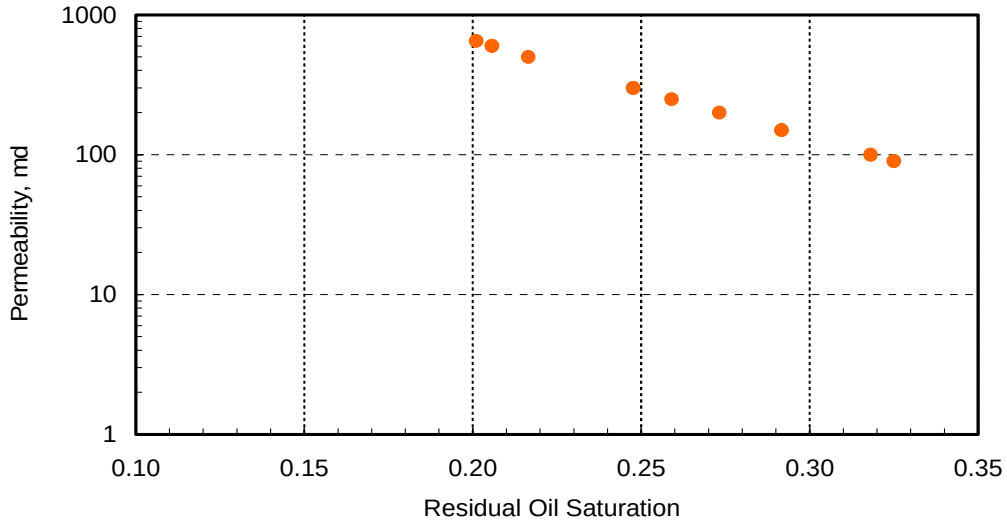

Figure 3.3 Correlation between the permeability and the oil saturation for the layered reservoir

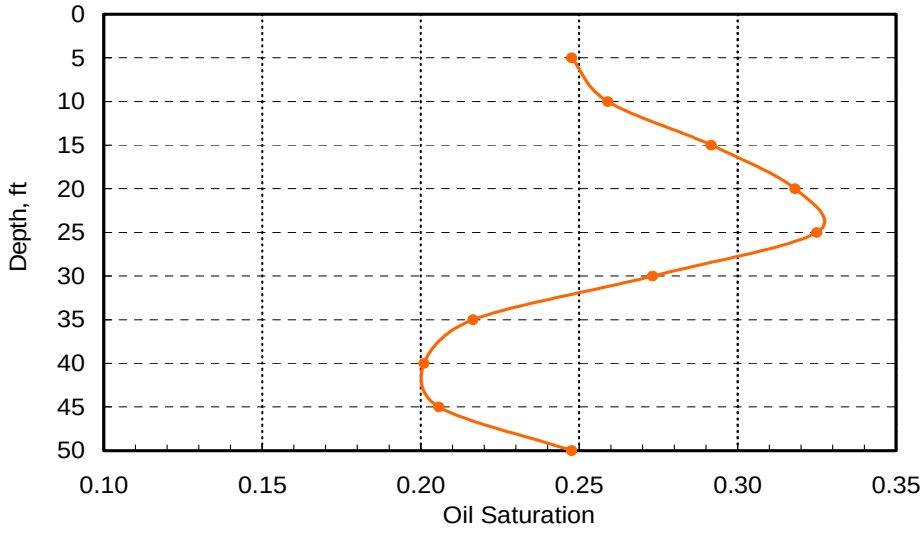

Figure 3.4 Vertical oil saturation distribution of the three-dimensional layered reservoir

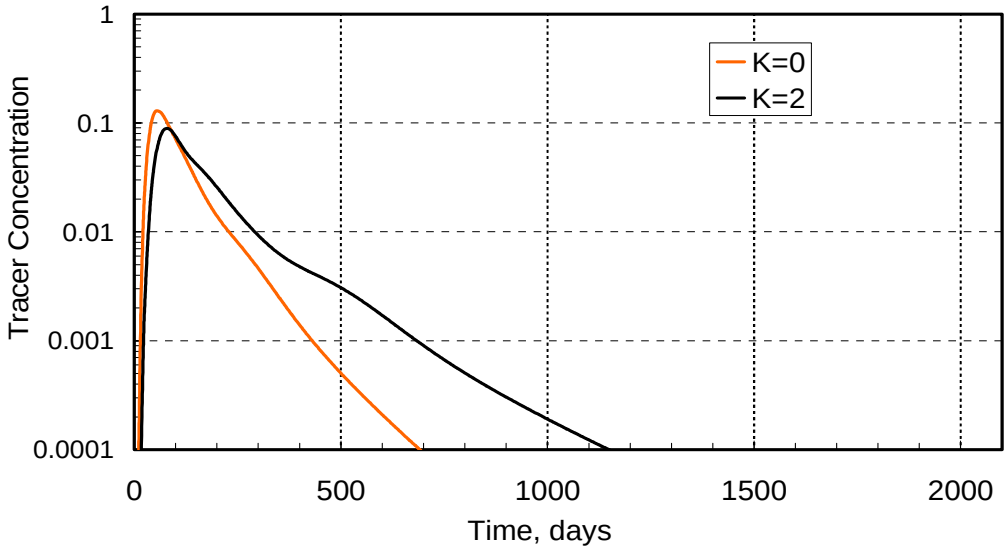

Figure 3.5. Forward model normalized tracer concentration response from the production well

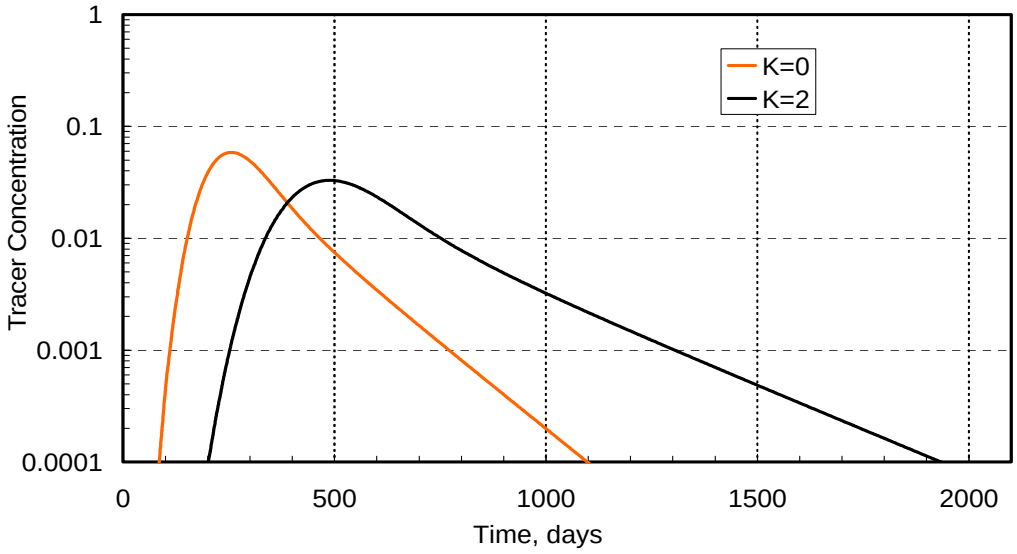

Figure 3.6 Forward model normalized tracer concentration response from the least permeable layer 5

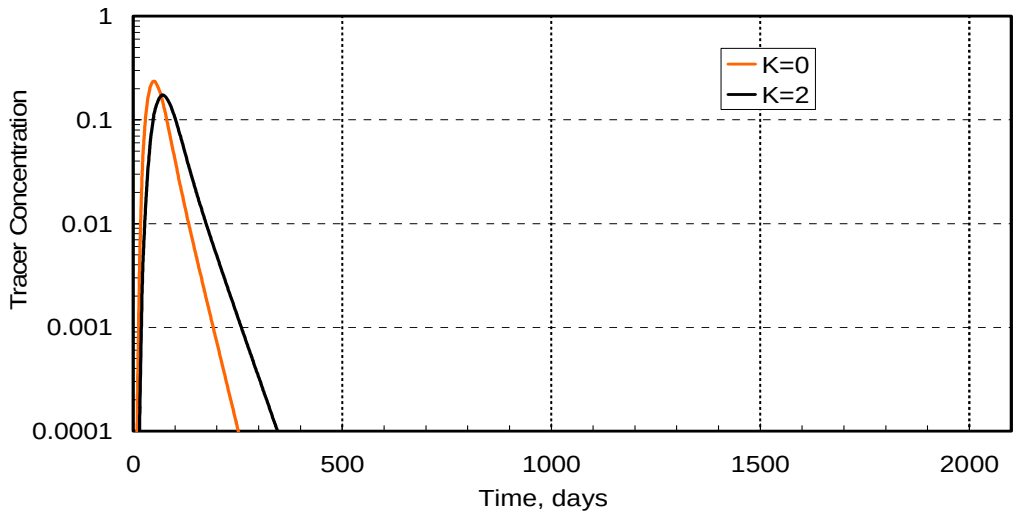

Figure 3.7 Forward model normalized tracer concentration response from the most permeable layer 8

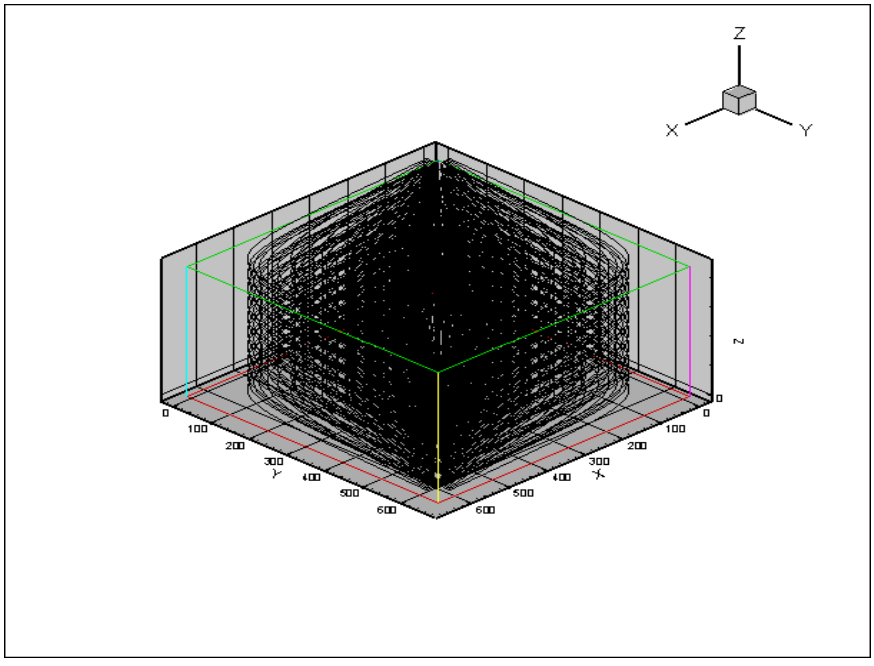

Figure 3.8 Streamline distribution after inverse modeling

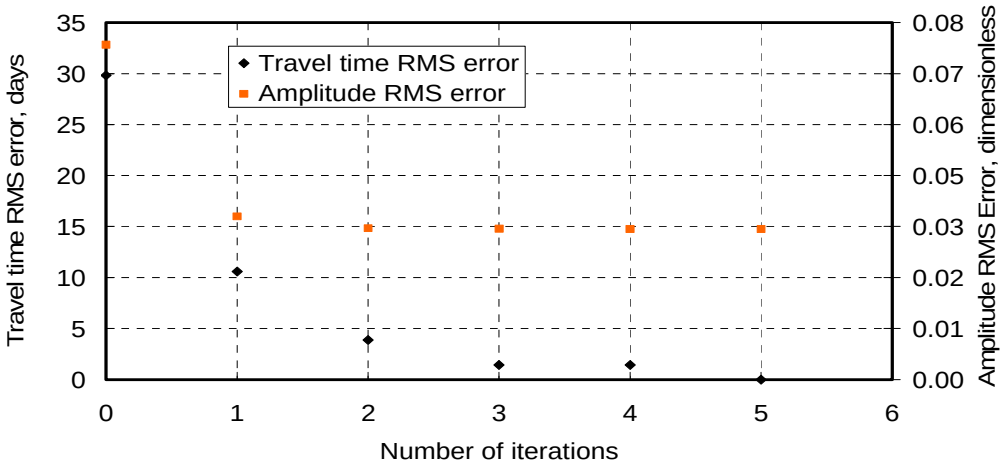

Figure 3.9 Root Mean Square error (RMS) change on travel time and amplitude during inversion

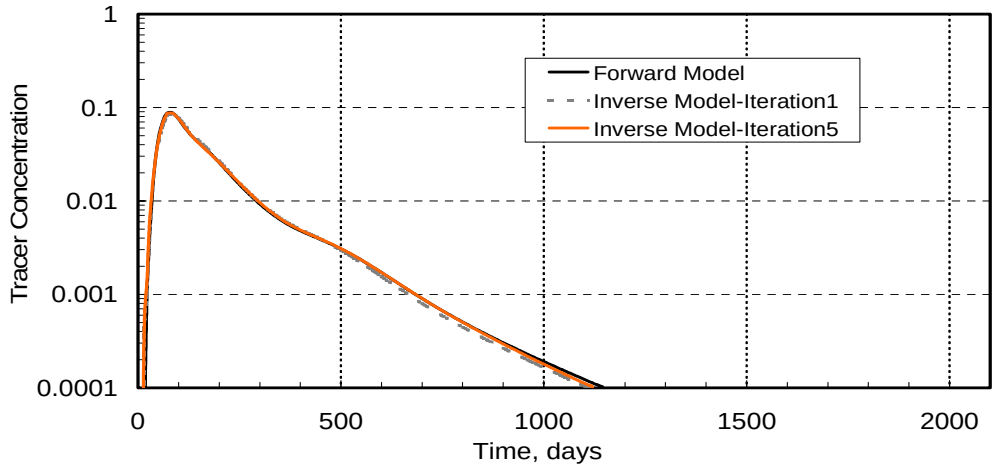

Figure 3.10 Match of the forward model tracer response from all layers by iterations 1 and 5 of the inverse model

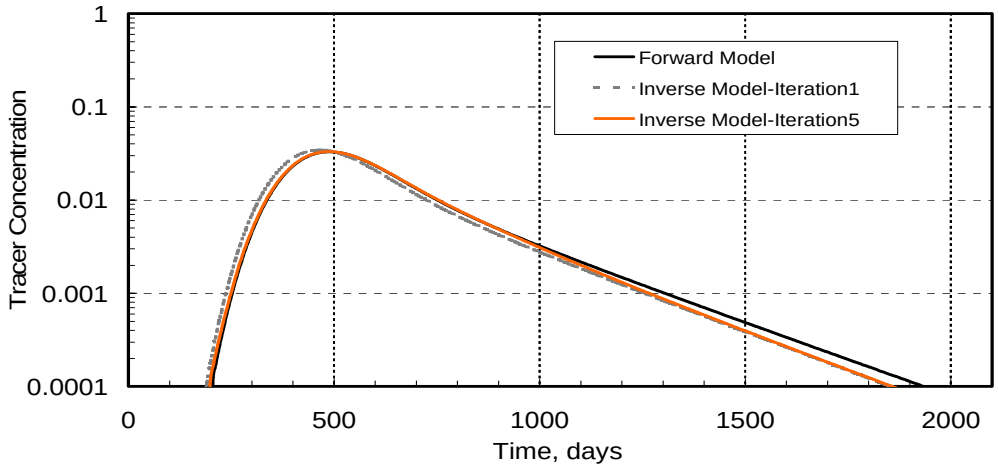

Figure 3.11 Match of the forward model tracer response from layer 5 by iterations 1 and 5 of the inverse model

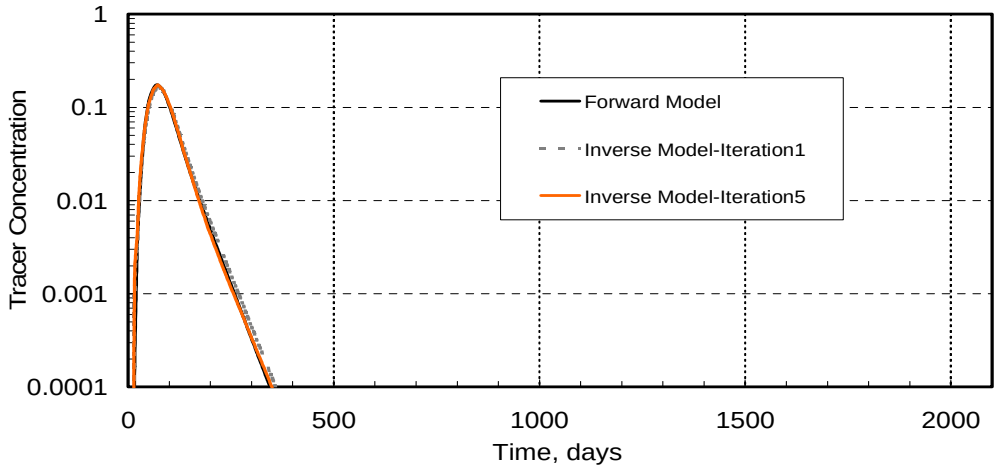

Figure 3.12 Match of the forward model tracer response from layer 8 by iterations 1 and 5 of the inverse model

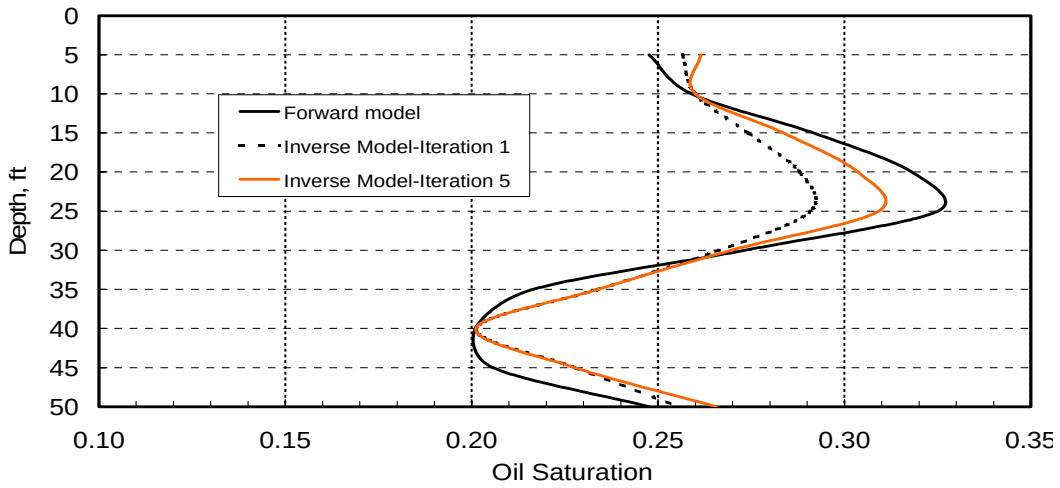

Figure 3.13 Vertical oil saturation distribution for the first and the fifth iteration of the inverse model compared to the forward model

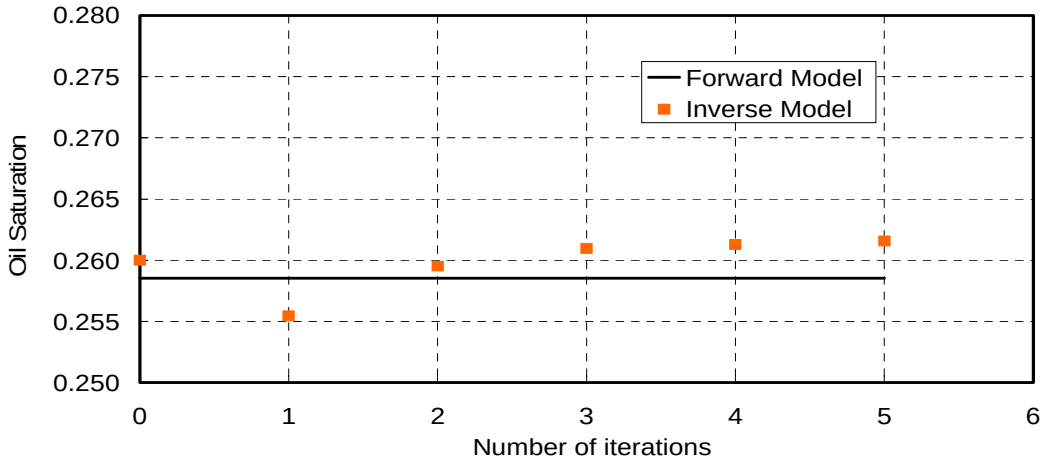

Figure 3.14. Inverse model oil saturation estimate change with the number of iterations.

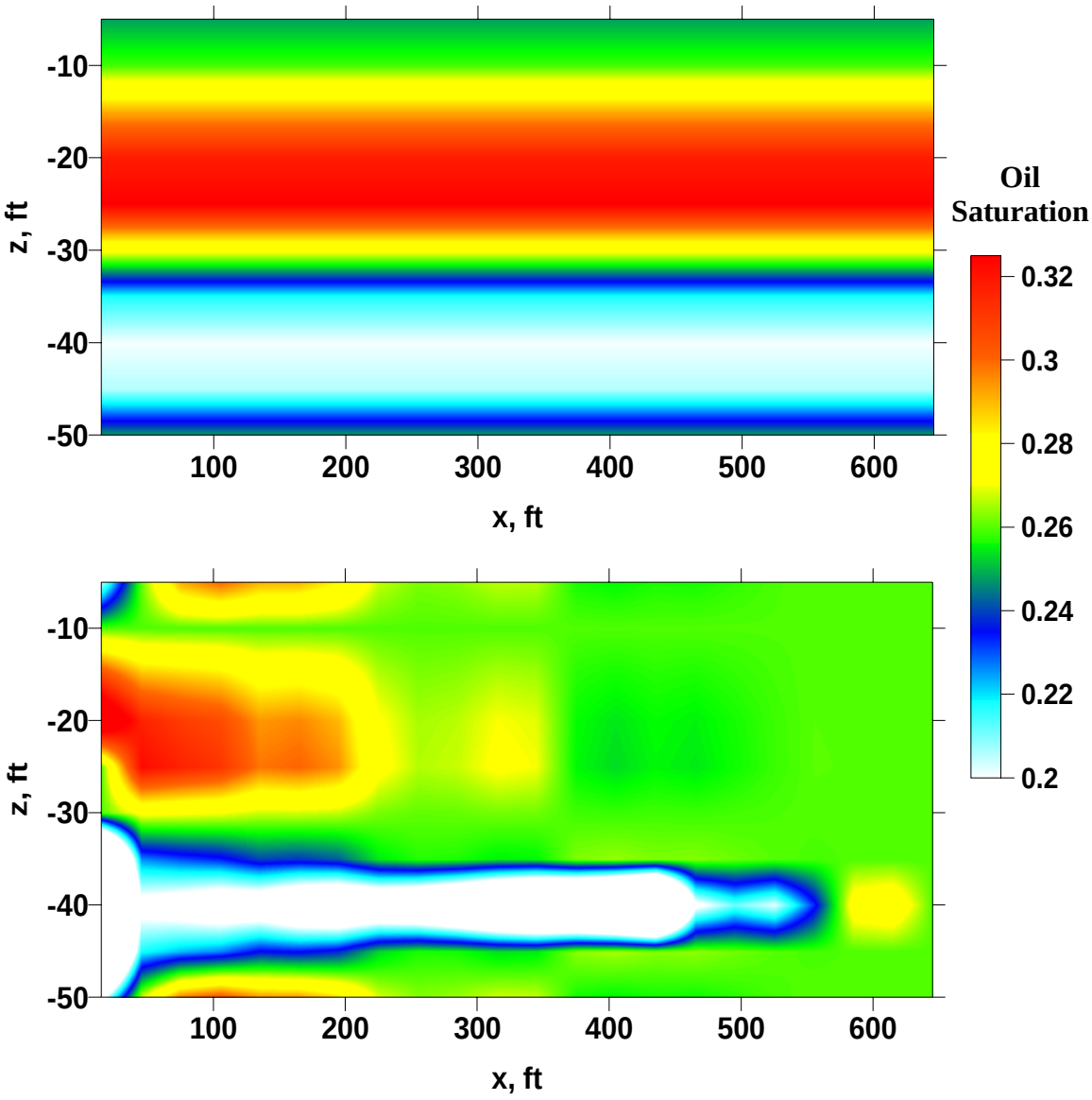

Figure 3.15 Comparison of forward model oil saturation distribution (top image) with inverse model oil saturation distribution (bottom image) at the fifth iteration

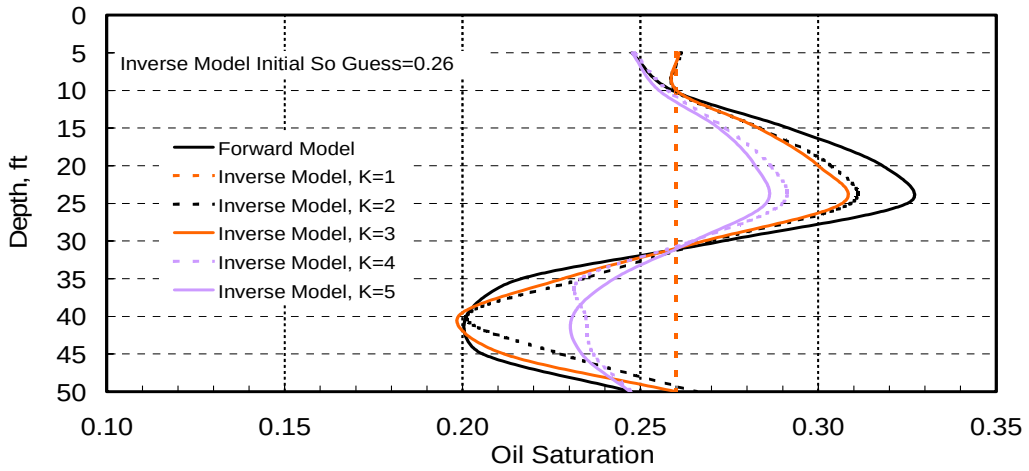

Figure 3.16 Inverse model vertical oil saturation distribution with partition coefficients K= 1, 2, 3, 4, and 5.

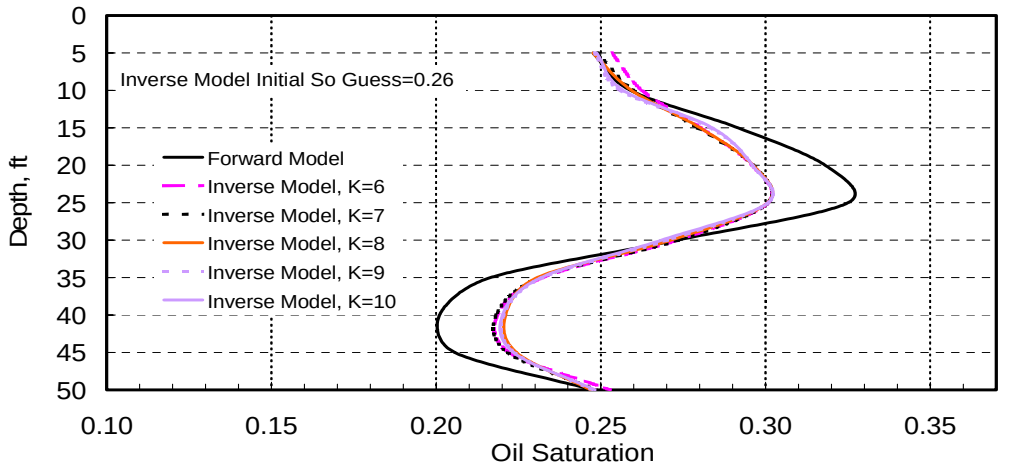

Figure 3.17. Inverse model vertical oil saturation distribution with partition coefficients K=6, 7, 8, 9 and 10.

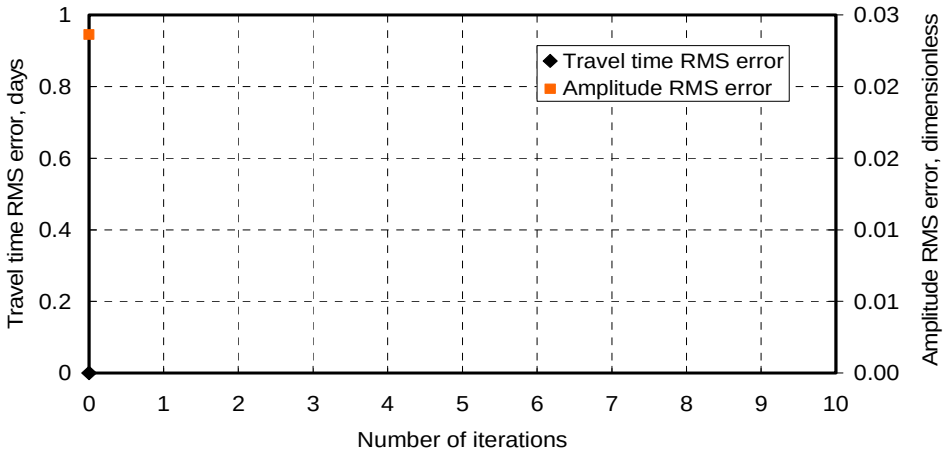

Figure 3.18. RMS error change on travel time and amplitude at partition coefficient K=1.

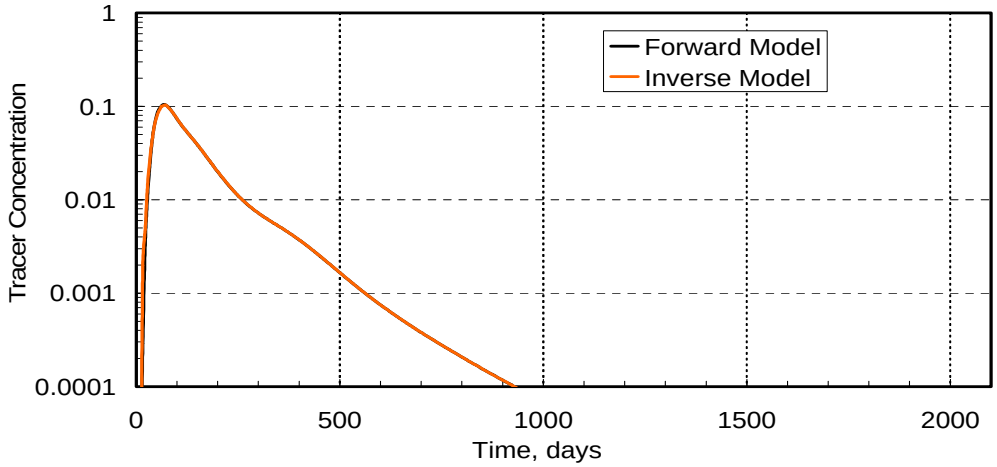

Figure 3.19. Match of the forward model tracer response from all layers with inverse model at tracer partition coefficient K=1

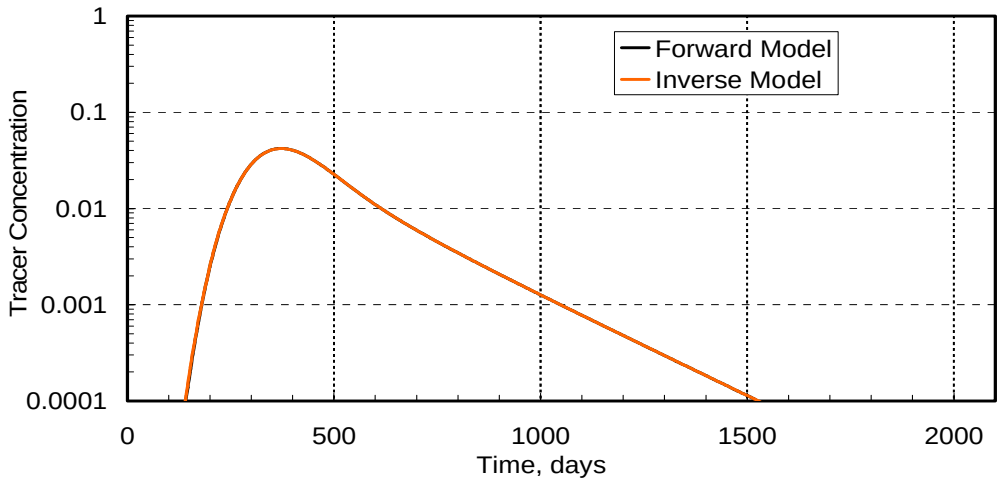

Figure 3.20. Match of the forward model tracer response from layer 5 with inverse model at tracer partition coefficient K=1.

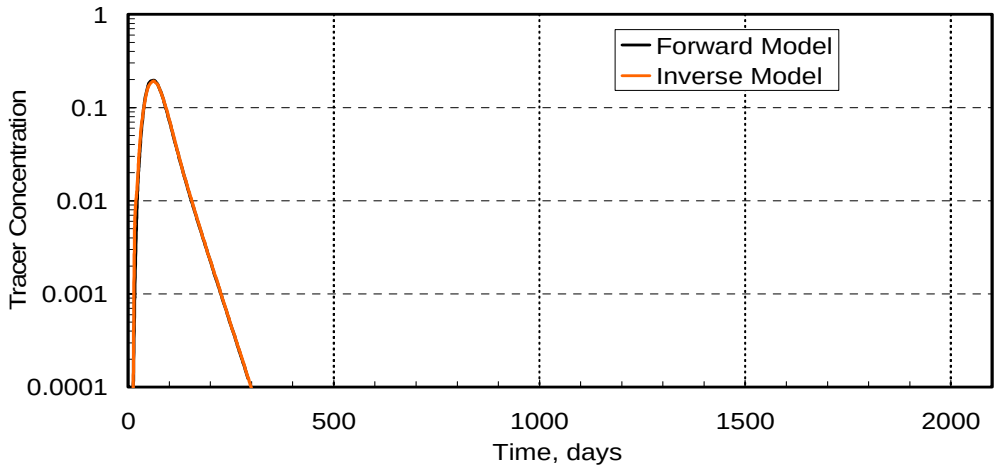

Figure 3.21. Match of the forward model tracer response from layer 8 with inverse model at tracer partition coefficient K=1.

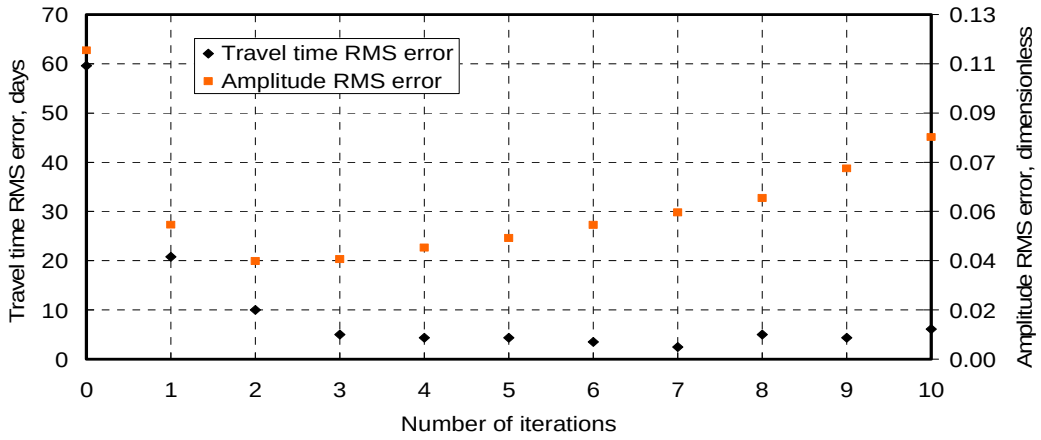

Figure 3.22. RMS error change on travel time and amplitude at partition coefficient 3.

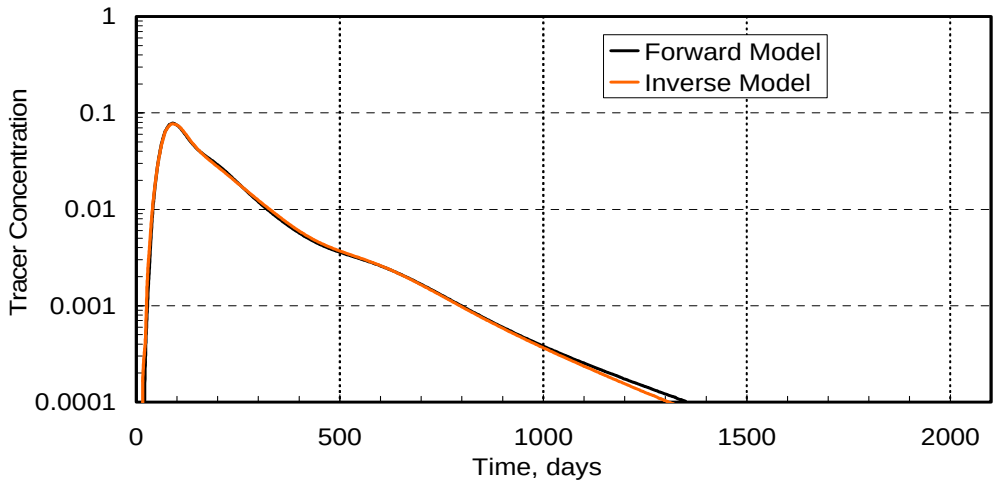

Figure 3.23. Match of the forward model tracer response from the all layers by iteration 3 of the inverse model at tracer partition coefficient K=3

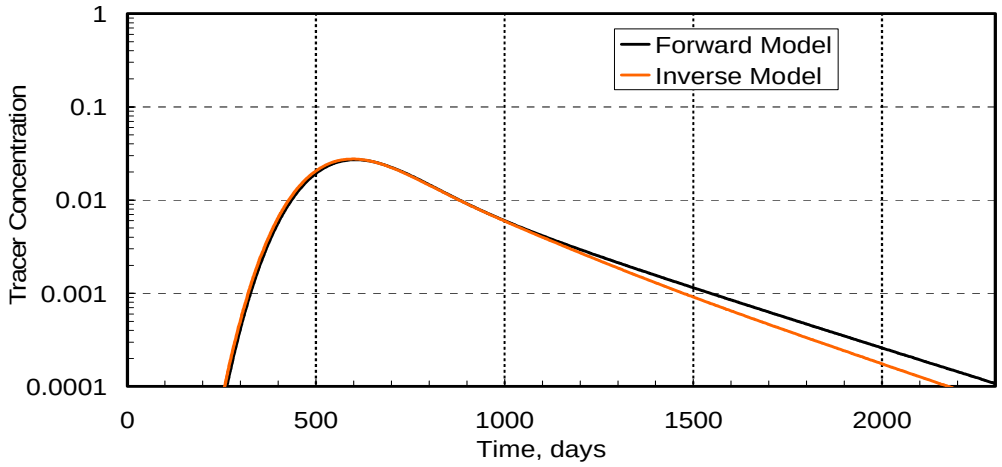

Figure 3.24. Match of the forward model tracer response from layer 5 by iteration 3 of the inverse model at tracer partition coefficient K=3

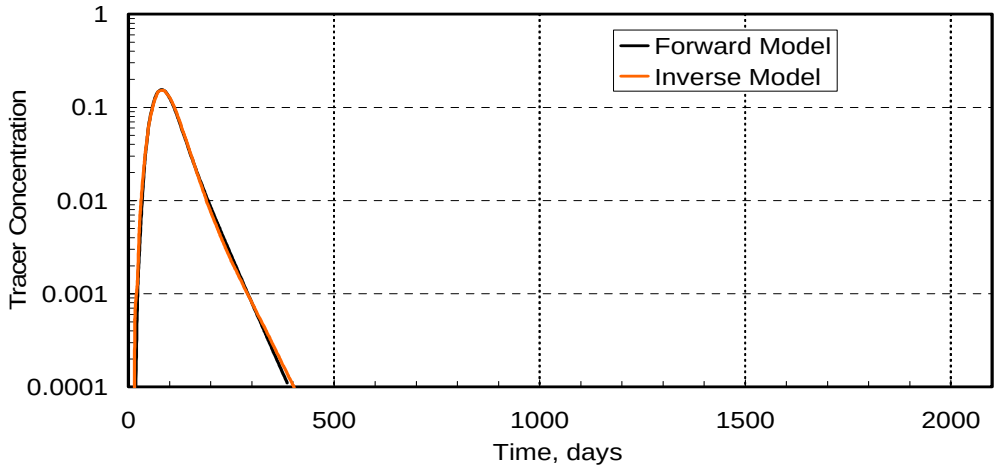

Figure 3.25. Match of the forward model tracer response from layer 8 by iteration 3 of the inverse model at tracer partition coefficient K=3

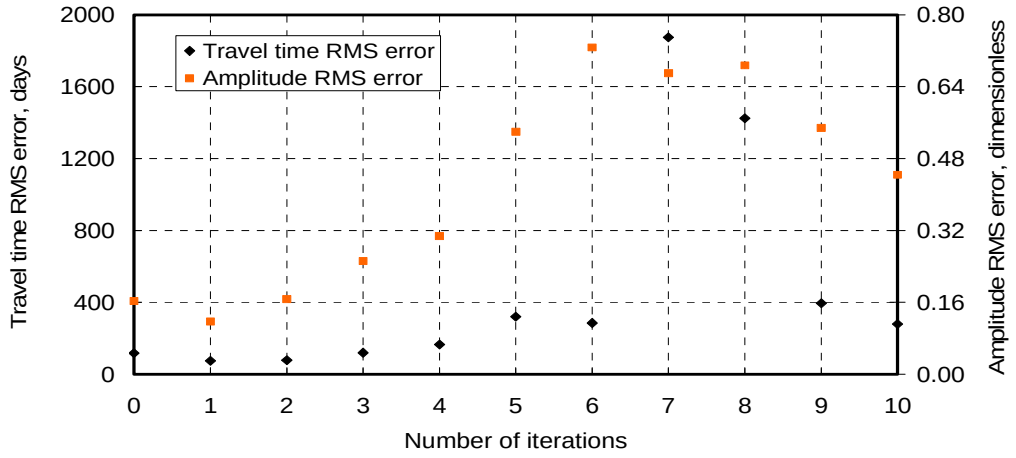

Figure 3.26. RMS error change on travel time and amplitude at partition coefficient 5.

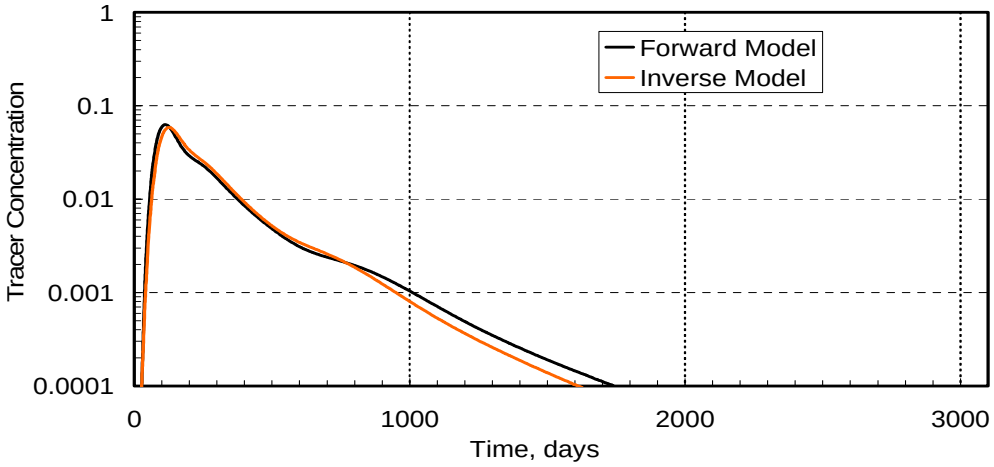

Figure 3.27. Match of the forward model tracer response from all layers by iteration 1 of the inverse model at tracer partition coefficient K=5

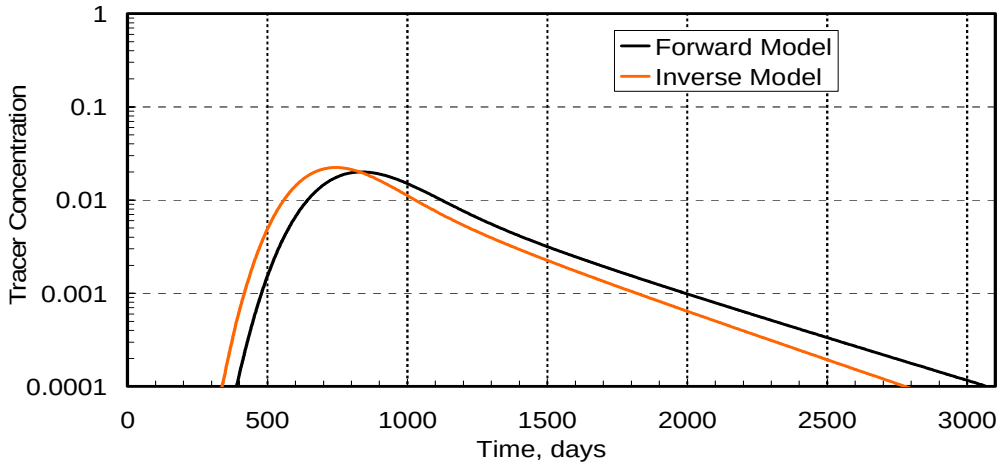

Figure 3.28. Match of the forward model tracer response from layer 5 by iteration 1 of the inverse model at tracer partition coefficient K=5

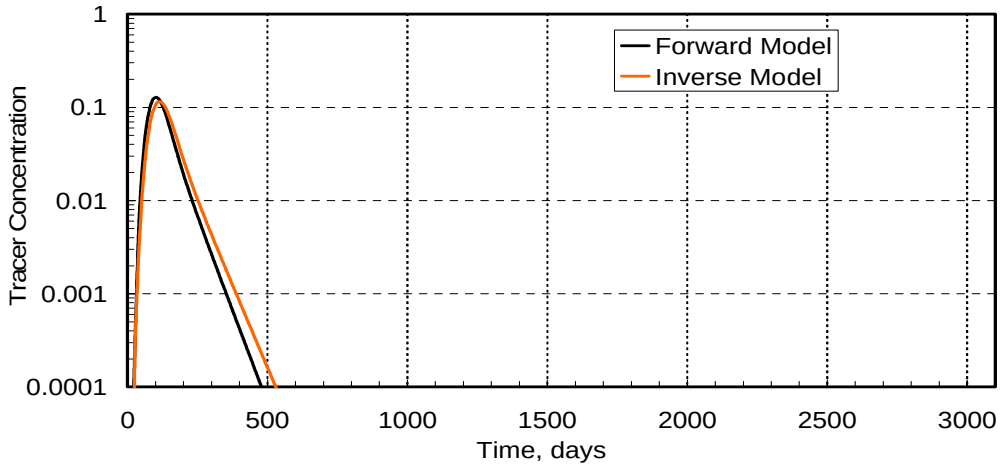

Figure 3.29. Match of the forward model tracer response from layer 8 by iteration 1 of the inverse model at tracer partition coefficient K=5

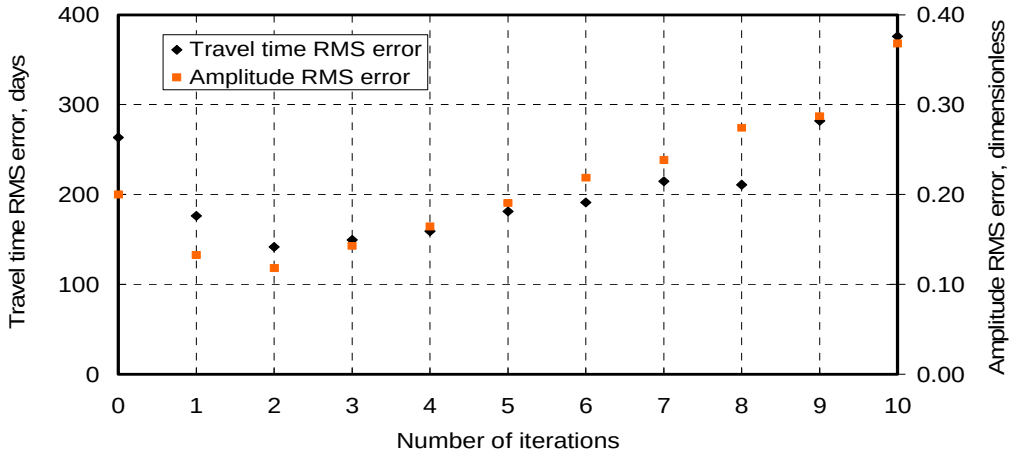

Figure 3.30. RMS error change on travel time and amplitude at partition coefficient 10

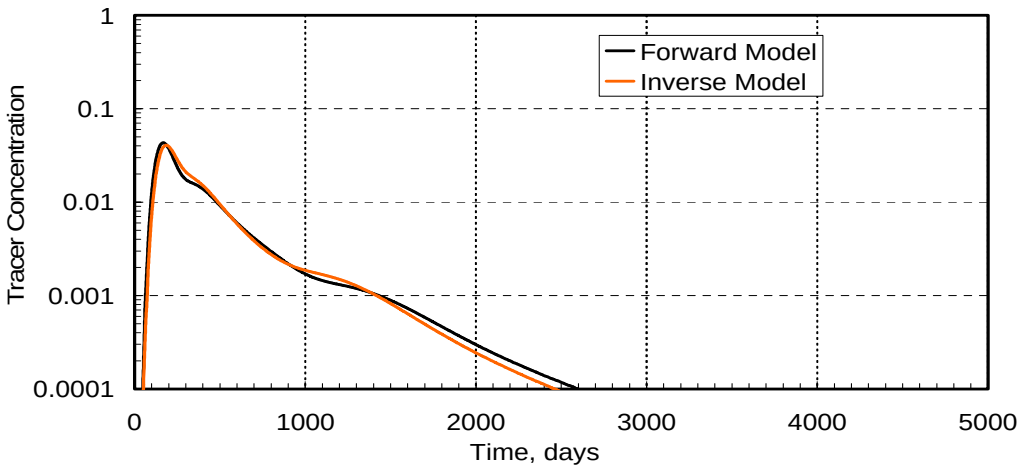

Figure 3.31. Match of the forward model tracer response from all layers by iteration 2 of the inverse model at tracer partition coefficient K=10

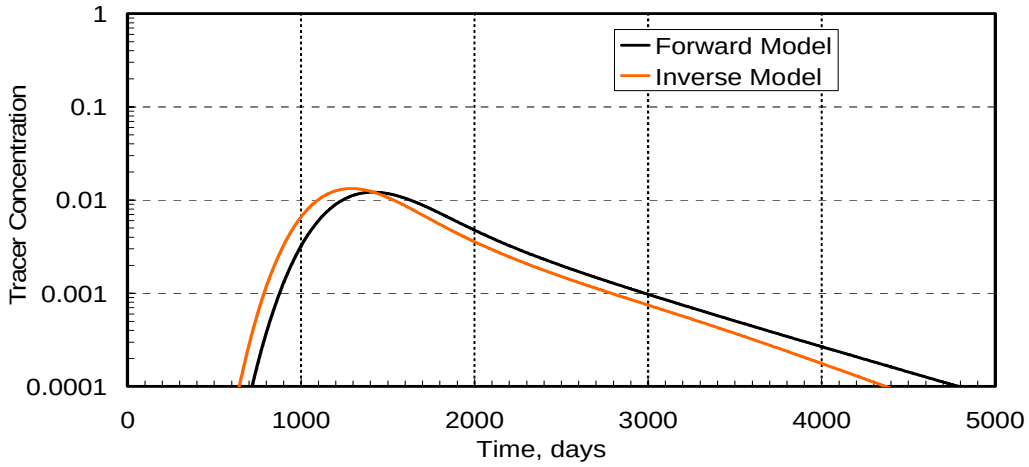

Figure 3.32.Match of the forward model tracer response from layer 5 by iteration 2 of the inverse model at tracer partition coefficient K=10.

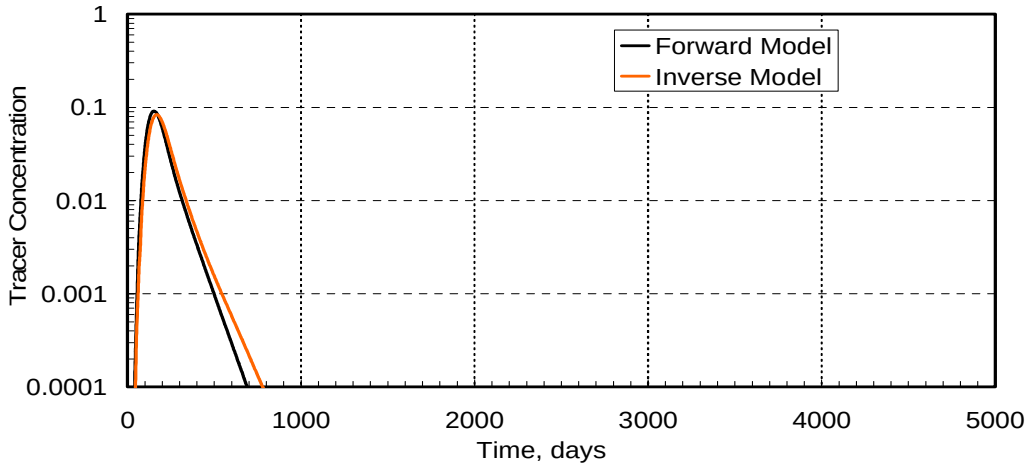

Figure 3.33. Match of the forward model tracer response from layer 8 by iteration 2 of the inverse model at tracer partition coefficient K=10.

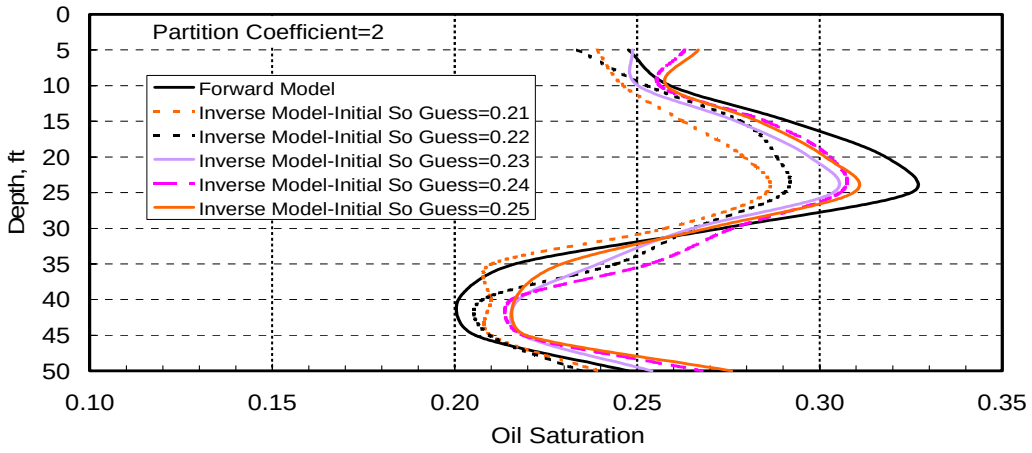

Figure 3.34. Inverse model vertical oil saturation estimates at initial oil saturations guesses 0.21, 0.22, 0.23, 0.24 and 0.25.

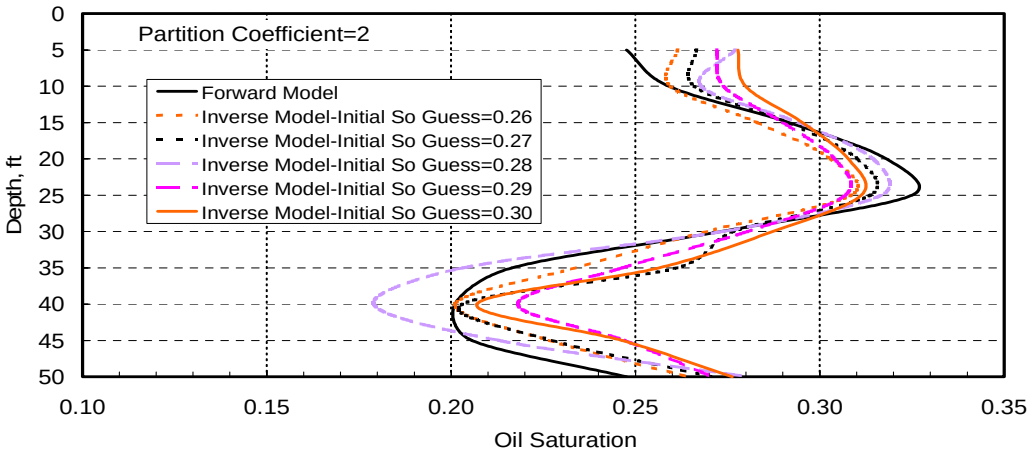

Figure 3.35. Inverse model vertical oil saturation estimates at initial oil saturations guesses 0.26, 0.27, 0.28, 0.29 and 0.30.

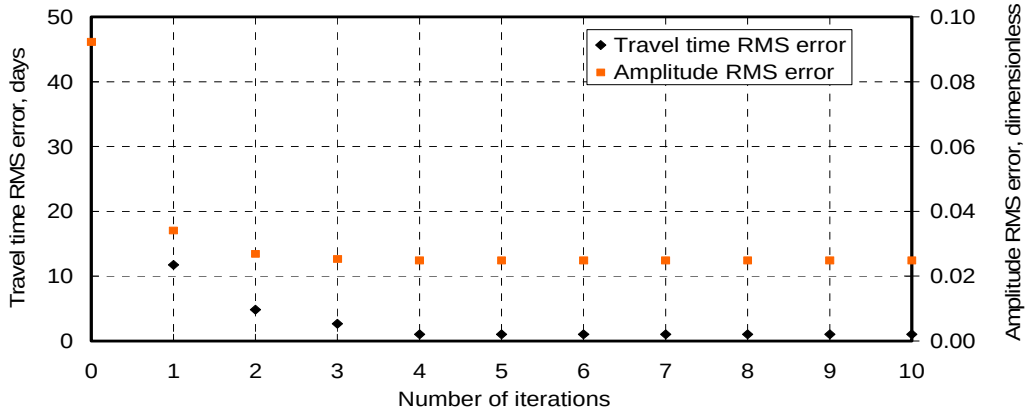

Figure 3.36. RMS error change on travel time and amplitude at initial oil saturation guess 0.21

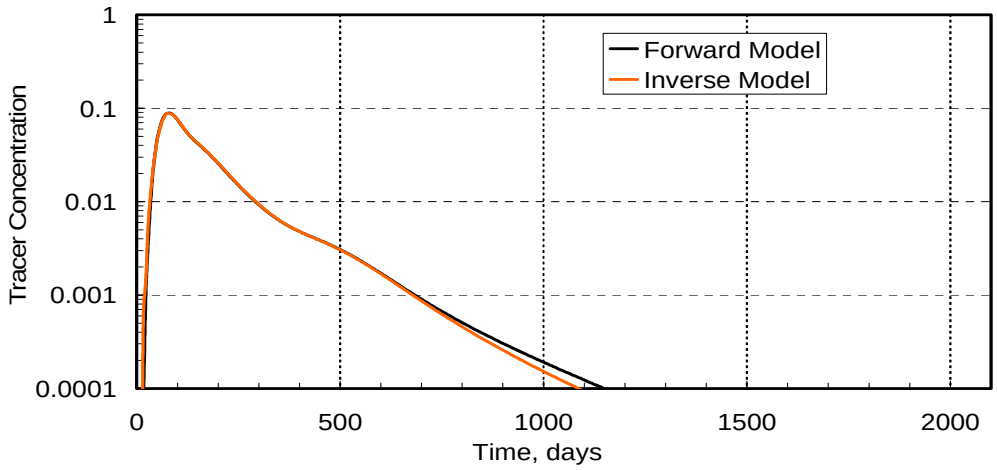

Figure 3.37. Match of the forward model tracer response from all layers by iteration 4 of the inverse model at the initial oil saturation guess 0.21.

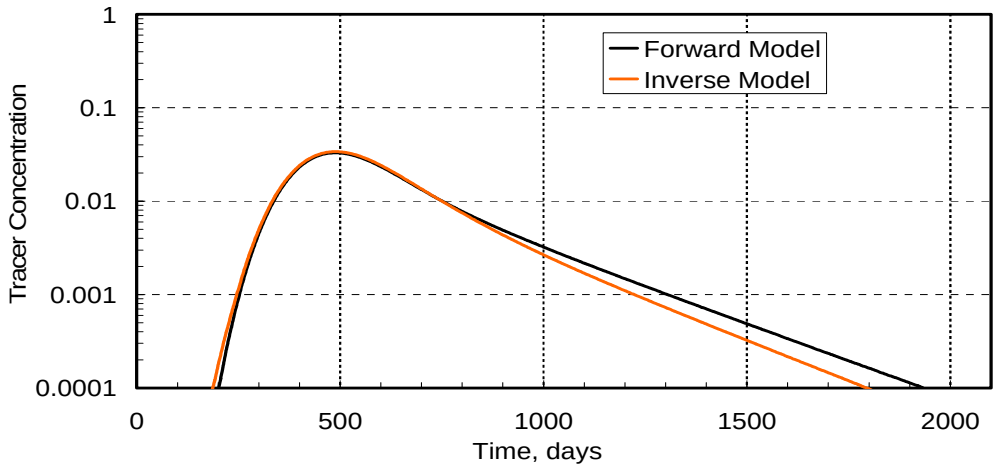

Figure 3.38. Match of the forward model tracer response from layer 5 by iteration 4 of the inverse model at the initial oil saturation guess 0.21.

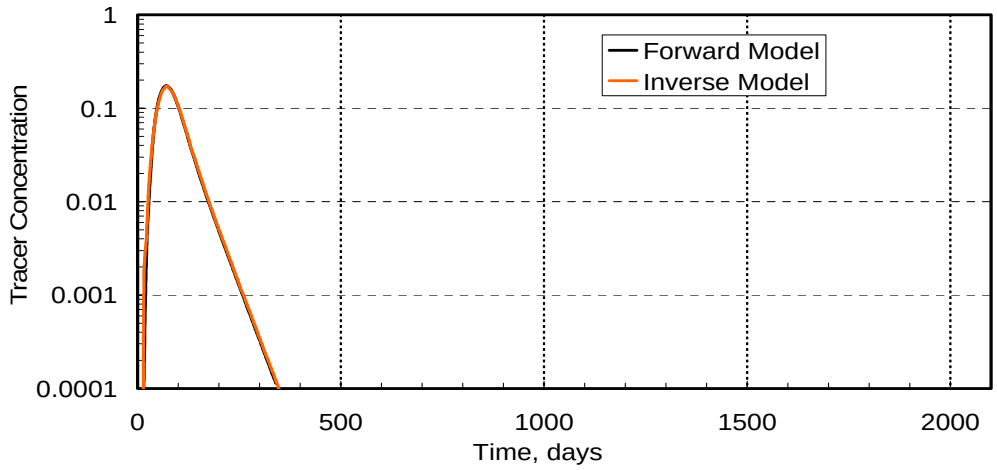

Figure 3.39. Match of the forward model tracer response from layer 8 by iteration 4 of the inverse model at the initial oil saturation guess 0.21.

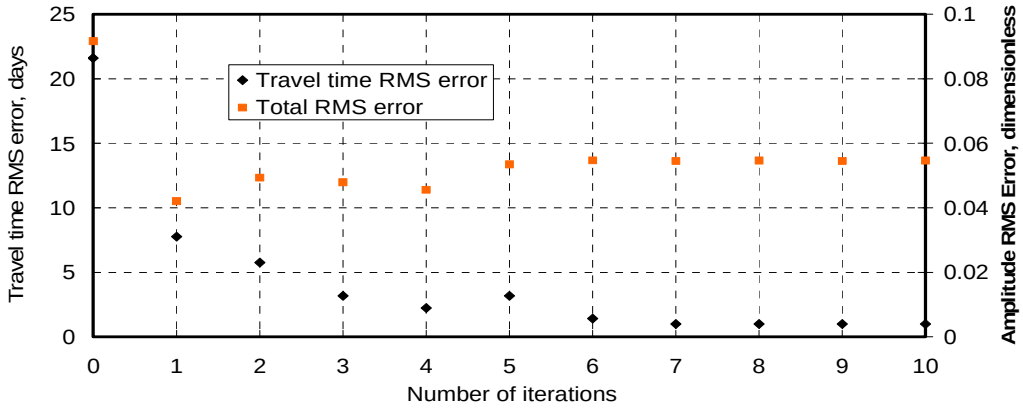

Figure 3.40. RMS error change on travel time and amplitude at initial oil saturation guess 0.28

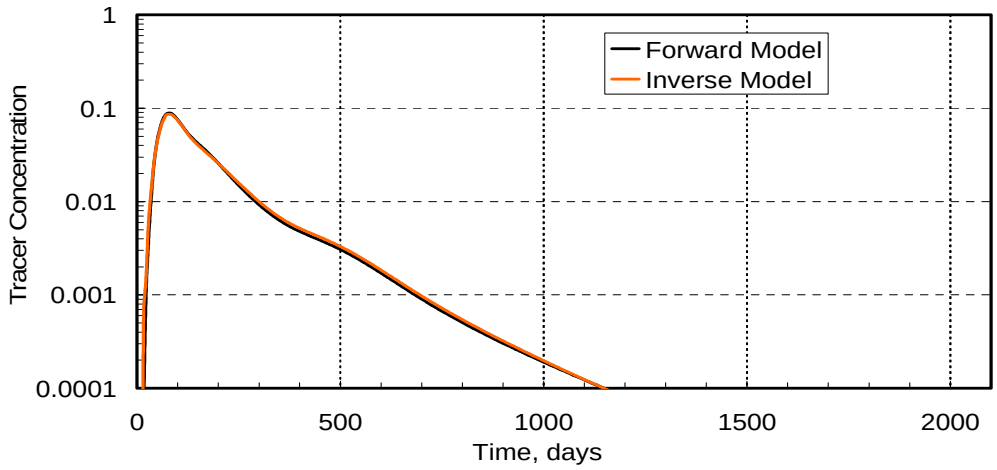

Figure 3.41. Match of the forward model tracer response from all layers by iteration 10 of the inverse model at the initial oil saturation guess 0.28.

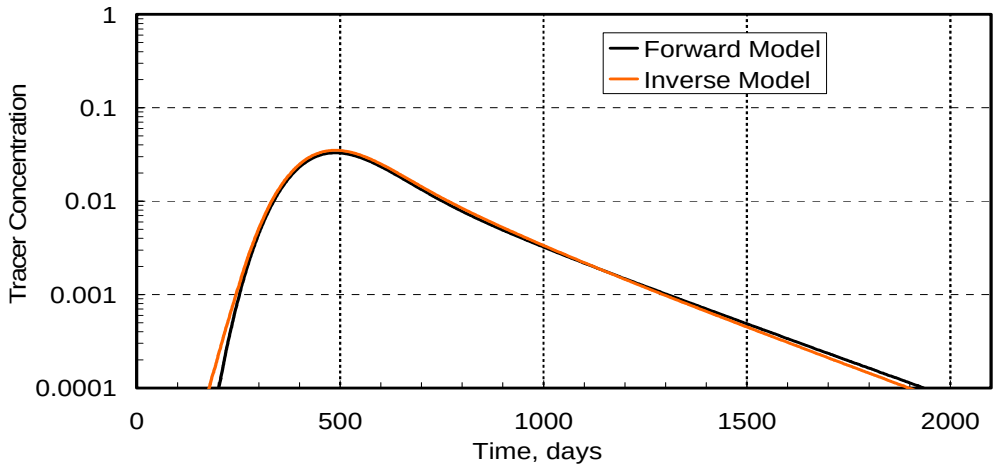

Figure 3.42. Match of the forward model tracer response from layer 5 by iteration 10 of the inverse model at the initial oil saturation guess 0.28.

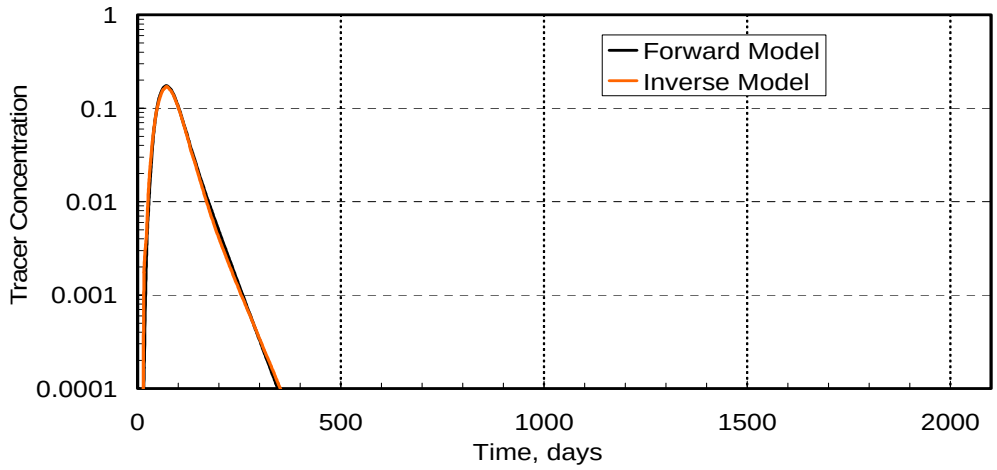

Figure 3.43. Match of the forward model tracer response from layer 8 by iteration 10 of the inverse model at the initial oil saturation guess 0.28.

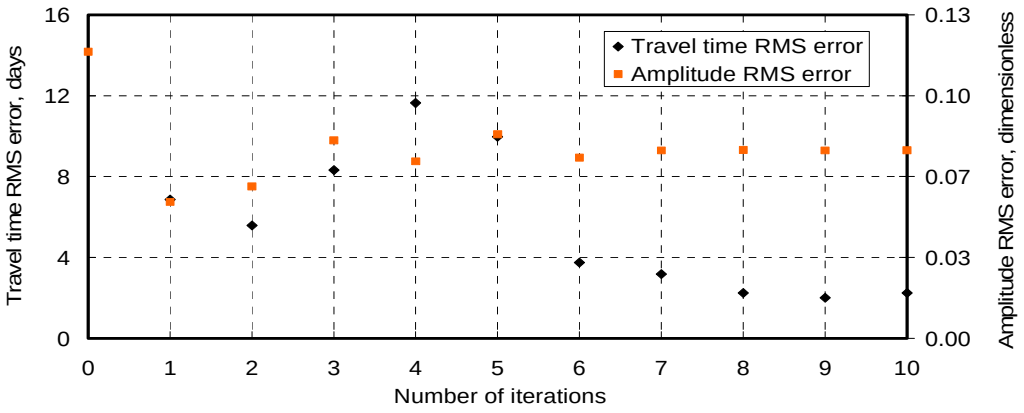

Figure 3.44. RMS error change on travel time and amplitude at initial oil saturation guess 0.30

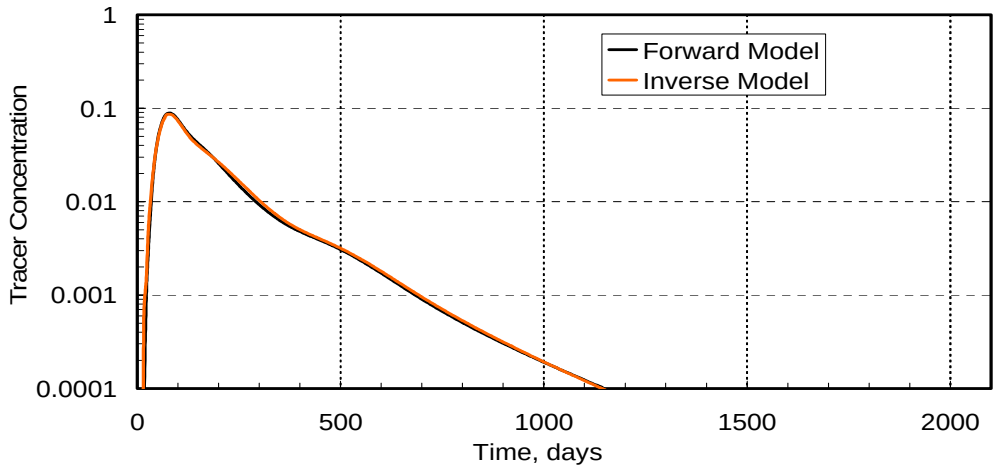

Figure 3.45. Match of the forward model tracer response from all layers by iteration 1 of the inverse model at the initial oil saturation guess 0.30.

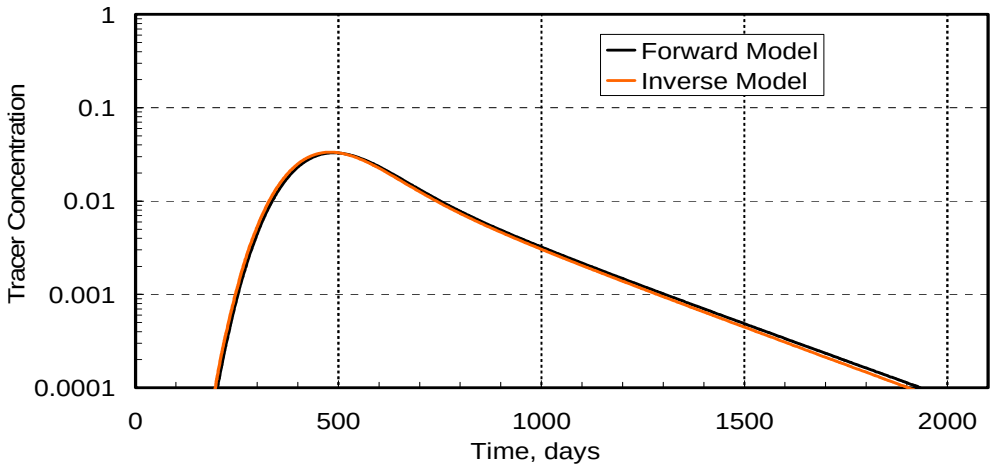

Figure 3.46. Match of the forward model tracer response from layer 5 by iteration 1 of the inverse model at the initial oil saturation guess 0.30.

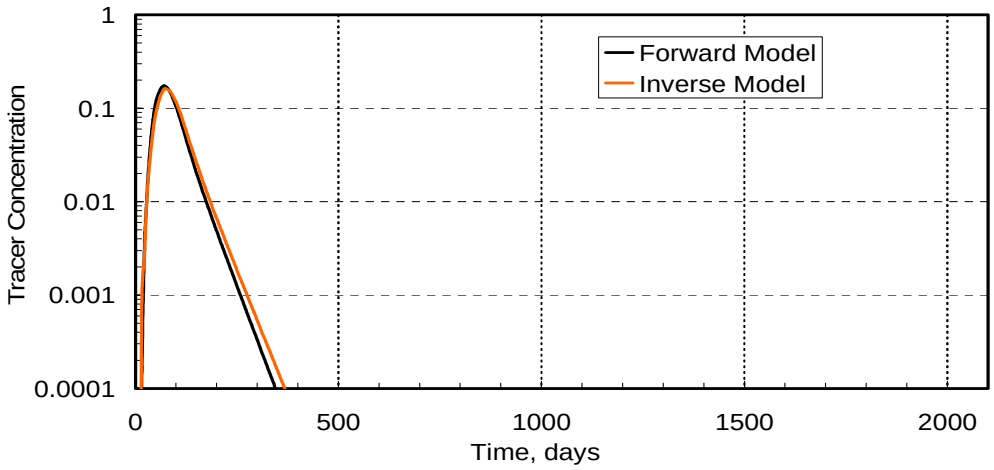

Figure 3.47. Match of the forward model tracer response from layer 8 by iteration 1 of the inverse model at the initial oil saturation guess 0.30.

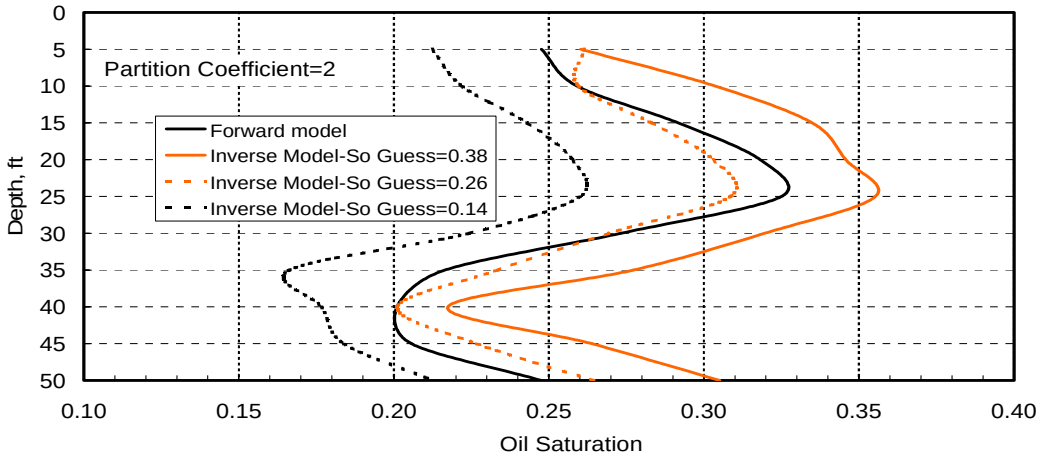

Figure 3.48. Inverse model vertical oil saturation estimates at initial oil saturations guesses 0.38, 0.26, and 0.14.

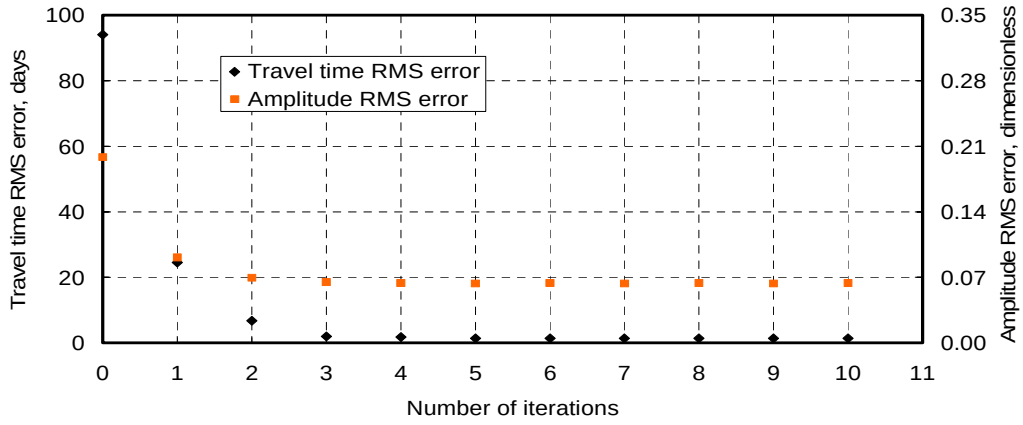

Figure 3.49. RMS error change on travel time and amplitude at initial oil saturation guess 0.14

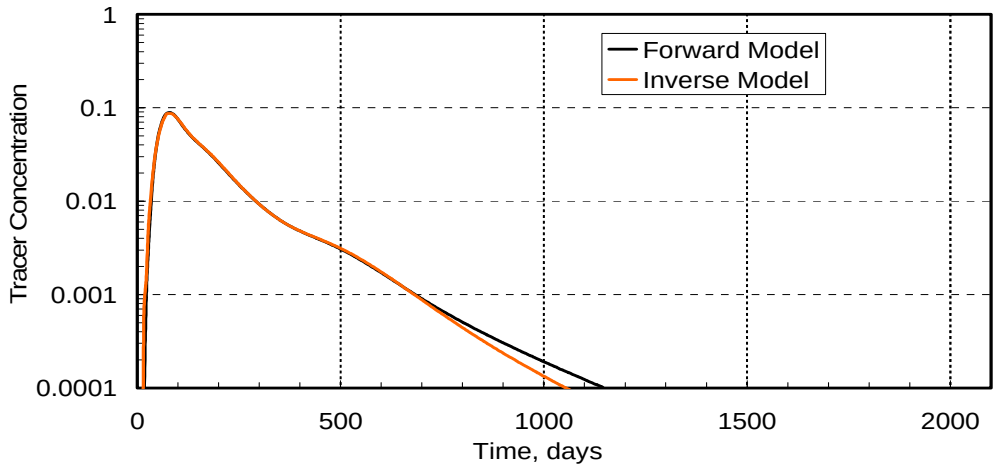

Figure 3.50. Match of the forward model tracer response from all layers by iteration 4 of the inverse model at the initial oil saturation guess 0.14.

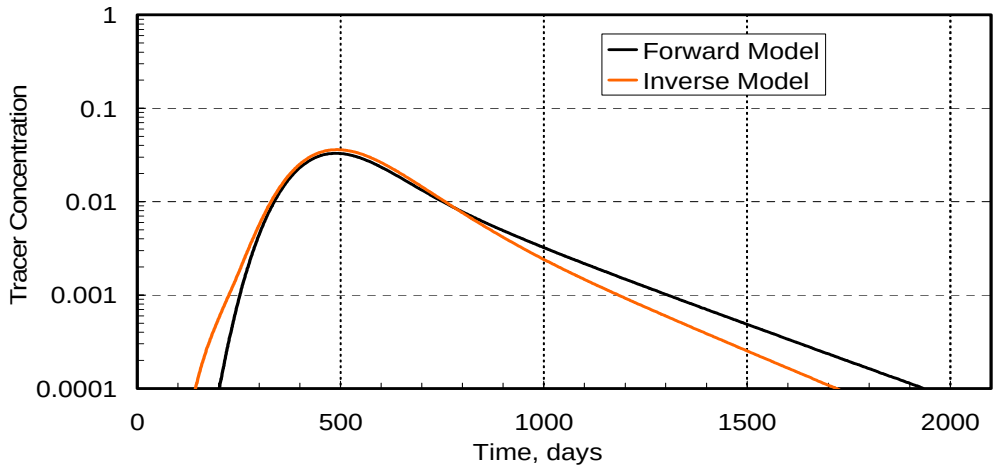

Figure 3.51. Match of the forward model tracer response from layer 5 by iteration 4 of the inverse model at the initial oil saturation guess 0.14.

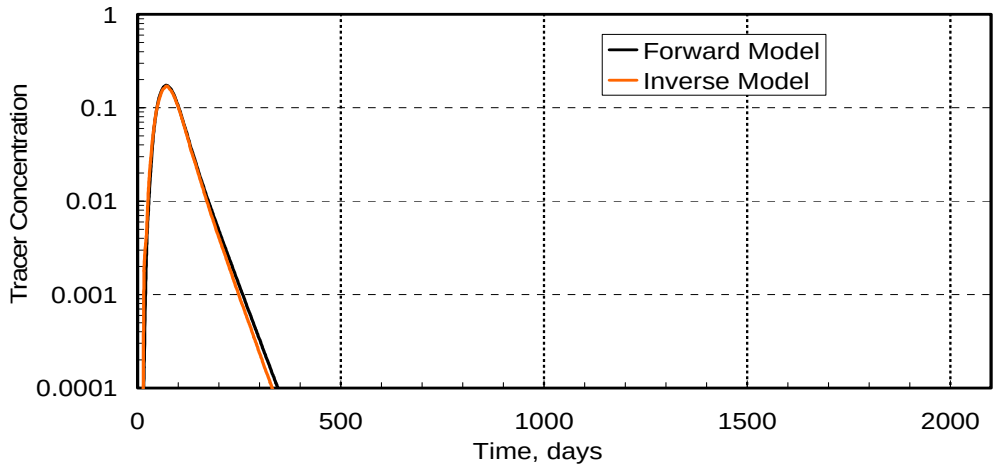

Figure 3.52. Match of the forward model tracer response from layer 8 by iteration 4 of the inverse model at the initial oil saturation guess 0.14.

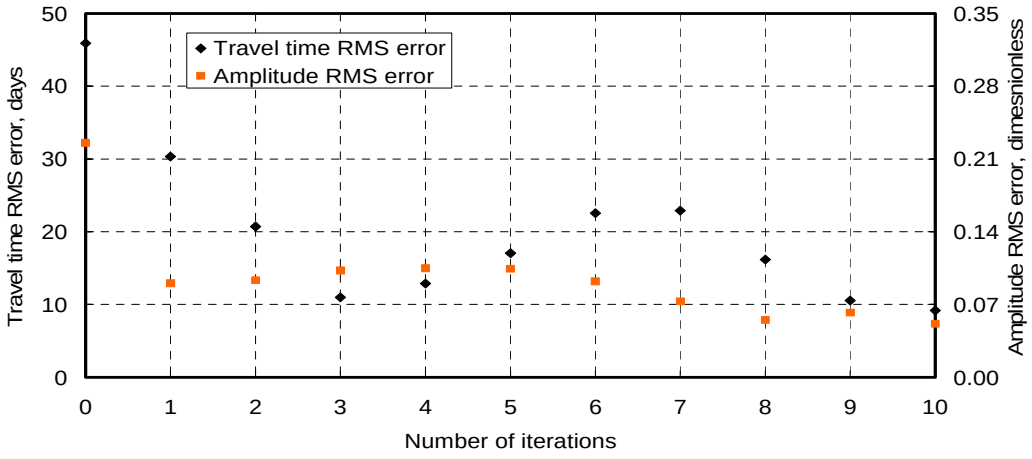

Figure 3.53. RMS error change on travel time and amplitude and at initial oil saturation guess 0.38

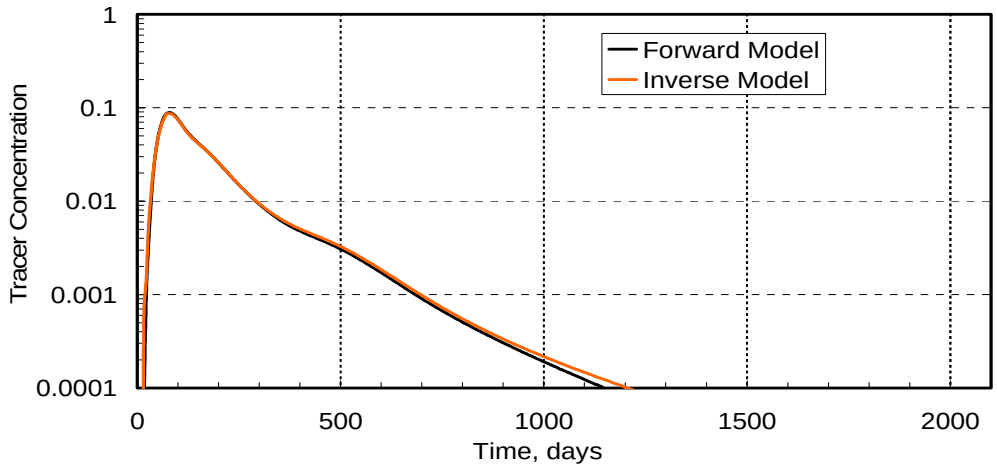

Figure 3.54. Match of the forward model tracer response from all layers by iteration 10 of the inverse model at the initial oil saturation guess 0.38.

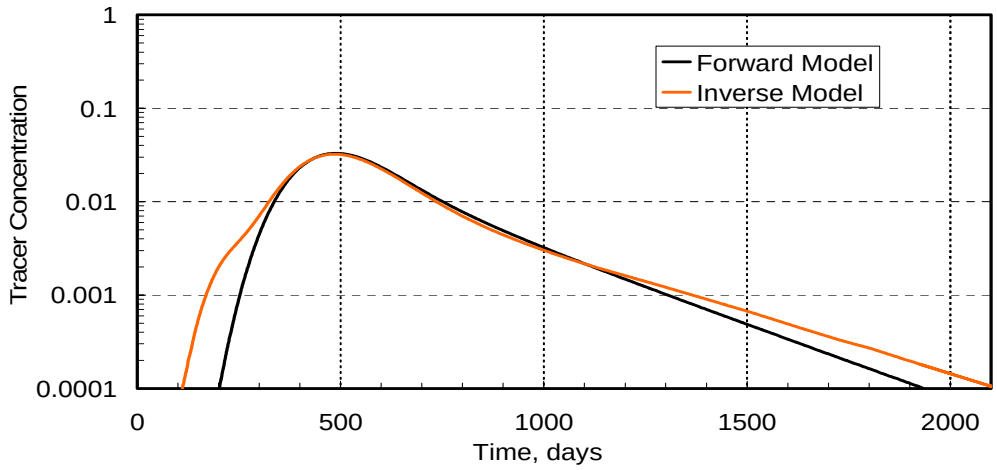

Figure 3.55. Match of the forward model tracer response from layer 5 by iteration 10 of the inverse model at the initial oil saturation guess 0.38.

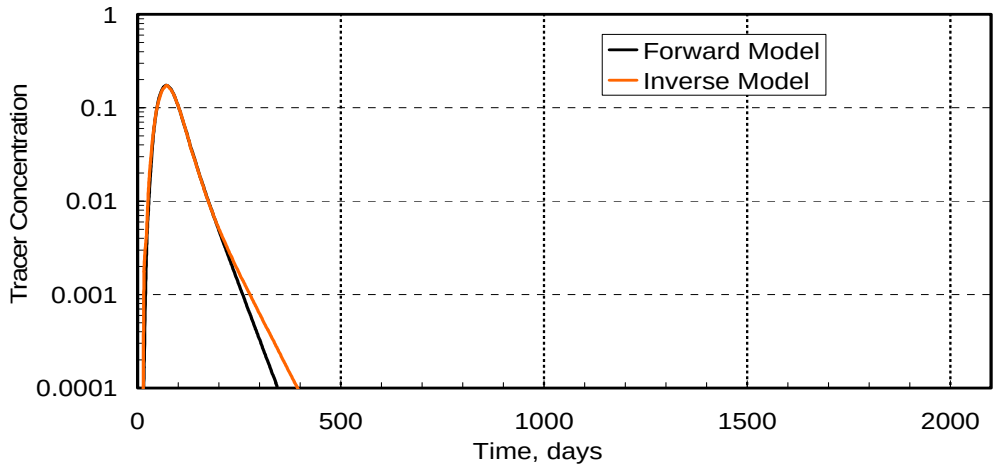

Figure 3.56. Match of the forward model tracer response from layer 8 by iteration 10 of the inverse model at the initial oil saturation guess 0.38.

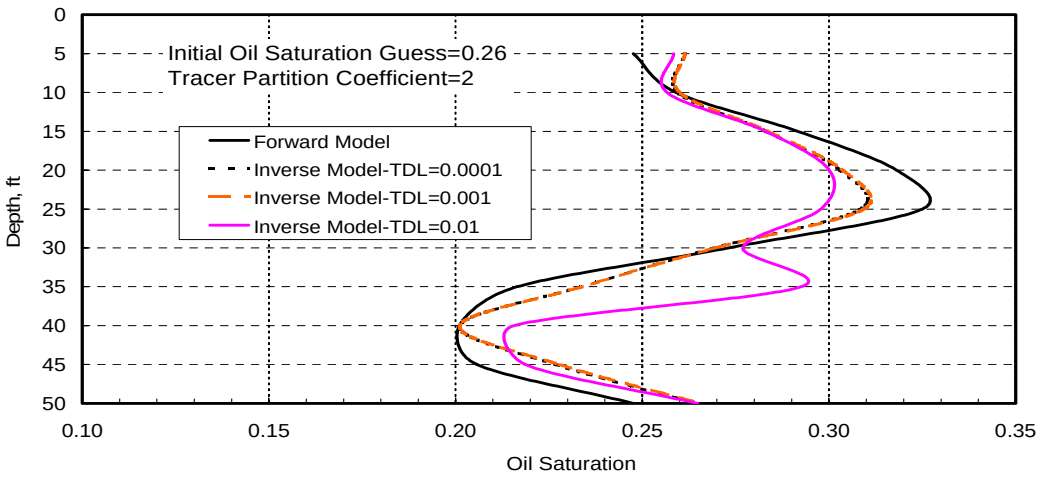

Figure 3.57. Inverse model vertical oil saturation distribution estimates for TDLs 0.0001, 0.001 and 0.01 at initial oil saturation guess 0.26.

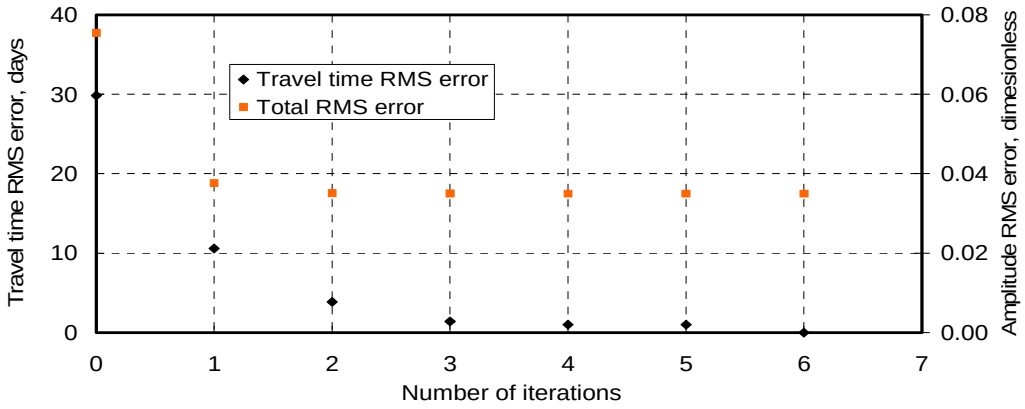

Figure 3.58. RMS error change on travel time and amplitude for TDL 0.001 at initial oil saturation guess 0.26.

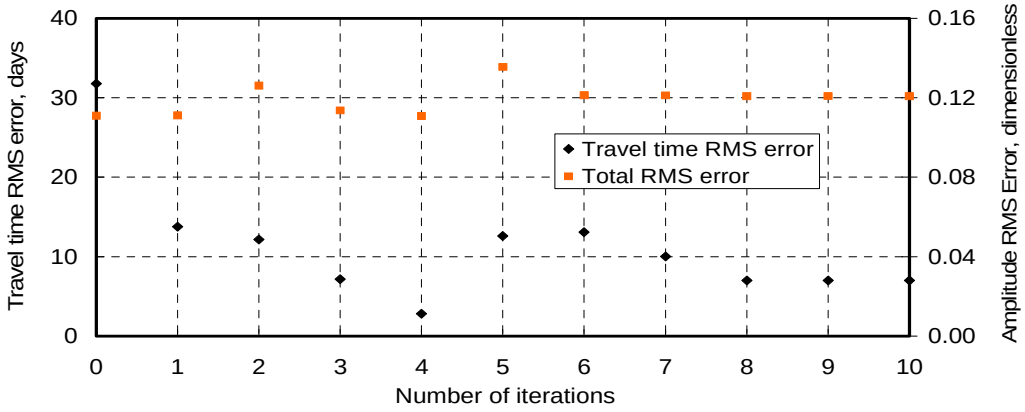

Figure 3.59. RMS error change on travel time and amplitude for TDL 0.01 at initial oil saturation guess 0.26.

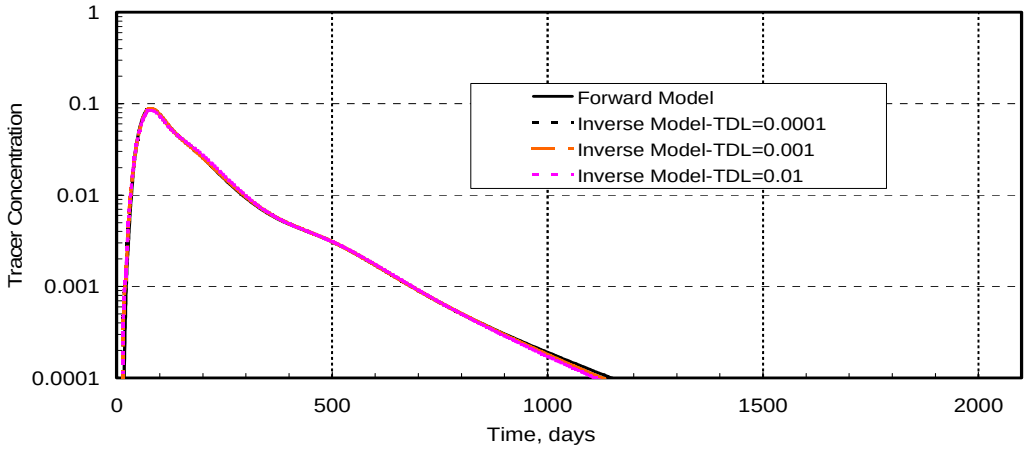

Figure 3.60. Match of the forward model tracer response from all layers with the inverse model for TDLs 0.0001, 0.001 and 0.01 at initial oil saturation guess 0.26.

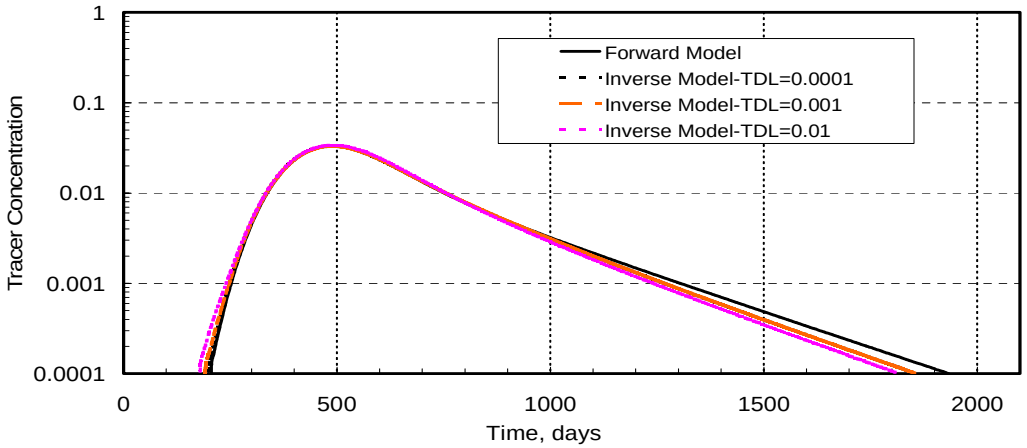

Figure 3.61. Match of the forward model tracer response from layer 5 with the inverse model for TDLs 0.0001, 0.001 and 0.01 at initial oil saturation guess 0.26.

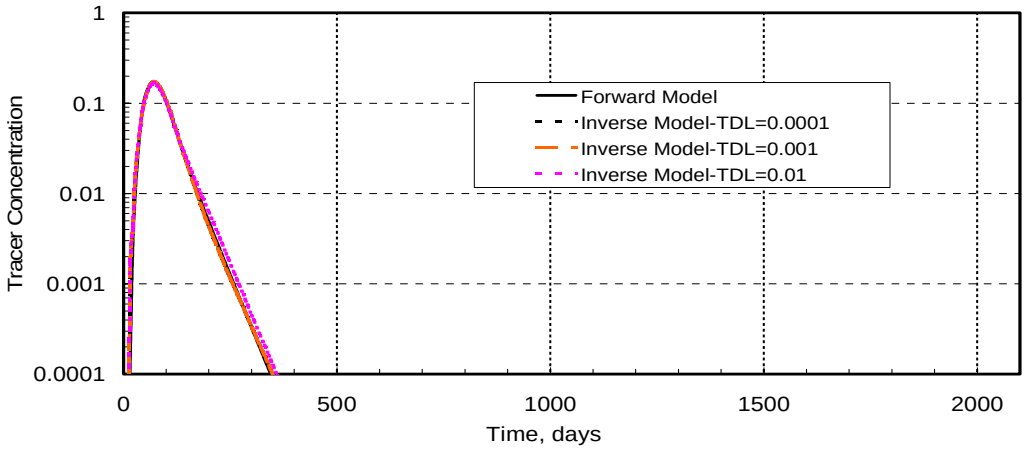

Figure 3.62. Match of the forward model tracer response from layer 8 with the inverse model for TDLs 0.0001, 0.001 and 0.01 at initial oil saturation guess 0.26.

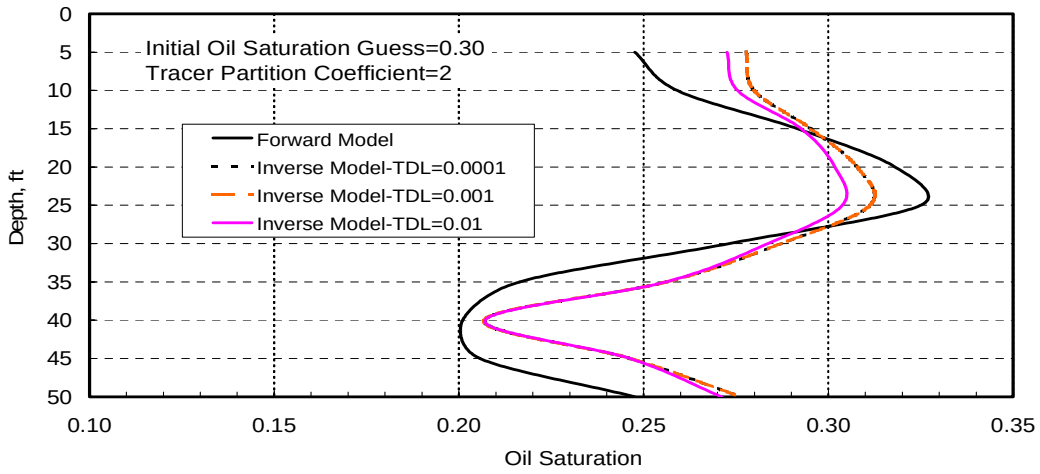

Figure 3.63. Inverse model vertical oil saturation distribution estimates for TDLs 0.0001, 0.001 and 0.01at initial oil saturations guess 0.30.

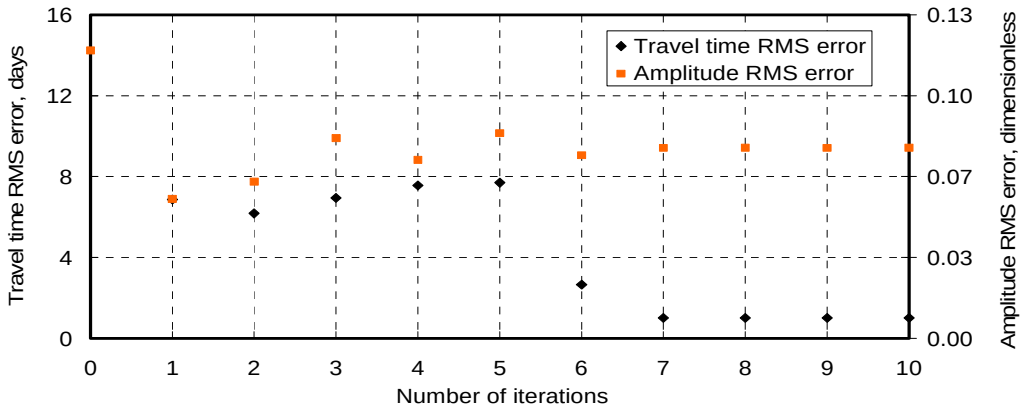

Figure 3.64. RMS error change on travel time and amplitude for TDL 0.001 and initial oil saturation guess 0.30.

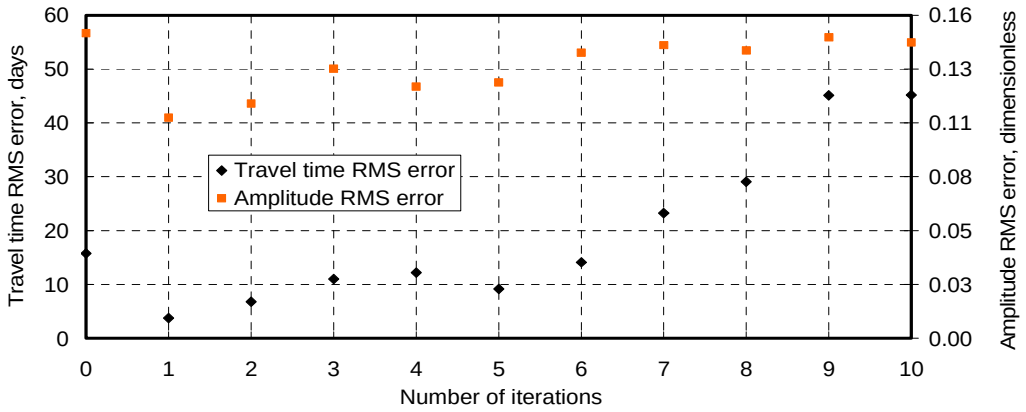

Figure 3.65. RMS error change on travel time and amplitude for tracer concentration detection limit 0.01 at initial oil saturation guess 0.30.

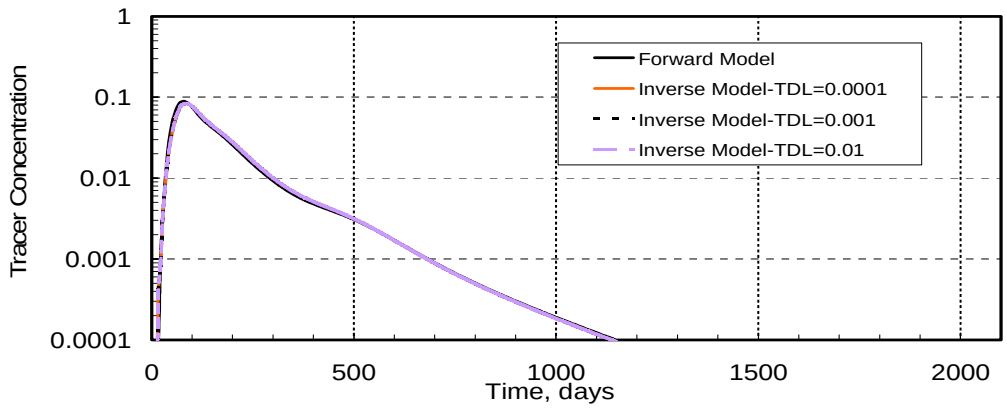

Figure 3.66. Match of the forward model tracer response from all layers with the inverse model for TDLs 0.0001, 0.001 and 0.01 at initial oil saturation guess 0.30.

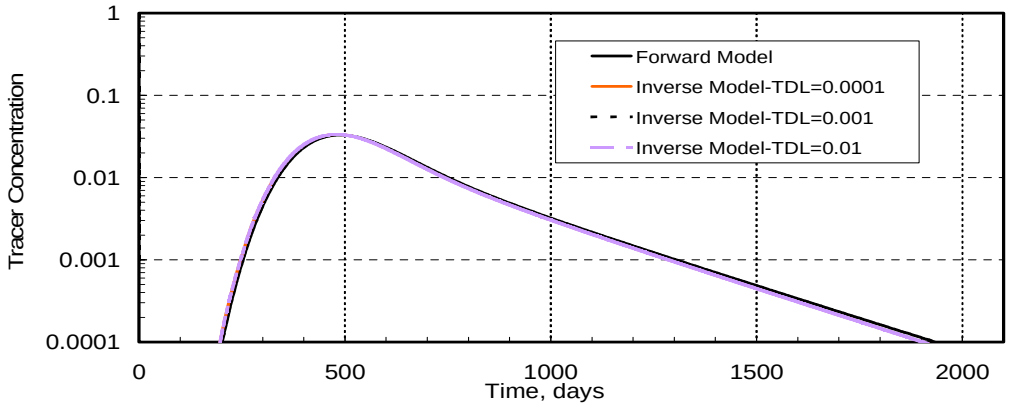

Figure 3.67. Match of the forward model tracer response from layer 5 with the inverse model for TDLs 0.0001, 0.001 and 0.01 at initial oil saturation guess 0.30.

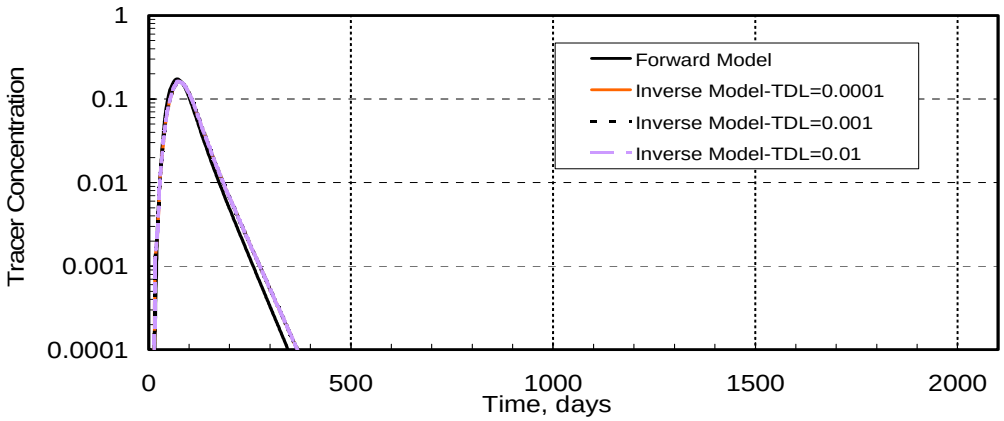

Figure 3.68. Match of the forward model tracer response from layer 8 with the inverse model for TDLs 0.0001, 0.001 and 0.01 at initial oil saturation guess 0.30.

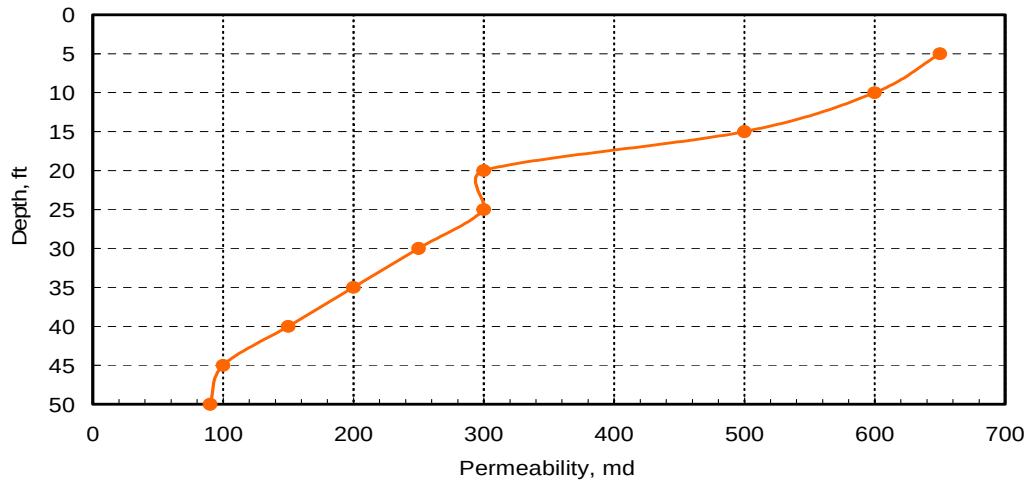

Figure 3.69 Rearranged vertical permeability distribution of the three-dimensional uniform layered permeability reservoir model

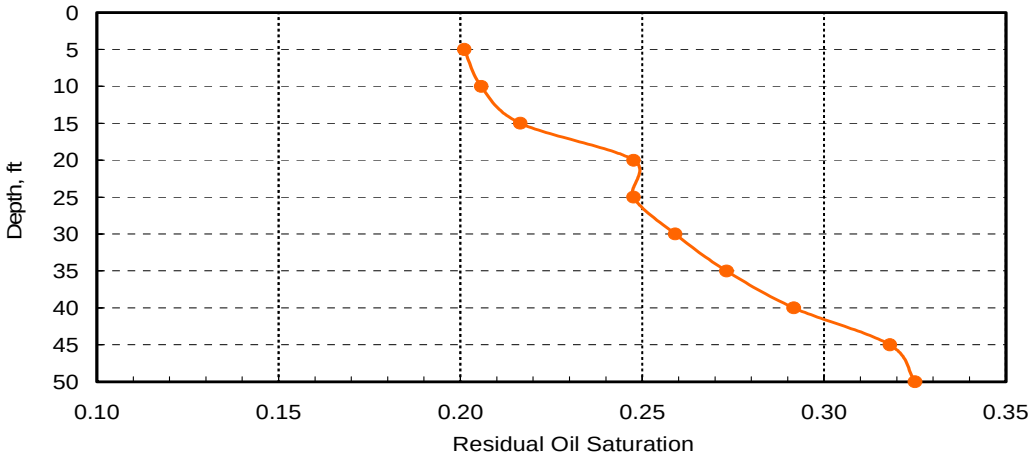

Figure 3.70 Rearranged vertical permeability distribution of the three-dimensional uniform layered permeability reservoir model

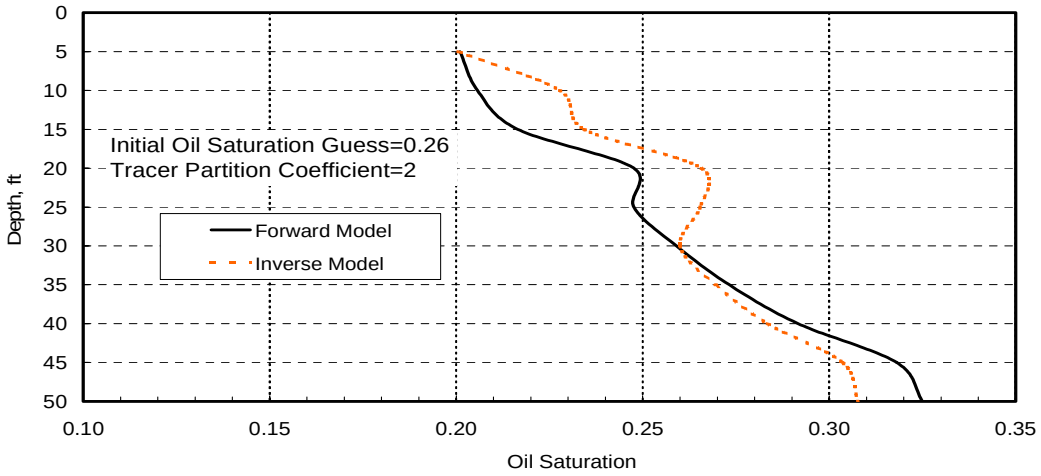

Figure 3.71 Inverse model vertical oil saturation distribution estimates in the reservoir model with the rearranged permeability field

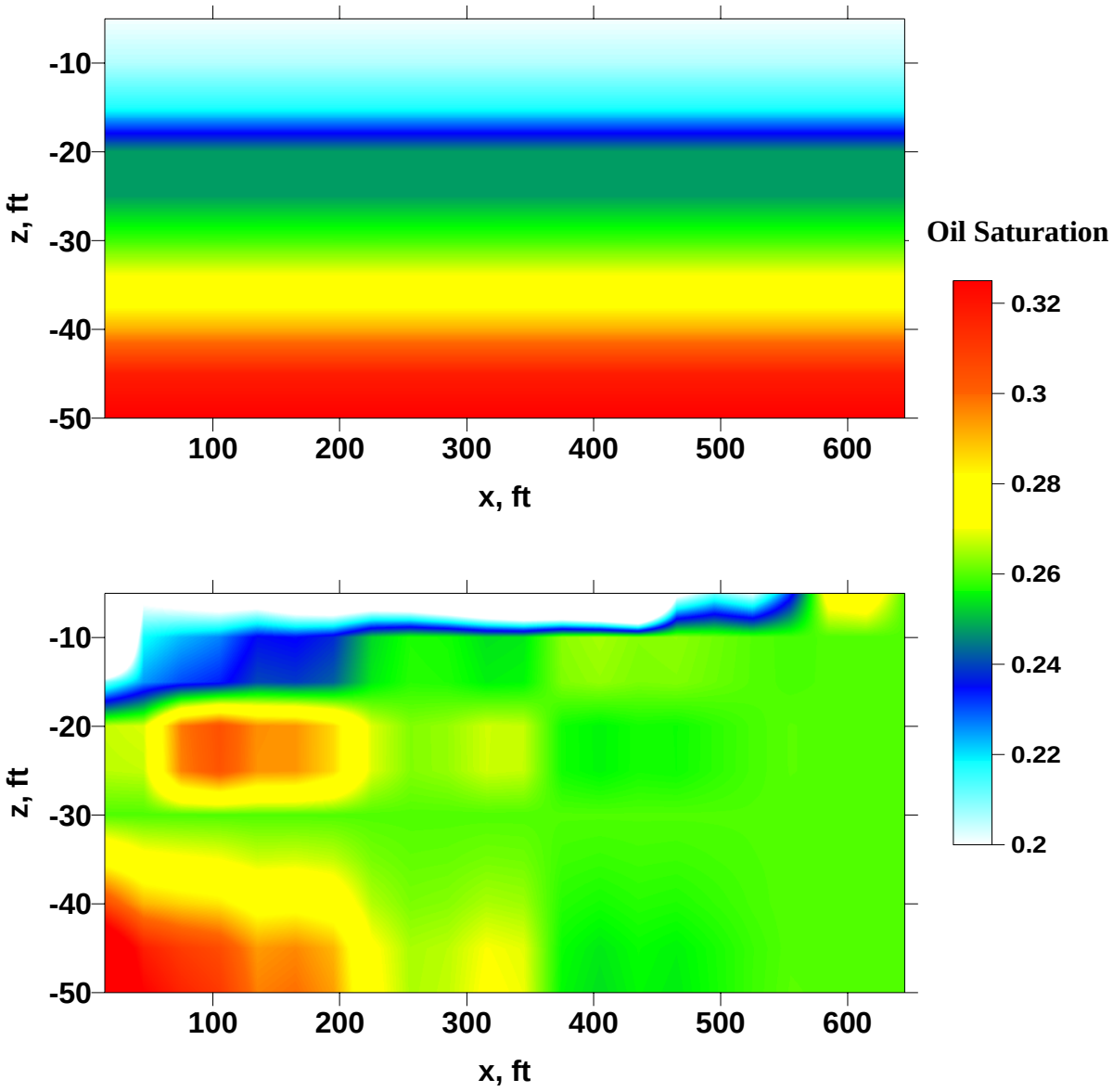

Figure 3.72. Comparison of forward model oil saturation distribution (top image) with inverse model oil saturation distribution (bottom image) in the rearranged permeability field.

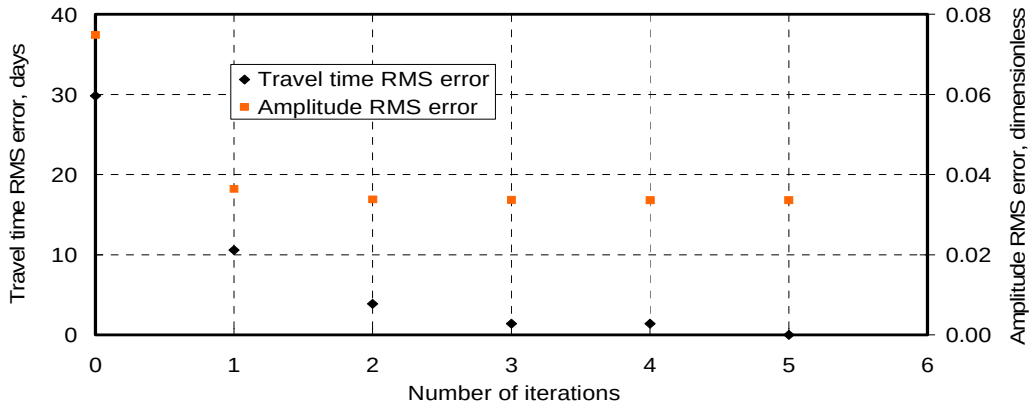

Figure 3.73. RMS error change on travel time and amplitude at in the rearranged permeability field.

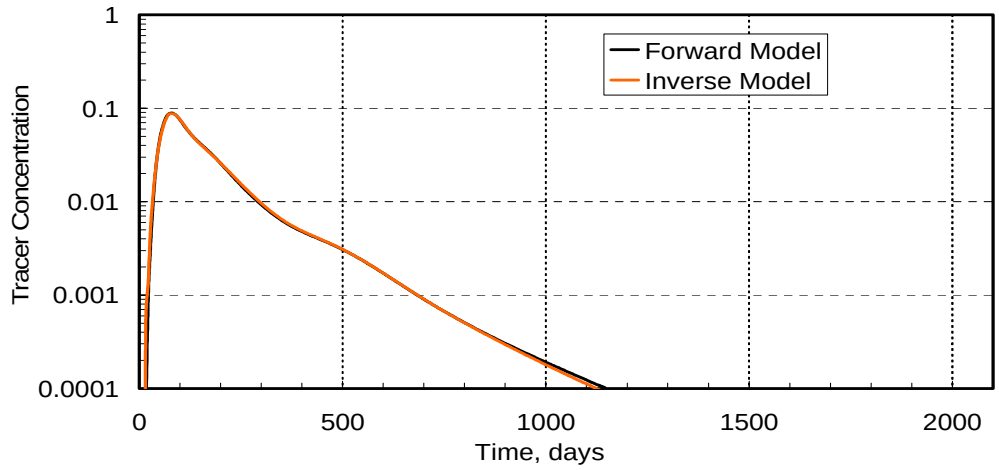

Figure 3.74. Match of the forward model tracer response from all layers by iteration 5 of the inverse model at the reservoir model with the rearranged permeability field.

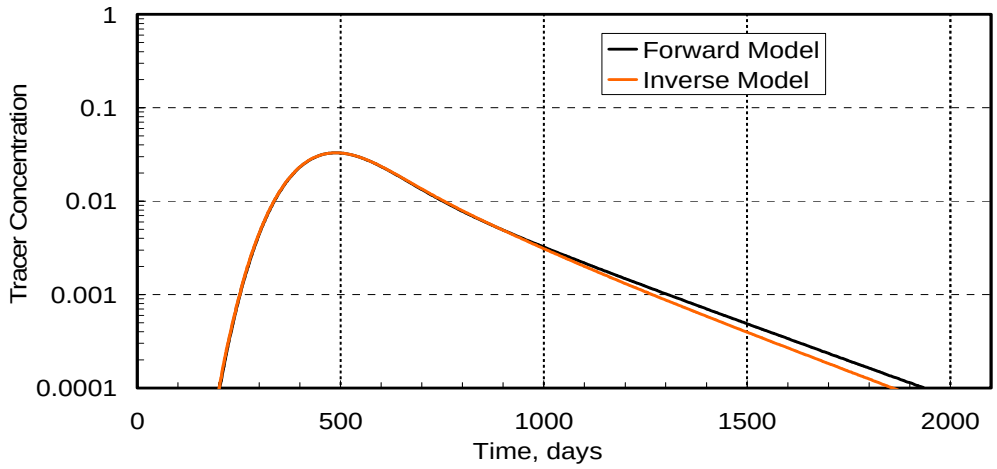

Figure 3.75. Match of the forward model tracer response from layer 5 by iteration 5 of the inverse model at the reservoir model with the rearranged permeability field.

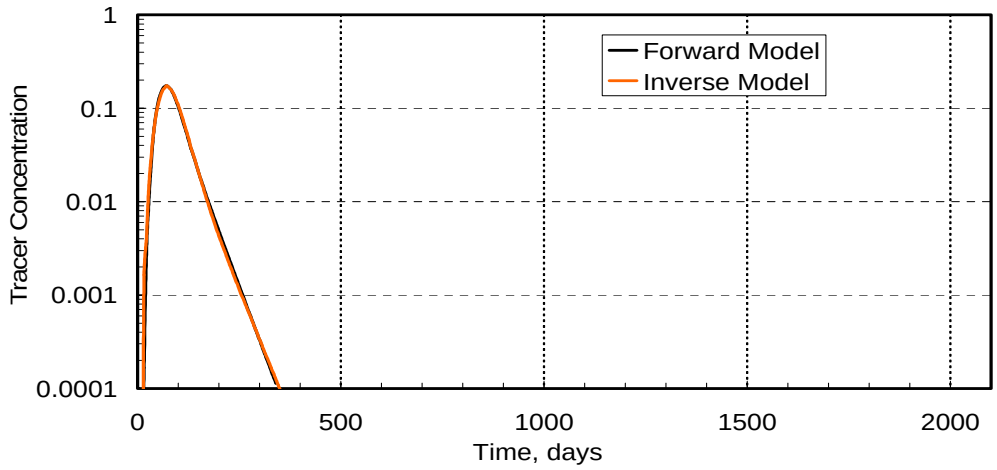

Figure 3.76. Match of the forward model tracer response from all layers by iteration 8 of the inverse model at the reservoir model with the rearranged permeability field.

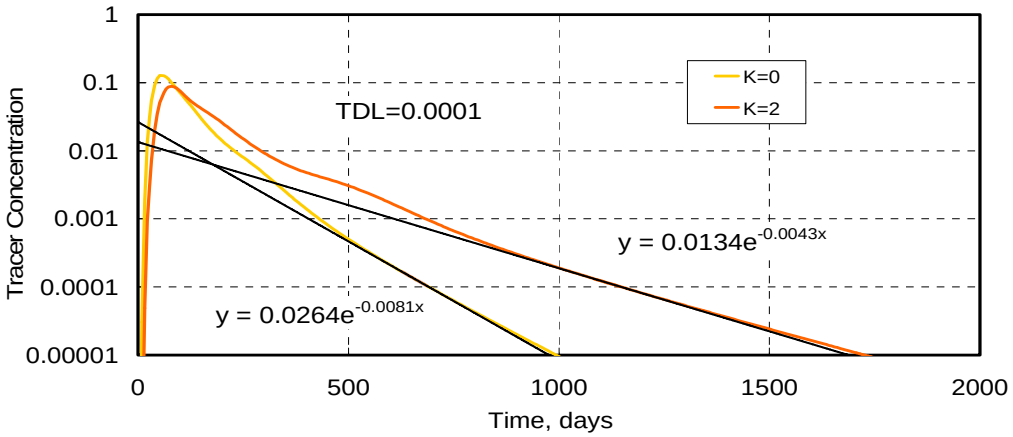

Figure 3.77. Extrapolation of tracer response from all layers for TDL =0.0001

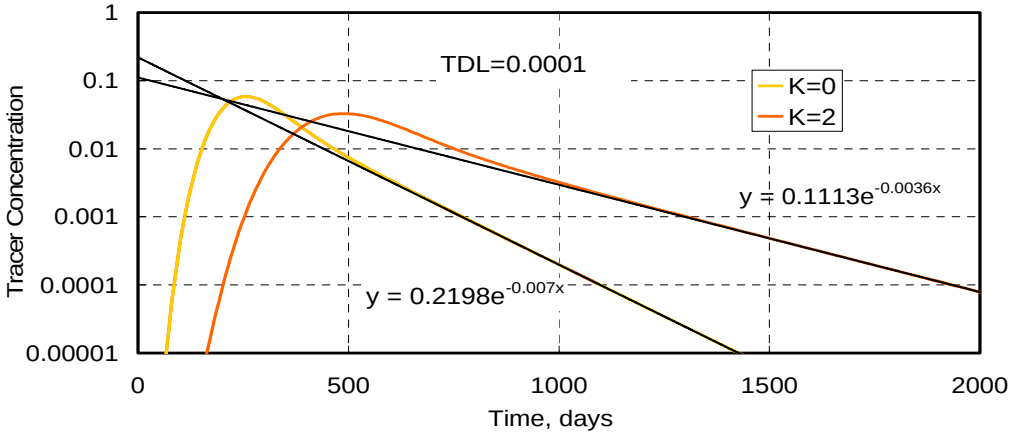

Figure 3.78. Extrapolation of tracer response from layer 5 for TDL =0.0001.

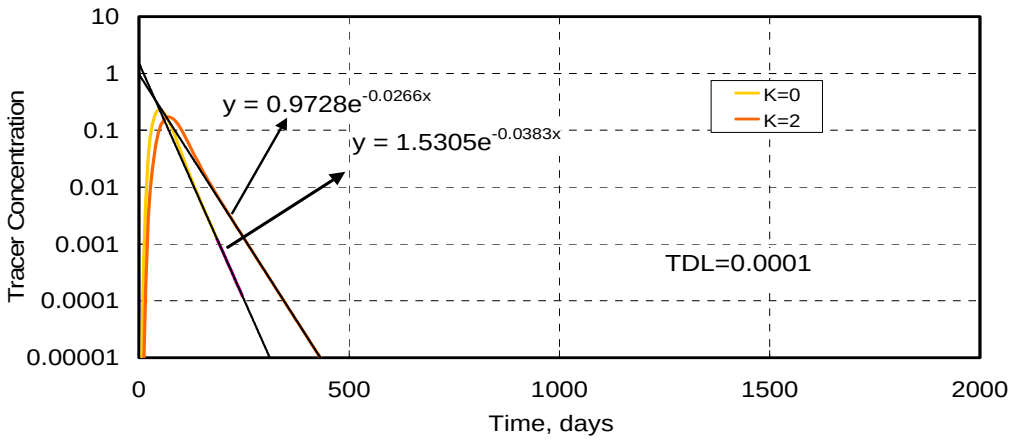

Figure 3.79. Extrapolation of tracer response from layer 8 for TDL =0.0001.

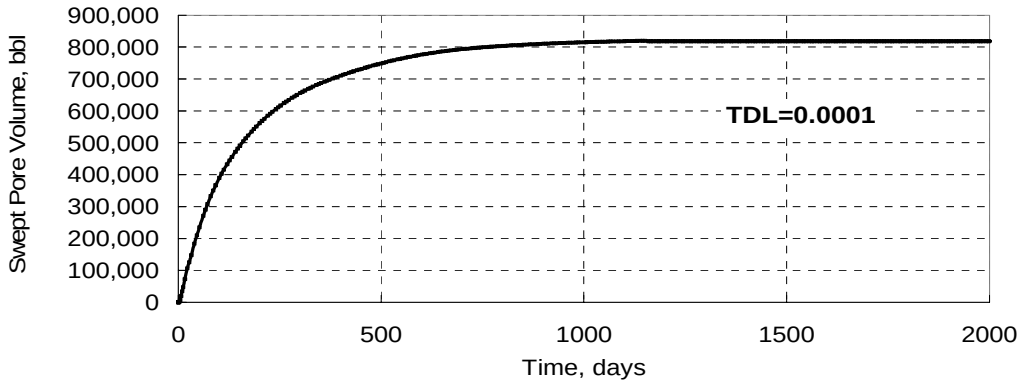

Figure 3.80. MOM swept pore volume estimate of the reservoir after extrapolation for TDL =0.0001

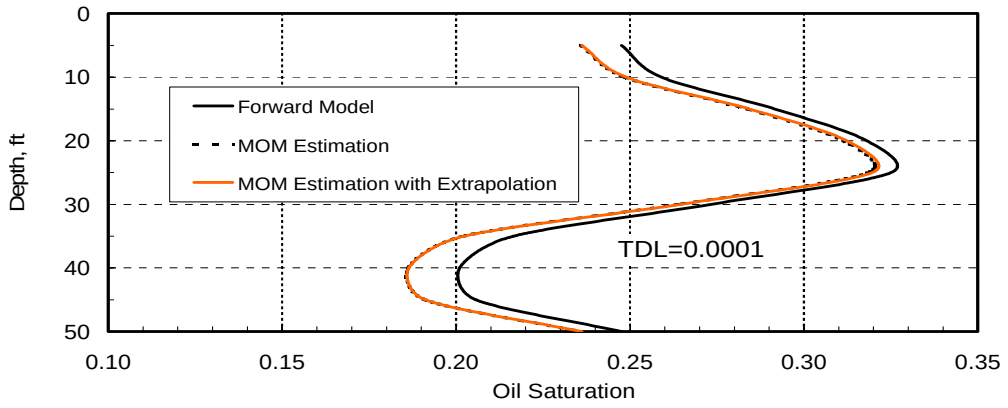

Figure 3.81. MOM oil saturation estimate with and without extrapolation for TDL 0.0001.

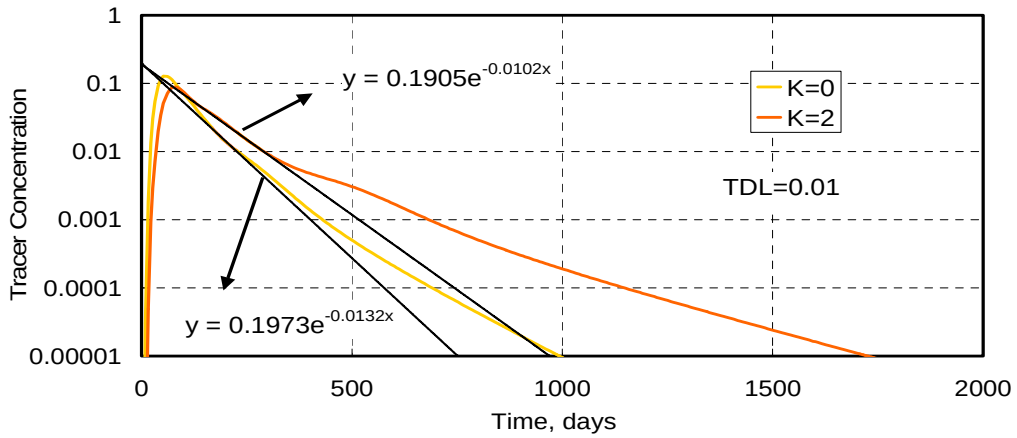

Figure 3.82. Extrapolation of tracer response from all layers for TDL =0.01

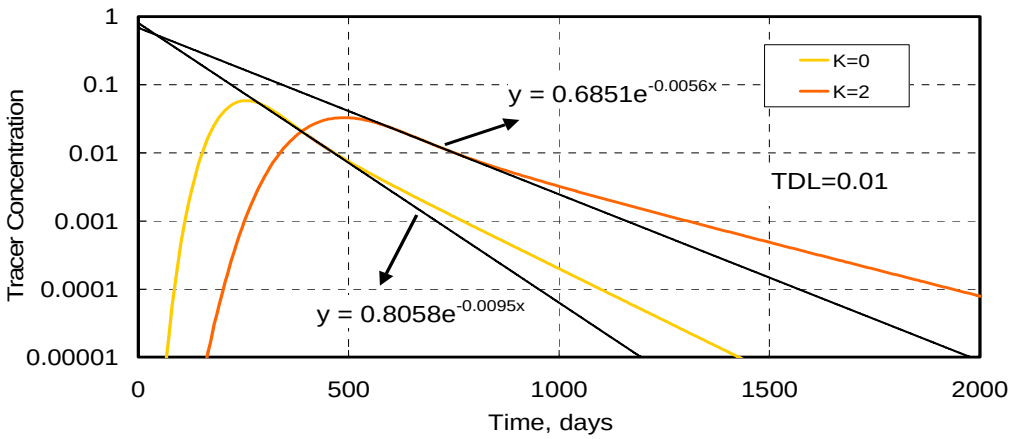

Figure 3.83. Extrapolation of tracer response from layer 5 for TDL =0.01.

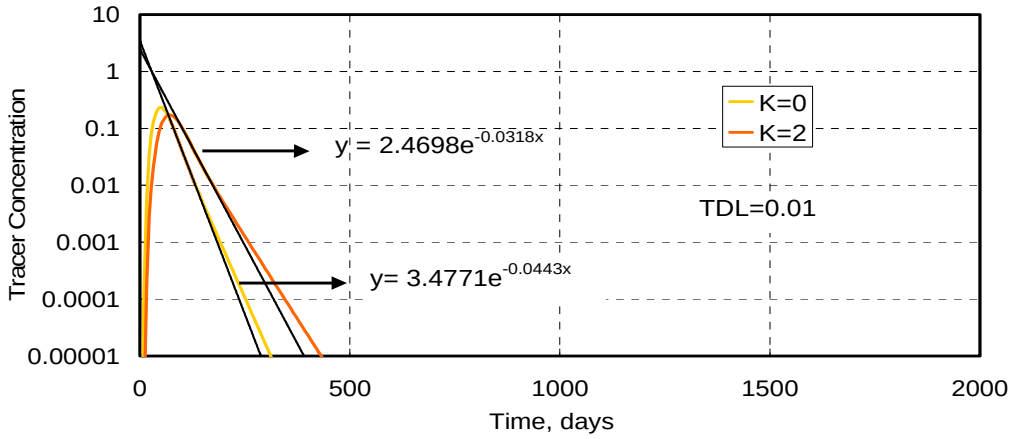

Figure 3.84.Extrapolation of tracer response from layer 8 for TDL =0.01.

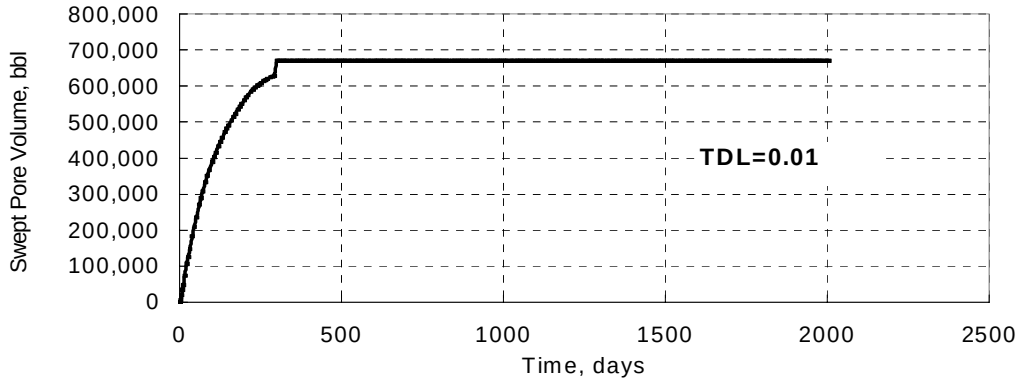

Figure 3.85. MOM swept pore volume estimate of the reservoir for TDL =0.01 after extrapolation

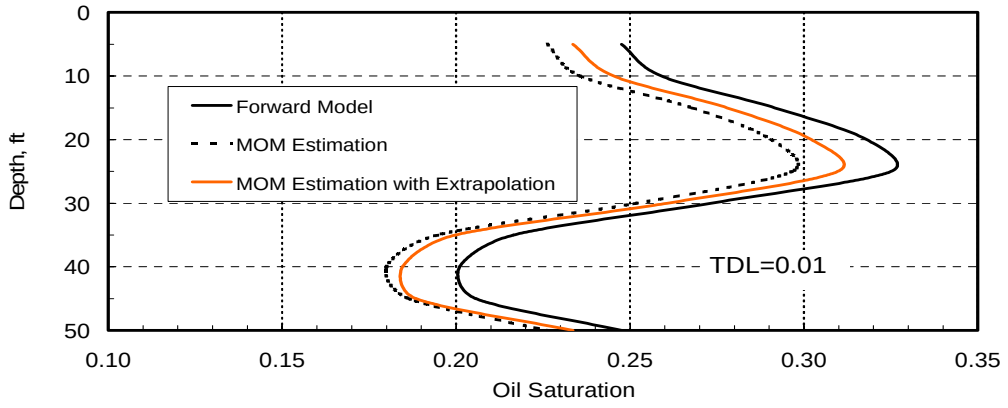

Figure 3.86. MOM oil saturation estimate with and without extrapolation for TDL 0.01.

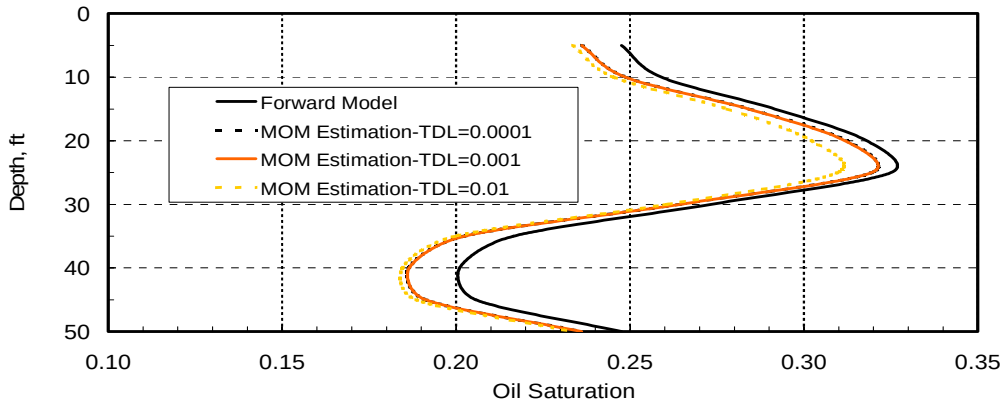

Figure 3.87. MOM oil saturation estimate with and with extrapolation at various TDLs.

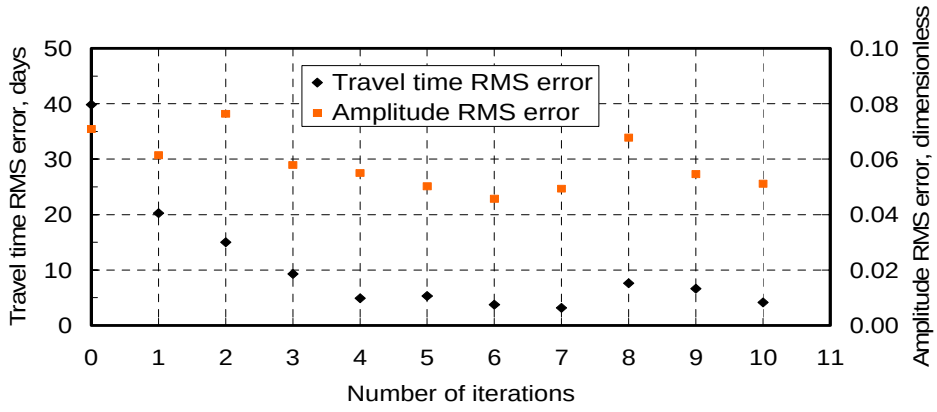

Figure 3.88. RMS error change on travel time and amplitude during the inverse model run at initial oil saturation guess 0.241 (average MOM estimate).

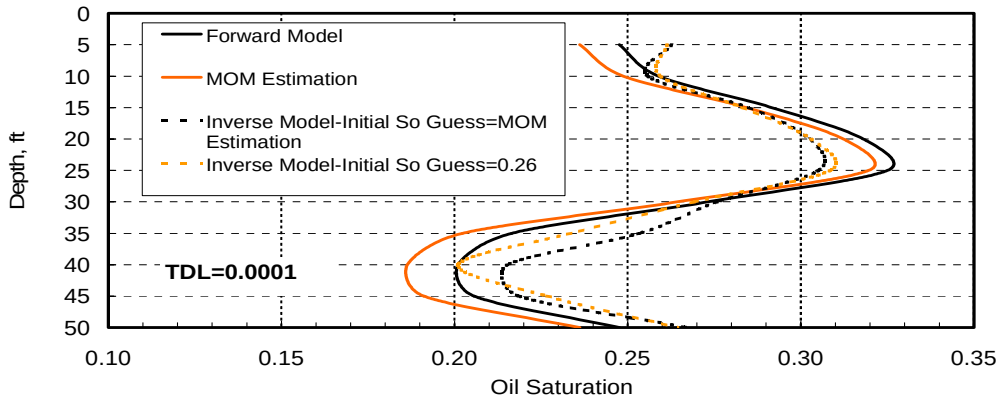

Figure 3.89. Comparison of MOM and inverse model oil saturation estimates.

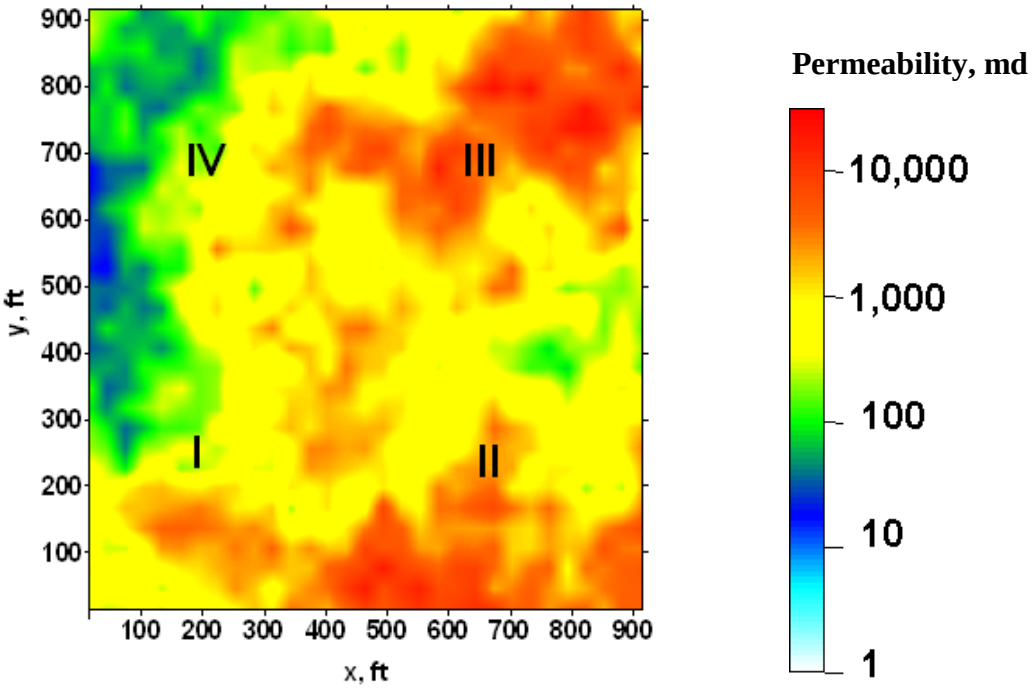

Figure 3.90. Stochastic permeability distribution at the vertical layer Z=7

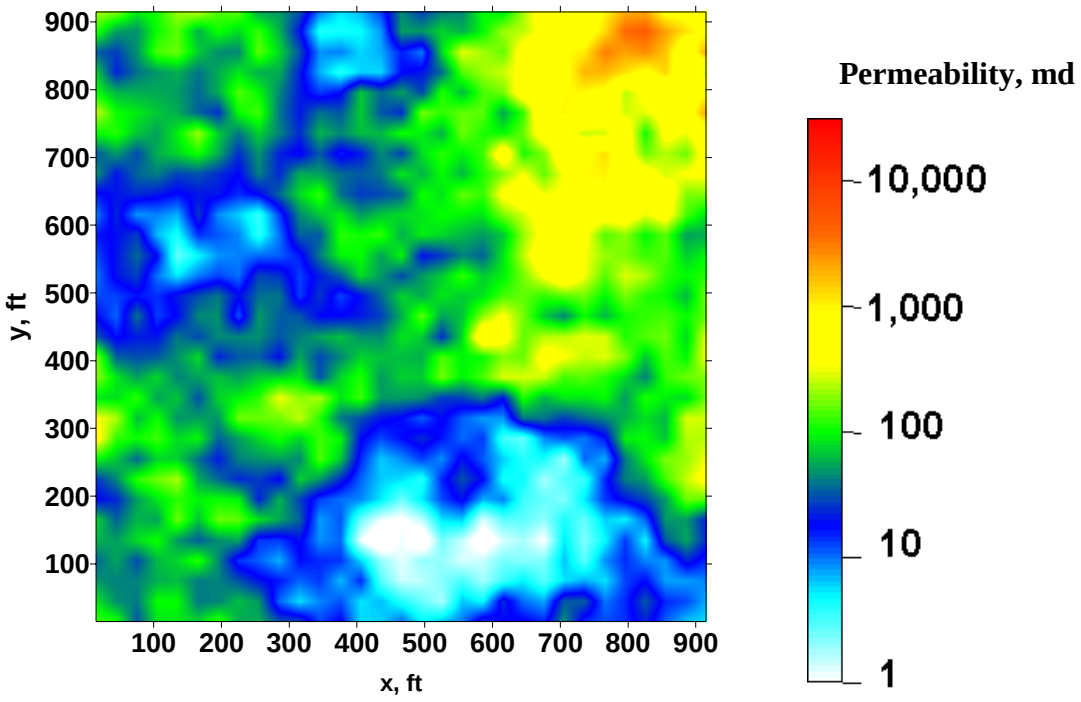

Figure 3.91. Stochastic permeability distribution at the vertical layer Z=3

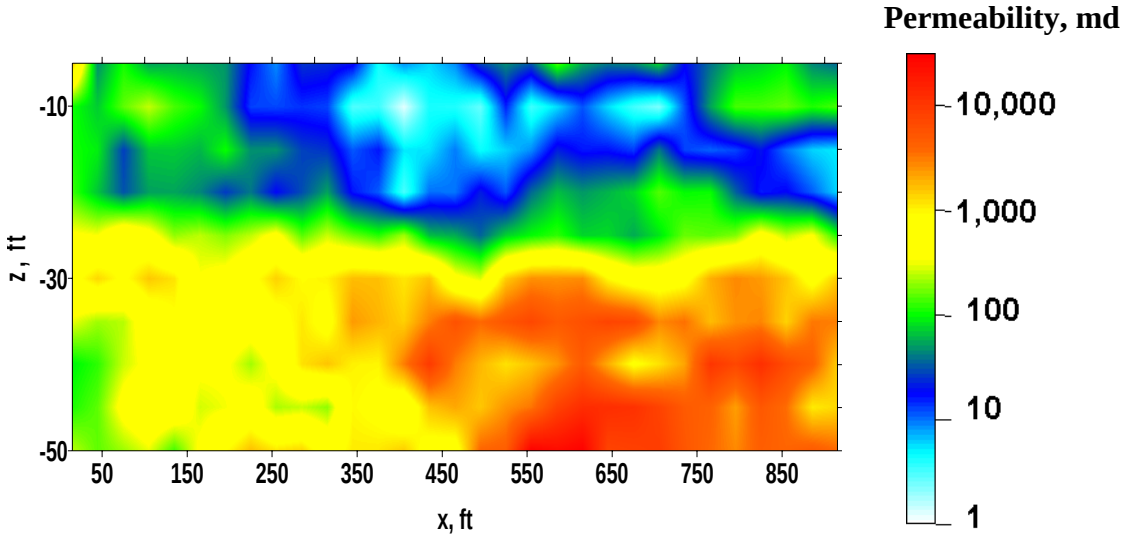

Figure 3.92. Stochastic permeability distribution in horizontal layer, Y=1

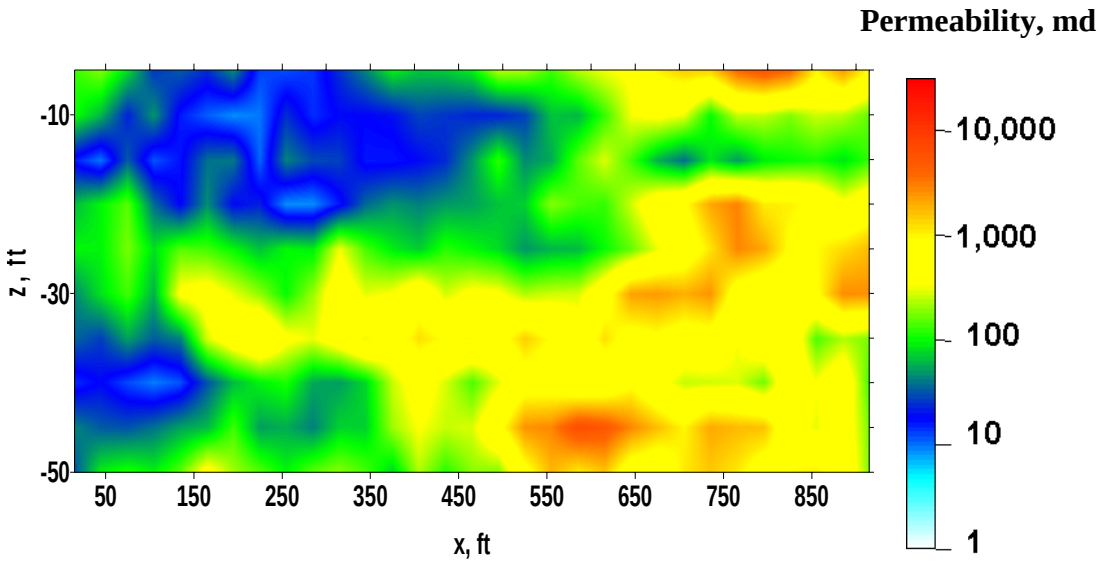

Figure 3.93. Stochastic permeability distribution in horizontal layer, Y=16

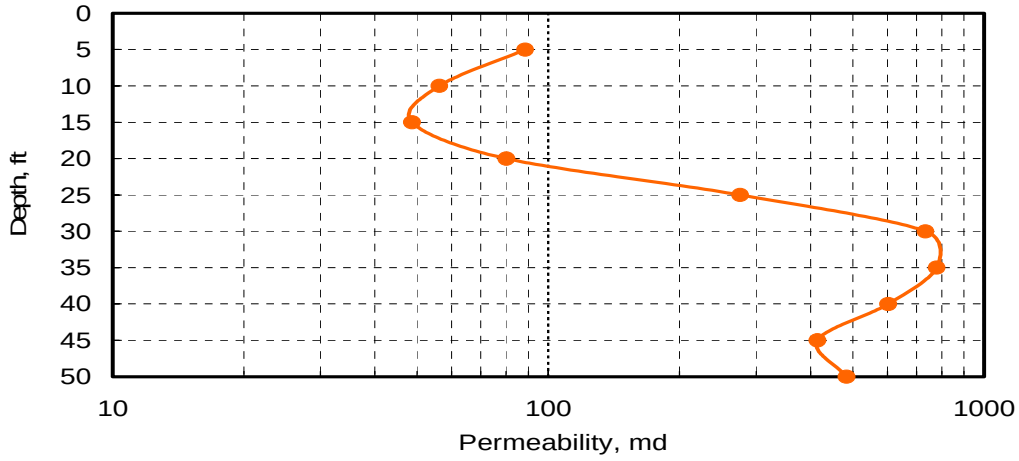

Figure 3.94. Vertical permeability distribution of the three-dimensional layered reservoir with the stochastic permeability field.

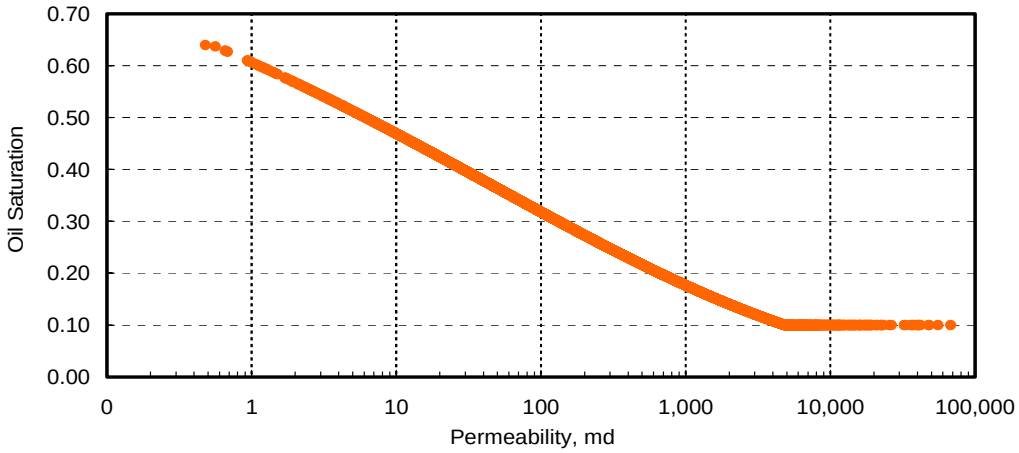

Figure 3.95. Correlation between the permeability and the oil saturation for the model with the stochastic permeability field.

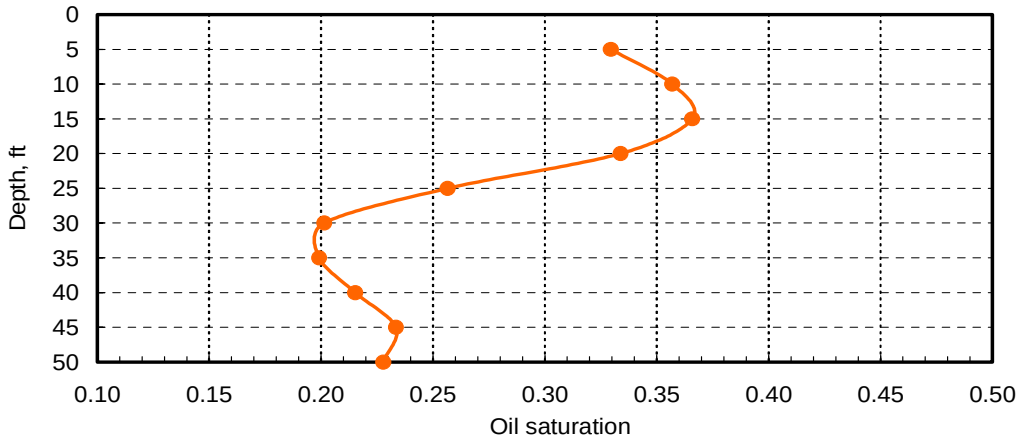

Figure 3.96. Vertical oil saturation distribution of the three-dimensional layered reservoir with the stochastic permeability field.

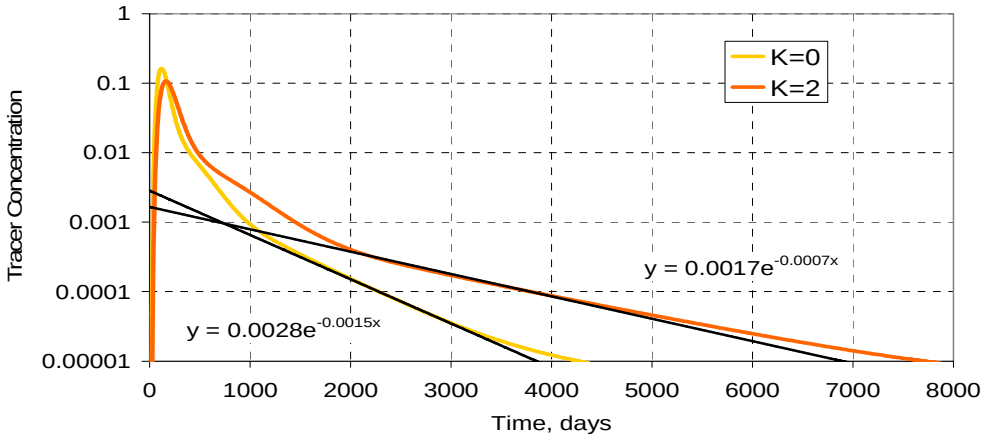

Figure 3.97. Extrapolation of tracer response in the first quadrant for TDL =0.0001 at kv/kh=0.1

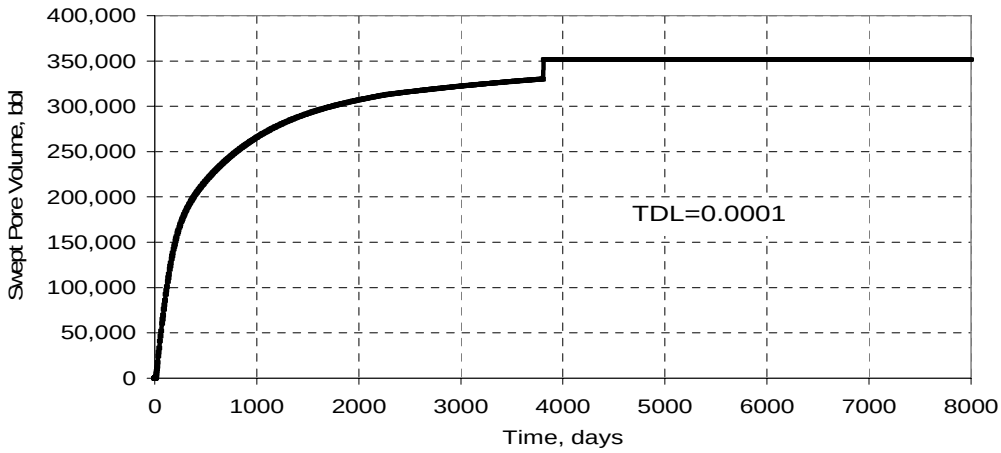

Figure 3.98. MOM swept pore volume estimate in the first quadrant after the extrapolation for TDL =0.0001 at kv/kh=0.1.

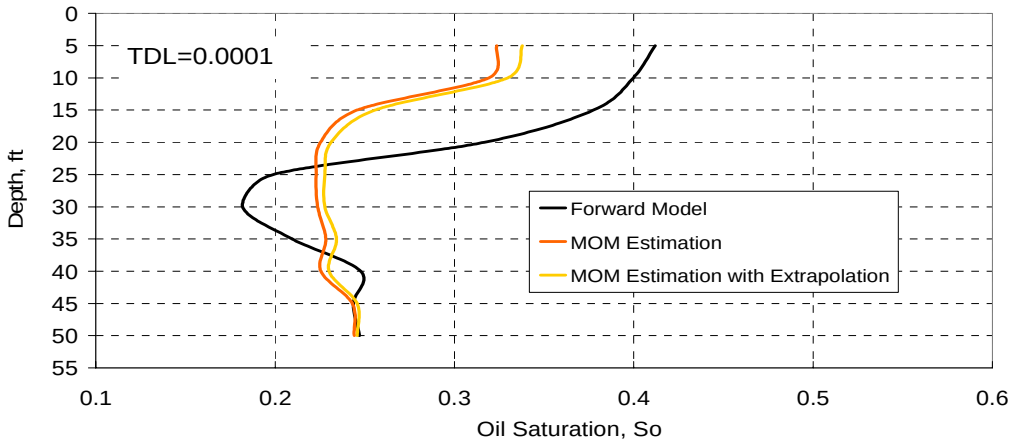

Figure 3.99. MOM oil saturation estimate with and without extrapolation in the first quadrant for TDL=0.0001 at kv/kh=0.1.

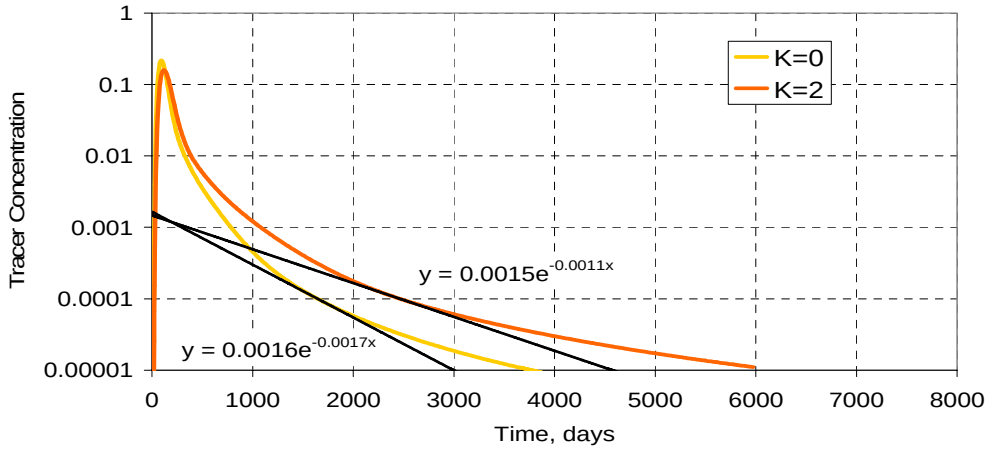

Figure 3.100. Extrapolation of tracer response in the second quadrant for TDL =0.0001 at kv/kh=0.1

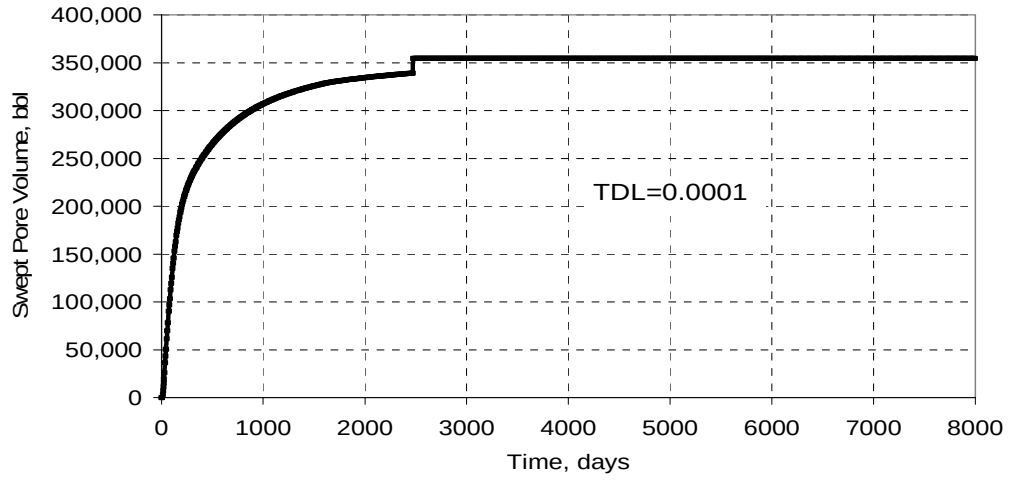

Figure 3.101. MOM swept pore volume estimate in the second quadrant after the extrapolation for TDL =0.0001 at kv/kh=0.1.

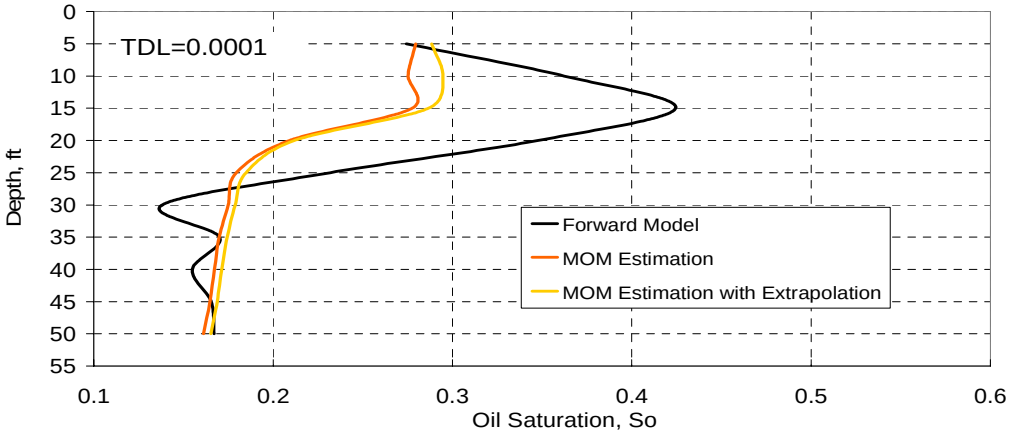

Figure 3.102. MOM oil saturation estimate with and without extrapolation in the second quadrant for TDL=0.0001 at kv/kh=0.1.

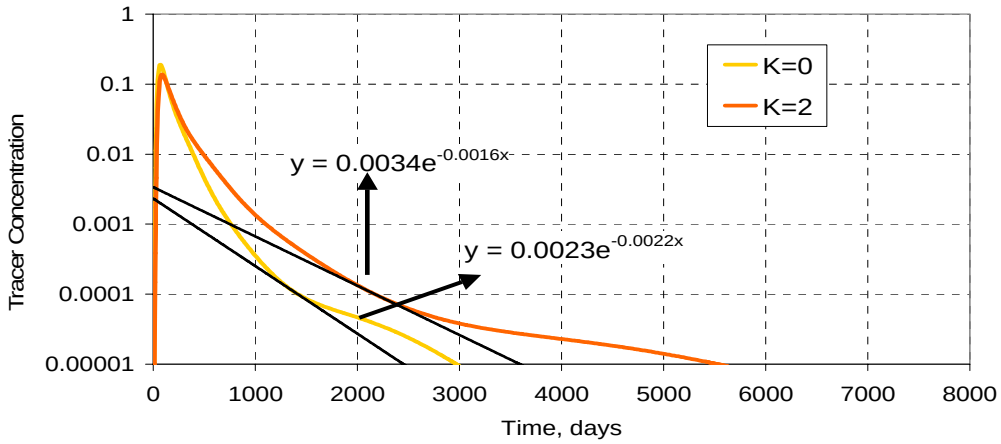

Figure 3.103. Extrapolation of tracer response in the third quadrant for TDL =0.0001 at kv/kh=0.1

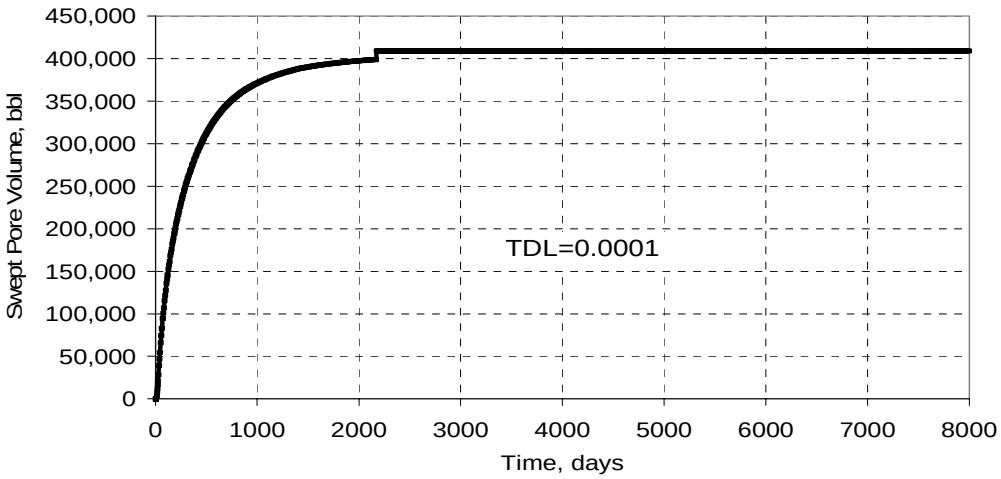

Figure 104. MOM swept pore volume estimate in the third quadrant after the extrapolation for TDL =0.0001 at kv/kh=0.1.

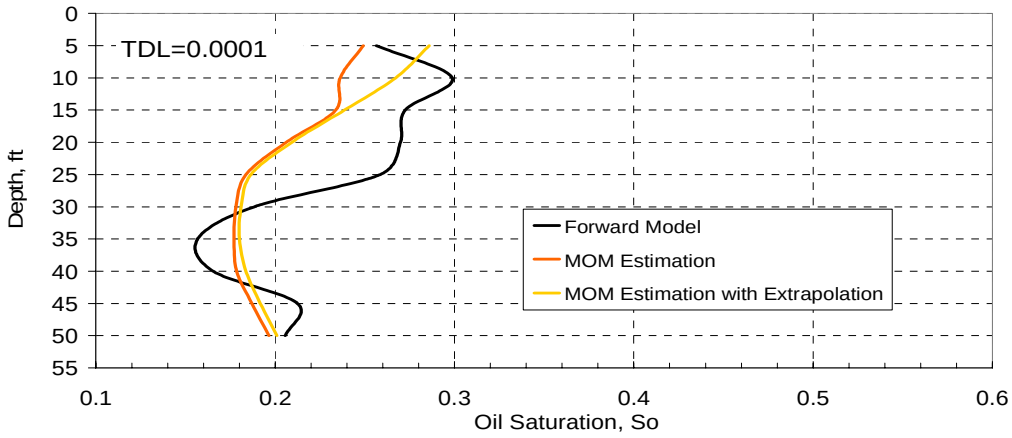

Figure 3.105. MOM oil saturation estimate with and without extrapolation in the third quadrant, for TDL=0.0001 at kv/kh=0.1.

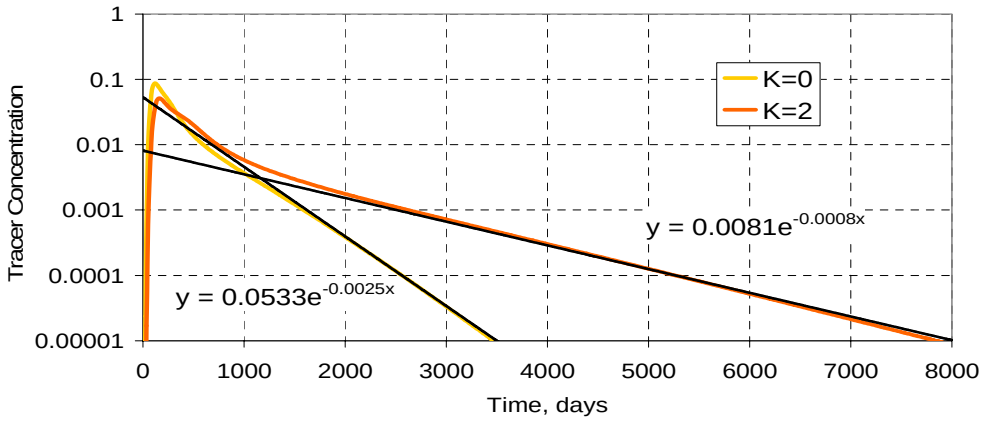

Figure 3.106. Extrapolation of tracer response in the fourth quadrant for TDL =0.0001 at at kv/kh=0.1

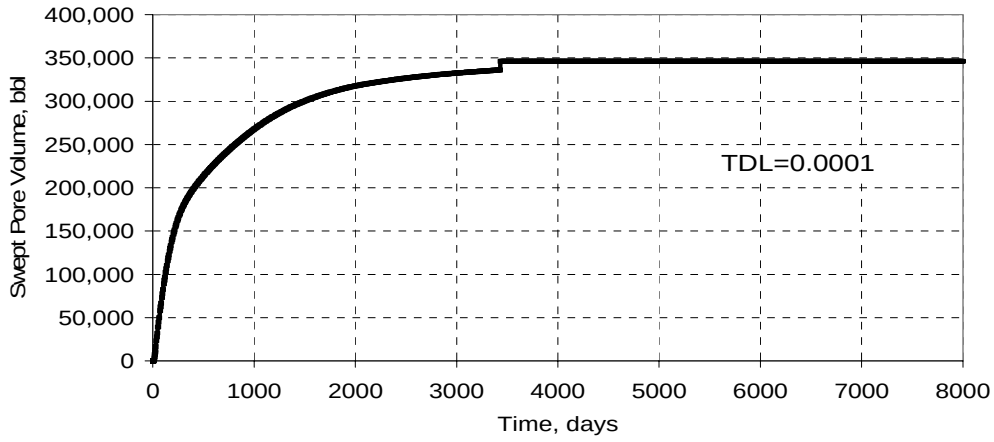

Figure 107. MOM swept pore volume estimate at the fourth quadrant after the extrapolation for TDL =0.0001 at kv/kh=0.1.

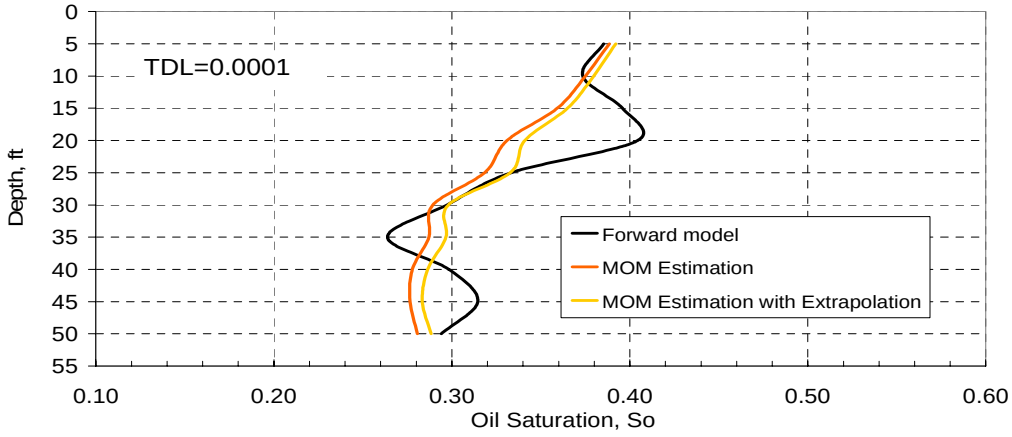

Figure 3.108. MOM oil saturation estimate with and without extrapolation in the fourth quadrant for TDL 0.0001 at kv/kh=0.1.

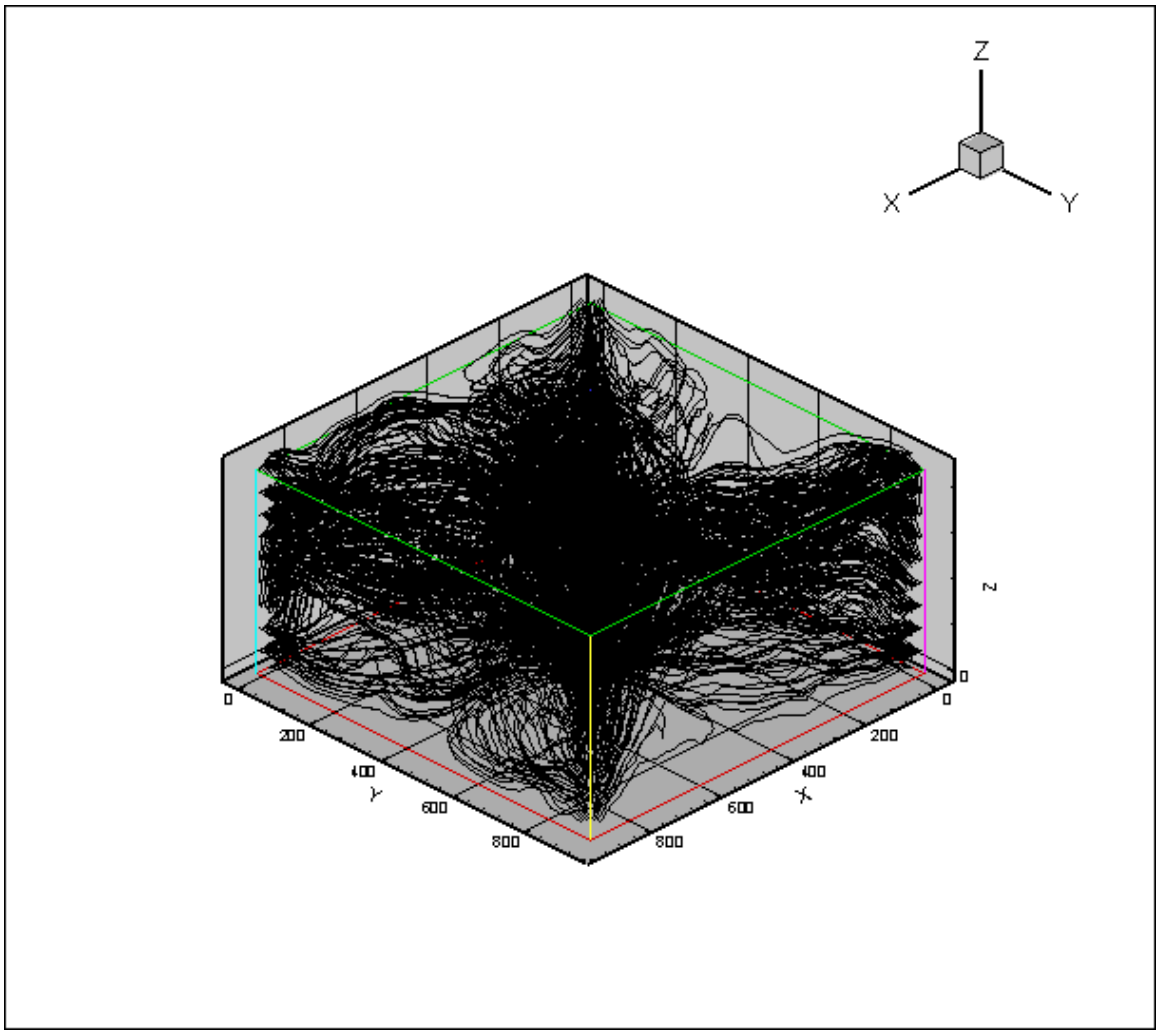

Figure 3.109. Streamline distribution after inverse modeling in the reservoir model with the stochastic permeability field at kv/kh=0.1.

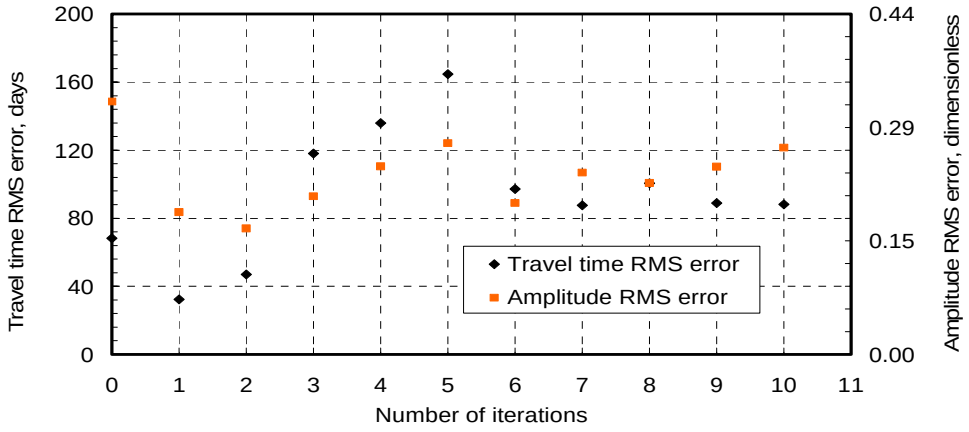

Figure 3.110. RMS error change on travel time and amplitude at the reservoir model with the stochastic permeability field at kv/kh=0.1.

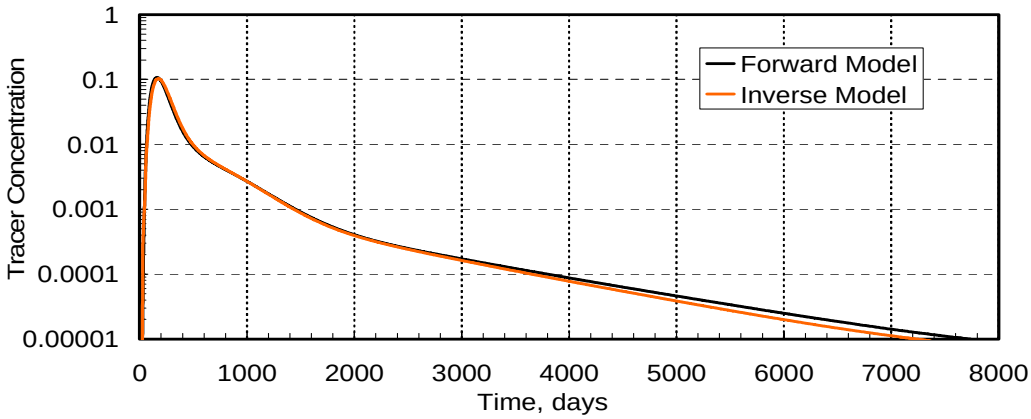

Figure 3.111. Match of the forward model tracer response from the first quadrant with the inverse model for TDL=0.0001 at kv/kh=0.1.

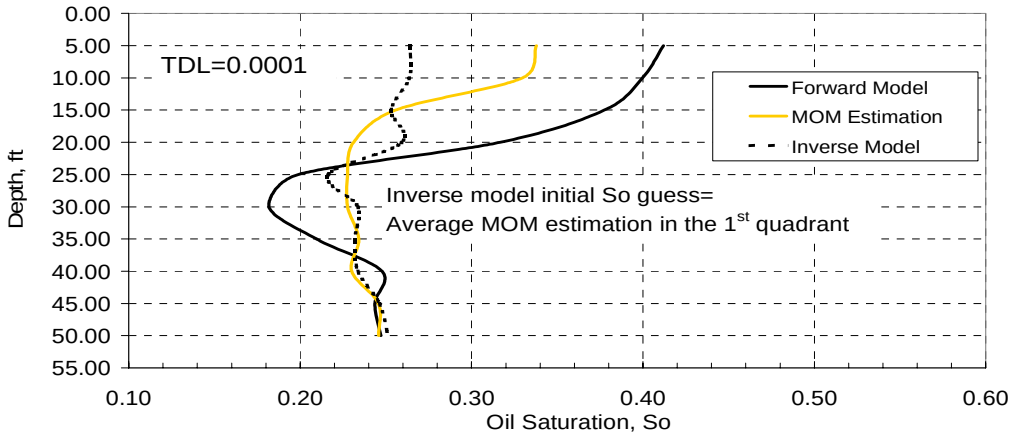

Figure 3.112. Comparison of MOM and inverse model oil saturation estimates in the first quadrant for TDL=0.0001 at kv/kh=0.1.

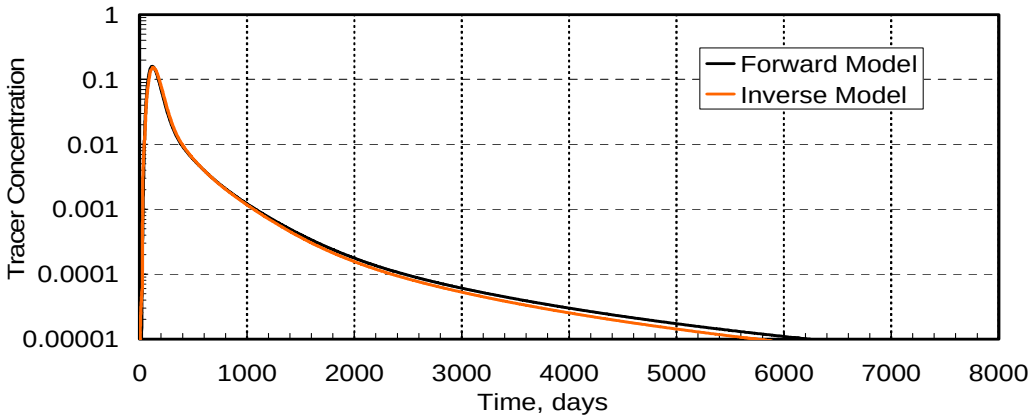

Figure 3.113. Match of the forward model tracer response from the second quadrant with the inverse model for TDL=0.0001 at kv/kh=0.1.

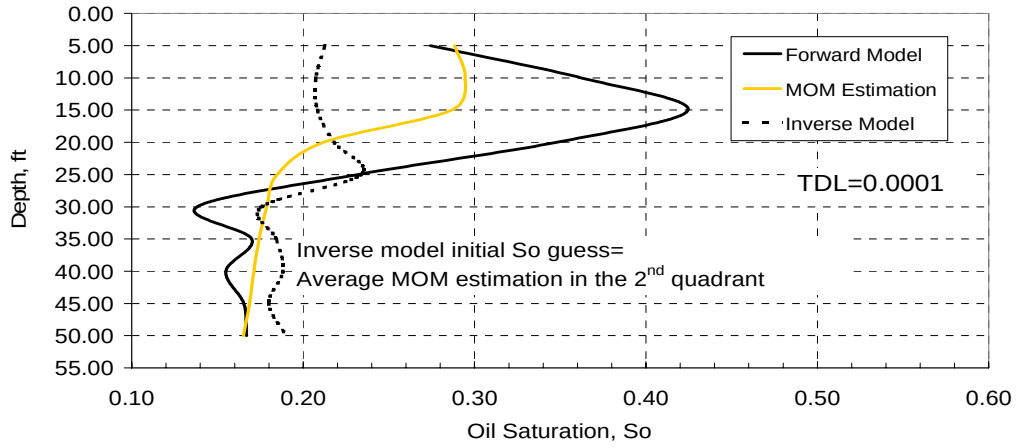

Figure 3.114. Comparison of MOM and inverse model oil saturation estimates in the second quadrant for TDL=0.0001 at kv/kh=0.1.

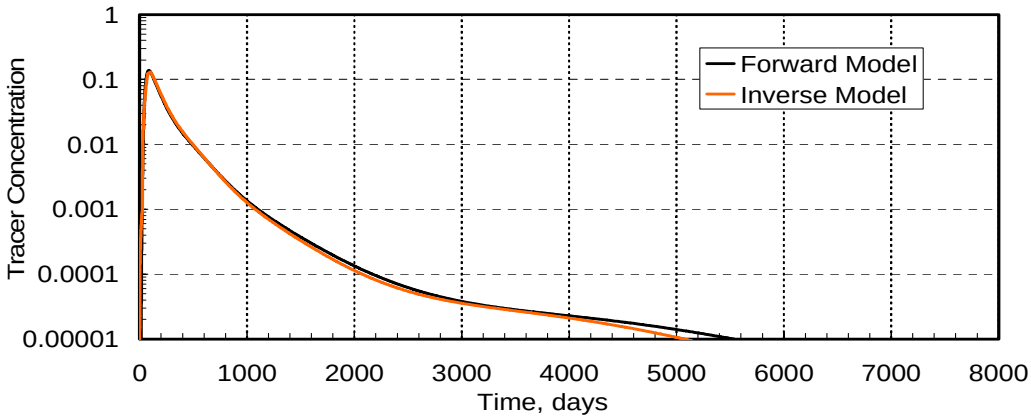

Figure 3.115. Match of the forward model tracer response from the third quadrant with the inverse model for TDL=0.0001 at kv/kh=0.1.

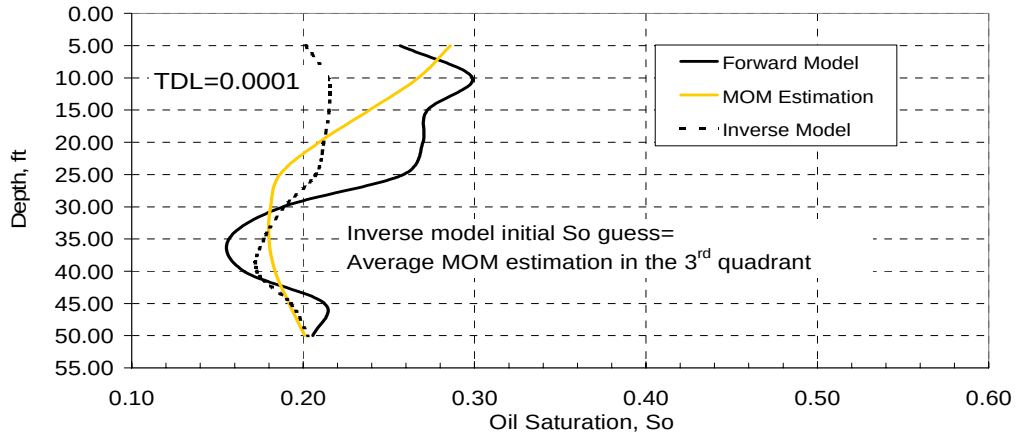

Figure 3.116. Comparison of MOM and inverse model oil saturation estimates in the third quadrant for TDL=0.0001 at kv/kh=0.1.

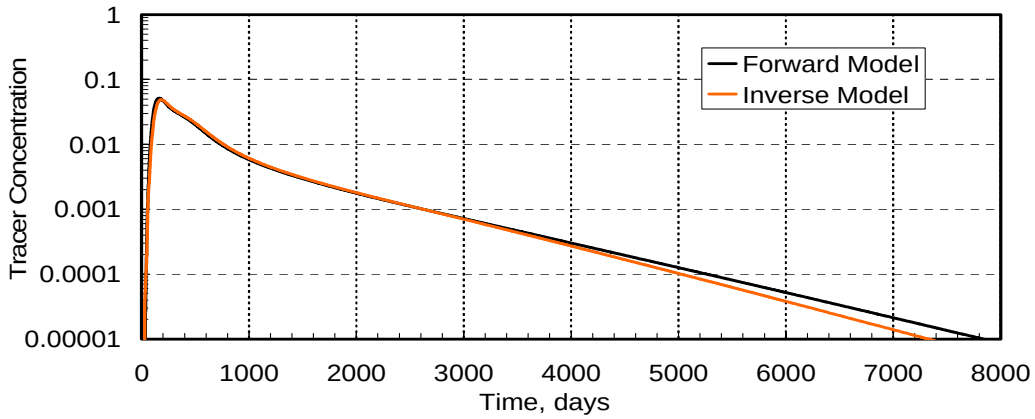

Figure 3.117. Match of the forward model tracer response from the fourth quadrant with the inverse model for TDL=0.0001 at kv/kh=0.1.

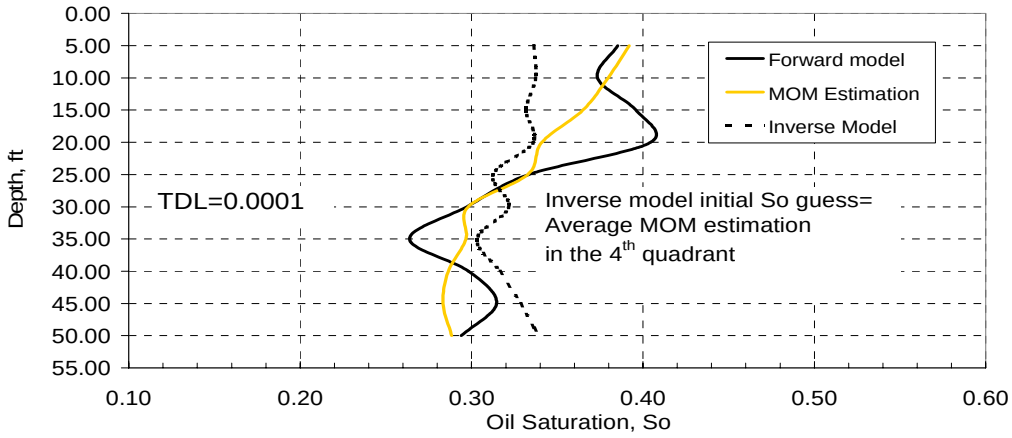

Figure 3.118. Comparison of MOM and inverse model oil saturation estimates in the fourth quadrant for TDL=0.0001 at kv/kh=0.1.

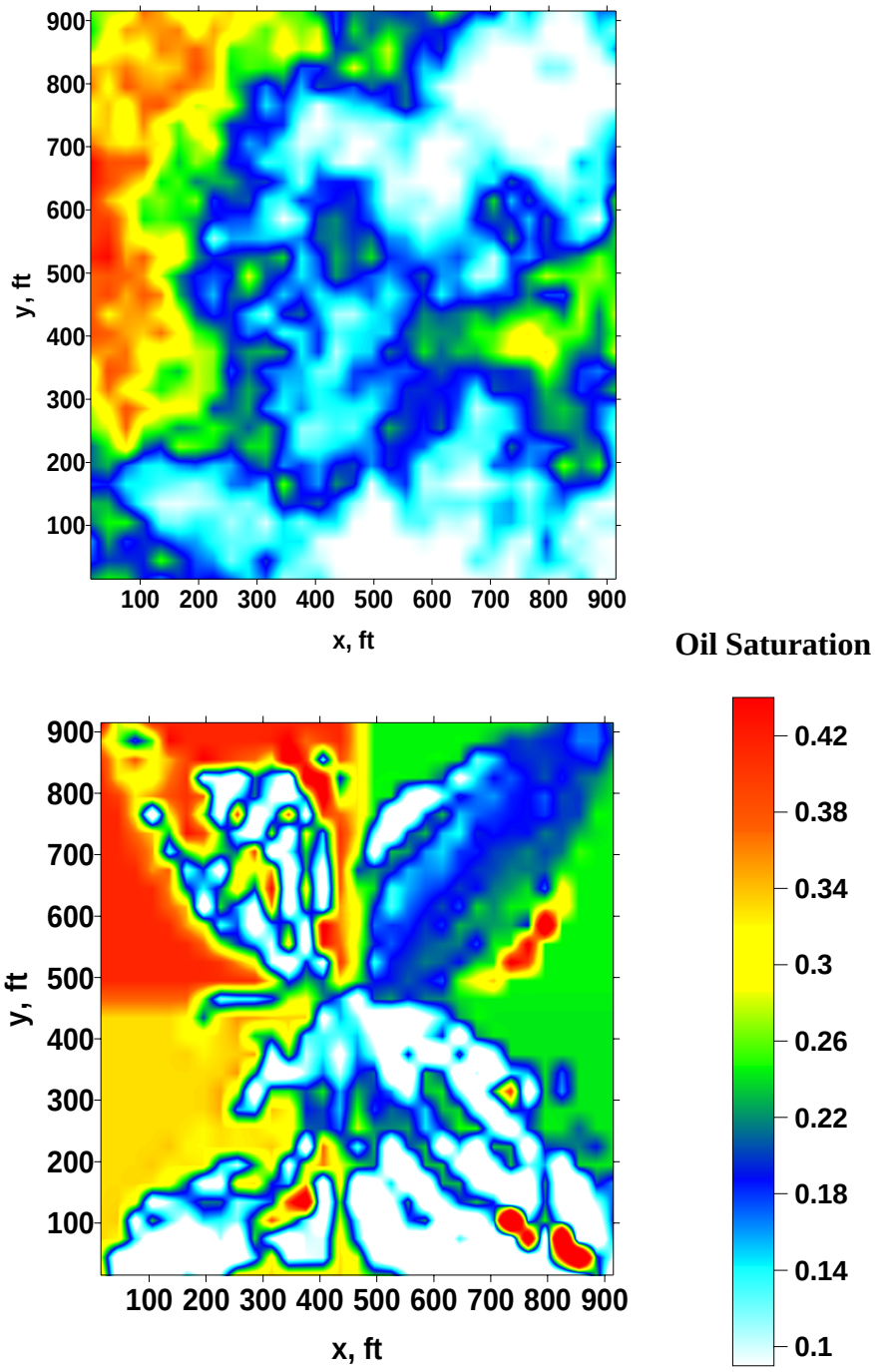

Figure 3.119 Comparison of forward model oil saturation distribution (top image) with inverse model oil saturation distribution (bottom image) in layer Z=7.

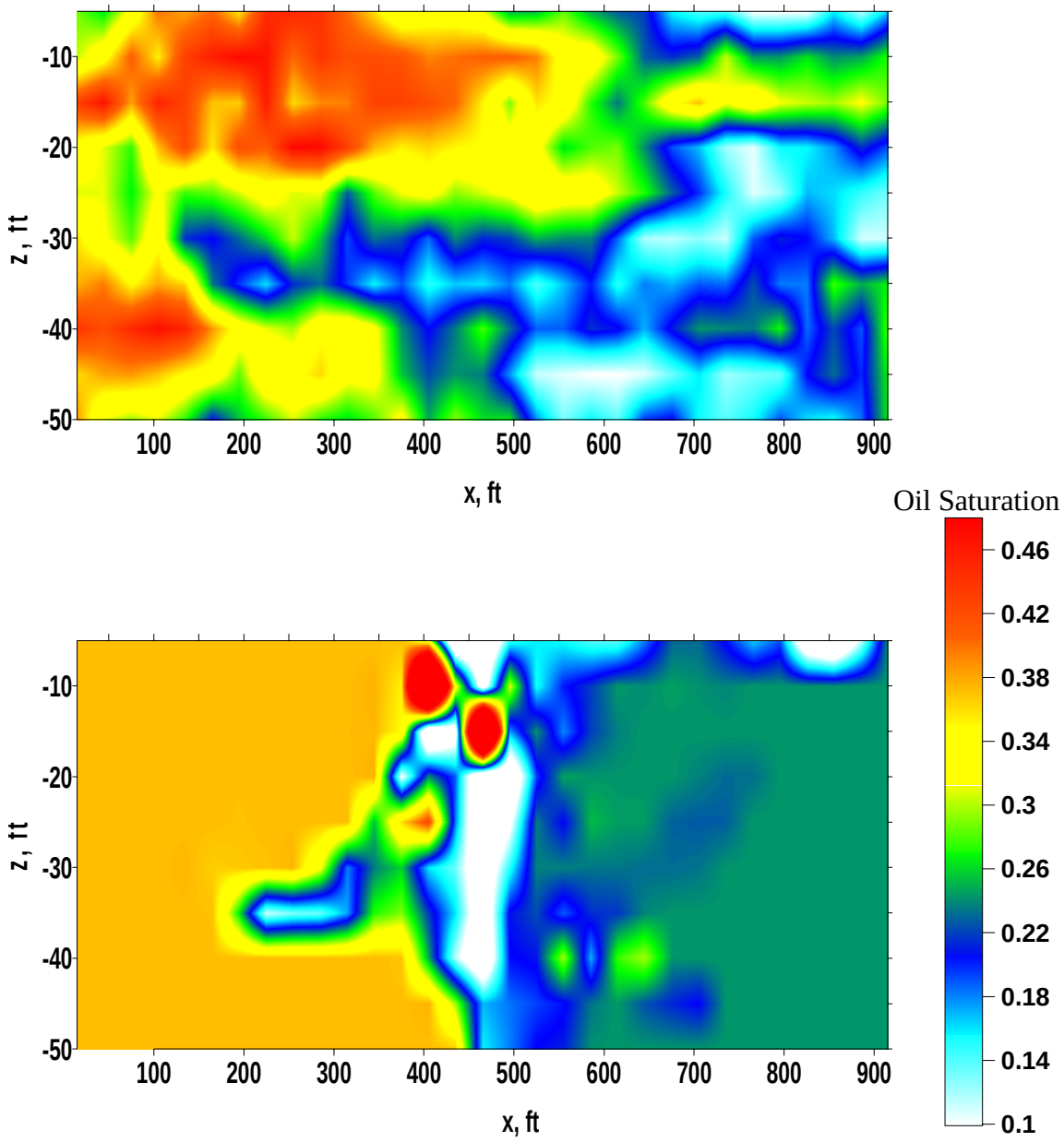

Figure 3.120 Comparison of forward model oil saturation distribution (top image) with inverse model oil saturation distribution (bottom image) in layer Y=16.

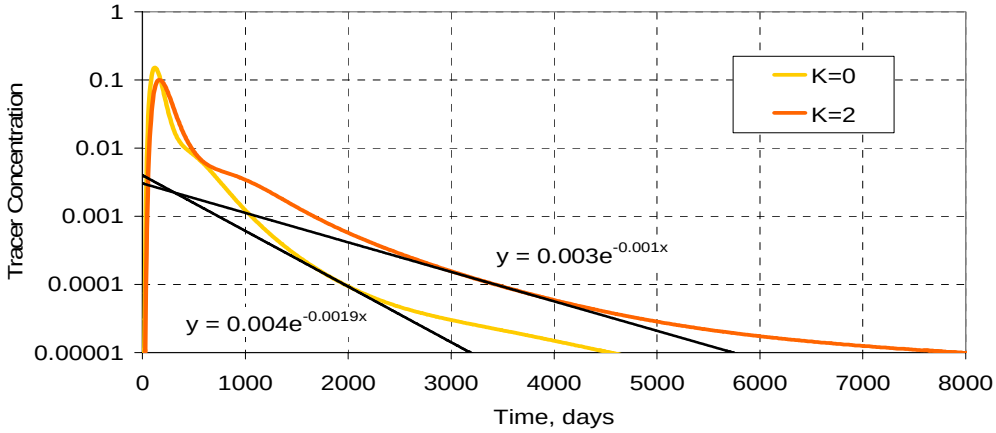

Figure 3.121. Extrapolation of tracer response from the first quadrant for TDL =0.0001 at kv/kh=0.01

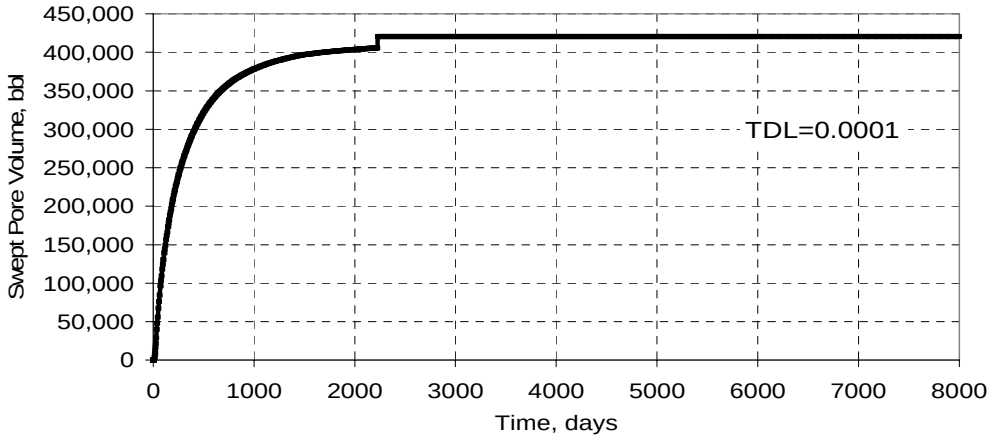

Figure 3.122. MOM swept pore volume estimate in the first quadrant after the extrapolation for TDL =0.0001 at kv/kh=0.01.

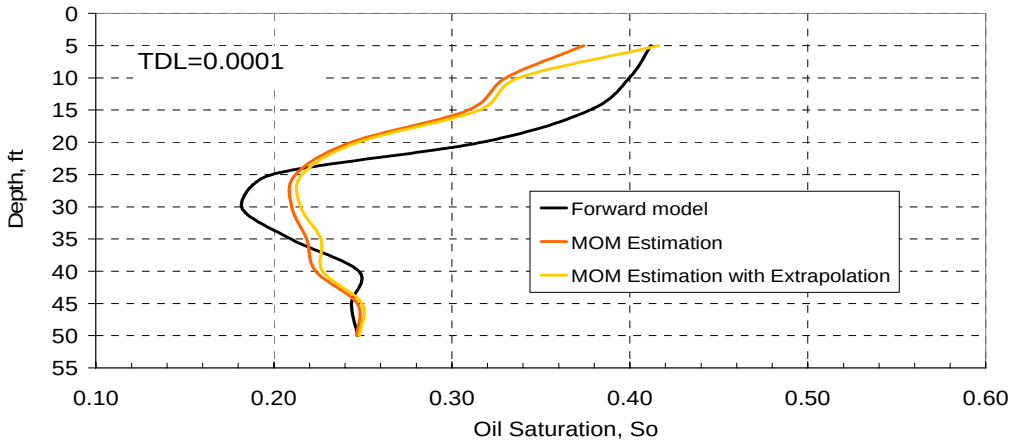

Figure 3.123. MOM oil saturation estimate with and without extrapolation in the first quadrant for TDL=0.0001 at kv/kh=0.01.

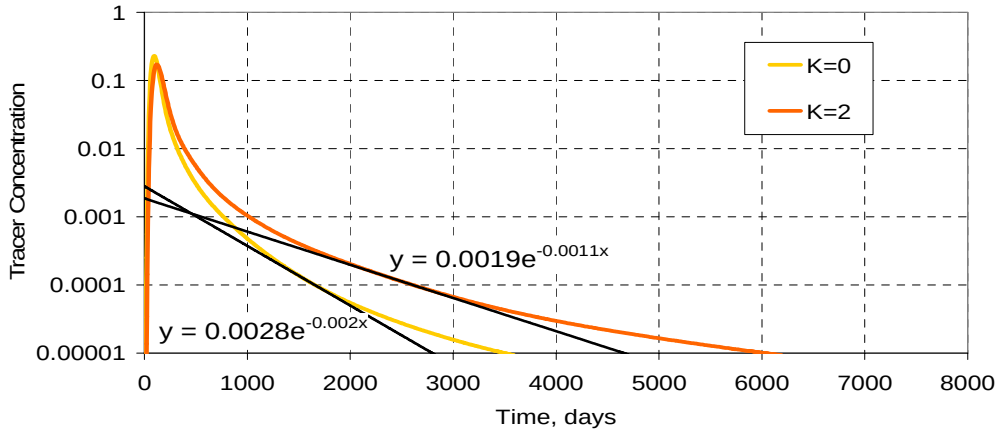

Figure 3.124. Extrapolation of tracer response from the second quadrant for TDL =0.0001 at kv/kh=0.01

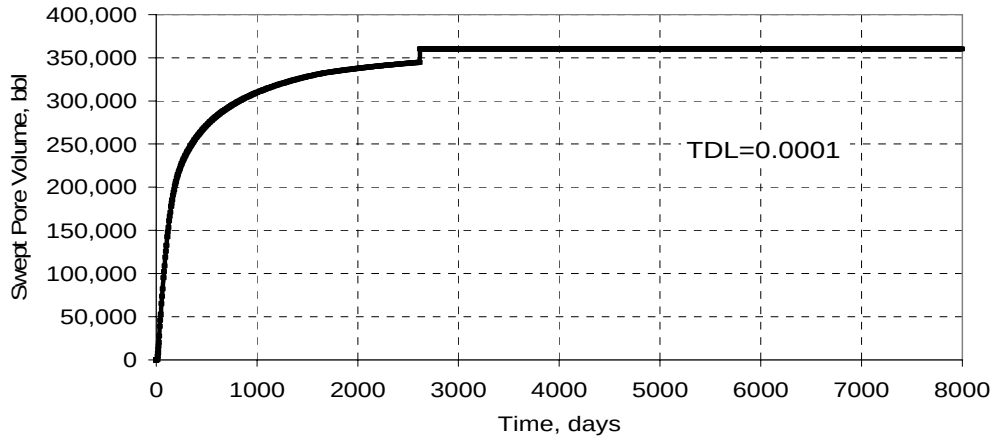

Figure 3.125. MOM swept pore volume estimate in the second quadrant after the extrapolation for TDL =0.0001 at kv/kh=0.01.

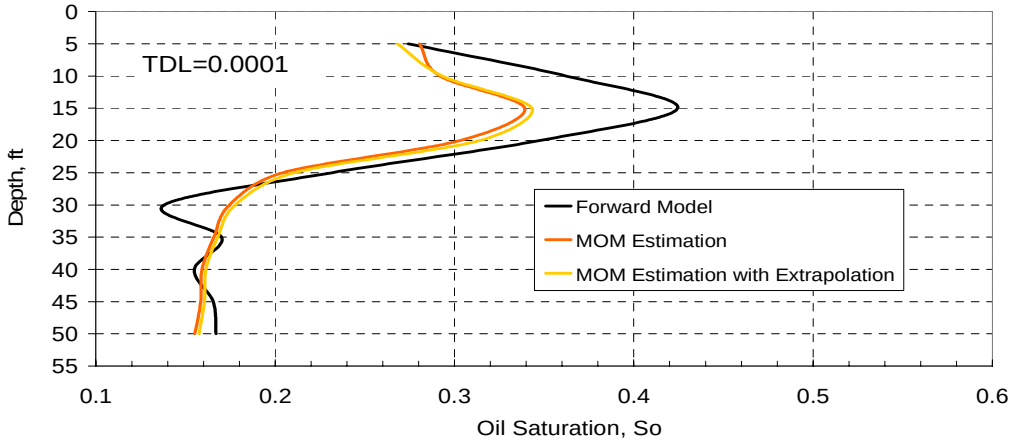

Figure 3.126. MOM oil saturation estimate with and without extrapolation in the second quadrant for TDL=0.0001 at kv/kh=0.01.

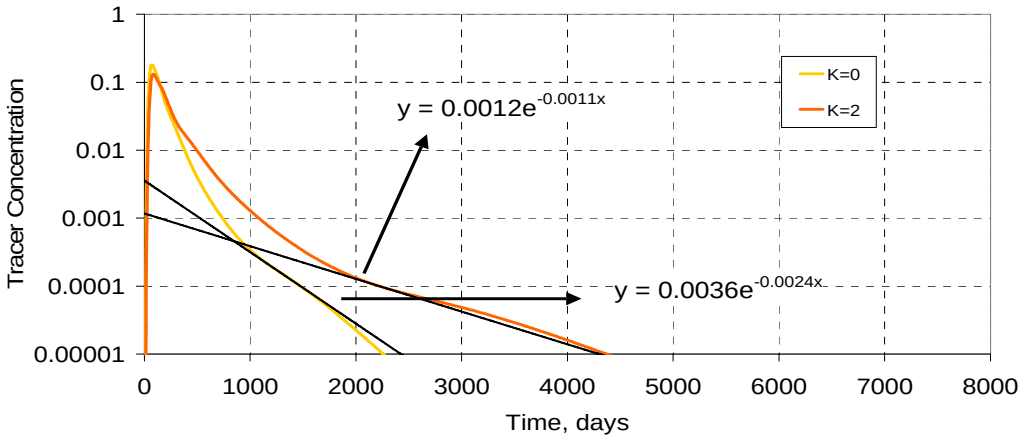

Figure 3.127. Extrapolation of tracer response from the third quadrant for TDL =0.0001 at kv/kh=0.01

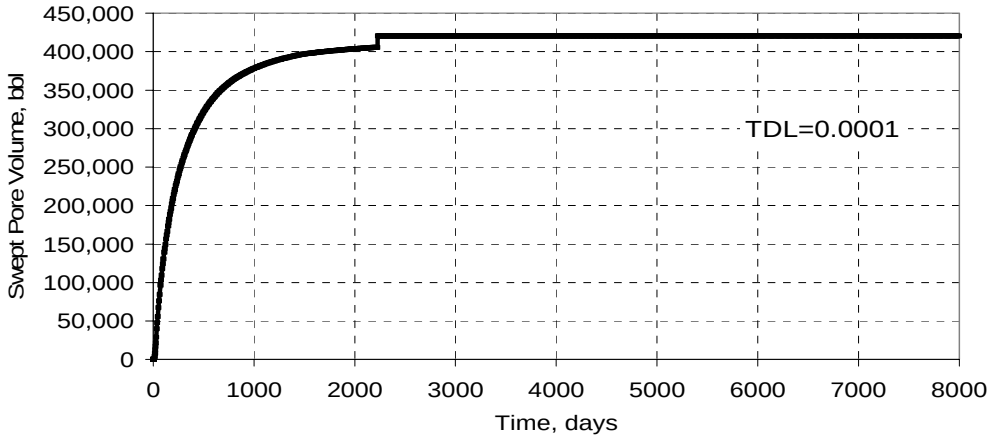

Figure 3.128. MOM swept pore volume estimate in the third quadrant after the extrapolation for TDL =0.0001 at kv/kh=0.01.

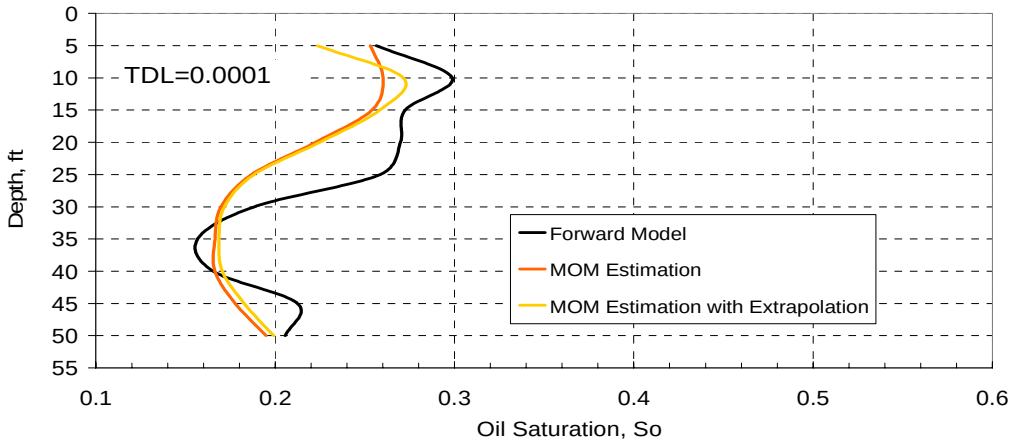

Figure 3.129. MOM oil saturation estimate with and without extrapolation in the third quadrant for TDL=0.0001 at kv/kh=0.01.

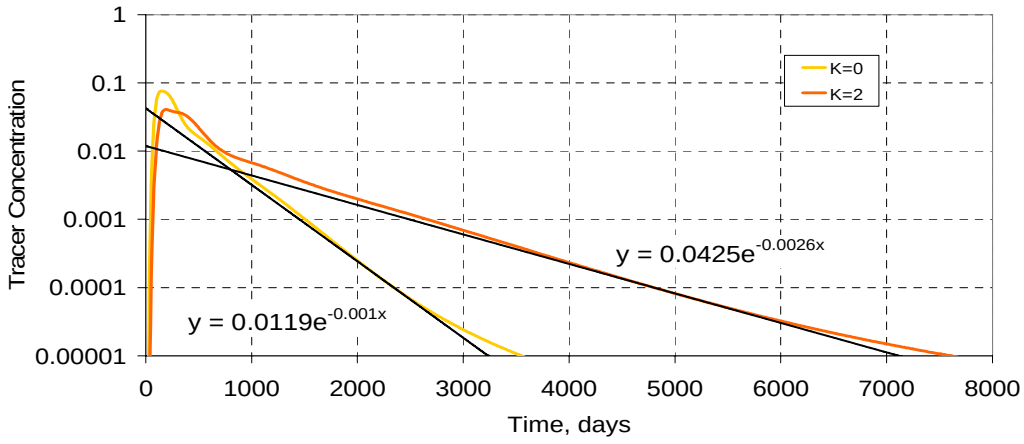

Figure 3.130. Extrapolation of tracer response from the fourth quadrant for TDL =0.0001 at kv/kh=0.01

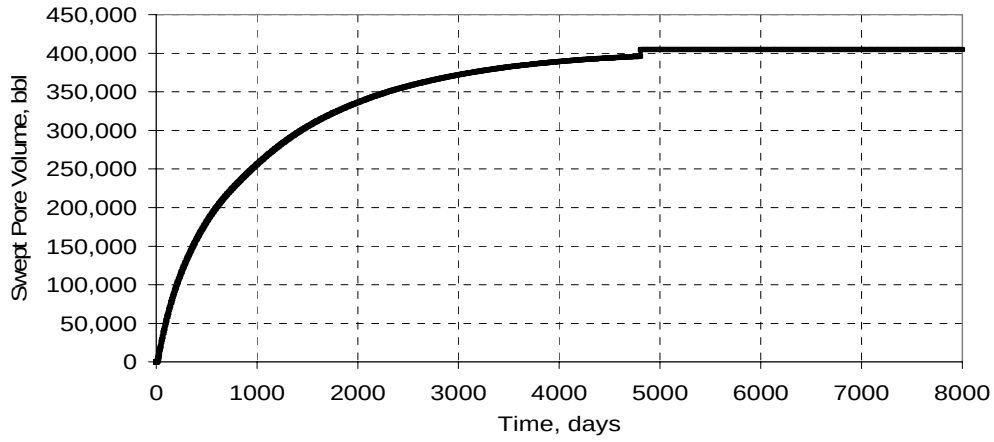

Figure 3.131. MOM swept pore volume estimate in the fourth quadrant after the extrapolation fourth TDL =0.0001 at kv/kh=0.01.

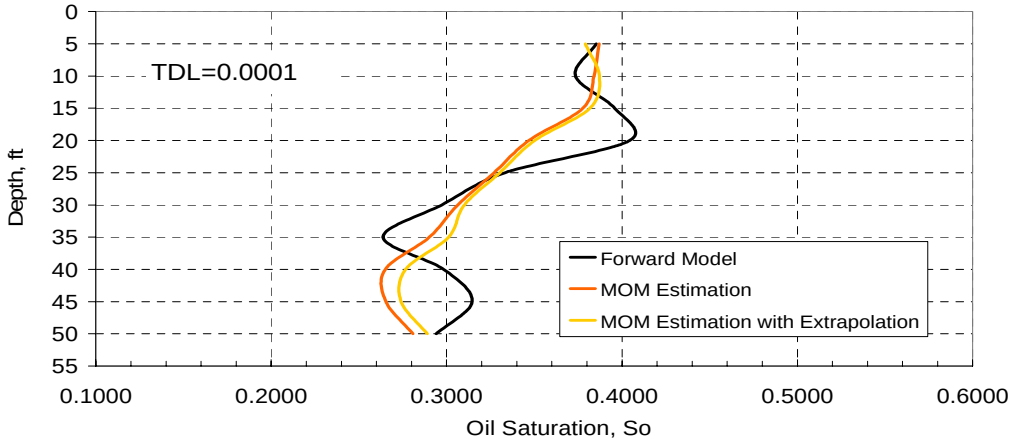

Figure 3.132. MOM oil saturation estimate with and without extrapolation in the fourth quadrant for TDL=0.0001 at kv/kh=0.01.

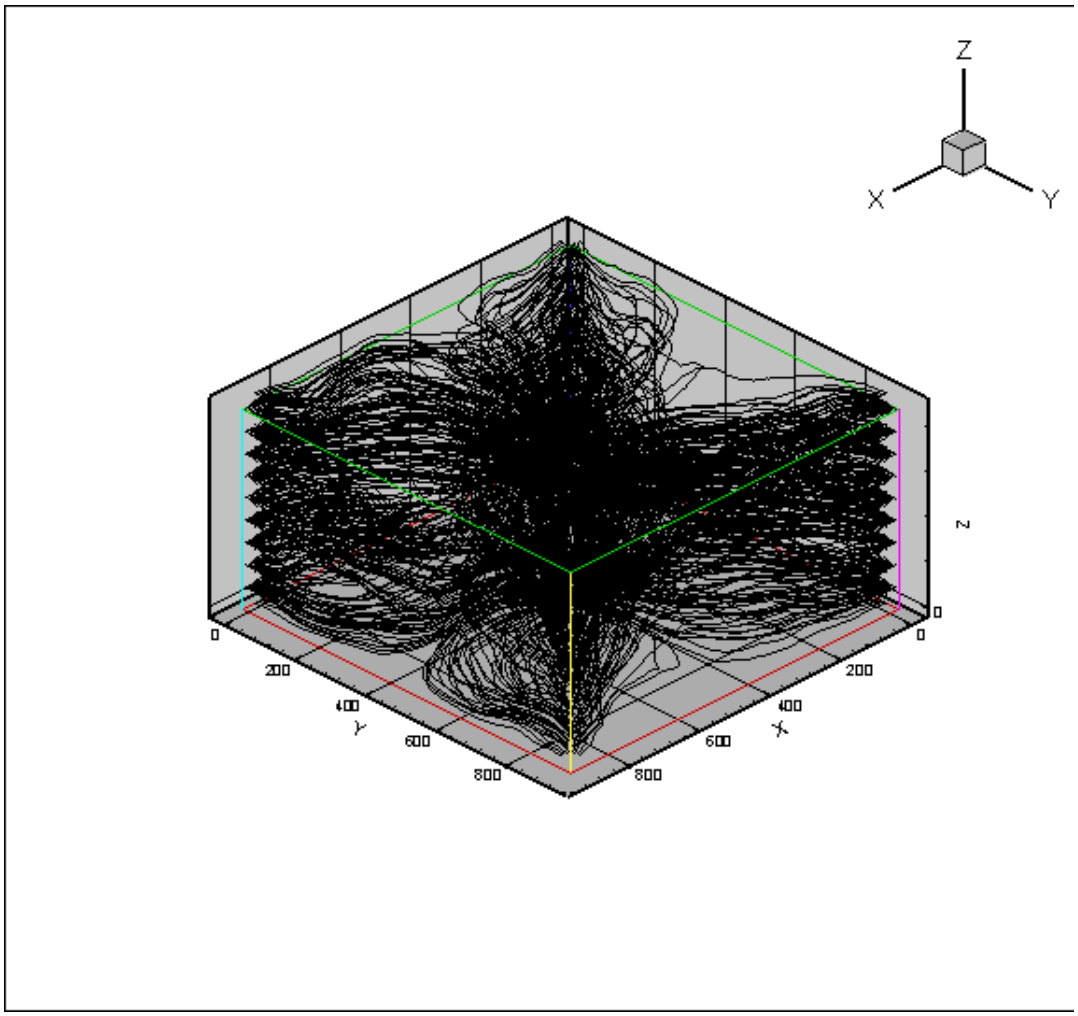

Figure 3.133. Streamline distribution after inverse modeling in the reservoir model with the stochastic permeability field at kv/kh=0.01.

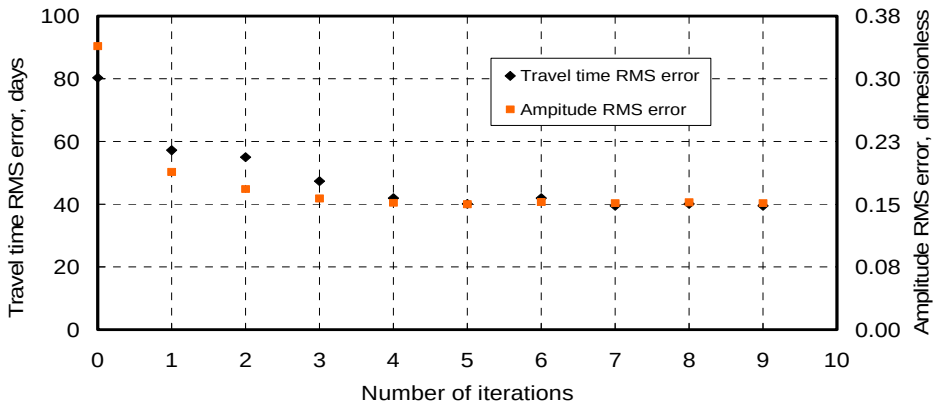

Figure 3.134. RMS error change on travel time and amplitude in the reservoir model with the stochastic permeability field at kv/kh=0.01.

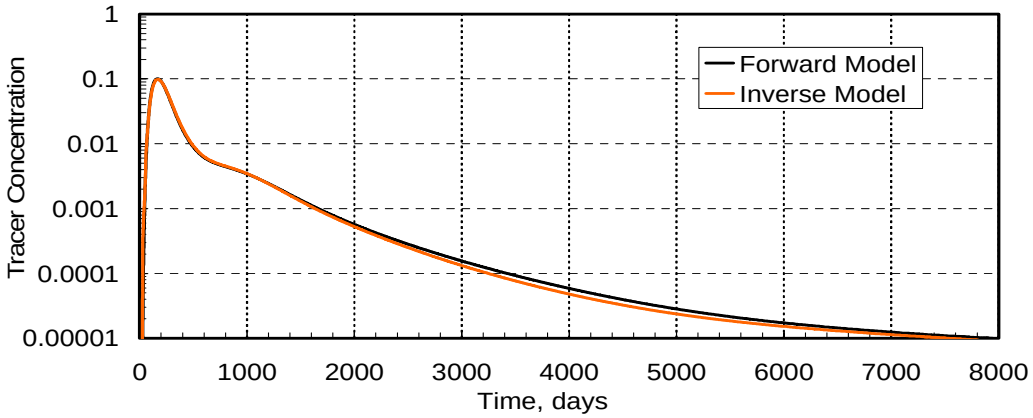

Figure 3.135. Match of the forward model tracer response from the first quadrant with the inverse model for TDL=0.0001 at kv/kh=0.01.

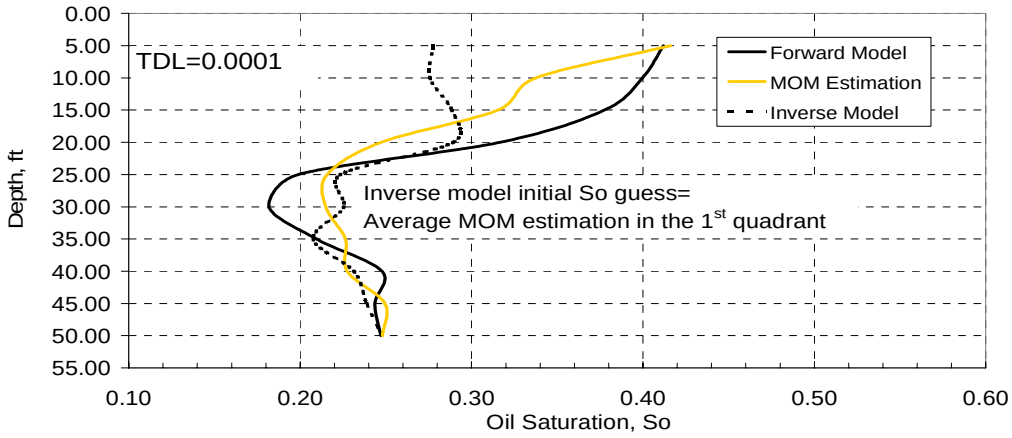

Figure 3.136. Comparison of MOM and inverse model oil saturation estimates in the first quadrant for TDL=0.0001 at kv/kh=0.01.

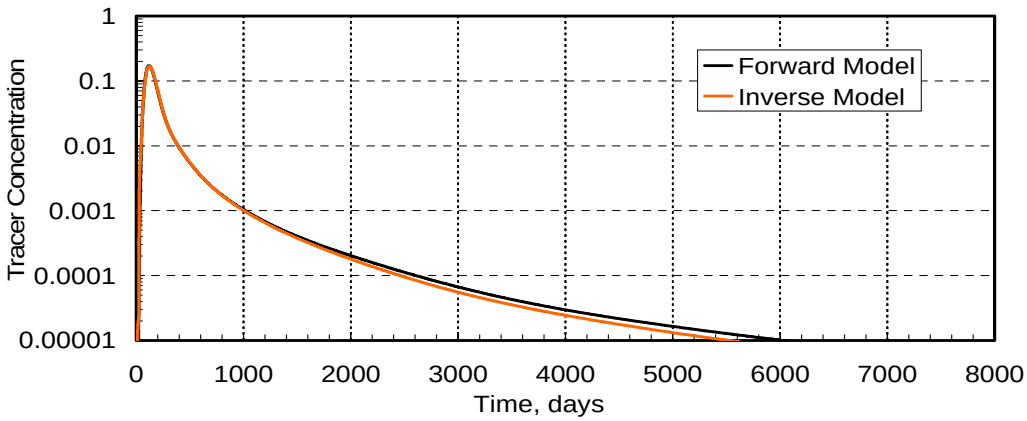

Figure 3.137. Match of the forward model tracer response from the second quadrant with the inverse model for TDL=0.0001 atkv/kh=0.01.

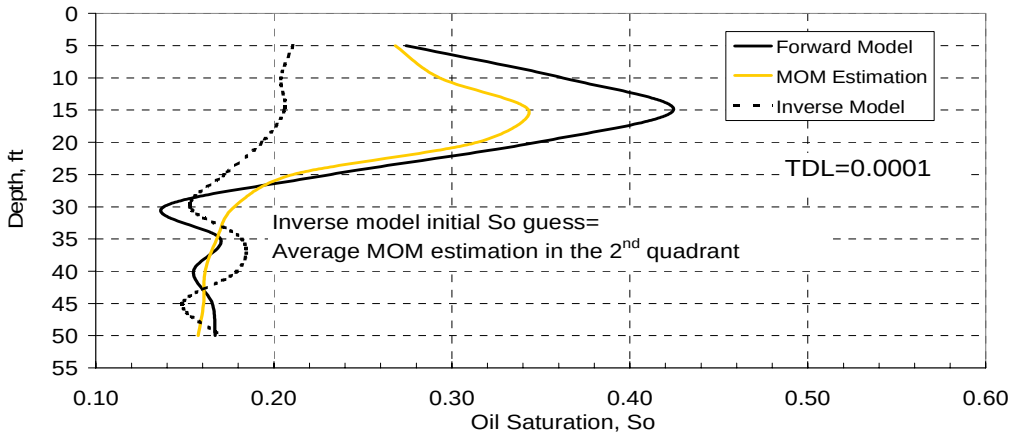

Figure 3.138. Comparison of MOM and inverse model oil saturation estimates in the second quadrant for TDL=0.0001 at kv/kh=0.01.

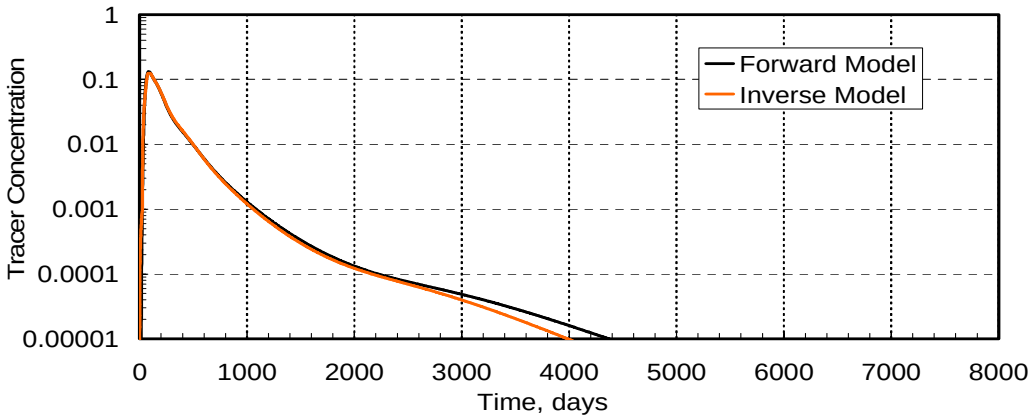

Figure 3.139. Match of the forward model tracer response from the third quadrant with the inverse model for TDL=0.0001 at kv/kh=0.01.

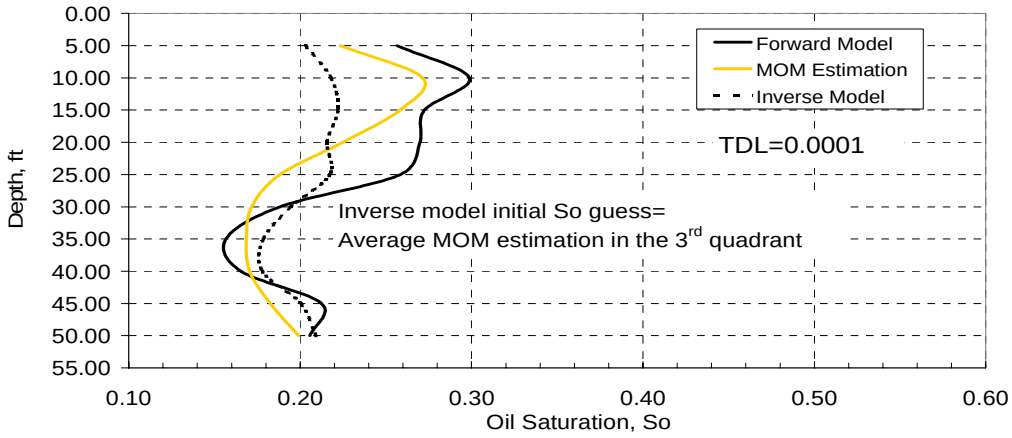

Figure 3.140. Comparison of MOM and inverse model oil saturation estimates in the third quadrant for TDL=0.0001 at kv/kh=0.01.

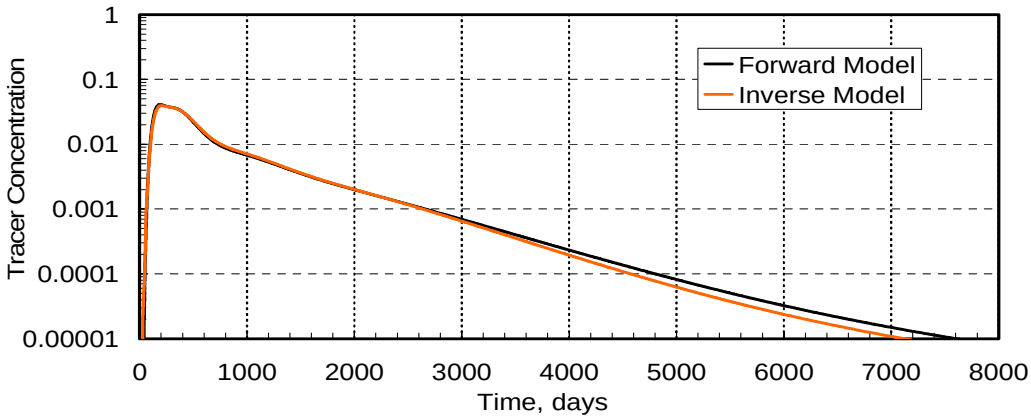

Figure 3.141. Match of the forward model tracer response from the fourth quadrant with the inverse model for TDL=0.0001 at kv/kh=0.01.

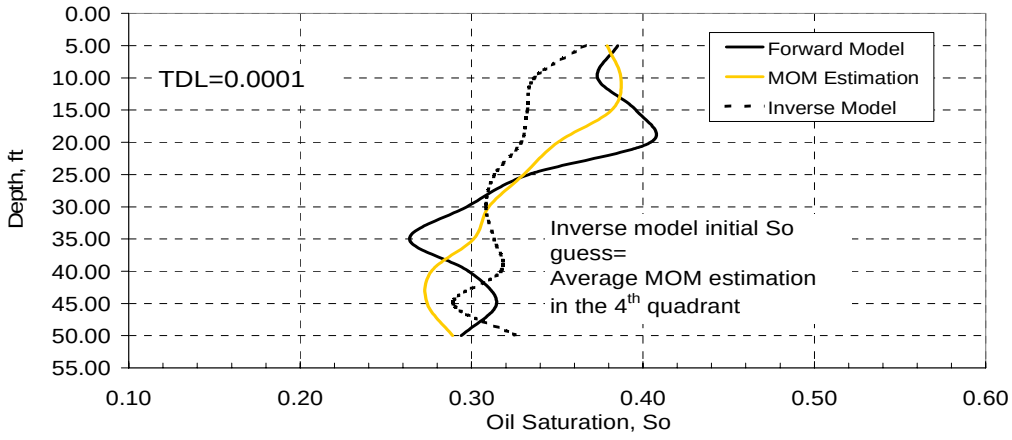

Figure 3.142. Comparison of MOM and inverse model oil saturation estimates in the fourth quadrant for TDL=0.0001 at kv/kh=0.01.

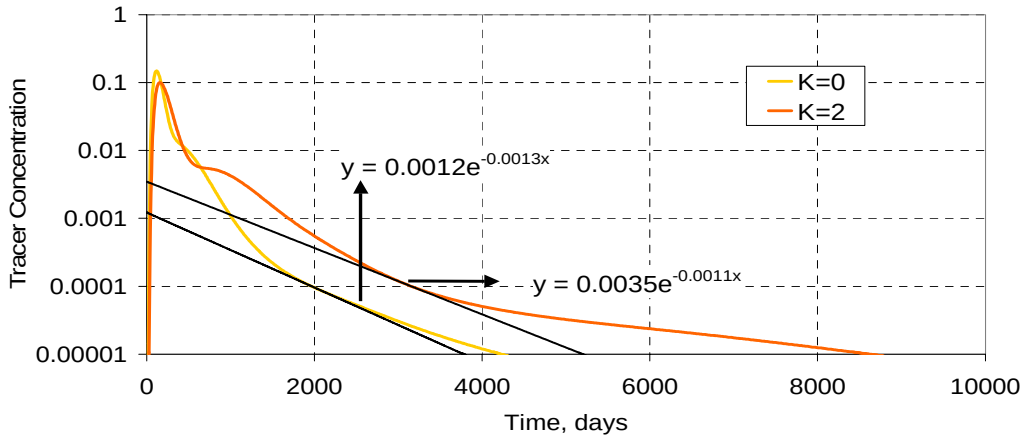

Figure 3.143. Extrapolation of tracer response in the first quadrant for TDL =0.0001 at kv/kh=0.001

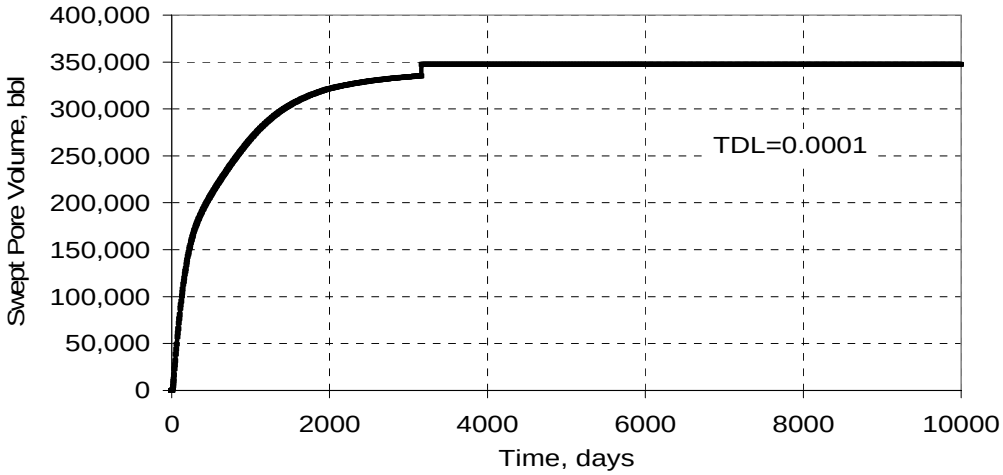

Figure 3.144. MOM swept pore volume estimate in the first quadrant after the extrapolation for TDL =0.0001 at kv/kh=0.001.

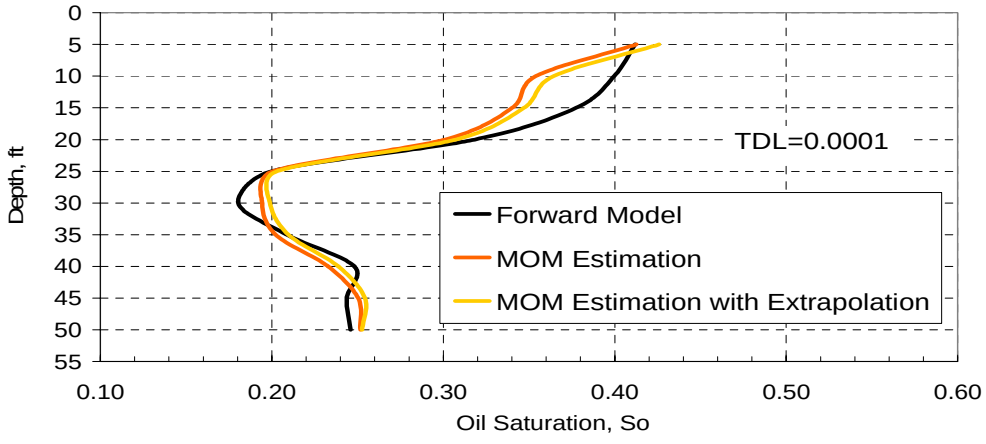

Figure 3.145. MOM oil saturation estimate with and without extrapolation in the first quadrant for TDL=0.0001 at kv/kh=0.001.

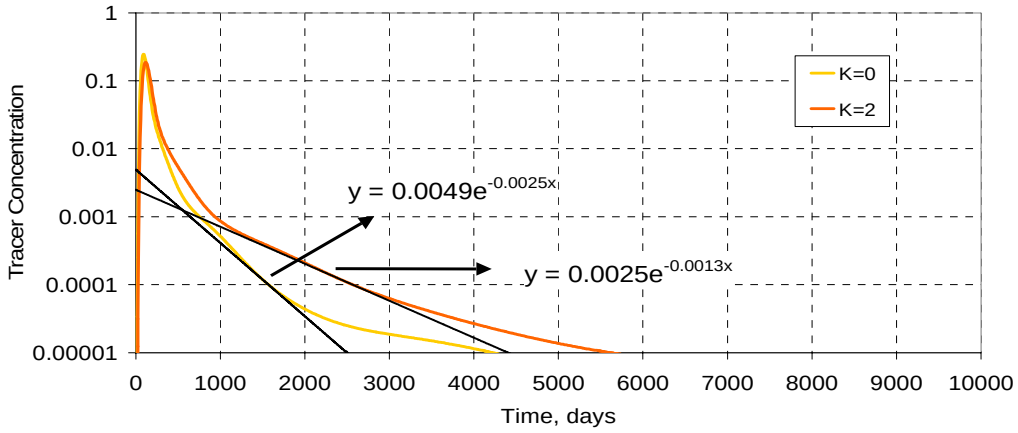

Figure 3.146. Extrapolation of tracer response in the second quadrant for TDL =0.0001 at kv/kh=0.001

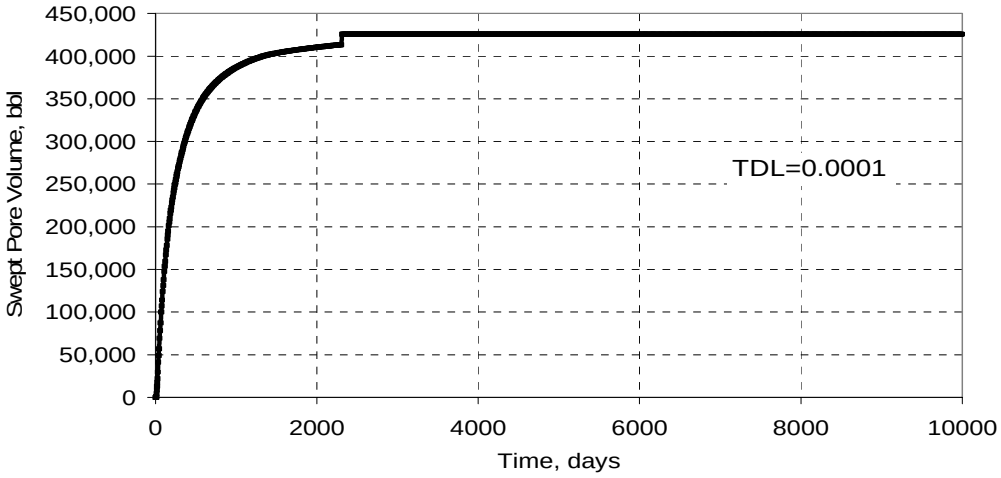

Figure 3.147. MOM swept pore volume estimate in the second quadrant for TDL =0.0001 at kv/kh=0.001.

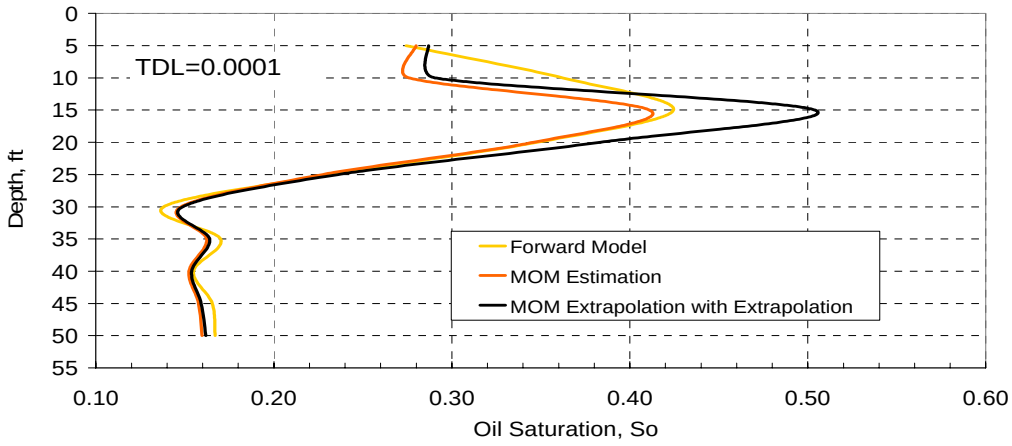

Figure 3.148. MOM oil saturation estimate with and without extrapolation in the second quadrant for TDL =0.0001 at kv/kh=0.001.

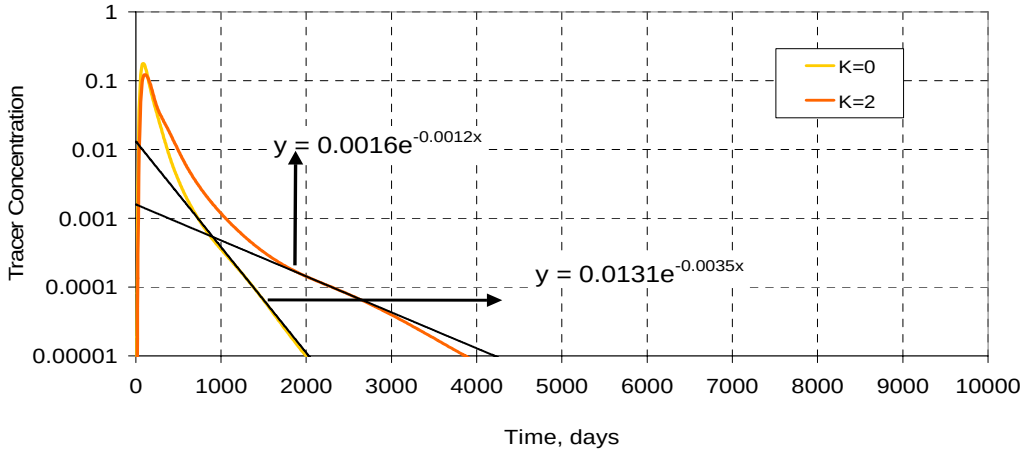

Figure 3.149. Extrapolation of tracer response in the second quadrant for TDL =0.0001 at kv/kh=0.001

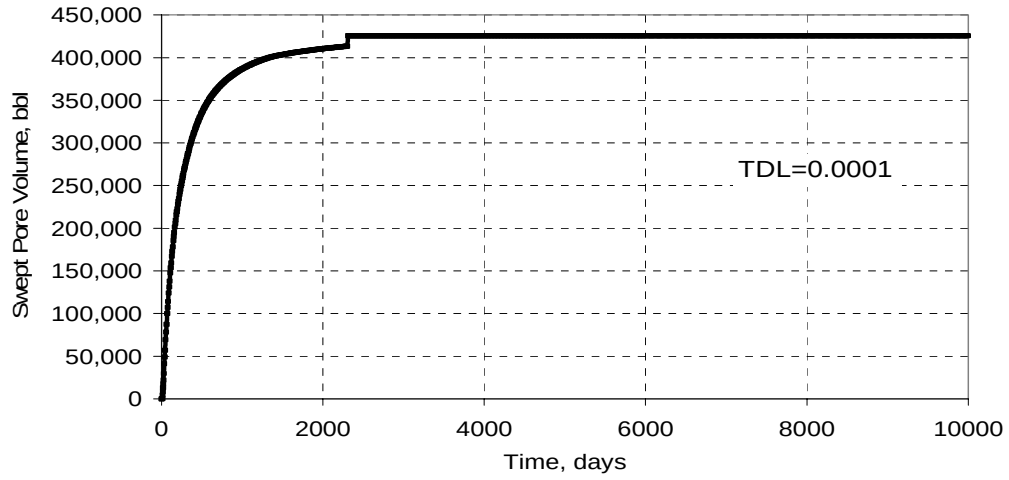

Figure 3.150. MOM swept pore volume estimate in the third quadrant after the extrapolation for TDL =0.0001 at kv/kh=0.001.

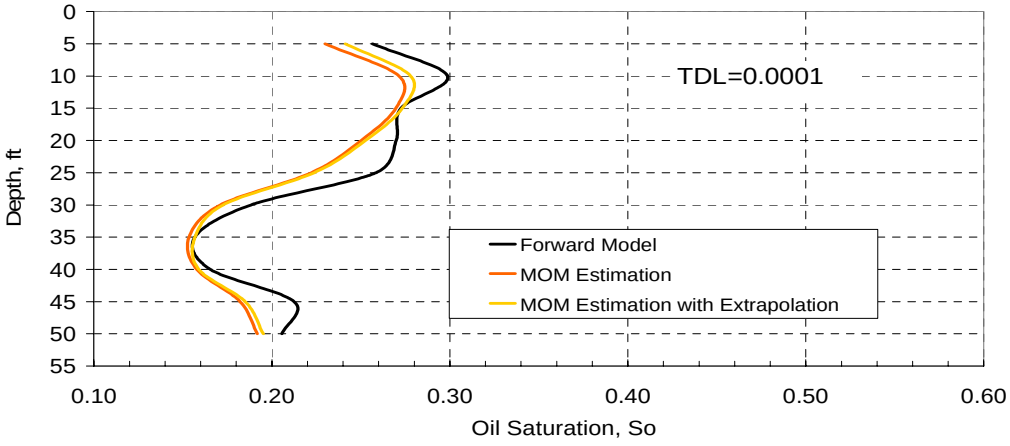

Figure 3.151. MOM oil saturation estimate with and without extrapolation in the third quadrant, for TDL=0.0001 at kv/kh=0.001.

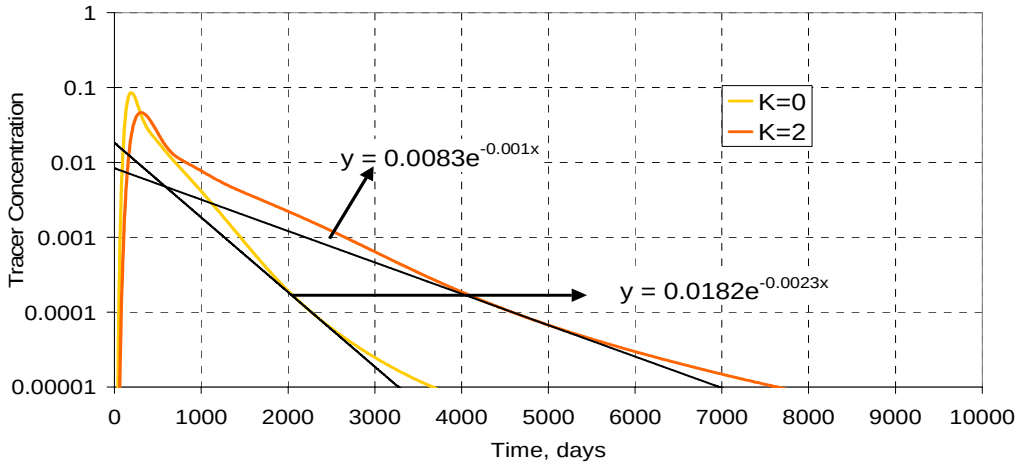

Figure 3.152. Extrapolation of tracer response in the fourth quadrant for TDL =0.0001 at at kv/kh=0.001

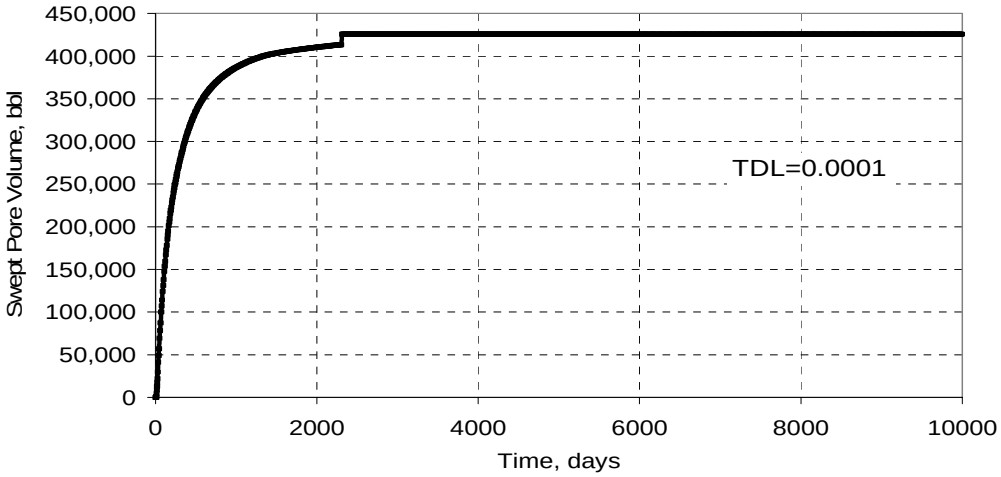

Figure 3.153. MOM swept pore volume estimate in the fourth quadrant after the extrapolation for TDL =0.0001 at kv/kh=0.001.

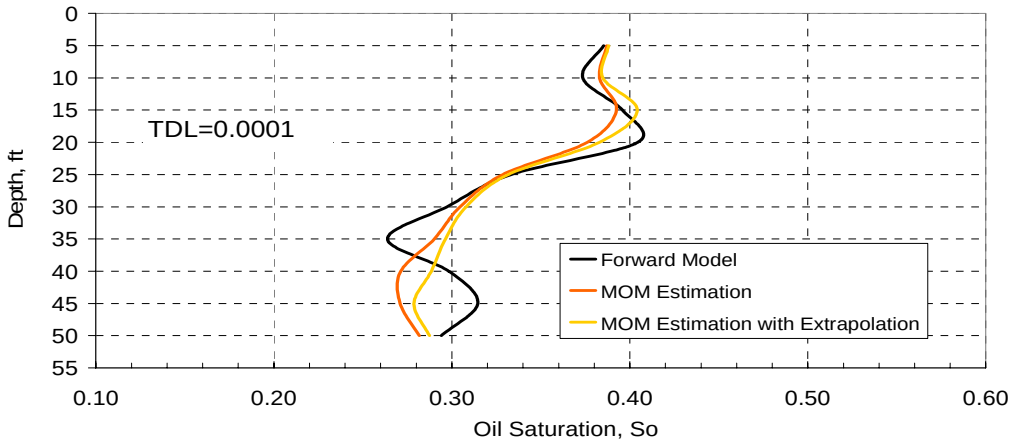

Figure 3.154. MOM oil saturation estimate with and without extrapolation in the fourth quadrant for TDL=0.0001 at kv/kh=0.001.

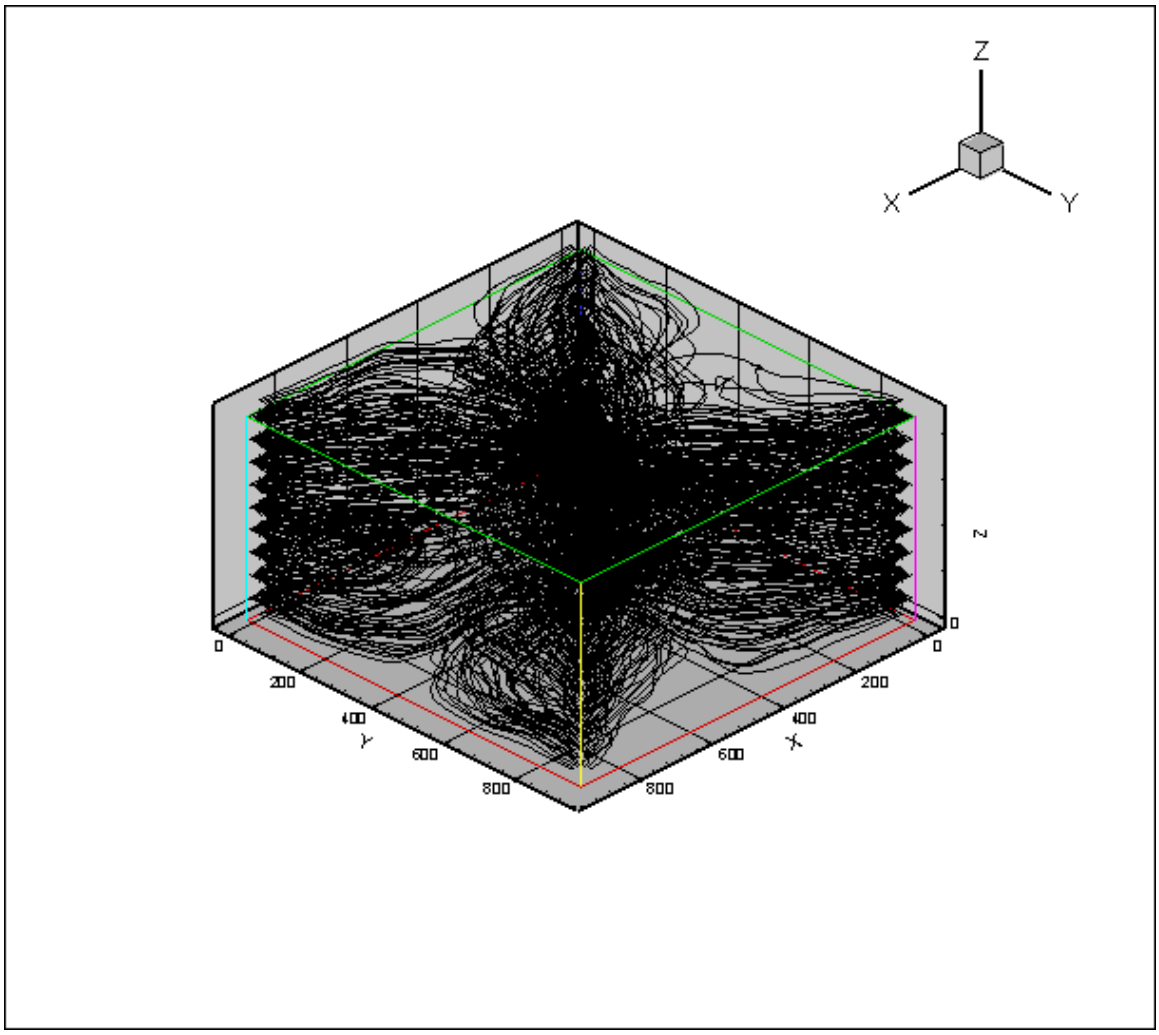

Figure 3.155. Streamline distribution after inverse modeling in the reservoir model with the stochastic permeability field at kv/kh=0.001.

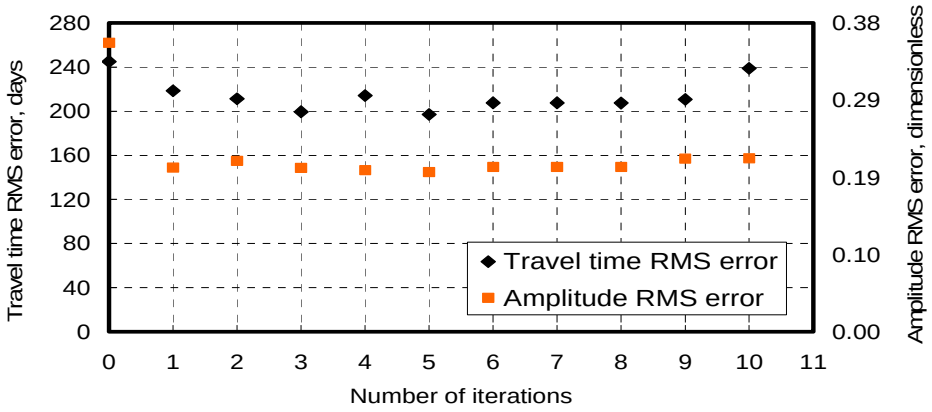

Figure 3.156. RMS error change on travel time and amplitude at the reservoir model with the stochastic permeability field at kv/kh=0.001.

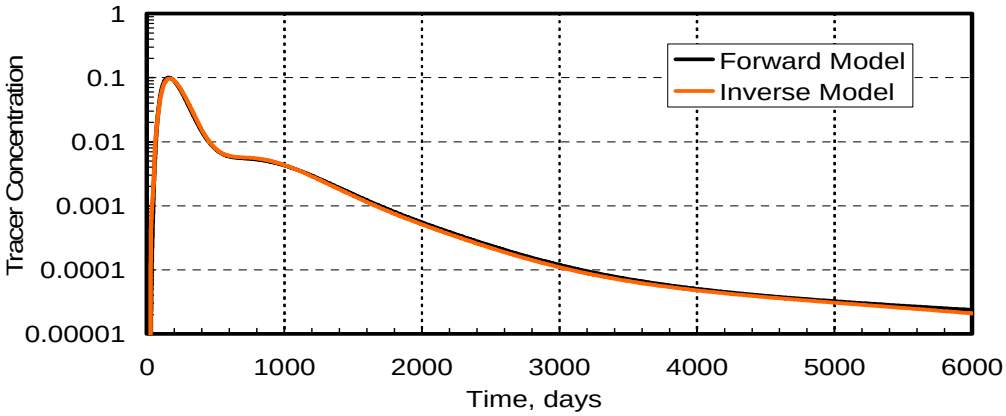

Figure 3.157. Match of the forward model tracer response from the first quadrant with the inverse model for TDL=0.0001 at kv/kh=0.001.

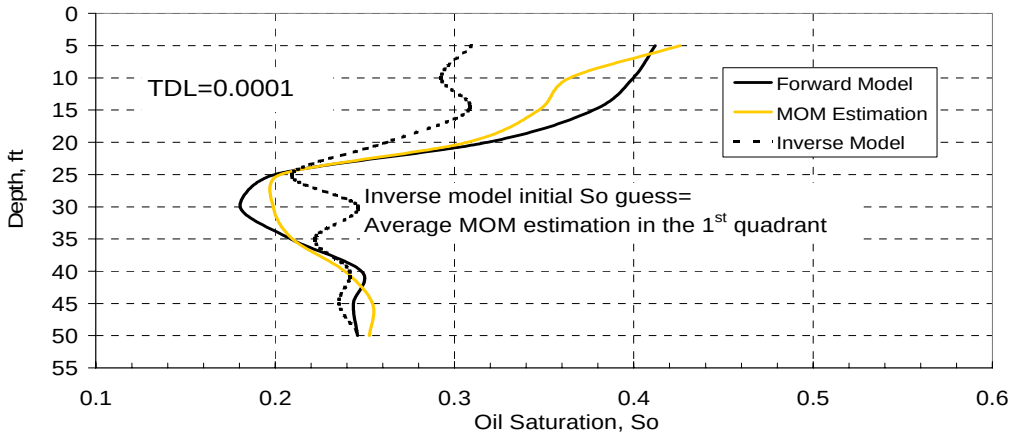

Figure 3.158. Comparison of MOM and inverse model oil saturation estimates in the first quadrant for TDL=0.0001 at kv/kh=0.001.

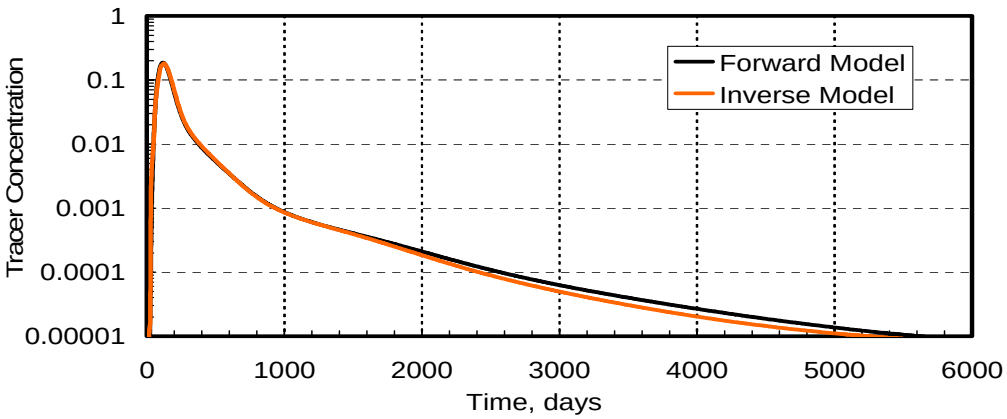

Figure 3.159. Match of the forward model tracer response from the second quadrant with the inverse model for TDL=0.0001 at kv/kh=0.001.

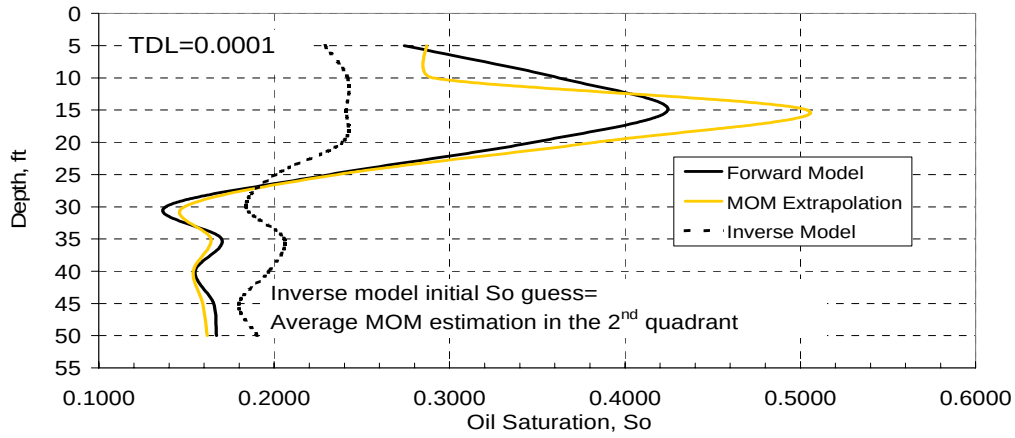

Figure 3.160. Comparison of MOM and inverse model oil saturation estimates in the second quadrant for TDL=0.0001 at kv/kh=0.001.

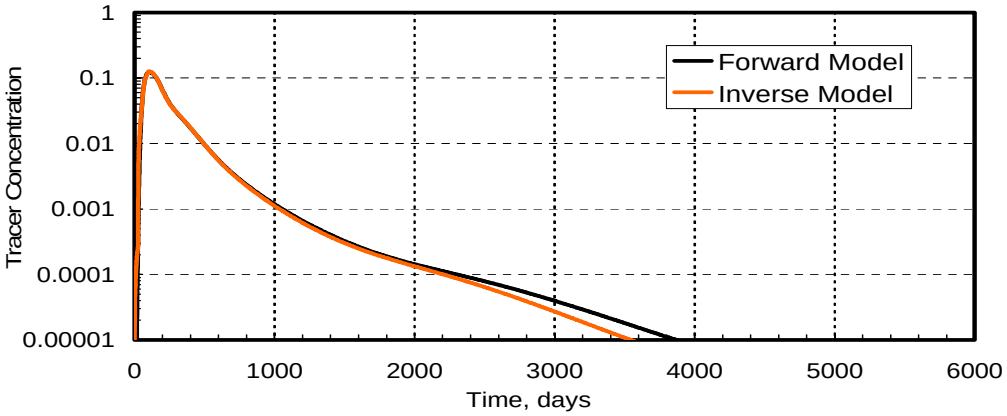

Figure 161. Match of the forward model tracer response from the third quadrant with the inverse model for TDL=0.0001 at kv/kh=0.001.

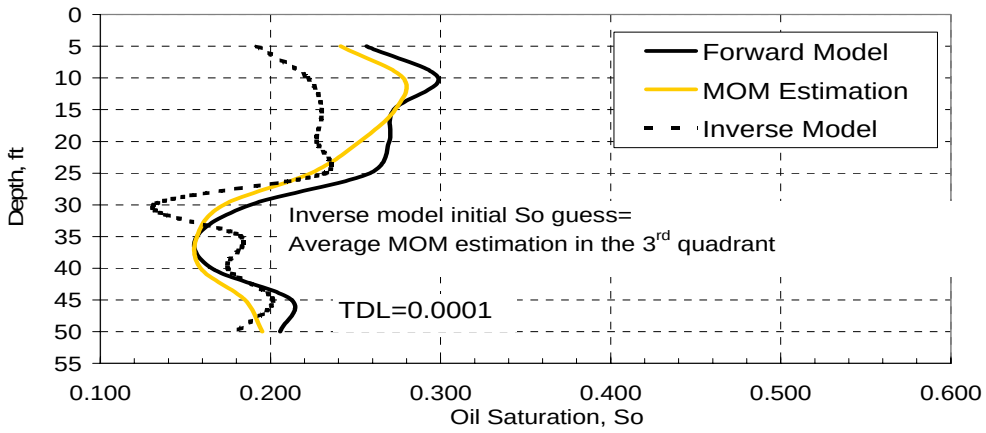

Figure 3.162. Comparison of MOM and inverse model oil saturation estimates in the third quadrant for TDL=0.0001 at kv/kh=0.001.

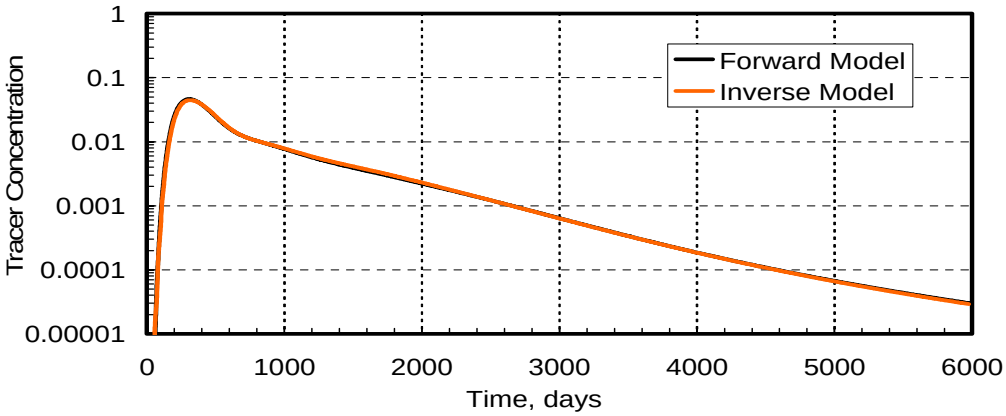

Figure 3.163. Match of the forward model tracer response from the fourth quadrant with the inverse model for TDL=0.0001 at kv/kh=0.001.

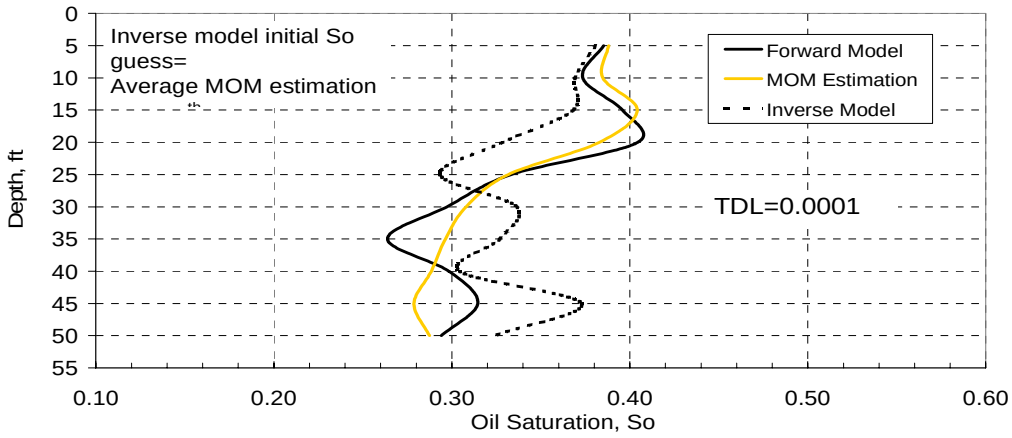

Figure 3.164. Comparison of MOM and inverse model oil saturation estimates in the fourth quadrant for TDL=0.0001 at kv/kh=0.001.

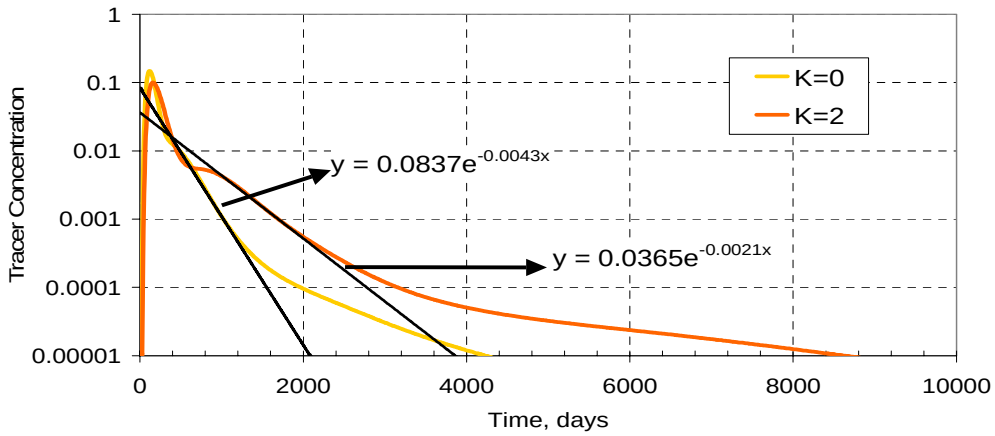

Figure 3.165. Extrapolation of tracer response from the first quadrant for TDL =0.001 at kv/kh=0.001

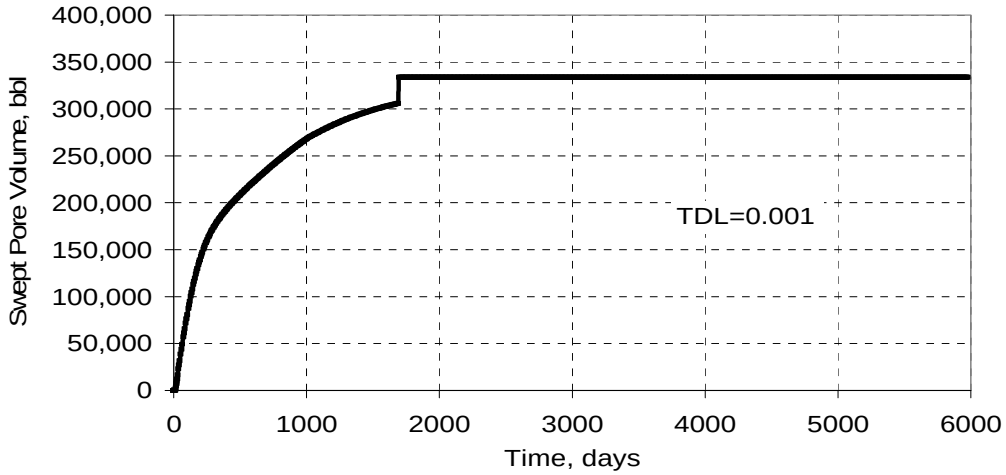

Figure 3.166. MOM swept pore volume estimate in the first quadrant after the extrapolation for TDL =0.001 at kv/kh=0.001.

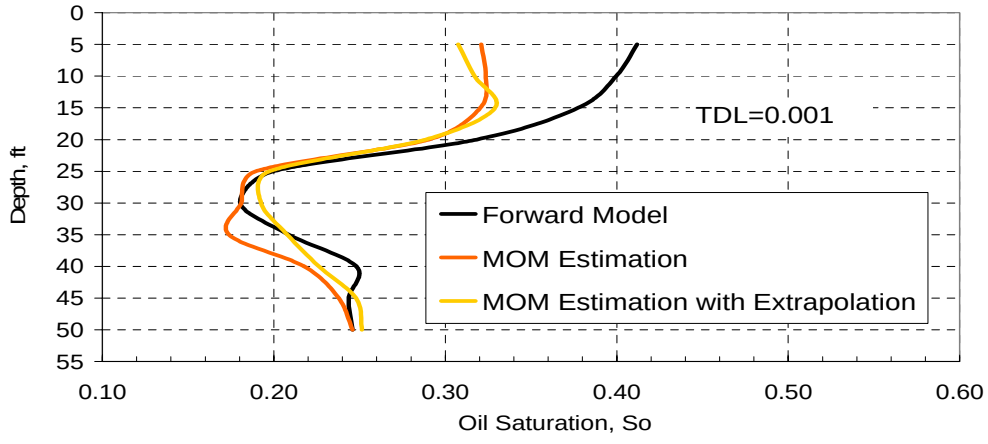

Figure 3.167. MOM oil saturation estimate with and without extrapolation in the first quadrant for TDL=0.001 at kv/kh=0.001.

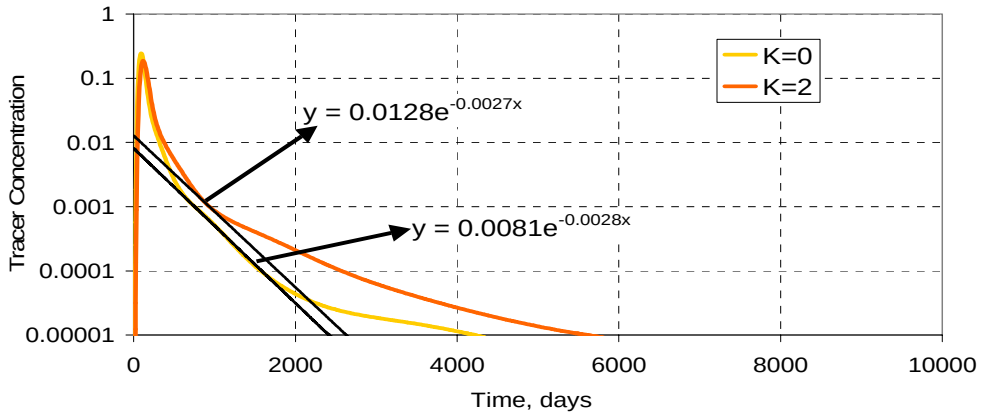

Figure 3.168.Extrapolation of tracer response from the second quadrant for TDL =0.001 at kv/kh=0.001

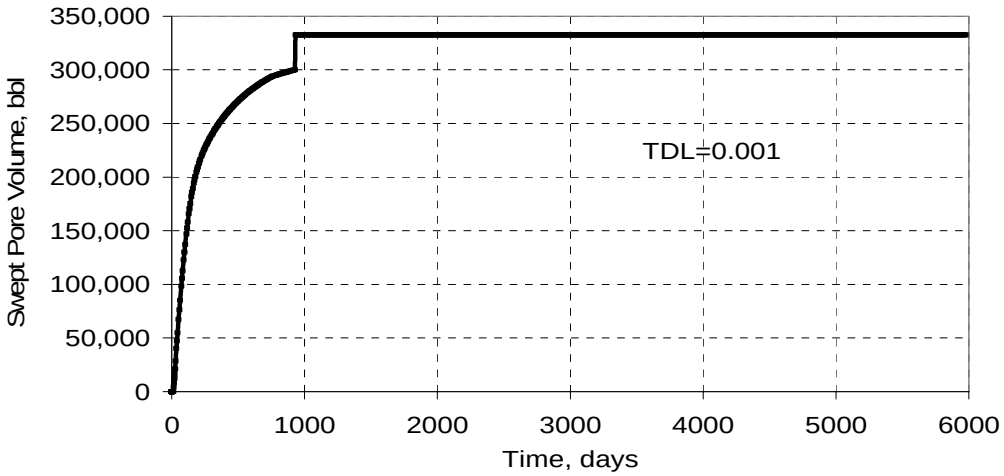

Figure 3.169. MOM swept pore volume estimate in the second quadrant after the extrapolation for TDL =0.001 at kv/kh=0.001.

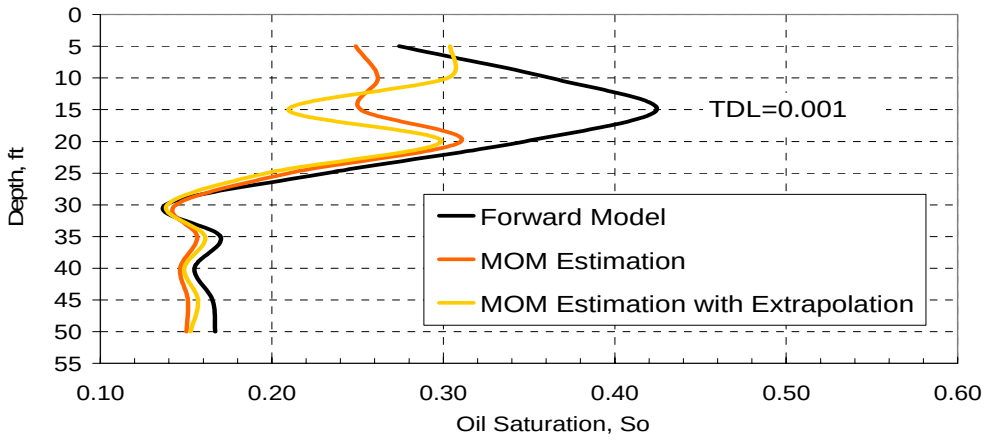

Figure 3.170. MOM oil saturation estimate with and without extrapolation in the second quadrant for TDL=0.001 at kv/kh=0.001.

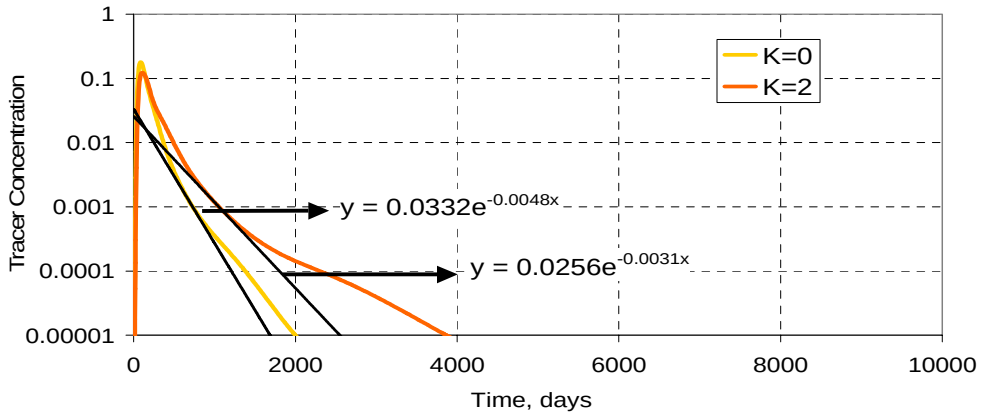

Figure 3.171. Extrapolation of tracer response from the third quadrant for TDL =0.001 at kv/kh=0.001

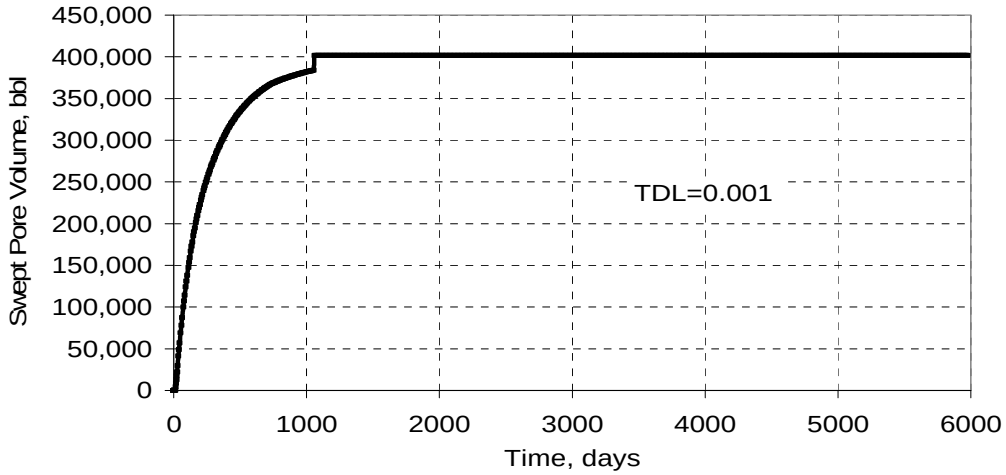

Figure 3.172. MOM swept pore volume estimate in the third quadrant after the extrapolation for TDL =0.001 at kv/kh=0.001.

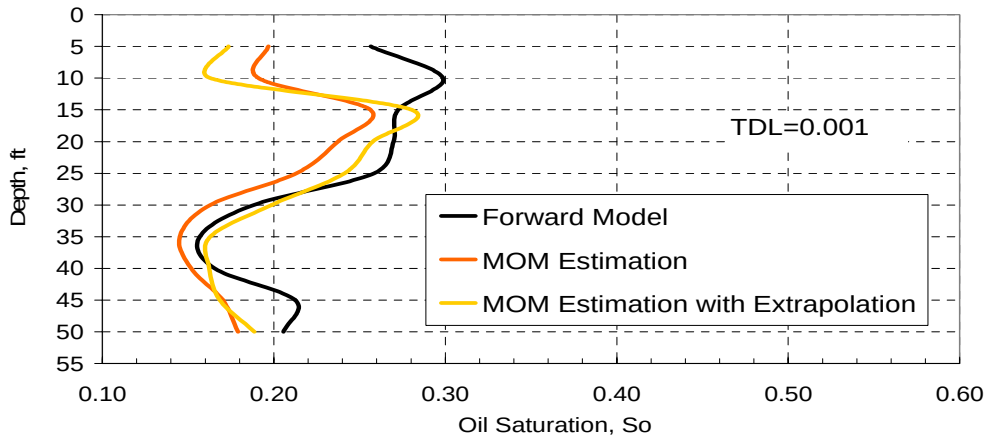

Figure 3.173. MOM oil saturation estimate with and without extrapolation in the third quadrant for TDL=0.001 at kv/kh=0.001.

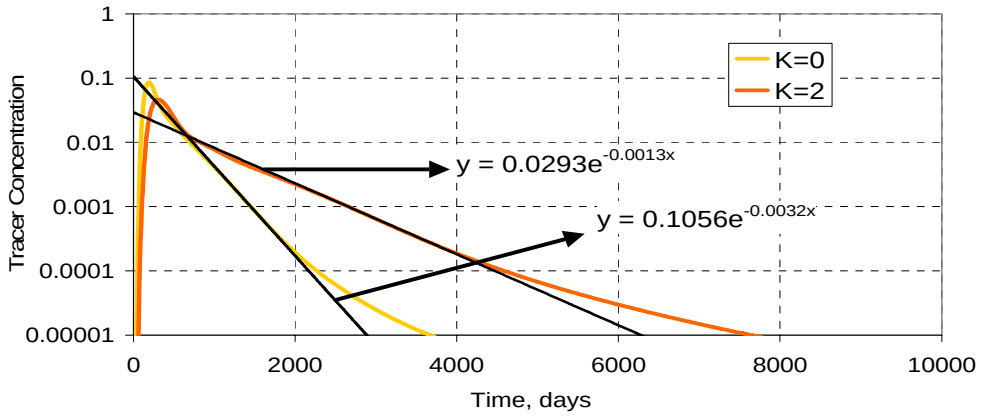

Figure 3.174. Extrapolation of tracer response from the fourth quadrant for TDL =0.001 at kv/kh=0.001

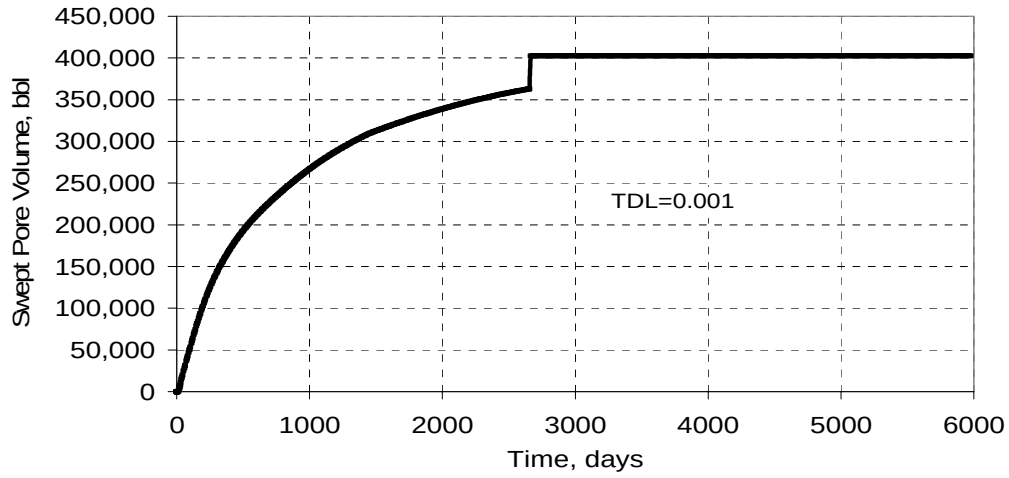

Figure 3.175. MOM swept pore volume estimate in the fourth quadrant after the extrapolation for TDL =0.001 at kv/kh=0.001.

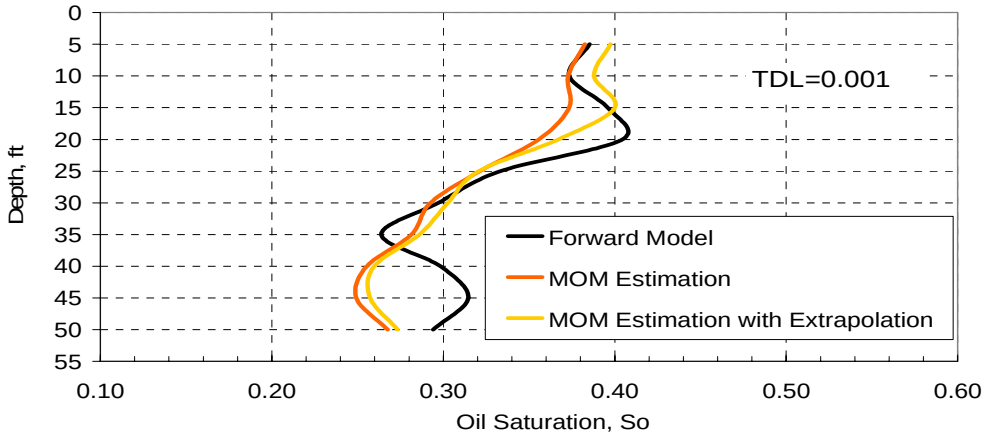

Figure 3.176. MOM oil saturation estimate with and without extrapolation in the fourth quadrant for TDL=0.001 at kv/kh=0.001.

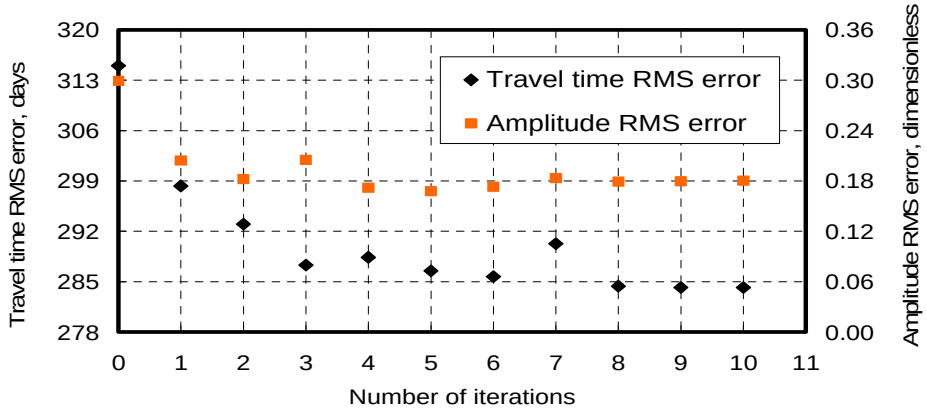

Figure 3.177. RMS error change on travel time and amplitude at the reservoir model with the stochastic permeability field for TDL=0.001 at kv/kh=0.001.

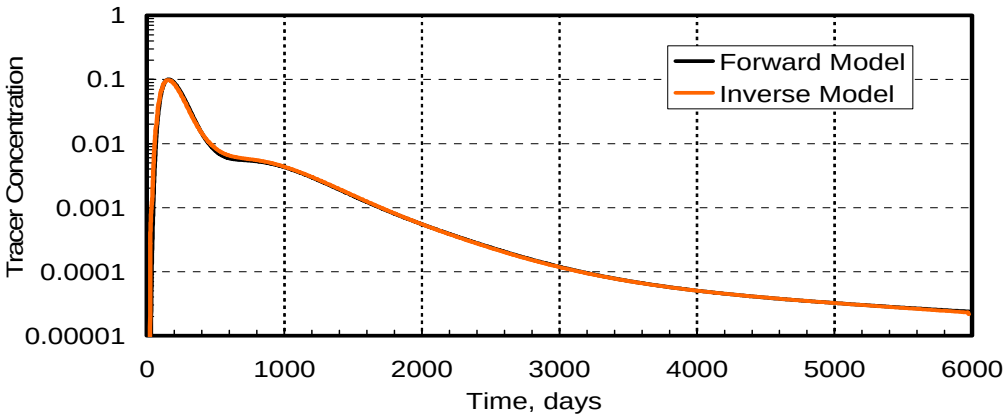

Figure 3.178.Extrapolation of tracer response from the second quadrant for TDL =0.001 at kv/kh=0.001

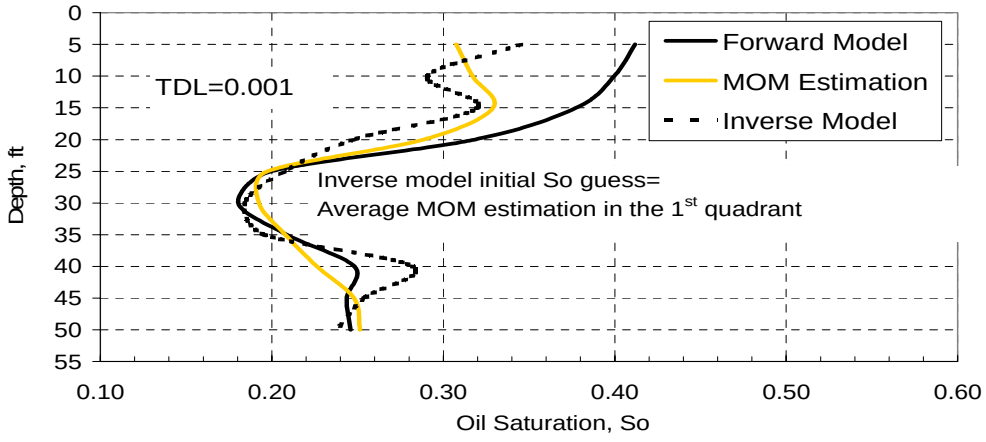

Figure 3.179. Comparison of MOM and inverse model oil saturation estimates in the first quadrant for TDL=0.001 at kv/kh=0.001.

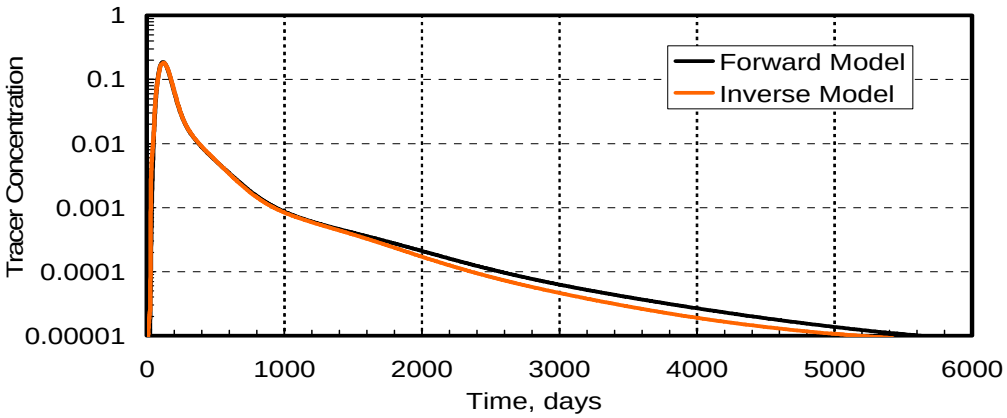

Figure 3.180.Extrapolation of tracer response from the second quadrant for TDL =0.001 at kv/kh=0.001

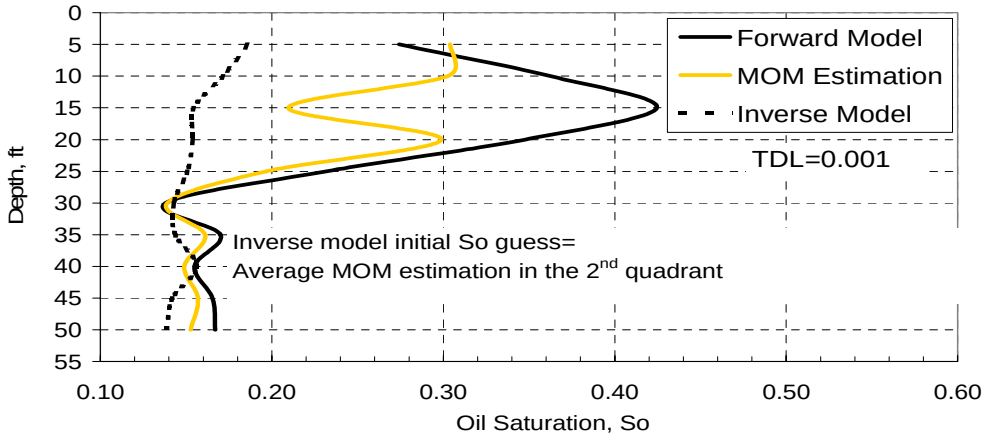

Figure 3.181. Comparison of MOM and inverse model oil saturation estimates in the second quadrant for TDL=0.001 at kv/kh=0.001.

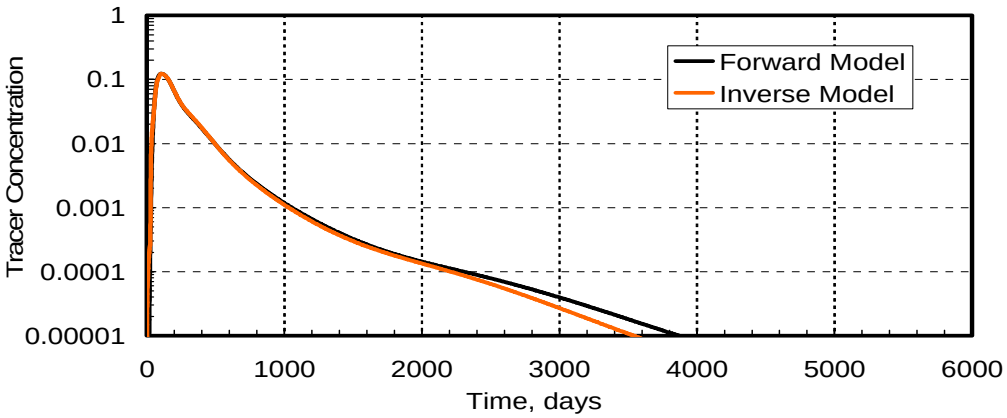

Figure 3.182.Extrapolation of tracer response from the third quadrant for TDL =0.001 at kv/kh=0.001

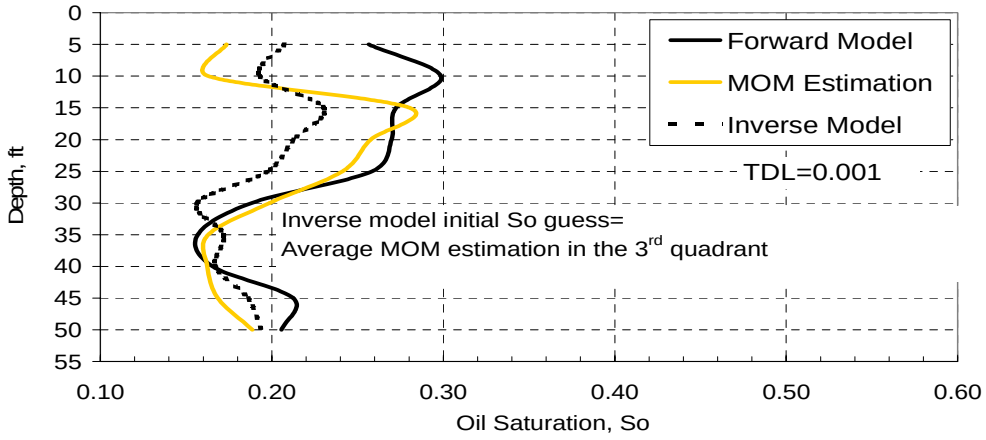

Figure 3.183. Comparison of MOM and inverse model oil saturation estimates in the third quadrant for TDL=0.001 at kv/kh=0.001.

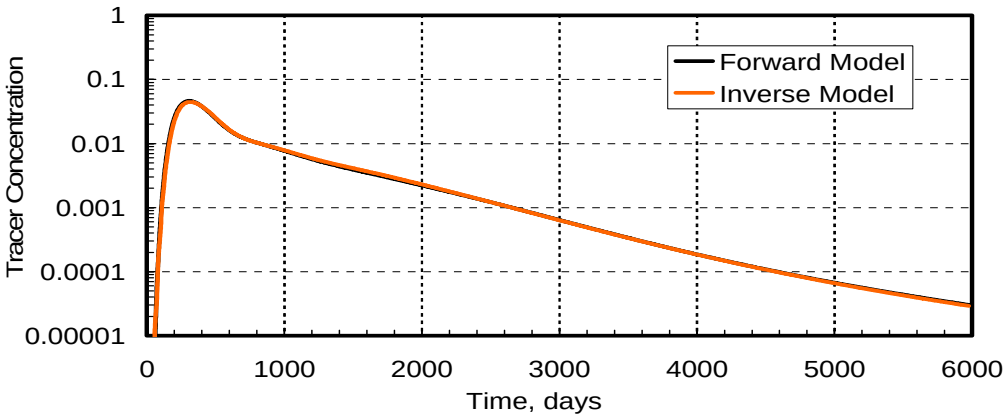

Figure 3.184.Extrapolation of tracer response from the fourth quadrant for TDL =0.001 at kv/kh=0.001

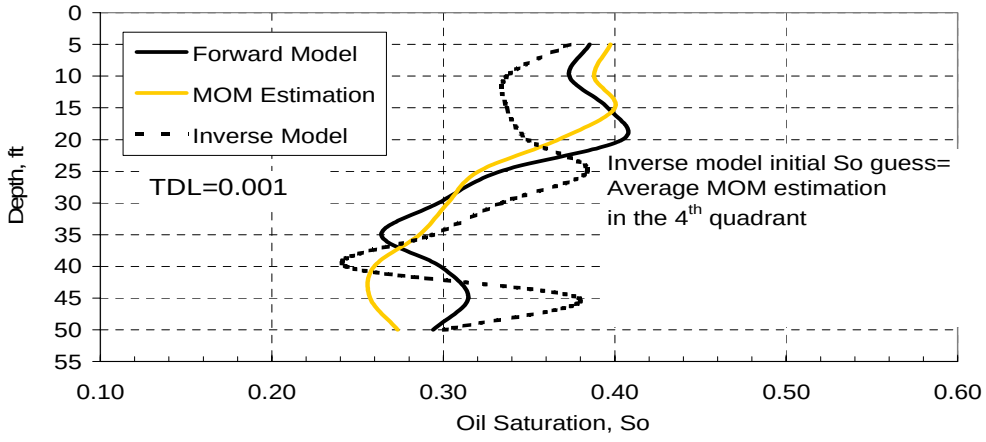

Figure 3.185. Comparison of MOM and inverse model oil saturation estimates in the fourth quadrant for TDL=0.001 at kv/kh=0.001.

CHAPTER 4: Use of Inverse Modeling in Two Phase Flow

In this part of the study, sensitivity analysis on inverse model is done at a very simple synthetic 2D reservoir model.

4.1 RESERVOIR DESCRIPTION

A 2-layer homogeneous cross sectional reservoir model is tested with the inverse model. The model has uniform permeability and porosity. Each layer has different uniform saturation values.

The reservoir is 660 ft in x direction, 330 ft in y direction and it has a 50 ft depth. The porosity is 0.2 and the pore volume is 387,900 bbl. Each layer has a 25ft thickness. The permeability is 100md in horizontal directions. The vertical permeability is taken as 0 md for no cross flow effects. The key parameters are tabulated in Table 4.1.

4.2 RUN DESCRIPTION

Two injectors are modeled, one for each layer. The injectors are controlled by constant flow rate of 500 bbl/day. And the partitioning tracer is injected for 50 days (0.129PV). The concentration is monitored at producer for 3000 days at both layers.

Simulations run here include models with and without cross flow effects and tracers with partition coefficients 10 and 2. The input file is given in Appendix B.

4.2 SENSITIVITY ANALYSIS

Five sets of simulations are performed to see the sensitivity of the tracer concentration response to relative permeability and viscosity. In these runs, tracer

partition coefficient is taken as 10. And the vertical permeability between the layers is zero. Table 4.2 summarizes the rest of the parameters. Two kinds of relative permeability used are shown in Figures 4.1 and 4.2. And, the fractional flow of water for runs 000, 600, 200, 100 and 500 are shown in Figures 4.3 to 4.7 respectively.

Simulations are run with water saturations 0.3, 0.5 and 0.7 for observing the sensitivity of tracers to different water saturations. The sensitivity of tracer response to saturation can be given by mean residence time. The mean residence time is given by the following equation (Oyerinde, 2004).

$$\overline{t^*_{Di}} = \frac{s_j + s_k K^i_{kj}}{f_j + f_k K^i_{kj}} \tag{4.1}$$

Here, $\overline{t^*_{Di}}$ is the corrected dimensionless mean residence time. K^i_{kj} is the partition coefficient of tracer i defined as the ratio of the concentration of tracer i in phase k to that in phase j. f_j, the fractional flow of phase j, and s_j the saturation of phase j. s_w and s_o are water and oil saturations respectively. f_w and f_o are the fractional flow of water and oil.

Tracer responses at these saturation values are shown in Figures 4.8 to 4.12. Each figure shows the mean residence time in both single-phase and two-phase flows. It is seen that the single-phase flow guarantees the monotonic change with oil saturation, whereas two-phase flow does not always guarantee a monotonic change. In Run 000 in Figure 4.8, the tracers are not sensitive when the oil saturation is low or high, i.e. 0.3<so<0.35 or 0.6<so<0.7. This insensitivity implies that the inverse model may fail to converge to the true saturation. In other words, the inverse model may only work in the oil saturation ranges between 0.35 and 0.6. In Run 600 in Figure 4.9, the inverse model may work in the range of 0.4<so<0.7. Figures 4.10 and 4.11 shows the mean residence

time in Runs 200 and 100. Under these specific relative permeability curves and viscosities, the mean residence time is monotonically decreasing with oil saturation, like seen in single-phase flow. In Run 500 in Figure 4.12, the tracer sensitivity is monotonically changing in the range of $0.3<so<0.45$ and $0.5<so<0.7$, where the inverse model may work. This sensitivity study shows that there is a possibility that the inverse model may work in some particular conditions.

In addition to the sensitivity discussed above, it is important to see how the initial oil saturation in the reservoir affects the produced tracer concentration. It is because the sensitivity studied above does not include the effect from the saturation changes with time. Also it is observed that the most of the tracer is transported in the water behind the oil bank causing the less sensitivity to the initial oil saturation. The tracer responses are shown in Figures 4.13 to 4.17. Almost no sensitivity is seen in Runs 000 and 200, and small sensitivity is seen in Run 100. Only Runs 600 and 500, where the contrast of the viscosity is high, have diversity in tracer response. If there is not much sensitivity in tracer response from the initial oil saturation in reservoir, it will possibly be hard to estimate oil saturation from tracer response.

4.3 APPLICATION OF INVERSE MODEL

After seeing the sensitivity to oil saturation and the initial saturation, the relative permeability and the viscosity from Run 500 are chosen for the further inverse simulations. The oil saturation in layer 1 is set to 0.4 and that in layer 2 to 0.6. The initial guess of the oil saturation is tabulated in Table 4.3 for Runs 511, 512, 513, and 514.

In Run 511, initial oil saturation guess for layer 1 is 0.35 while it is 0.55 for layer 2. Figure 4.18 demonstrates the decrease in RMS error change over the number of

iterations. 6 iterations are enough to reduce the error. Figures 4.19 and 4.20 show the tracer response curve matches in both layers. In layer 1, the tracer response from the inverse model is merging to the forward model. In layer2, the initial guess gives a very close tracer response to the forward model that no significant change in tracer response is seen. Figures 4.21 and 4.22 shows the oil saturation estimates in each layer. The saturation in layer 1 is estimated very well, while that in layer 2 is estimated not as good as in layer 1. However, the estimate is going towards the right direction.

In Run 512, initial oil saturation guess for layer 1 is 0.35 and 0.65 for layer 2. Figures 4.23 to 4.27 show the RMS error change, tracer response curves for layers 1 and 2 and the oil saturation estimate of inverse model for each layer of Run 512 respectively. In Figure 4.23, RMS error is decreasing with number of iterations. Although tracer response curve changes between the iterations in Figure 4.24, no change is observed in the tracer response coming from Figure 4.25. In Figure 4.26 oil saturation estimate catches the forward model value in layer. But in layer 2, saturation estimate is not getting further away from the initial guess in Figure 4.27.

The initial oil saturation estimate for layer 1 is 0.45 and 0.55 for layer 2 in Run 513. Figures 4.28 to 4.32 show the RMS error change, tracer response match and the oil saturation estimates of inverse model respectively. RMS is decreasing as desired in Figure 4.28. The tracer response curves are matching with the forward model in Figure 4.29 and 4.30. Oil saturation estimates approach the forward model in Figures 4.31 and 4.32 even though the estimate in layer 2 doesn't reach to the forward model.

Initial oil saturation guess for Run 514 for layer 1 is 0.45 and 0.65 for layer 2. The RMS error change, tracer response match and the oil saturation estimates of inverse model in Run 514 are shown in Figures 4.33 to 4.37. The results are very similar to the previous runs. RMS error decreases over number of iterations. Tracer responses match

with the forward model but in second layer tracer is not sensitive to the oil saturation. And the oil saturation estimates are approaching to the forward model in each layer.

In addition to the runs demonstrated above, inverse model is run without controlling the flow rate in each layer. In this run (run513-b), the total injection rate is kept at 1000bbl/day like in the previous runs, but the flow rate in each layer is changing with time as shown in Figure 4.38. Initial oil saturation guess is same as in run 513. Figure 4.39 shows the error change over the number of iterations. The inverse model does not offer converging result; instead RMS error oscillates over the number of iterations. And, if the travel time RMS error scale is checked, it is seen that the travel time error is really big. Third iteration is taken as the inverse model result. Figures 4.40 and 4.41 show the poor tracer concentration match. In both layers, it is observed that the first iteration results are closer to the forward model than the third iteration. Figure 4.42 and 4.43 show the inverse mode oil saturation estimates. Saturation estimates are very poor showing that the changing flow rate effects the inverse model estimates a lot.

Inverse model is also tested with different relative permeability. The permeability curve used has an end point relative permeability of 0.15 for water and 0.85 for oil. The run demonstrated here with a specific initial guess is Run 613. The parameters of this run can be seen in Table 4.4. Figure 4.44 shows the decrease in RMS error with iterations. Many times, in two-phase flow simulations inverse model crushes after a few iterations and the reason has not been found yet. It happens at the demonstrated run too. That's why the furthest iteration reached at run 613 is 7. And, 7^{th} iteration is taken as the inverse model estimate. Figures 4.45 and 4.46 show the tracer response matches of inverse and the forward models. It is seen that tracer concentrations match well starting from the first iteration. Figures 4.47 and 4.48 show the oil saturation estimates in two layers. The estimate is approaching to the forward model in the first layer. But, initial

guess is not improved in the second layer although the initial guess and the forward model values are in the sensitive region in Figure 4.9.

As a second step, for adding cross flow to the model, kv/kh ratio is increased to 0.1 by keeping every other parameter same (run 713 in Table 4.4). Sensitivity to different water saturations at this kv/kh ratio and partition coefficient is shown in Figure 4.49. It is noticed that tracer response for initial water saturation 0.7 is overlapping with response of water saturation 0.4 and it is in the middle of tracer response of water saturations 0.3 and 0.5. This may lead to errors in inverse model oil saturation estimate since one tracer response may present more than one saturation value. In Figure 4.50 RMS error change is shown. Amplitude RMS error flatten out after the 6th iteration. Figure 4.51 and 4.52 show the perfect tracer concentration match even at the first iteration. Figures 4.53 and 4.54 show the close oil saturation estimates in both layers.

As a third step, kv/kh ratio is kept at 0.1 and a tracer with a partition coefficient 2 instead of 10 is used since it is more practical to use in field conditions. Again the parameters for this run (run723) is shown in Table 4.4. Figure 4.55 shows the mean residence time change with oil saturation at this partition coefficient. Sensitivity is observed between oil saturations 0.45 and 0.7. The effect of the initial water saturation on the tracer response is demonstrated in Figure 4.56. Figure 4.57 illustrates the RMS error convergence. Tracer concentration responses for both layers at iteration 6 are shown in Figures 4.58 and 4.59. Although convergence is observed at 6th iteration in the RMS error plot, tracer concentration matches are not satisfactory. Figures 4.60 and 4.61 show the unsatisfactory oil saturation estimates. As the Figures show partition coefficient 2 does not work for this case.

4.3 CONCLUSIONS

The sensitivity of oil saturation to tracer response is not monotonic, like seen in single-phase flow. Second, the tracer response is not really sensitive to the initial oil saturation in the reservoir because the most of the tracer is in the water behind the oil bank. Third, the flow rate change seems to seriously affect the inverse calculation rather than the initial oil saturation in the reservoir does. Relative permeability change and cross flow do not make much difference in the inverse model estimate at the specific case it is used. Lastly, inverse model does not work with tracer partition coefficient 2. It is not a desired result since small partition coefficients are needed for practical and economical purposes in the field studies.

Table 4.1 Description of the two dimensional reservoir model

Number of gridblocks	66x1x2
Size of gridblocks (ftxftxft)	10x330x25
Area of the reservoir, acres	5
Reservoir pore volume, bbl	387,890
Porosity	0.2
Lateral permeability, md	100
Residual oil saturation	0.3
Residual water saturation	0.3

Table 4.2. Relative permeability parameters and viscosities.

Run number	Endpoint relative permeability		Exponent of relative permeability		Viscosity [cp]	
	Water	Oil	Water	Oil	Water	oil
000	0.15	0.85	1.5	2	0.7	5
600	0.15	0.85	1.5	2	0.7	20
100	1	1	1	1	0.7	5
200	1	1	1	1	0.7	0.7
500	1	1	1	1	0.7	20

Table 4.3. Run summary of oil saturation estimate

Run number	Initial saturation		Saturation initial guess		Saturation from inverse model	
	Layer1	Layer2	Layer1	Layer2	Layer1	Layer2
511	0.400	0.600	0.35	0.55	0.400	0.561
512	0.400	0.600	0.35	0.65	0.399	0.644
513	0.400	0.600	0.45	0.55	0.400	0.561
514	0.400	0.600	0.45	0.65	0.400	0.644

Table 4.4. Run summary of oil saturation estimate

Run number	kv/kh	Partition coefficient	Initial saturation		Saturation initial guess		Saturation from inverse model	
			Layer 1	Layer 2	Layer 1	Layer 2	Layer 1	Layer 2
613	0	10	0.4	0.6	0.45	0.55	0.43	0.56
713	0.1	10	0.4	0.6	0.45	0.55	0.38	0.6
723	0.1	2	0.4	0.6	0.45	0.55	0.19	0.98

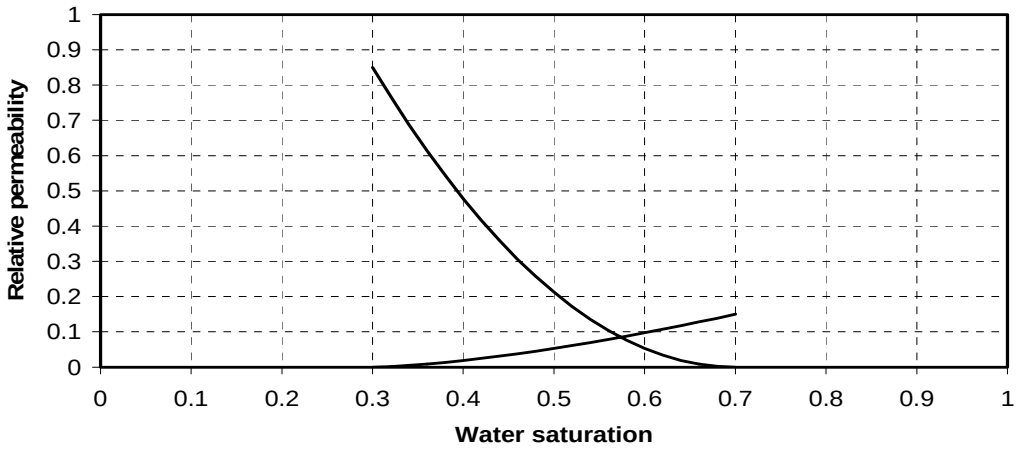

Figure 4.1. Relative permeability curves in Runs 000 and 600

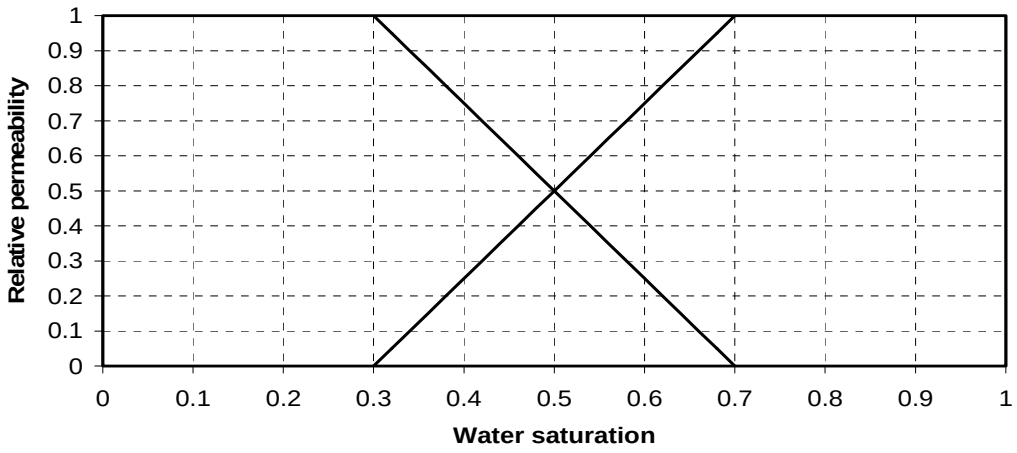

Figure 4.2. Relative permeability curves in Runs 200, 100, and 500.

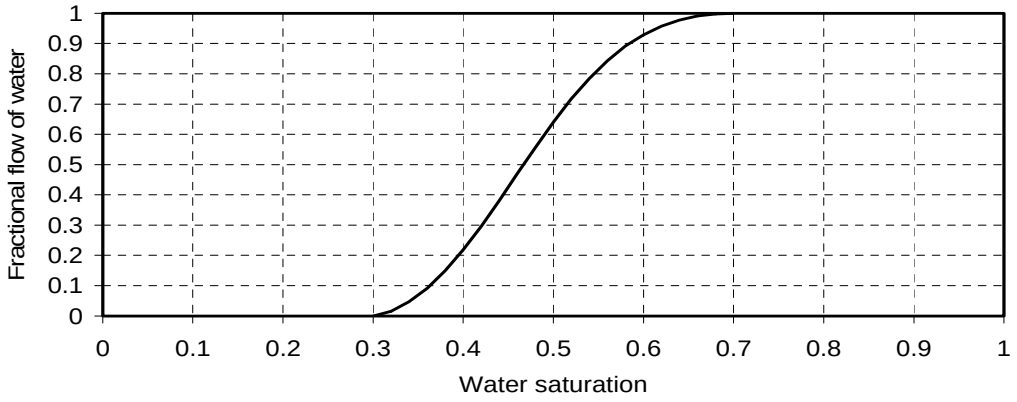

Figure 4.3. Fractional flow of water in Run 000

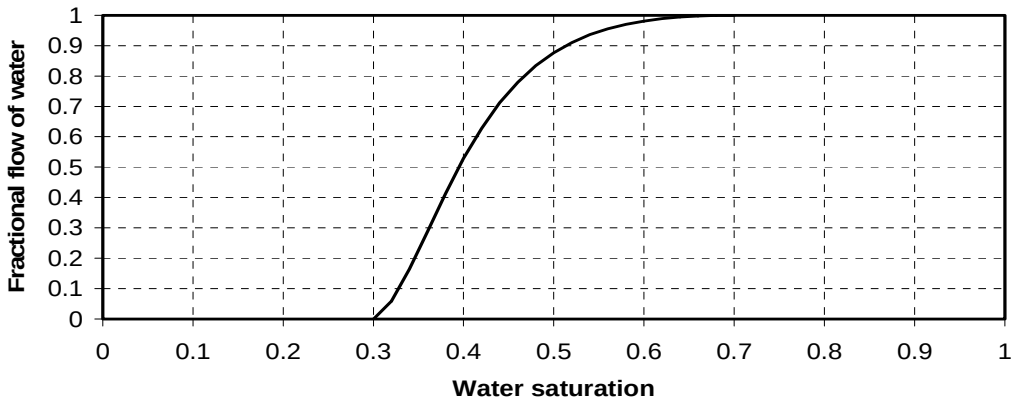

Figure 4.44. Fractional flow of water in Run 600 and Run 700

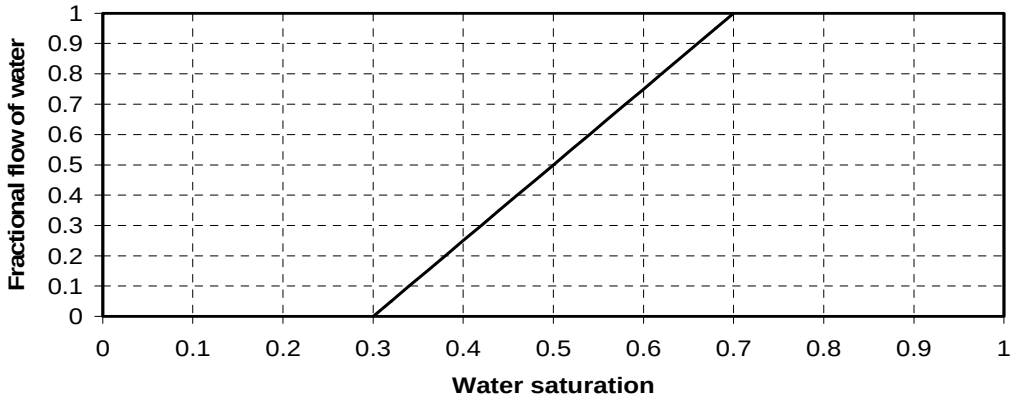

Figure 4.5. Fractional flow of water in Run 200

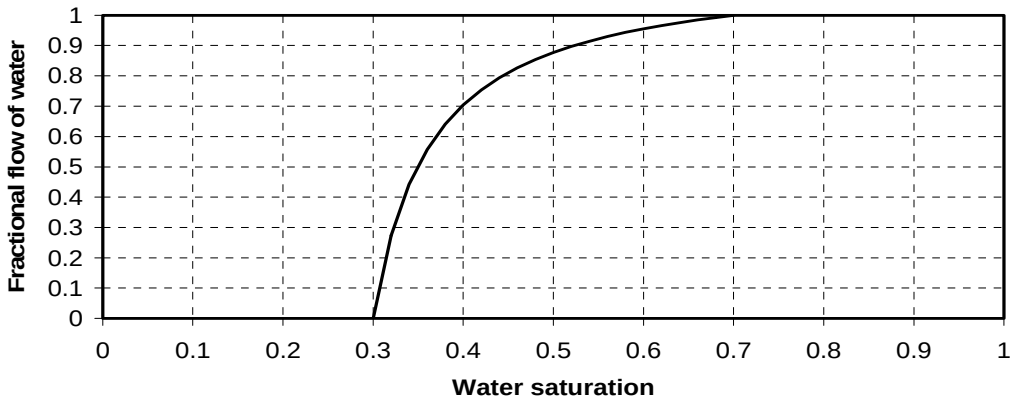

Figure 4.6. Fractional flow of water in Run 100

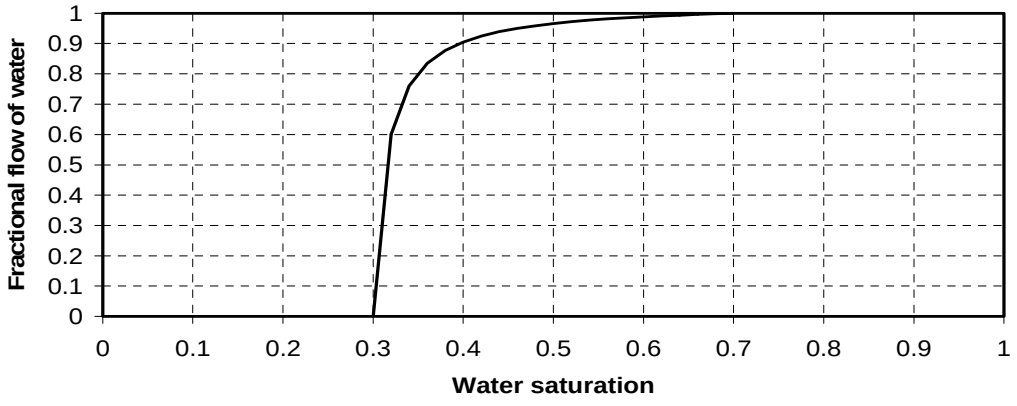

Figure 4.7. Fractional flow of water in Run 500

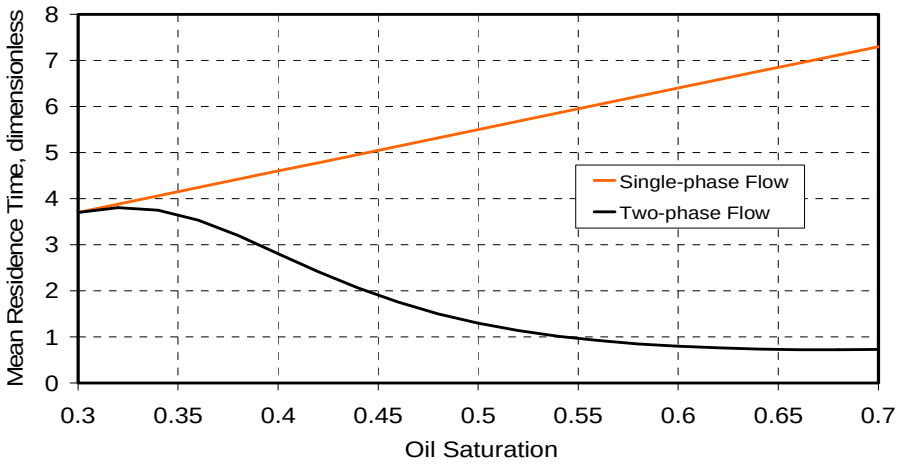

Figure 4.8. Mean residence time sensitivity to the oil saturation in Run000 at partition coefficient 10

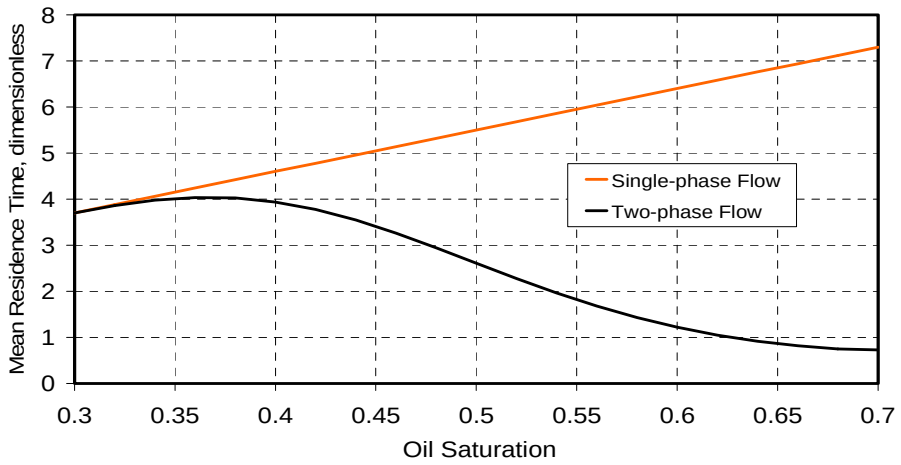

Figure 4.9. Mean residence time sensitivity to the oil saturation in Run600 at partition coefficient 10

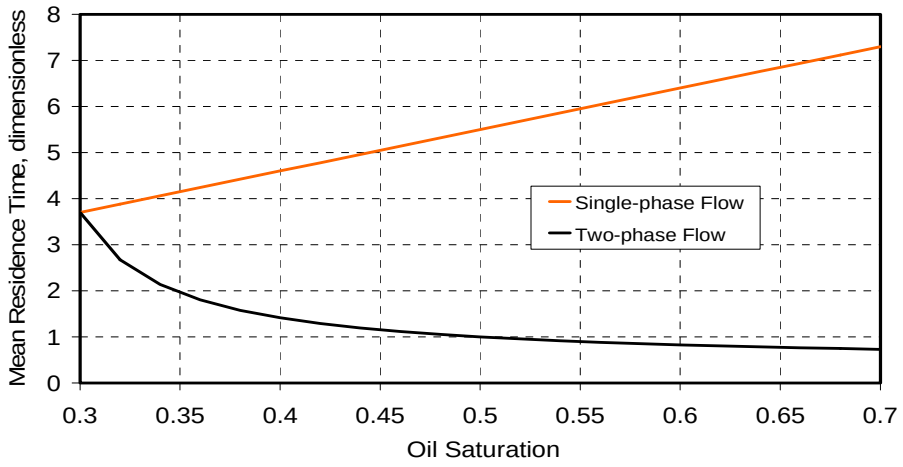

Figure 4.10. Mean residence time sensitivity to the oil saturation in Run200 at partition coefficient 10

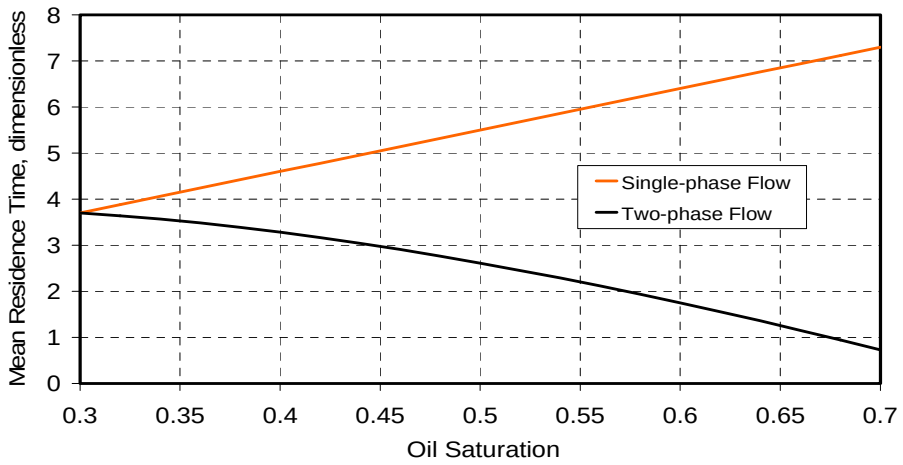

Figure 4.11. Mean residence time sensitivity to the oil saturation in Run100 at partition coefficient 10

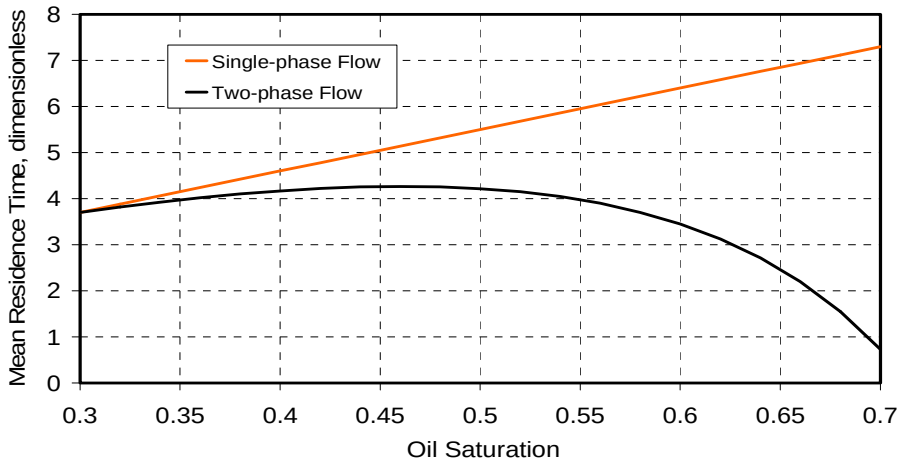

Figure 4.12. Mean residence time sensitivity to the oil saturation in Run500 at partition coefficient 10

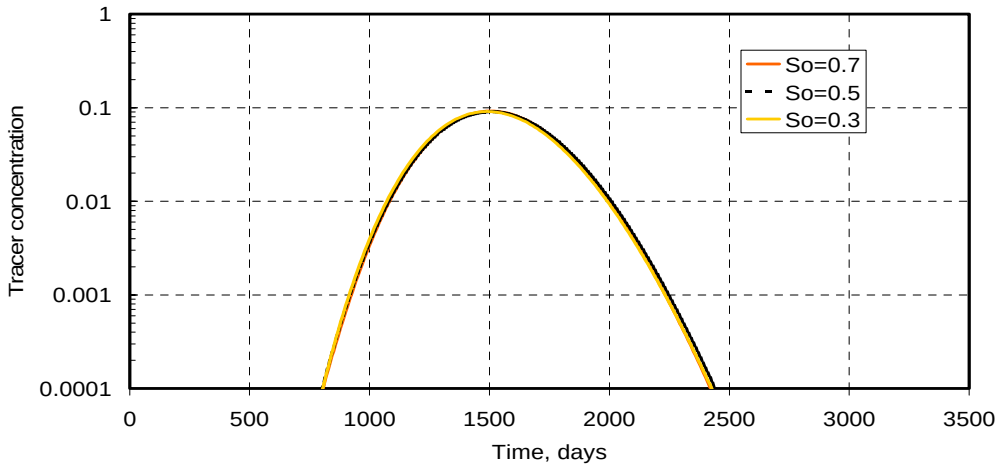

Figure 4.13. The effect of the initial water saturation on the tracer response in Run 000

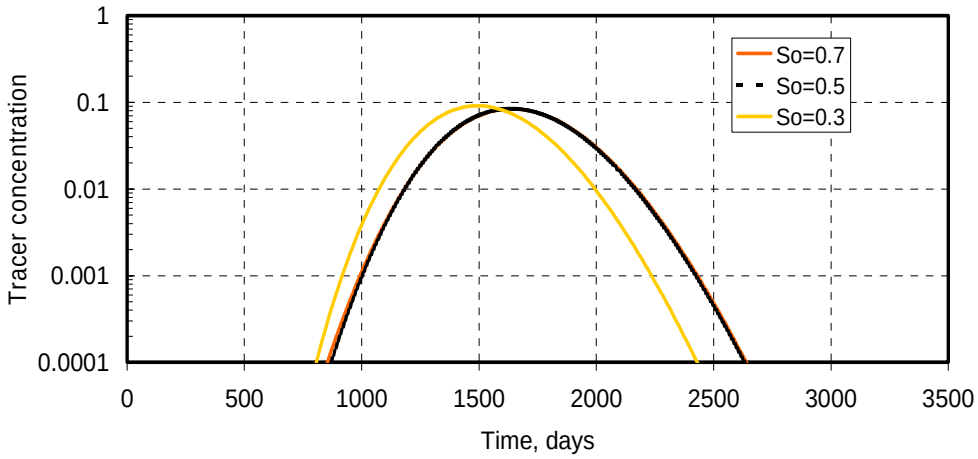

Figure 4.14. The effect of the initial water saturation on the tracer response in Run 600

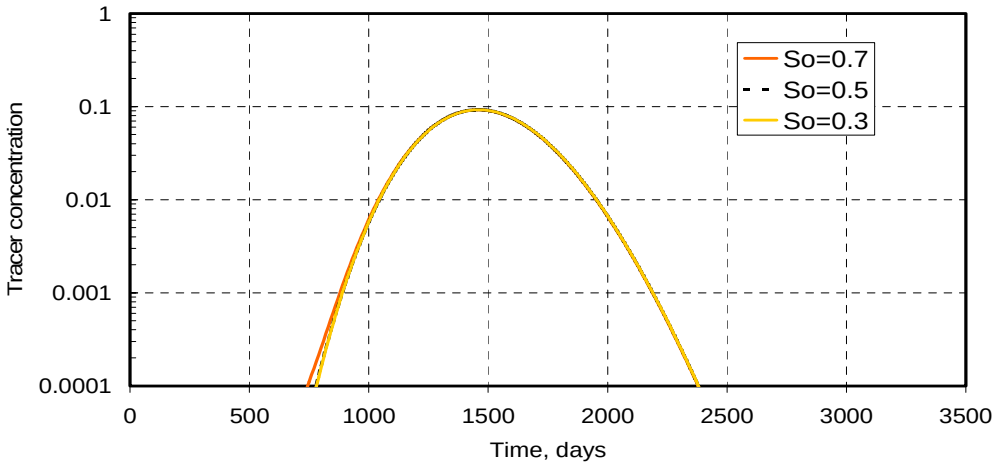

Figure 4.15. The effect of the initial water saturation on the tracer response in Run 200

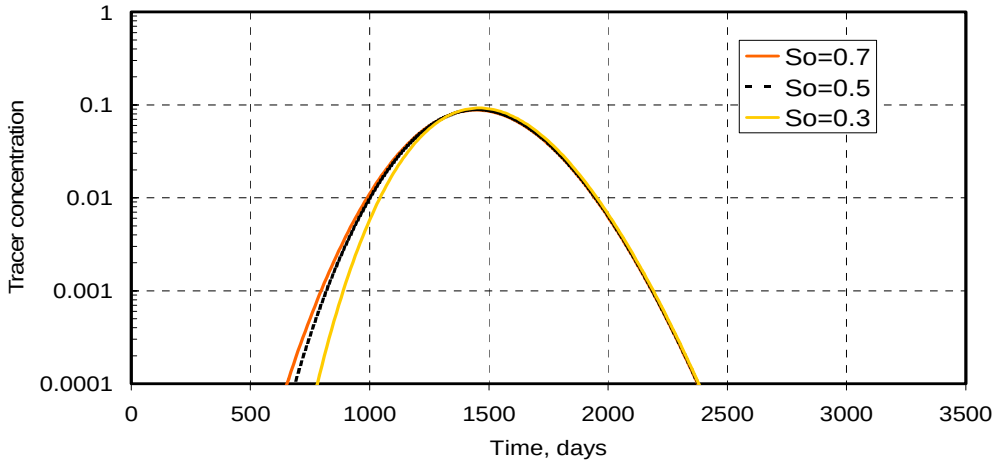

Figure 4.16. The effect of the initial water saturation on the tracer response in Run 100

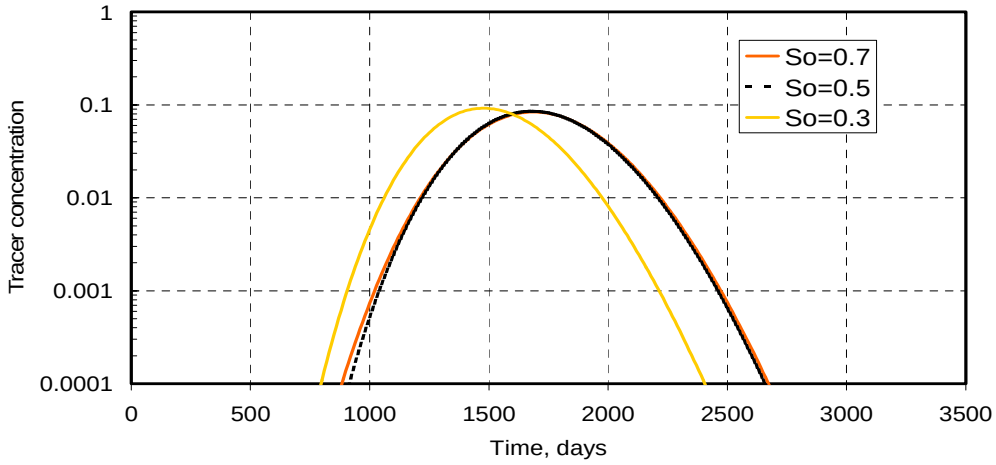

Figure 4.17. The effect of the initial water saturation on the tracer response in Run 500

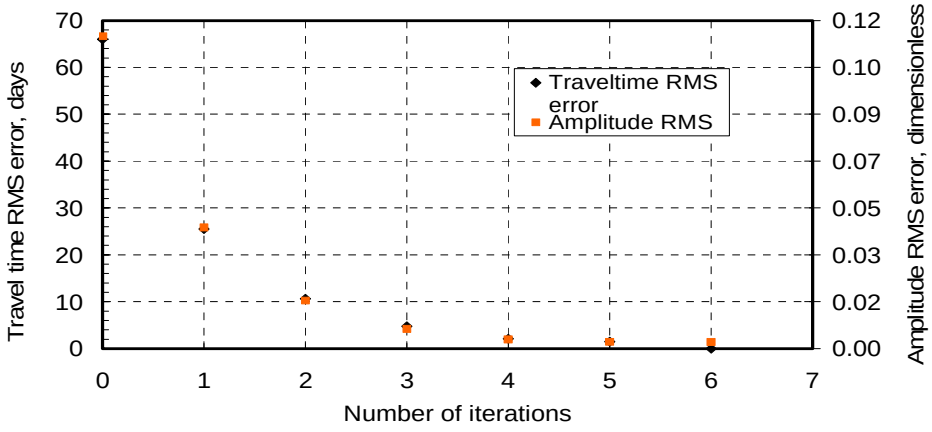

Figure 4.18. Root Mean Square error (RMS) change on travel time and amplitude during inversion in Run 511

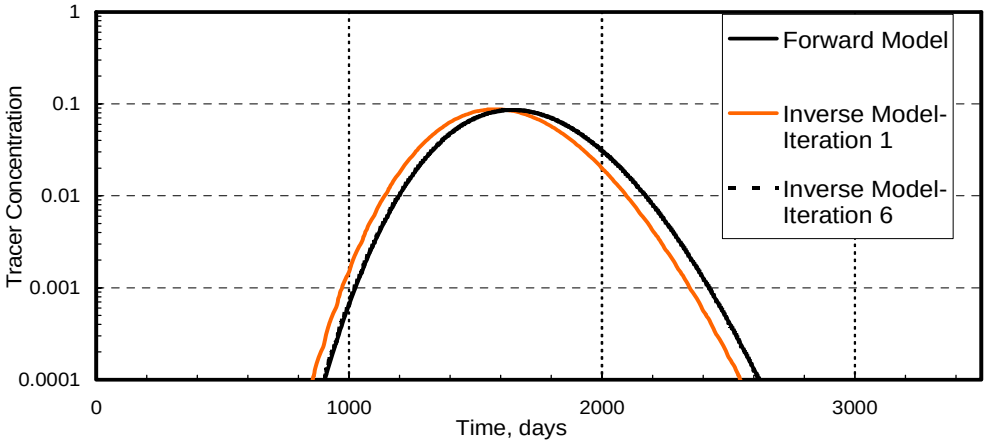

Figure 4.19. Match of the forward model tracer response from layer 1 by iteration 1 and 6 of inverse model in Run 511

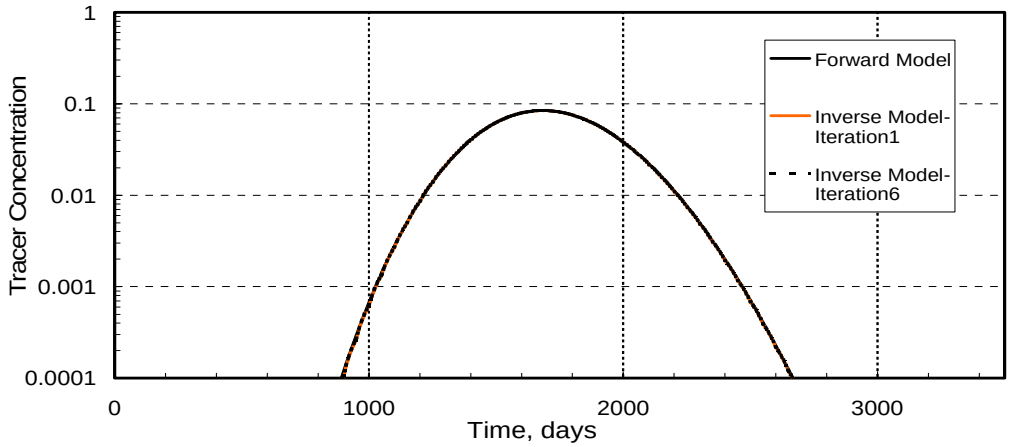

Figure 4.20. Match of the forward model tracer response from layer 2 by iteration 1 and 6 of inverse model in Run 511

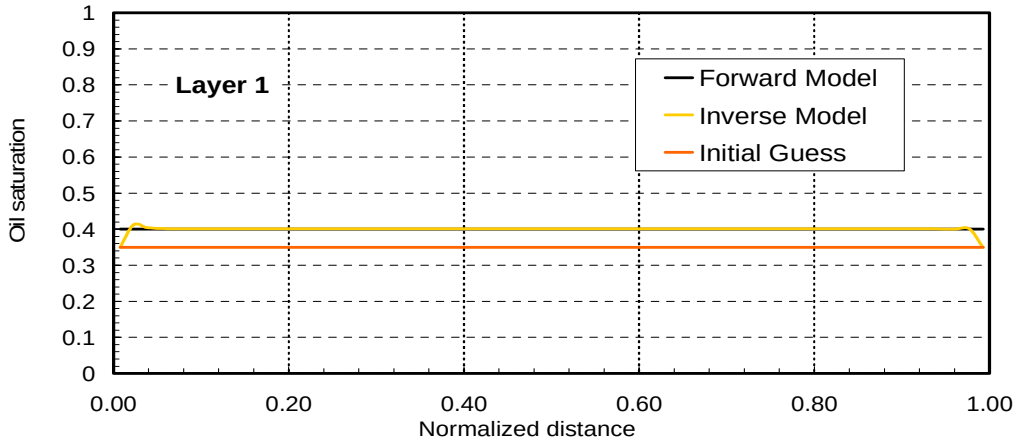

Figure 4.21. Inverse model oil saturation estimate in layer 1 in Run 511

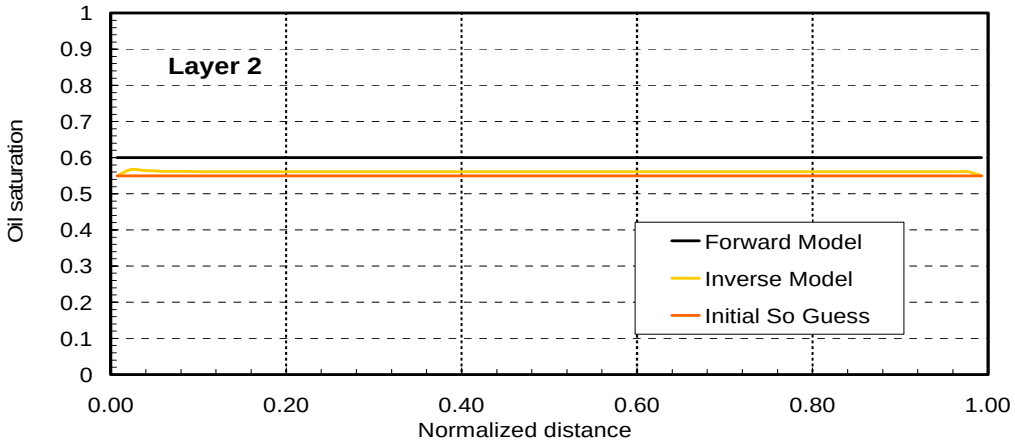

Figure 4.22. Inverse model oil saturation estimate in layer 2 in Run 511

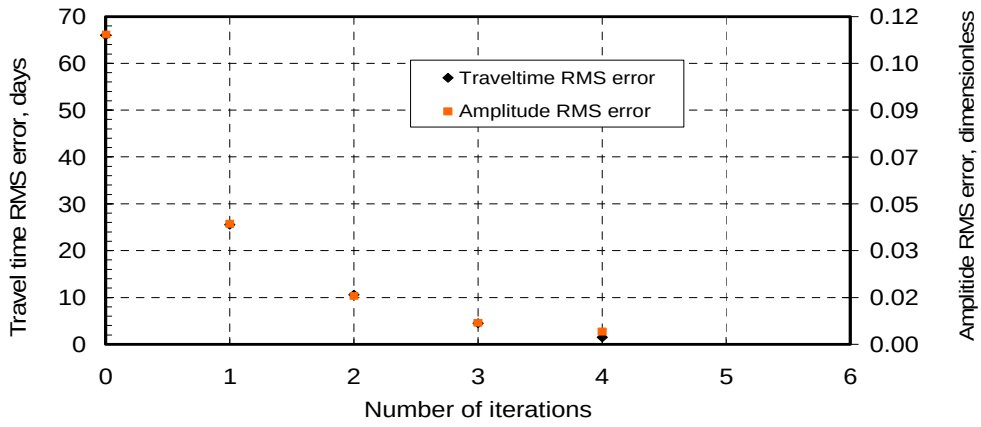

Figure 4.23. Root Mean Square error (RMS) change on travel time and amplitude during inversion in Run 512

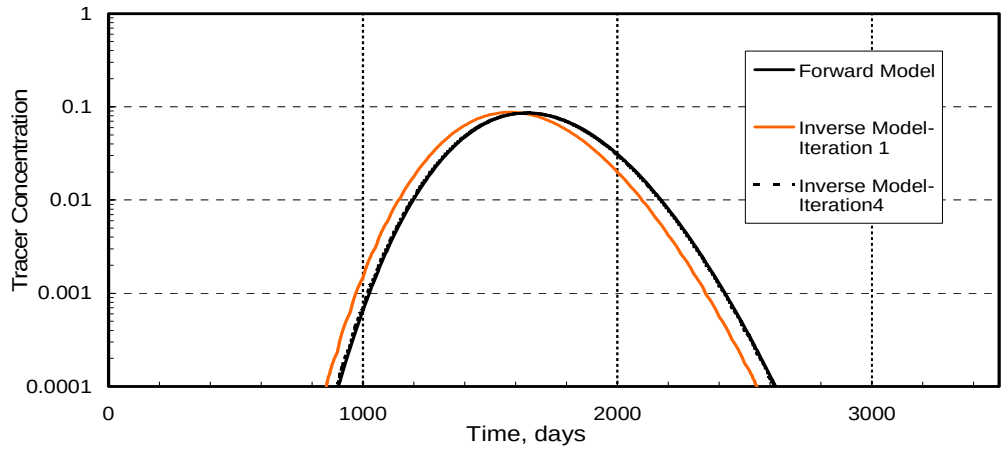

Figure 4.24. Match of the forward model tracer response from layer 1 by iteration 1 and 4 of inverse model in Run 512

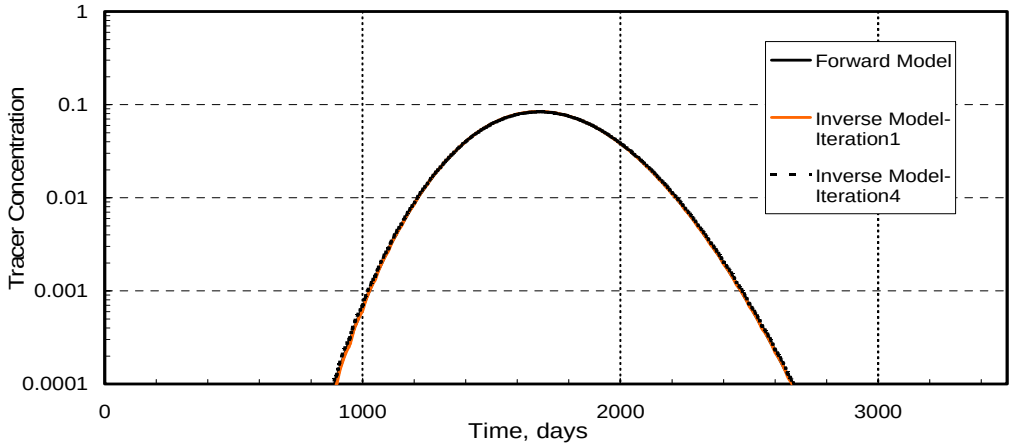

Figure 4.25. Match of the forward model tracer response from layer 2 by iteration 1 and 4 of inverse model in Run 512

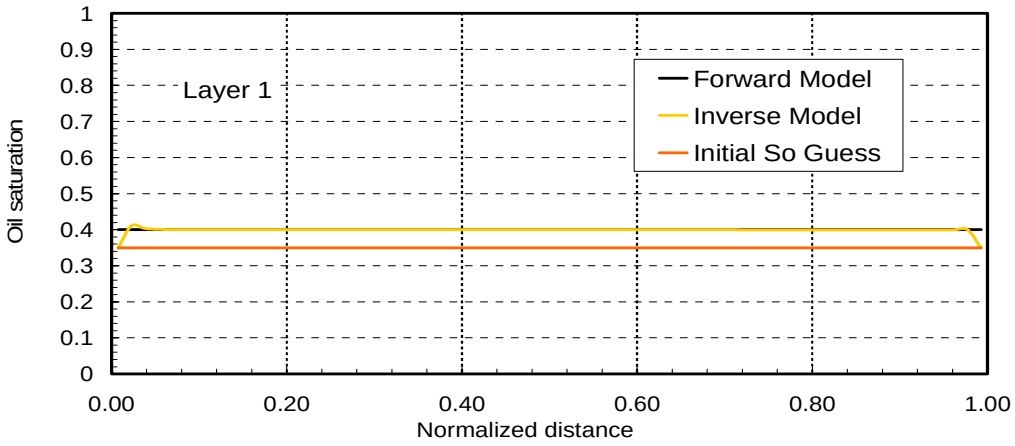

Figure 4.26. Inverse model oil saturation estimate in layer 1 in Run 512.

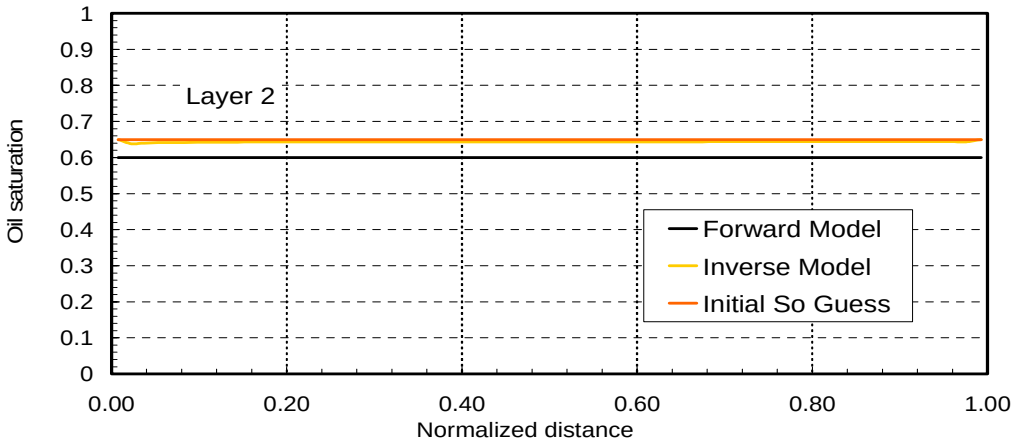

Figure 4.27. Inverse model oil saturation estimate in layer 2 in Run 512.

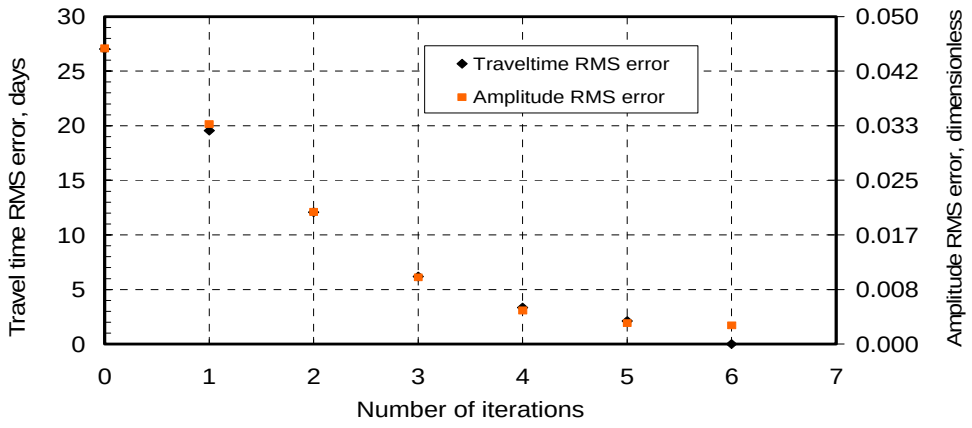

Figure 4.28. Root Mean Square error (RMS) change on travel time and amplitude during inversion in Run 513

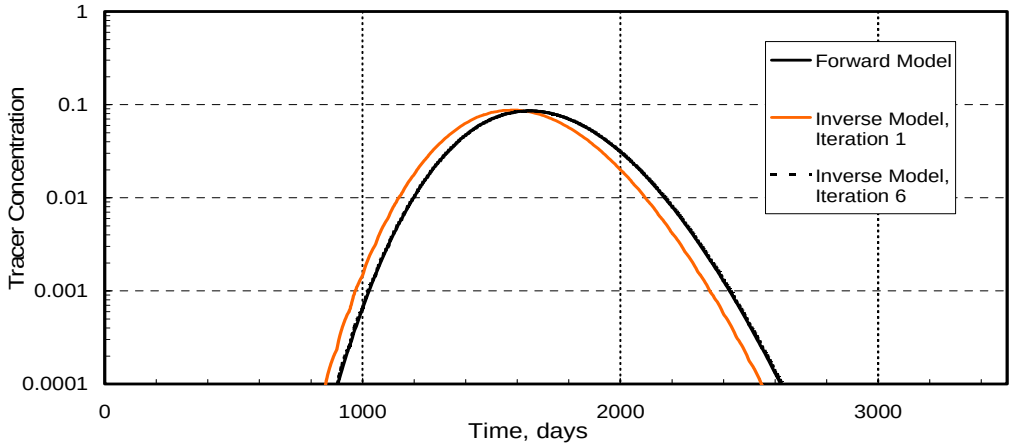

Figure 4.29. Match of the forward model tracer response from layer 1 by iteration 1 and 6 of inverse model in Run 513

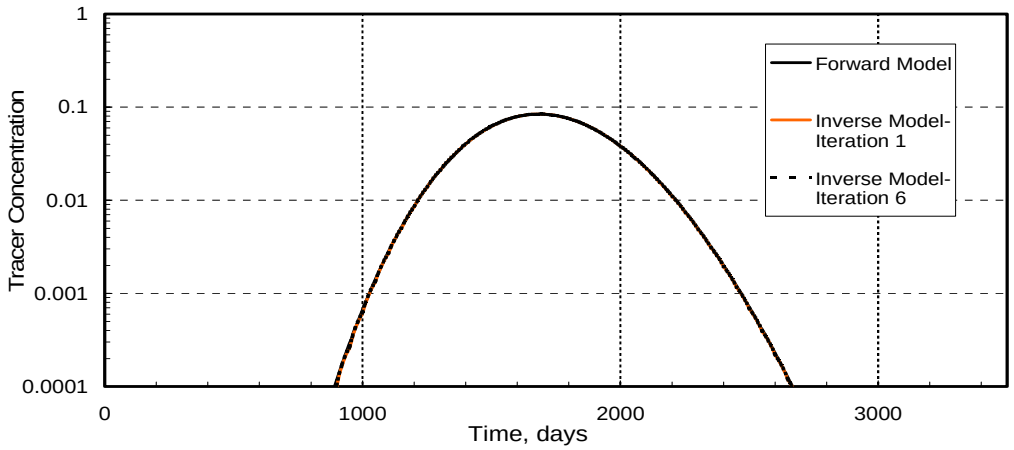

Figure 4.30. Match of the forward model tracer response from layer 1 by iteration 1 and 6 of inverse model in Run 513

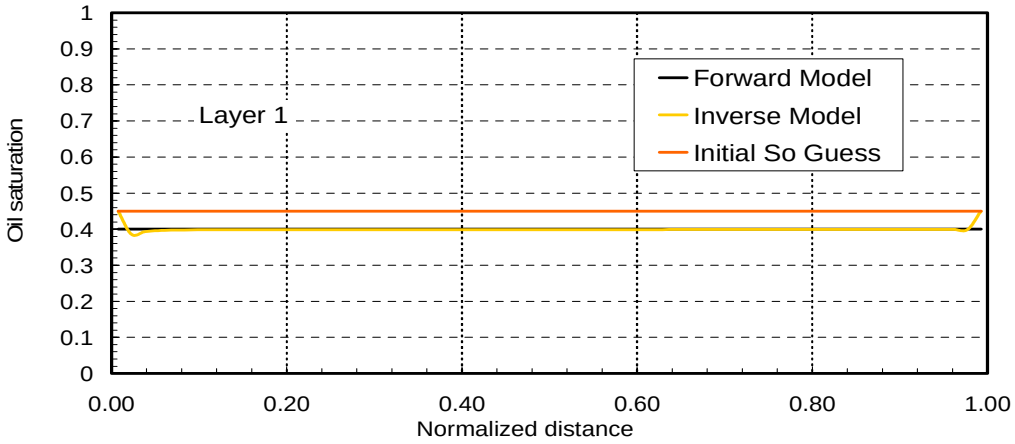

Figure 4.31. Inverse model oil saturation estimate in layer 1 in Run 513

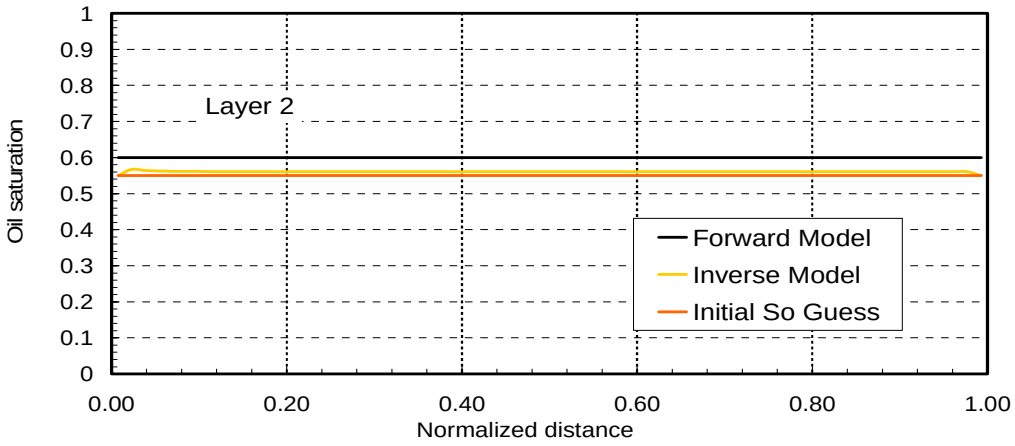

Figure 4.32. Inverse model oil saturation estimate in layer 2 in Run 513

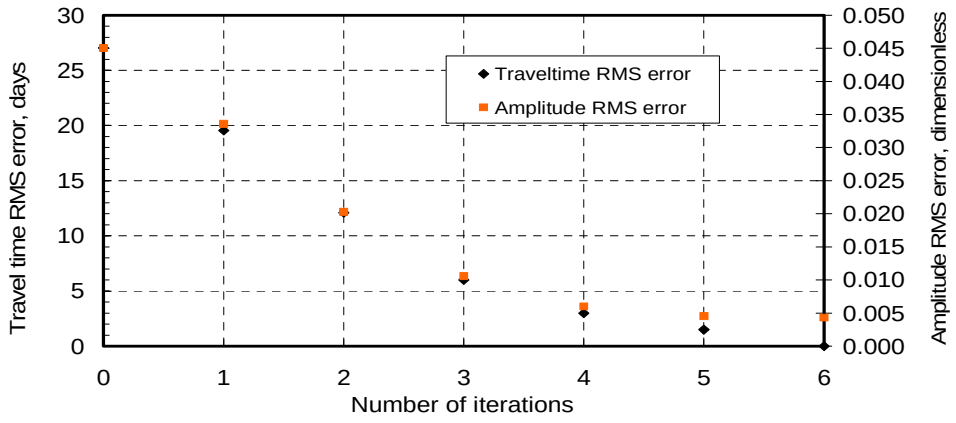

Figure 4.33. Root Mean Square error (RMS) change on travel time and amplitude during inversion in Run 514

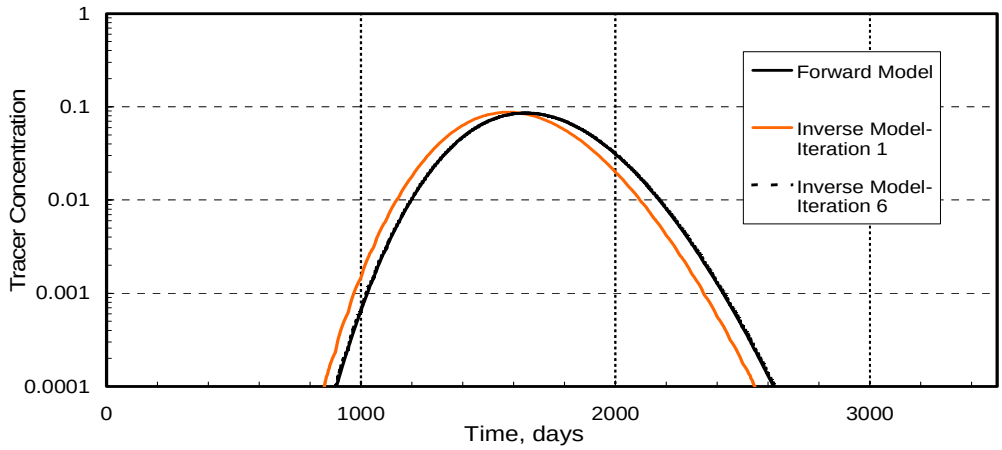

Figure 4.34. Match of the forward model tracer response from layer 1 by iteration 1 and 6 of inverse model in Run 514

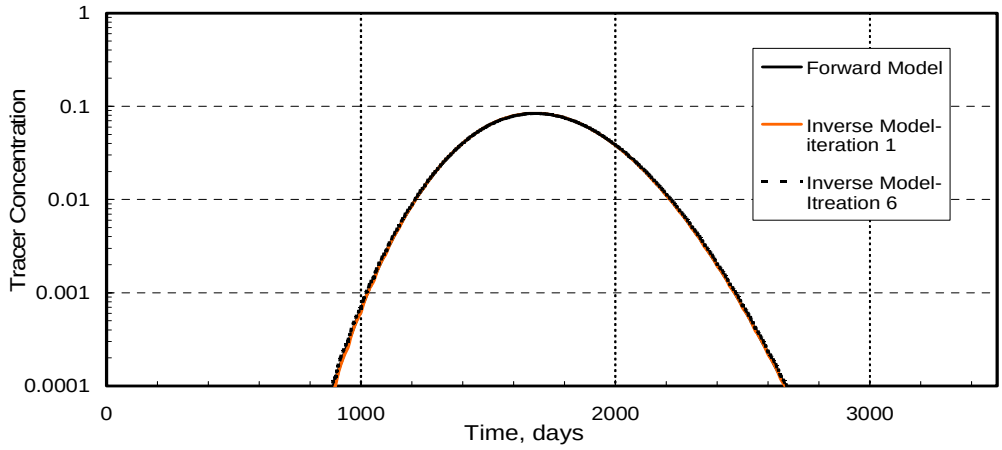

Figure 4.35. Match of the forward model tracer response from layer 2 by iteration 1 and 6 of inverse model in Run 514

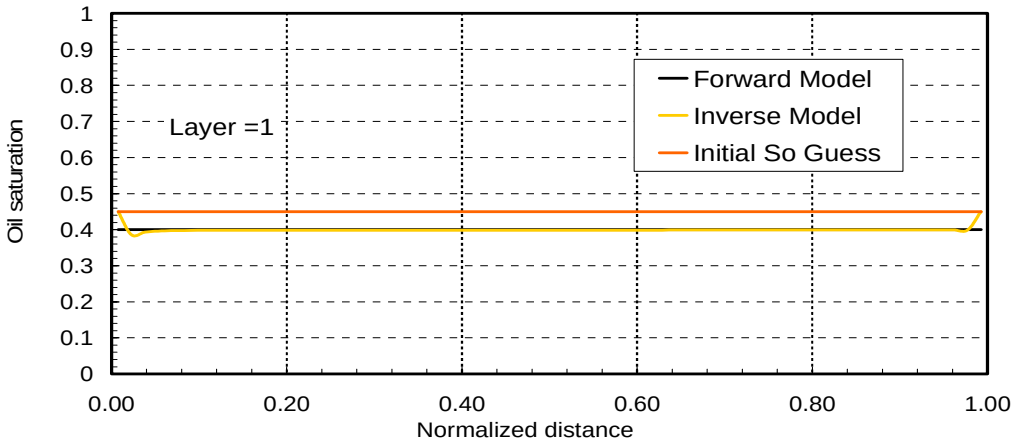

Figure 4.36. Inverse model oil saturation estimate in layer 1 in Run 514

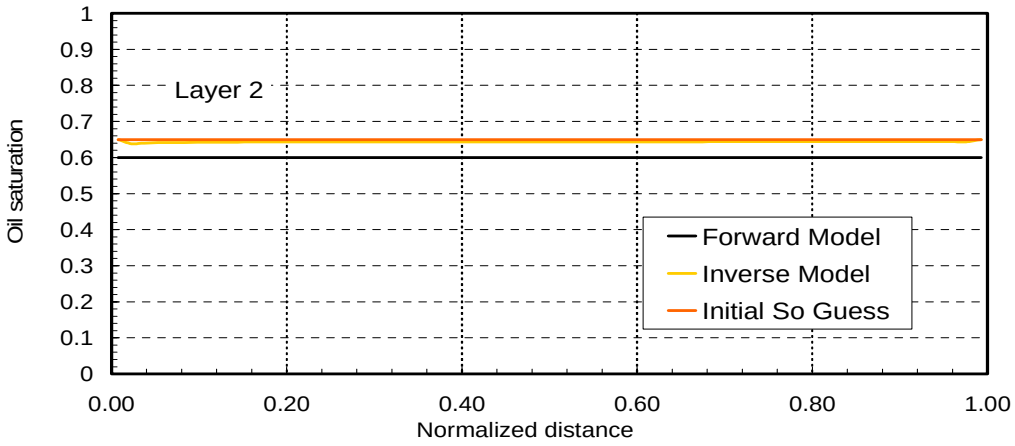

Figure 4.37. Inverse model oil saturation estimate in layer 2 in Run 514

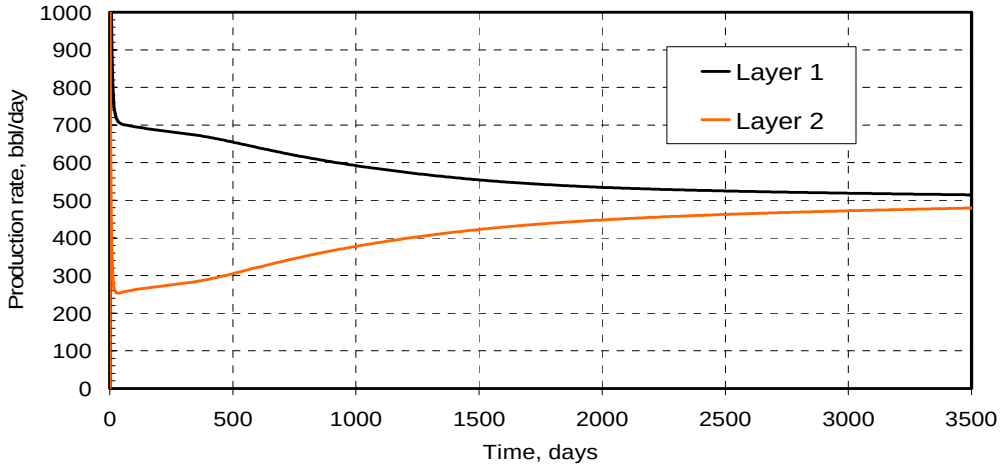

Figure 4.38. Injection rate change in Run 513-b

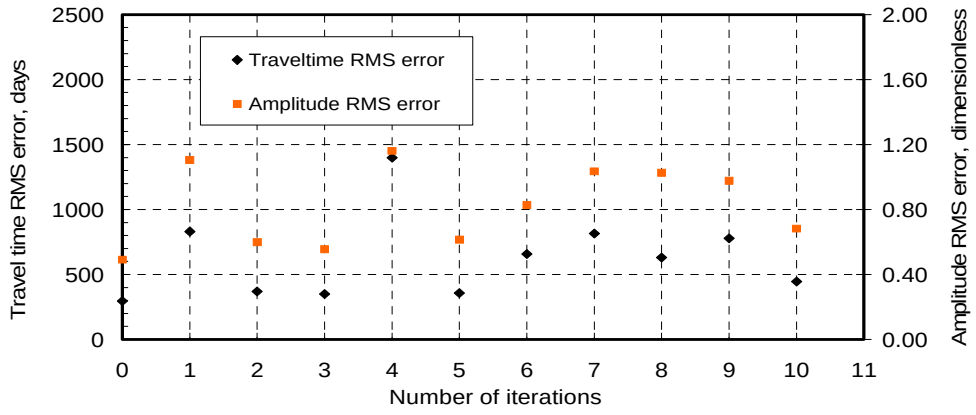

Figure 4.39. Root Mean Square error (RMS) change on travel time and amplitude during inversion in Run 513-b with changing flow rate in each layer

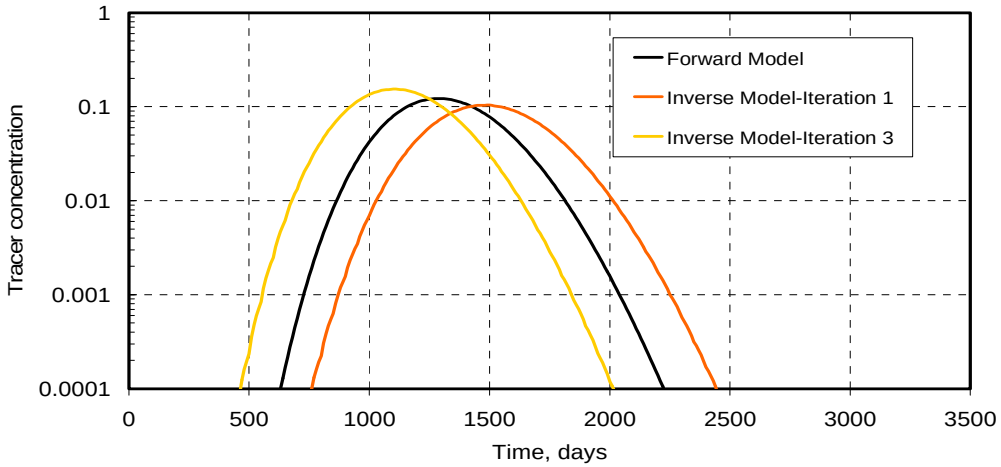

Figure 4.40. Match of the forward model tracer response from layer 1 by iteration 1 and 3 of inverse model in Run 513-b with changing flow rate in each layer

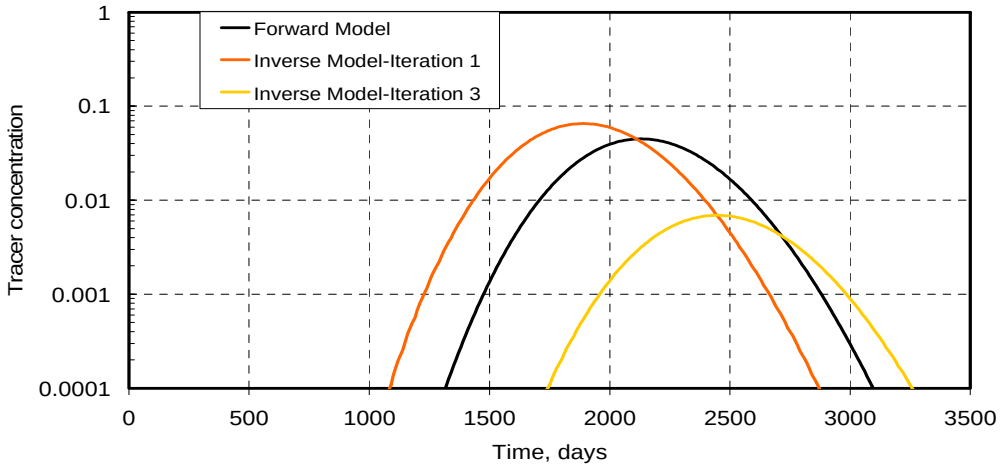

Figure 4.41. Match of the forward model tracer response from layer 2 by iteration 1 and 3 of inverse model in Run 513-b with changing flow rate in each layer

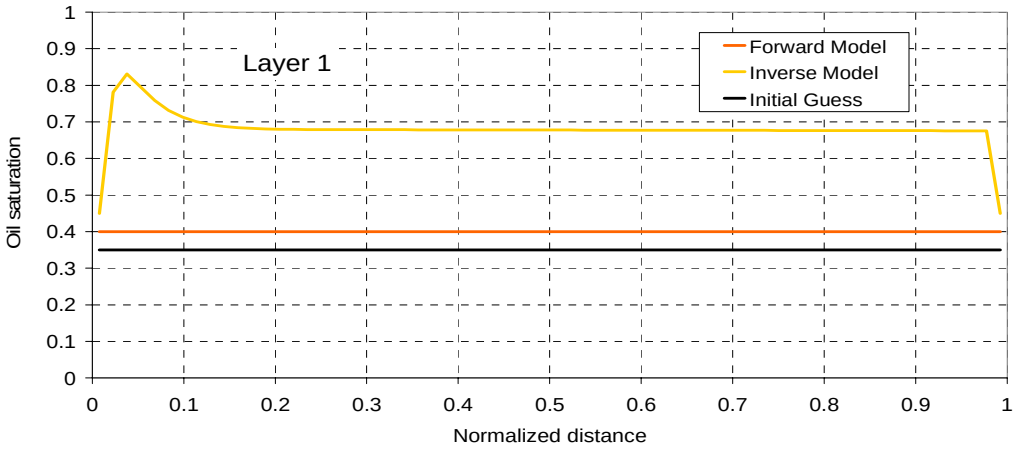

Figure 4.42. Inverse model oil saturation estimate in layer 1 in Run 513-b with changing flow rate in each layer

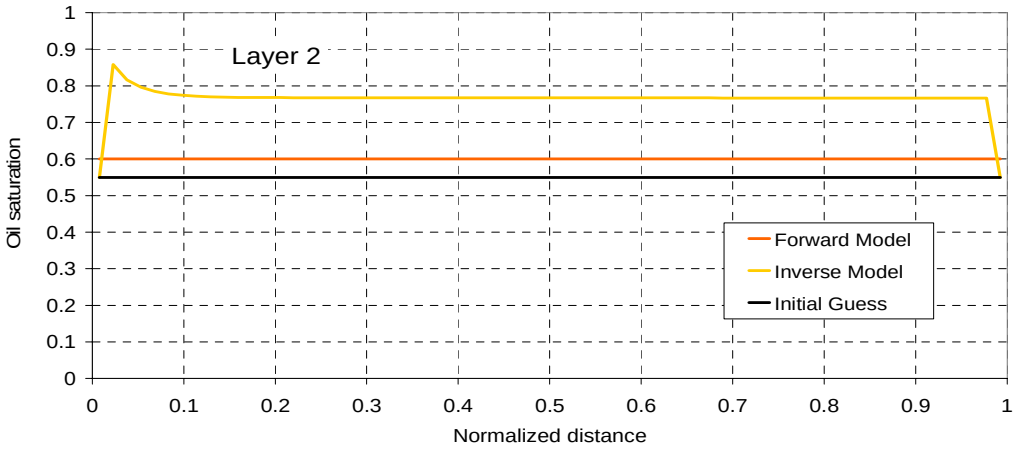

Figure 4.43. Inverse model oil saturation estimate in layer 2 in Run 513-b with changing flow rate in each layer

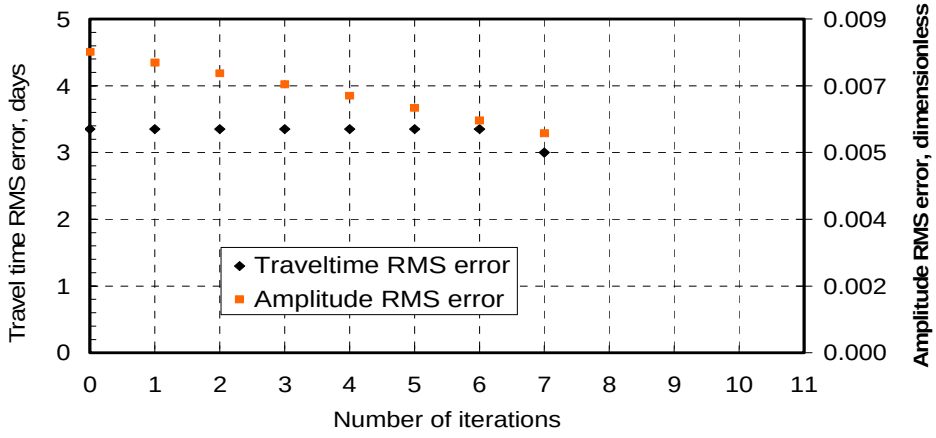

Figure 4.44. Root Mean Square error (RMS) change on travel time and amplitude during inversion in Run 613

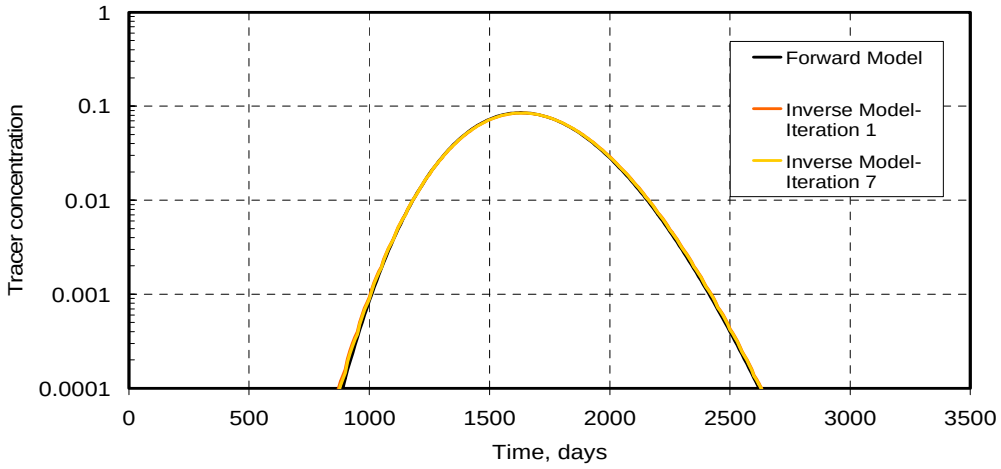

Figure 4.45. Match of the forward model tracer response from layer 1 by iteration 1 and 7 of inverse model in Run 613

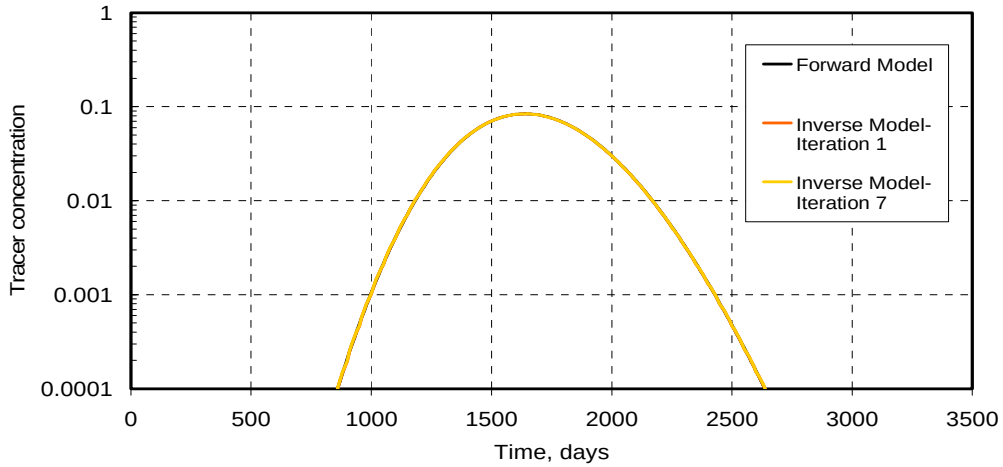

Figure 4.46. Match of the forward model tracer response from layer 2 by iteration 1 and 7 of inverse model in Run 613

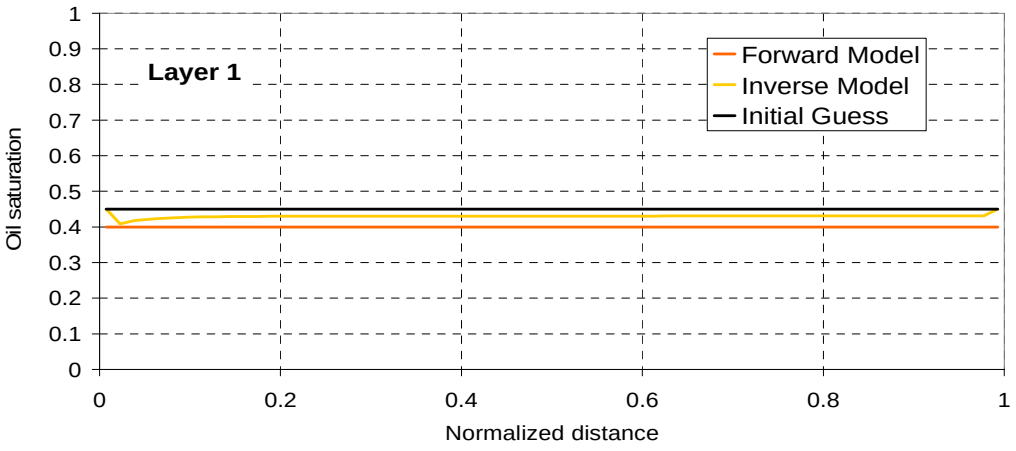

Figure 4.47. Inverse model oil saturation estimate in layer 1 in Run 613

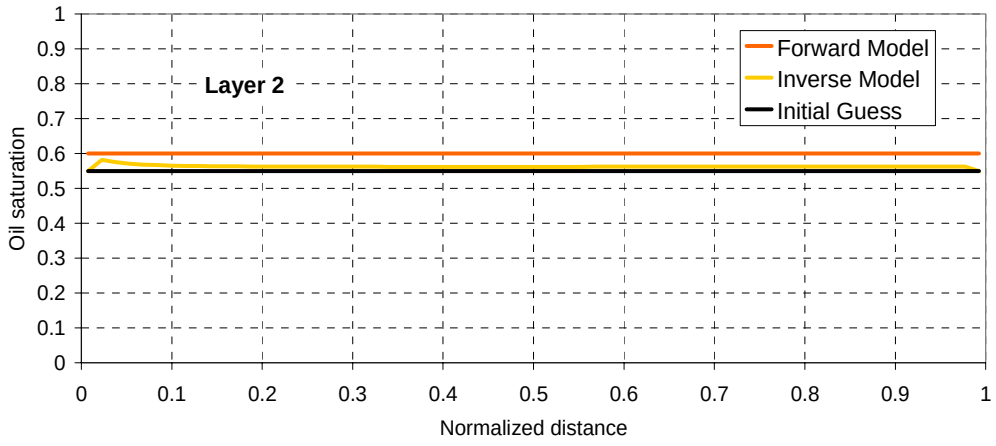

Figure 4.48. Inverse model oil saturation estimate in layer 2 in Run 613

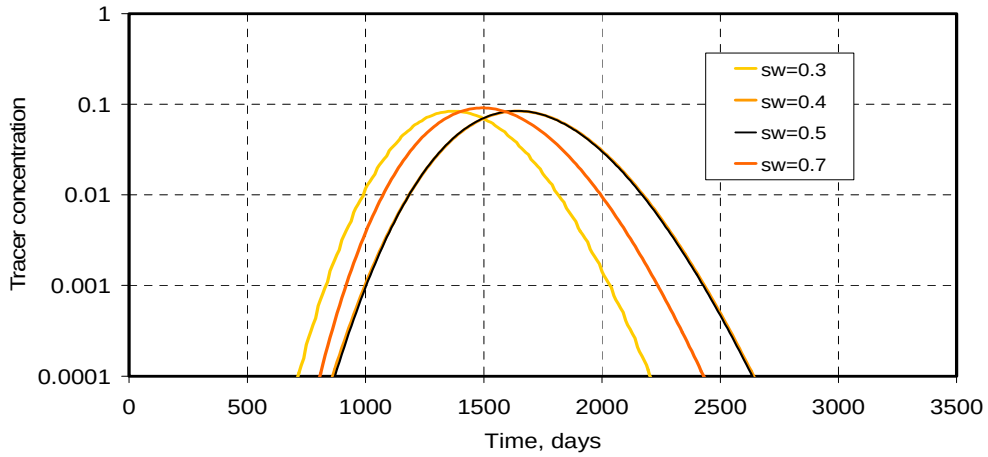

Figure 4.49. The effect of the initial water saturation on the tracer response in Run 713

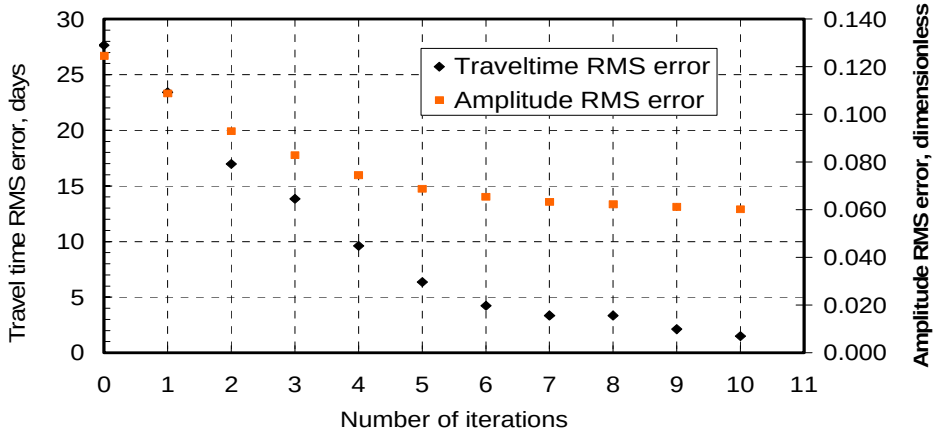

Figure 4.50. Root Mean Square error (RMS) change on travel time and amplitude during inversion in Run 713

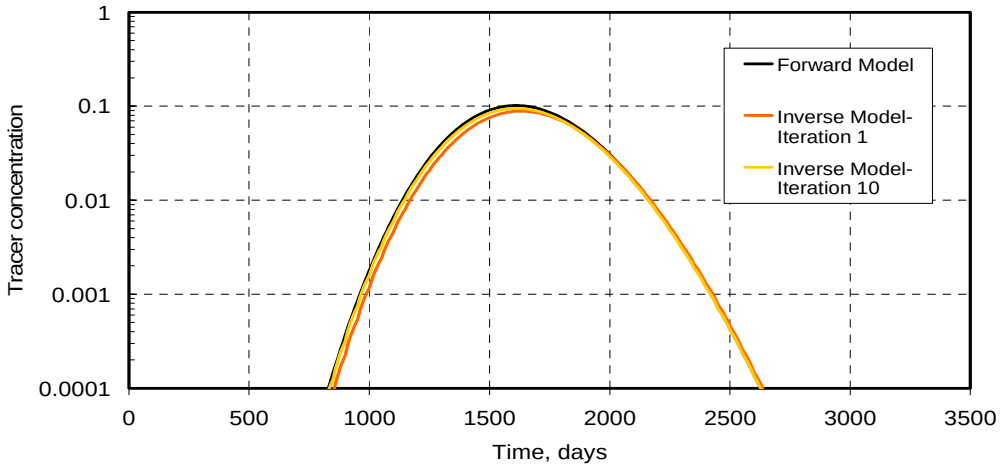

Figure 4.51. Match of the forward model tracer response from layer 1 by iteration 1 and 10 of inverse model in Run 713

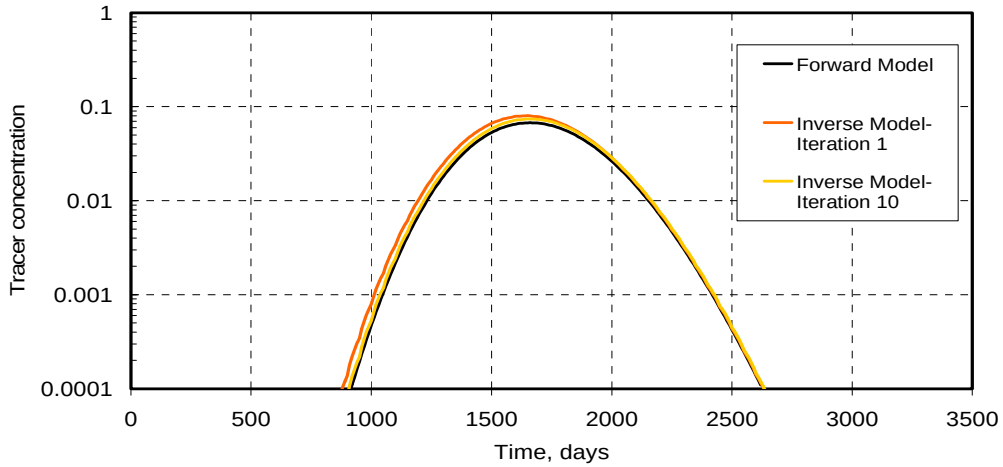

Figure 4.52. Match of the forward model tracer response from layer 2 by iteration 1 and 10 of inverse model in Run 713

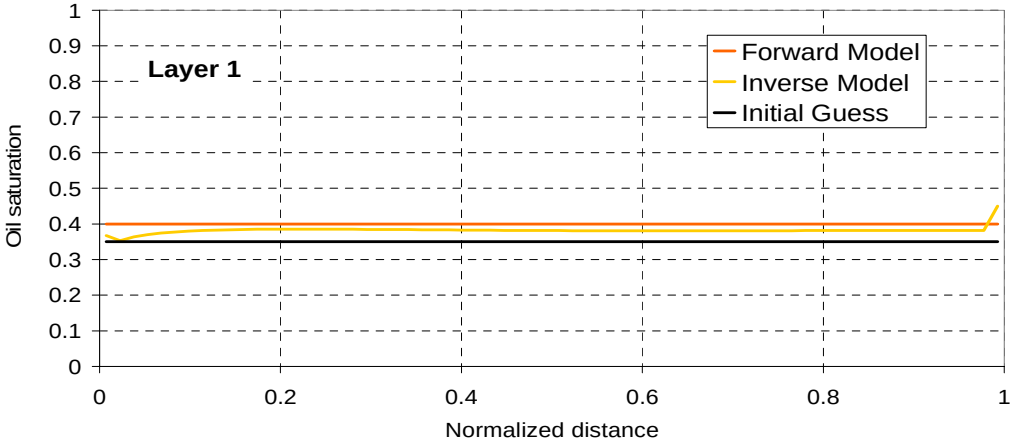

Figure 4.53. Inverse model oil saturation estimate in layer 1 in Run 713

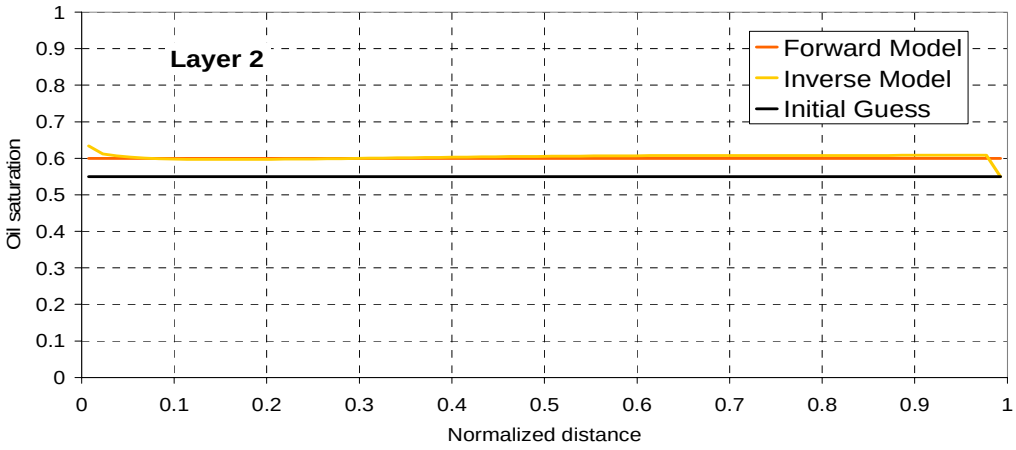

Figure 4.54. Inverse model oil saturation estimate in layer 2 in Run 713

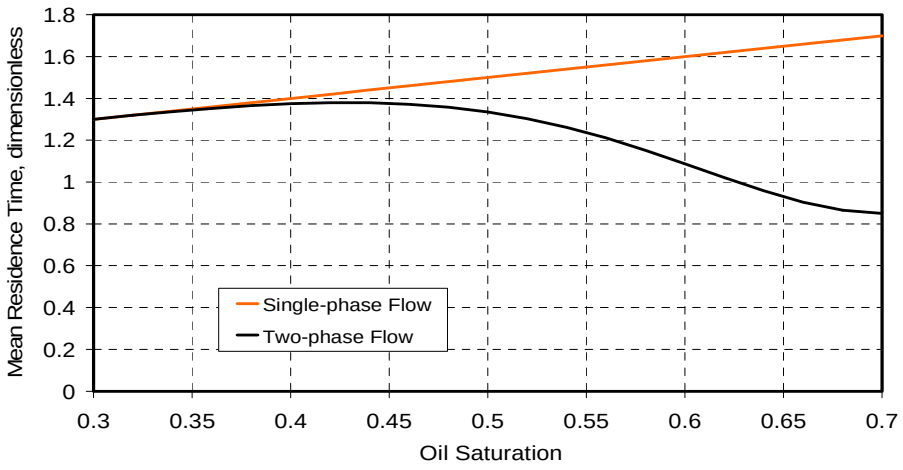

Figure 4.55. Mean residence time sensitivity to the oil saturation in Run723

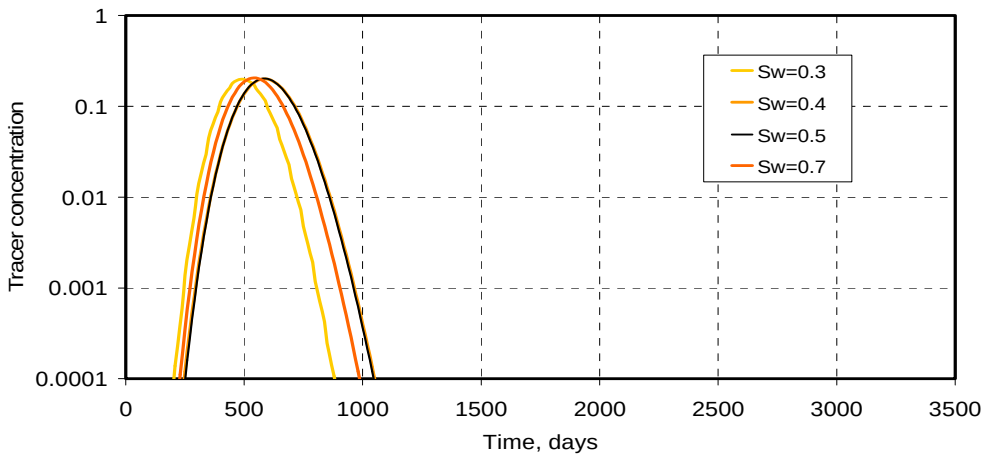

Figure 4.56. The effect of the initial water saturation on the tracer response in Run 723.

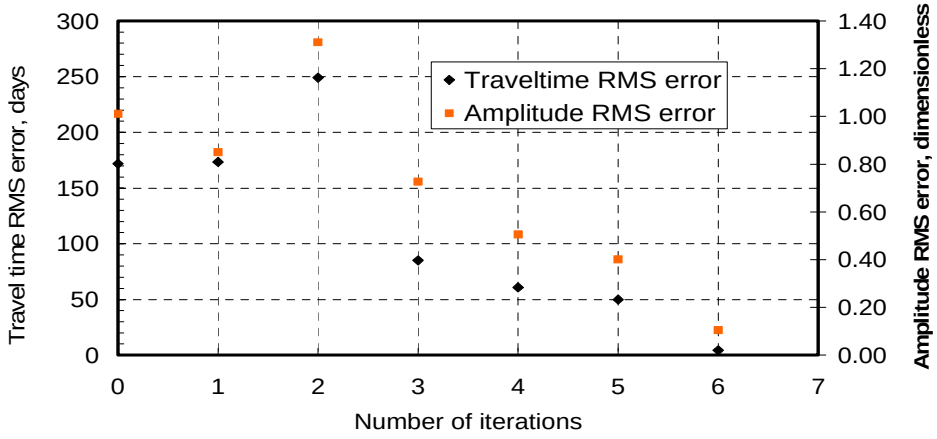

Figure 4.57. Root Mean Square error (RMS) change on travel time and amplitude during inversion in Run 723

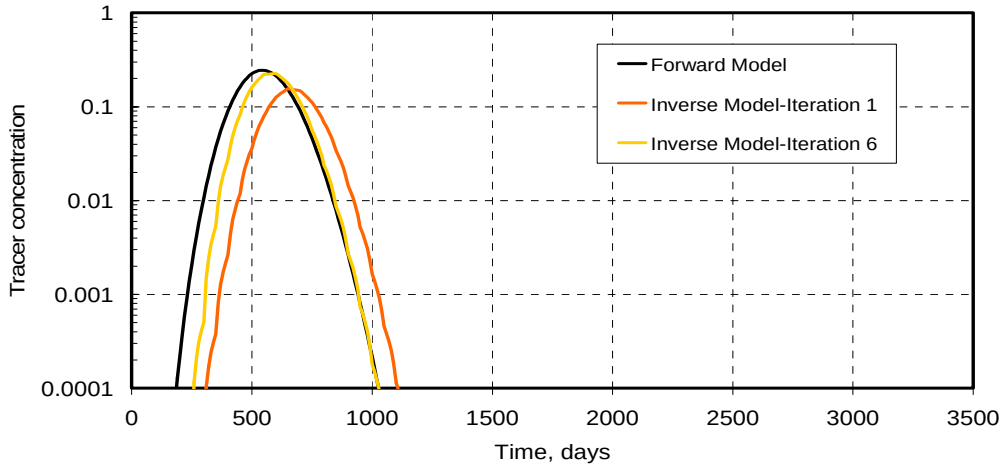

Figure 4.58. Match of the forward model tracer response from layer 1 by iteration 1 and 6 of inverse model in Run 723

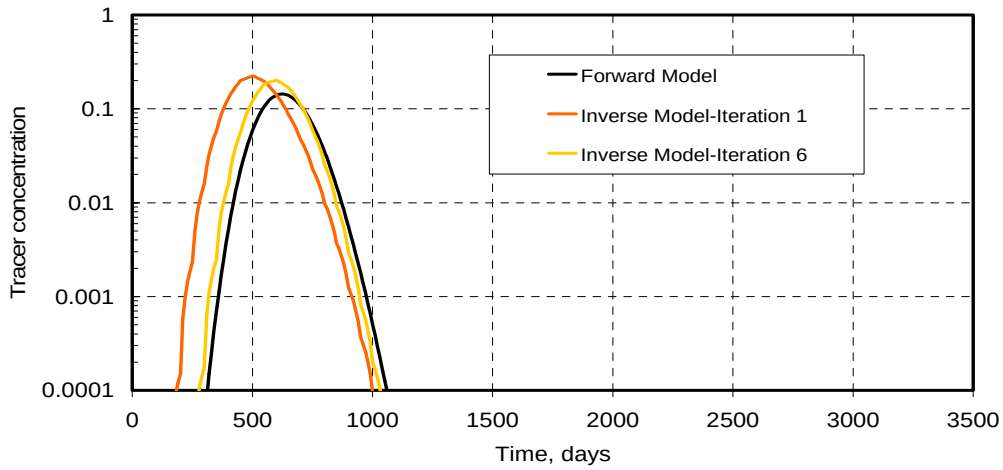

Figure 4.59. Match of the forward model tracer response from layer 2 by iteration 1 and 6 of inverse model in Run 723

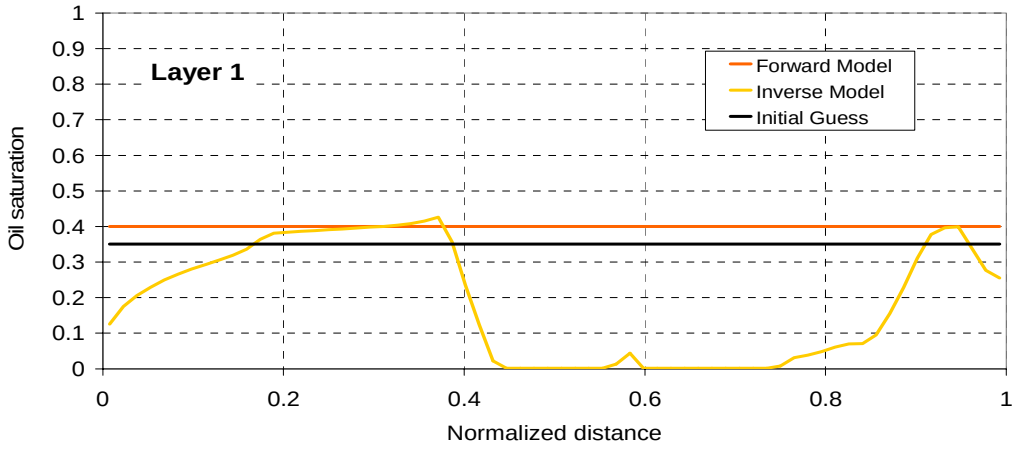

Figure 4.60. Inverse model oil saturation estimate in layer 1 in Run 723

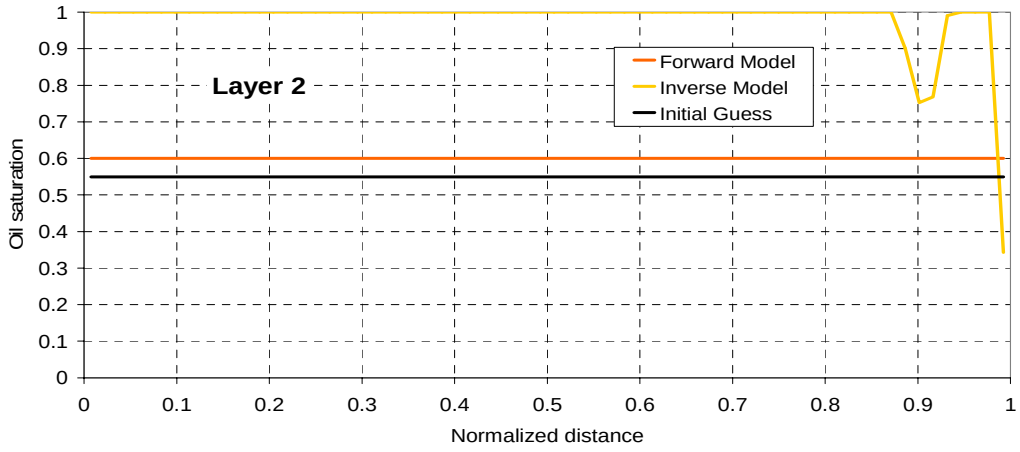

Figure 4.61. Inverse model oil saturation estimate in layer 2 in Run 723

CHAPTER 5: Conclusions and Recommendations for Future Work

5.1 INVERSE MODEL IN SINGLE-PHASE FLOW

Inverse modeling was applied to two cases: a reservoir with uniform permeability layers and a reservoir with a stochastically permeability distribution. In the layered permeability case, the sensitivity to tracer partition coefficient, initial oil saturation guess, tracer concentration detection limit and to the order of the geological layers are was investigated. Next, the MOM calculations were performed at various tracer detection limits and the results are compared with inverse model saturation estimates. Lastly, the methods were used in a complementary way by using the oil saturation from the MOM as the initial guess for the inverse calculation.

MOM and inverse model techniques were also applied to an inverted full five-spot well pattern with the stochastic permeability field. The MOM and inverse model techniques were applied for various kv/kh ratios. The average MOM oil saturation estimates in each quadrant of the five spot were used as initial guesses for the inverse modeling.

It is concluded that a perfect tracer concentration match between the inverse and the forward models does not guarantee accurate oil saturation estimates. Moreover, inverse modeling is sensitive to tracer partition coefficient and initial oil saturation guesses. In addition, RMS error does not always decrease over the number of iterations. The inverse model is more successful in estimating the average oil saturation than the oil saturation distribution in the reservoir. One big advantage of inverse modeling is that it extrapolates the tracer concentration response at any detection limit in a way that is in

general more accurately than the empirical exponential extrapolation of the tracer tail. Inverse modeling gave a good estimate of oil saturation for TDLs of 0.0001, 0.001 and 0.01 for the layered permeability reservoir case.

For the full five-spot case with the stochastic permeability field, oil saturation estimates were not as good as they were in the layered reservoir case. Although the MOM average oil saturation estimates, which are the initial oil saturation guesses for inverse model, in each quadrant are quite close to the forward model values, inverse model estimates were poor. The accuracy of vertical oil saturation distribution estimates using the MOM are better for low vertical permeability, but this is not true for the inverse model technique. Instead in some quadrants, inverse model oil saturation estimate error increases with the decreasing vertical permeability. Lastly, it can be said that MOM oil saturation estimates always have less error than inverse model oil saturation estimates. The important conclusions on inverse model, which can be obtained from both cases,

- Inverse model is very sensitive to the initial guess.
- Inverse model is sensitive to tracer partition coefficient
- The RMS error on travel time and amplitude does not always decrease over the number of iterations.
- A perfect tracer concentration match between the inverse and the forward models does not guarantee accurate oil saturation estimate.
- Inverse model extrapolates the tracer concentration response at any detection limit accurately.
- Inverse model is not depended on the kv/kh ratio as much as MOM.

5.2 INVERSE MODEL IN TWO-PHASE FLOW

Inverse model is tested in two-phase flow simulations with a two-dimensional synthetic reservoir model. First, sensitivity of oil saturation to tracer partition coefficient is analyzed by observing the mean residence time variation with changing oil saturation. In addition to the sensitivity of oil saturation to the tracer partition coefficient, the affect of the initial oil saturation in the reservoir to the produced tracer concentration is studied. Then, sensitivity of inverse model to two different relative permeability curves, changing injection rate, cross-flow and to two different partition coefficients are studied. Below are the conclusions reached.

- The mean residence time versus oil saturation is changing monotonically in two-phase flow, like it is in single-phase flow.
- The tracer response is not really sensitive to the initial oil saturation in the reservoir because the most of the tracer is in the water behind the oil bank.
- Different oil saturations may have the same tracer response curve and this decreases the uniqueness of the inverse model oil saturation estimate.
- The flow rate change seems to seriously affect the inverse calculation rather than the initial oil saturation in the reservoir does.
- Relative permeability change and cross flow do not make much difference in the inverse model estimate at the specific case it is used.
- Inverse model does not work with tracer partition coefficient 2 in two-phase flow.

5.3 RECOMMENDATIONS FOR THE FUTURE WORK

From this thesis study it is seen that inverse model is giving promising results but needs improvement. In all the cases studied, tracer response curves of the inverse and the forward models are matching very well most of the time. But, the oil saturation estimate

is not always satisfactory even if the initial oil saturation guess is very close to forward model value. This non-unique behavior may be avoided by including a conservative tracer with the partitioning tracer into the inverse model calculations. Concentration matches obtained with two tracers may decrease the non-uniqueness of the estimate. Also, matching inverse model tracer concentration and production rate with forward model together can be another way of obtaining accurate oil saturation estimates from inverse model.

Appendix A: Fundamentals of Streamline Simulation for Obtaining Analytical Sensitivities

The information given in Appendix A is taken from Oyerinde's (2004) master thesis.

A.1 CONVECTIVE TRACER TRANSPORT

Because tracers are often injected as a finite slug in small quantities, avoiding numerical dispersion in tracer transport modeling is a major concern. Utilizing streamline method in solute transport modeling is particularly useful because of its dispersion free simulation characteristic. For a solute transport, the convection-diffusion equation is given as

$$\phi \frac{\partial C(x,t)}{\partial t} = \nabla.\left[D(x)\nabla C(x,t)\right] - v\nabla C(x,t) \tag{A.1}$$

where C is the tracer concentration and D is the dispersion coefficient. If we assume convective transport only due to heterogeneous flow geometry, the neutral tracer transport equation becomes

$$\phi \frac{\partial C(x,t)}{\partial t} + v\nabla C(x,t) = 0 \tag{A.2}$$

Neglecting dispersion effects is tolerable assumption for the field-scale solute transports, because the macroscopic mixing is mainly attributed to the convective velocity variations from the subsurface heterogeneity. Applying coordinate transformation to time of flight, equation describing the transport of a neutral tracer in a

heterogeneous permeable medium, Equation A.2, can be written in the time of flight coordinates as follows

$$\frac{\partial C(\tau,t)}{\partial t}+\frac{\partial C(\tau,t)}{\partial \tau}=0 \qquad \text{(A.3)}$$

For a unit impulse concentration source at (τ, t) = (0, 0), the solution to the above equation or the impulse response is given by

$$C(x,t)=\delta(t-\tau(x)) \qquad \text{(A.4)}$$

where δ is the Dirac delta function. For an input with temporal variation $C_0(t)$ at injection well, the observed concentration at producer can be obtained by convolution of the input and the impulse response as

$$C(t)=C_0(t-\tau) \qquad \text{(A.5)}$$

The overall concentration response at the producer will be given by summing over the responses from all the streamlines reaching the producing well. The tracer response at a producer is obtained by integrating the contributions of individual streamlines

$$C(t)=\int_{all\,\psi} C_0(t-\tau)d\psi \qquad \text{(A.6)}$$

Crane and Blunt provides recent review of the convective as well as reactive solute transport modeling using streamline models.

A.2. COMPUTATION OF SENSITIVITY OF TRACER RESPONSE TO RESERVOIR PARAMETERS

Sensitivity calculations constitute a critical aspect of inverse modeling. By sensitivity, we mean the partial derivative of the production response with respect to model parameters such as permeability, porosity and saturation. Although several

methods are available for computing sensitivities, for example, numerical perturbation method, direct method, or adjoint state method, these are limited by their computational costs and complex implementations. The streamline based analytic sensitivity computation approach is extremely efficient and requires only a single simulation run.

For incompressible water flooding in nondeformable media and given constant well conditions, change of pressure profile (and consequently of streamline trajectory) is mainly due to total mobility change via saturation change. However, the total mobility stays more or less constant for most of the moderate to unfavorable mobility ratio water flooding, making stationary streamline assumption quite tolerable. Yoon (2000) presented a synthetic water flooding example for the end point mobility ratio of 1.43 that verified the assumption above. He demonstrated that a saturation solution with one pressure solving was nearly identical to the saturation from the numerical solution with 10 pressure solving. No significant difference among the saturation profiles indicates that single pressure update at the beginning of simulation and stationary streamlines thereafter would be a valid assumption.

It is possible to analytically derive a relationship between perturbations in reservoir properties, such as permeability, porosity or saturation, and changes in dynamic data such as water-cut and tracer response under the stationary streamline assumption. The relationship can be framed entirely in terms of quantities computed by a streamline simulator. Then sensitivities of the production response with respect to reservoir parameters are formulated along streamlines.

As described earlier, streamline method decouples flow and transport by a coordinate transformation from the physical space to one following flow directions - the tracer time of flight along streamlines. The time of flight can be defined as

$$\tau = \int_{\psi} s(x)dr \qquad \text{(A.7)}$$

where the integral is along the streamline trajectory, ψ, r is measured along streamlines, and *s(x)* is the ‘slowness’, defined as a reciprocal of magnitude of interstitial velocity v adjusted for partitioning properties of the tracer, is given by

$$s(x) = \frac{1}{|v(x)|}\left(S_w + K_0 S_0\right) \tag{A.8}$$

where Ko is the partitioning coefficient of tracer defined as the ratio of tracer concentration in oil phase to that in water phase. Introducing the Darcy equation, the slowness becomes

$$s(x) = \frac{\phi(x)}{\lambda_t k(x)|\nabla P|}\left(S_w + K_0 S_0\right) \tag{A.9}$$

Because s(x) is a composite function involving reservoir properties, its first order variation will be given by

$$\delta s(x) = \frac{\partial s(x)}{\partial k}\delta k(x) + \frac{\partial s(x)}{\partial \phi}\delta\phi(x) + \frac{\partial s(x)}{\partial S_w}\delta S_w \tag{A.10}$$

where the partial derivatives are

$$\begin{aligned}
\frac{\partial s(x)}{\partial k} &= \frac{-\phi(x)}{\lambda_t k^2(x)|\nabla P|}(S_w + K_0 S_0) = -\frac{s(x)}{k} \\
\frac{\partial s(x)}{\partial \phi} &= \frac{1}{\lambda_t k(x)|\nabla P|}(S_w + K_0 S_0) = \frac{s(x)}{\phi} \\
\frac{\partial s(x)}{\partial S_w} &= \frac{\phi(x)}{\lambda_t k(x)|\nabla P|}(1 - K_0) = \frac{(1-K_0)}{(S_w + K_0 S_0)} s(x)
\end{aligned} \tag{A.11}$$

Note that for unit partitioning coefficient, the tracer response will be insensitive to saturation changes as one might expect. Also, in the above expressions, we have ignored pressure changes resulting from small variations in permeability and assumed that the end point water relative permeability varies little with saturation change near residual oil saturation (Yoon, 2000). Under these assumptions, since streamline trajectory is a function of pressure, it is natural to assume that streamlines do not shift as a result of

small perturbation in permeability or saturation. Now it is possible to relate the change in traveltime δτ to the change in slowness:

$$\delta\tau = \int_{\psi} \delta s(x)dr = \int_{\psi} \left[-\frac{s(x)}{k(x)}\delta k(x) + \frac{s(x)}{\phi(x)}\delta\phi(x) + \frac{(1-K_0)}{(S_w + K_0 S_0)} s(x)\delta S_w \right] dr \quad \text{(A.12)}$$

Under the stationary streamline assumption, streamline tracer traveltime sensitivity along a single streamline ψ at a producer with respect to permeability, porosity, and saturation at particular grid block containing x is given by integrating Equation (A.13) from the inlet to the outlet of streamline within the grid block:

$$\begin{aligned}
\frac{\partial\tau(\psi)}{\partial k} &= \int_{inlet}^{outlet} \left[-\frac{s(x)}{k(x)} \right] dr(\psi) \\
\frac{\partial\tau(\psi)}{\partial \phi} &= \int_{inlet}^{outlet} \left[-\frac{s(x)}{\phi(x)} \right] dr(\psi) \\
\frac{\partial\tau(\psi)}{\partial \phi} &= \int_{inlet}^{outlet} \left[-\frac{s(x}{\phi(x)} \right] dr(\psi)
\end{aligned} \quad \text{(A.13)}$$

Note that the slowness in the grid block of interest is known from pressure solution and the integration can be carried out while tracing streamlines. The travel time sensitivity can then be obtained by integrating the streamline sensitivities over all streamlines contributing a producer from a single streamline simulation.

For an injected concentration history $C_0(t)$, the corresponding tracer concentration response at the producer along with single streamline can be written as

$$C(t) = C_0\left(t - \int_{\psi} s(x)dr \right) \quad \text{(A.14)}$$

Consider a small perturbation in reservoir properties about an initial reservoir model, δm. The resulting changes in slowness and tracer concentrations can be written as

$$s(x) = s^0(x) + \delta s(x)$$
$$C(x,t) = C^0(x,t) + \delta C(x,t) \tag{A.15}$$

where s^0 and C^0 are initial slowness distribution in the reservoir and the associated tracer response, respectively. If we assume that streamlines do not shift as a result of small perturbations in medium properties, then the change in concentration response at the producing well can be derived based on a Taylor series expansion

$$\delta C(x,t) = -C_0^{'}(t-\tau)\int_{\psi}\delta s(x)dr \tag{A.16}$$

Tracer travel time and concentration sensitivities with respect to permeability, porosity, and water saturation can be obtained by integrating Equation A.16 over all streamlines contributing to a producer.

Also, we can see that the above expressions for sensitivity of tracer concentration and water cut response only involve quantities that are readily available once we generate the velocity field and define the streamline trajectories in a streamline simulator. Thus, in a single forward run of a streamline simulator we may derive all the sensitivity coefficients required to solve the inverse problem.

The estimated change in δC due to a perturbation in reservoir properties, δm, is used in construction of sensitivity matrix, G, for minimization of the objective function.

A.3. ACCOUNTING FOR MOBILE OIL SATURATIONS

The general form of Equation A.1 for an ideal water flood tracer is given by

$$\phi\frac{\partial\left(\left(S_w + K_0S_0\right)C\right)}{\partial t} + \vec{u}\nabla\left(\left(F_w + K_0S_0\right)C\right) = Q_1M\delta(t) \tag{A.17}$$

The source term represents a spike of tracer of total mass or activity M, injected into the reservoir over a very short time interval. (For a finite tracer slug, “t=0” corresponds to the time at which half the tracer has been injected. The delta function approximation is an excellent one at the field scale. Only the nearest and quickest of field tracer response curves have sufficiently small dispersion to resolve the width of the original spike). The velocity u is the total of the two phases, and is used to define the time of flight,

$$\vec{u}.\nabla\tau = \phi \tag{A.18}$$

Expanding from conservation form and utilizing the time of flight gives

$$(S_w + K_0 S_0)\frac{\partial C}{\partial \tau} + \left(F_w + K_0 F_0\right) \tag{A.19}$$

In essence, compared to the total two phase flow, the tracer moves with a retardation factor of

$$\frac{S_w + K_o S_o}{F_w + K_o F_o} \tag{A.20}$$

The dependence of the retardation factor on fractional flow indicates that when both water and oil phases are flowing, the interpretation may be fairly complicated.

Taking the retardation factor into consideration, the “slowness” defined in Equation A.2 can be generalized as

$$s(x) = \frac{\phi(x)}{\lambda_t k(x)\left|\nabla P\right|}\left(\frac{S_w + K_o S_o}{F_w + K_o F_o}\right) \tag{A.21}$$

Since S(x) is a composite function involving reservoir properties, the partial derivatives of its first order variation will be given by

$$\frac{\partial s(x)}{\partial k} = \frac{\partial}{\partial k}\left\{\left(\frac{S_w + K_o S_o}{F_w + K_o F_o}\right).\frac{\phi(x)}{\lambda_t k(x)|\nabla P|}\right\} = \left(\frac{S_w + K_o S_o}{F_w + K_o F_o}\right).\frac{s(x)}{k(x)} \tag{A.22}$$

$$\frac{\partial s(x)}{\partial \phi} = \frac{\partial}{\partial \phi}\left\{\left(\frac{S_w + K_o S_o}{F_w + K_o F_o}\right).\frac{\phi(x)}{\lambda_t k(x)|\nabla P|}\right\} = \left(\frac{S_w + K_o S_o}{F_w + K_o F_o}\right).\frac{s(x)}{\phi(x)} \tag{A.23}$$

$$\frac{\partial s(x)}{\partial S_w} = \frac{\partial}{\partial S_w}\left\{\left(\frac{S_w + K_o S_o}{F_w + K_o F_o}\right).\frac{\phi(x)}{\lambda_t k(x)|\nabla P|}\right\} \tag{A.24}$$

Assuming total mobility is constant, the partial derivative in Equation A.24 reduces to

$$\frac{\partial s(x)}{\partial S_w} = \left\{\frac{(1-K_o)\left\{F_w + K_o F_o - (S_w + K_o S_o)\frac{\partial f_w}{\partial S_w}\right\}}{F_w + K_o F_o}\right\} s(x) \tag{A.25}$$

It is these modifications made to the sensitivity calculations that facilitate the inversion process in the presence of mobile oil saturations.

Appendix B: Sample Input Files

B.1 INVERSE MODEL FORWARD RUN ECLIPSE INPUT FILE FOR SINGLE PHASE FLOW

```
-- 3D layered permeability model.
-- Tracer test simulation with the use of downhole sensors for vertical charachterization of reservoir
-- Eclipse input file
--    * regular grid
--    * tracer simulation
-- ********************************************************************
-- ********************************************************************

NOECHO

RUNSPEC

TITLE
3D, heterogeneous, 22x22x10, 29/11/04

oil
water
field

start    --   start date
1 'JAN' 2000 /

dimens   --   nx   ny   nz
              22   22  10  /

eqldims  --  ntequl  ndprvd  ndrxvd  nttrvd  nstrvd
                1     100      10       1      20 /

endscale --  directional  reversible  tables  nodes
             'NODIR'      'REVERS'         2      5  /

tabdims  --  ntsfun  ntpvt  nssfun  nppvt  ntfip  nrpvt
                1      1     101     12      1     12   /

welldims --  wells  connect per well  groups  wells per group
                40                75       2               40 /

nstack   --  linear solver stack size
             100 /
TRACERS   --    oil   water   gas  environ  diffusion
                 0       4     0      0      'DIFF'/
PARTTRAC
4   4   3/

UNIFOUT

IMPLICIT

--UNIFIN

--  ************************************************************
--  ******  End    RUNSPEC section    *******************
--  ******                            *******************
--  ******  Begin  GRID section       *******************
--  ************************************************************

GRID

-- PSEUDOS    -- Write binary files for input to Pseudo

-- RPTGRID
--   'TRANX' 'TRANZ'  'NNC' 'PORV' /

DX
 4840*30 /

DY
 4840*30 /

DZ
 4840*5 /

--BOX     - ix1 ix2 jy1 jy2 kz1 kz2
 --           1 22   1   22   1   1 /

TOPS
484*0 /

--ENDBOX

PORO
 4840*0.2 /

PERMX
484*300
484*250
484*150
484*100
484*90
484*200
484*500
484*650
484*600
```

484*300
/

COPY

PERMX PERMY /
PERMX PERMZ /
/

MULTIPLY
PERMZ 0.1 1 22 1 22 1 10/
/

GRIDFILE
  2
/

INIT

-- **
-- ****** End GRID ******************
-- ****** ******************
-- ****** Begin PROPS ******************
-- **

PROPS

swof -- sw krw kro pcow
0.0000E+00 0.0000E+00 1.0000E+00 0.0000
1.0000E-02 1.2023E-03 9.7862E-01 0.0000
2.0000E-02 3.3075E-03 9.5749E-01 0.0000
3.0000E-02 5.9786E-03 9.3661E-01 0.0000
4.0000E-02 9.0993E-03 9.1597E-01 0.0000
5.0000E-02 1.2604E-02 8.9558E-01 0.0000
6.0000E-02 1.6448E-02 8.7544E-01 0.0000
7.0000E-02 2.0599E-02 8.5554E-01 0.0000
8.0000E-02 2.5033E-02 8.3588E-01 0.0000
9.0000E-02 2.9730E-02 8.1647E-01 0.0000
1.0000E-01 3.4674E-02 7.9730E-01 0.0000
1.1000E-01 3.9850E-02 7.7837E-01 0.0000
1.2000E-01 4.5249E-02 7.5969E-01 0.0000
1.3000E-01 5.0858E-02 7.4125E-01 0.0000
1.4000E-01 5.6669E-02 7.2306E-01 0.0000
1.5000E-01 6.2675E-02 7.0510E-01 0.0000
1.6000E-01 6.8868E-02 6.8739E-01 0.0000
1.7000E-01 7.5241E-02 6.6991E-01 0.0000
1.8000E-01 8.1790E-02 6.5268E-01 0.0000
1.9000E-01 8.8508E-02 6.3569E-01 0.0000
2.0000E-01 9.5390E-02 6.1893E-01 0.0000
2.1000E-01 1.0243E-01 6.0242E-01 0.0000
2.2000E-01 1.0963E-01 5.8614E-01 0.0000
2.3000E-01 1.1698E-01 5.7011E-01 0.0000
2.4000E-01 1.2448E-01 5.5431E-01 0.0000
2.5000E-01 1.3213E-01 5.3874E-01 0.0000
2.6000E-01 1.3991E-01 5.2342E-01 0.0000
2.7000E-01 1.4784E-01 5.0833E-01 0.0000
2.8000E-01 1.5590E-01 4.9347E-01 0.0000
2.9000E-01 1.6410E-01 4.7886E-01 0.0000
3.0000E-01 1.7242E-01 4.6447E-01 0.0000
3.1000E-01 1.8088E-01 4.5032E-01 0.0000
3.2000E-01 1.8946E-01 4.3641E-01 0.0000
3.3000E-01 1.9817E-01 4.2273E-01 0.0000
3.4000E-01 2.0699E-01 4.0928E-01 0.0000
3.5000E-01 2.1594E-01 3.9606E-01 0.0000
3.6000E-01 2.2501E-01 3.8308E-01 0.0000
3.7000E-01 2.3419E-01 3.7032E-01 0.0000
3.8000E-01 2.4349E-01 3.5780E-01 0.0000
3.9000E-01 2.5290E-01 3.4551E-01 0.0000
4.0000E-01 2.6243E-01 3.3345E-01 0.0000
4.1000E-01 2.7206E-01 3.2161E-01 0.0000
4.2000E-01 2.8180E-01 3.1001E-01 0.0000
4.3000E-01 2.9165E-01 2.9863E-01 0.0000
4.4000E-01 3.0161E-01 2.8748E-01 0.0000
4.5000E-01 3.1167E-01 2.7655E-01 0.0000
4.6000E-01 3.2183E-01 2.6586E-01 0.0000
4.7000E-01 3.3210E-01 2.5538E-01 0.0000
4.8000E-01 3.4246E-01 2.4514E-01 0.0000
4.9000E-01 3.5293E-01 2.3511E-01 0.0000
5.0000E-01 3.6349E-01 2.2531E-01 0.0000
5.1000E-01 3.7416E-01 2.1574E-01 0.0000
5.2000E-01 3.8492E-01 2.0638E-01 0.0000
5.3000E-01 3.9577E-01 1.9725E-01 0.0000
5.4000E-01 4.0672E-01 1.8833E-01 0.0000
5.5000E-01 4.1776E-01 1.7964E-01 0.0000
5.6000E-01 4.2890E-01 1.7117E-01 0.0000
5.7000E-01 4.4013E-01 1.6291E-01 0.0000
5.8000E-01 4.5145E-01 1.5488E-01 0.0000
5.9000E-01 4.6285E-01 1.4706E-01 0.0000
6.0000E-01 4.7435E-01 1.3945E-01 0.0000
6.1000E-01 4.8594E-01 1.3207E-01 0.0000
6.2000E-01 4.9761E-01 1.2489E-01 0.0000
6.3000E-01 5.0937E-01 1.1793E-01 0.0000
6.4000E-01 5.2122E-01 1.1119E-01 0.0000
6.5000E-01 5.3316E-01 1.0465E-01 0.0000
6.6000E-01 5.4517E-01 9.8329E-02 0.0000
6.7000E-01 5.5727E-01 9.2216E-02 0.0000
6.8000E-01 5.6946E-01 8.6312E-02 0.0000
6.9000E-01 5.8173E-01 8.0617E-02 0.0000
7.0000E-01 5.9408E-01 7.5130E-02 0.0000
7.1000E-01 6.0651E-01 6.9848E-02 0.0000
7.2000E-01 6.1902E-01 6.4772E-02 0.0000
7.3000E-01 6.3161E-01 5.9901E-02 0.0000
7.4000E-01 6.4429E-01 5.5232E-02 0.0000
7.5000E-01 6.5704E-01 5.0766E-02 0.0000
7.6000E-01 6.6987E-01 4.6500E-02 0.0000
7.7000E-01 6.8277E-01 4.2434E-02 0.0000
7.8000E-01 6.9576E-01 3.8566E-02 0.0000
7.9000E-01 7.0882E-01 3.4896E-02 0.0000

```
8.0000E-01      7.2196E-01      3.1421E-02      0.0000
8.1000E-01      7.3517E-01      2.8140E-02      0.0000
8.2000E-01      7.4846E-01      2.5052E-02      0.0000
8.3000E-01      7.6182E-01      2.2155E-02      0.0000
8.4000E-01      7.7526E-01      1.9447E-02      0.0000
8.5000E-01      7.8877E-01      1.6928E-02      0.0000
8.6000E-01      8.0236E-01      1.4594E-02      0.0000
8.7000E-01      8.1601E-01      1.2445E-02      0.0000
8.8000E-01      8.2975E-01      1.0477E-02      0.0000
8.9000E-01      8.4355E-01      8.6895E-03      0.0000
9.0000E-01      8.5742E-01      7.0795E-03      0.0000
9.1000E-01      8.7137E-01      5.6444E-03      0.0000
9.2000E-01      8.8538E-01      4.3817E-03      0.0000
9.3000E-01      8.9947E-01      3.2882E-03      0.0000
9.4000E-01      9.1362E-01      2.3606E-03      0.0000
9.5000E-01      9.2785E-01      1.5951E-03      0.0000
9.6000E-01      9.4214E-01      9.8725E-04      0.0000
9.7000E-01      9.5650E-01      5.3188E-04      0.0000
9.8000E-01      9.7093E-01      2.2244E-04      0.0000
9.9000E-01      9.8543E-01      5.0119E-05      0.0000
1.0000E+00      1.0000E+00      0.0000E+00      0.0000
/

swl     -- connate water end point saturations
4840*0. /

swcr    -- crtical water end point saturations
4840*0. /

swu
484*0.752388
484*0.740974
484*0.708338
484*0.681914
484*0.674995
484*0.726825
484*0.783535
484*0.798976
484*0.79431
484*0.752388
/
sowcr
484*0.247612
484*0.259026
484*0.291662
484*0.318086
484*0.325005
484*0.273175
484*0.216465
484*0.201024
484*0.20569
484*0.247612
/

pvtw    -- pref  fvf  compressibility  viscosity  viscosibility
           14.7  1.0             0.0        0.5           0.0 /

rock    --  reference pressure (psia)   compressibility (1/psi)
           14.7                    10e-6 /

density --   oil   water    gas  (lb/ft^3)
           52.848    62.352   1e-4  /

pvdo    --   poil   fvfo    viso
             100   1.0001   2
           10000   1.0      2 /
TRACER
                      'TR1'                                  'WAT'  ''   'OIL'  1   /
                      'TR2'                                  'WAT'  ''   'OIL'  1   /
                      'TR3'                                  'WAT'  ''   'OIL'  1   /
                      'TR4'                                  'WAT'  ''   'OIL'  1   /

 /

TRACERKP
0.0001    0
1000000   0/

0.0001    0.5
1000000   0.5/

0.0001    1
1000000   1/

0.0001    2
1000000   2/

TRACTVD
/
rptprops
'swfn' 'pvtw' 'pvdo' 'rock' /

REGIONS    ====================================================

TRKPFTR1
4840*1/

TRKPFTR2
4840*2/

TRKPFTR3
4840*3/

TRKPFTR4
4840*4/

SOLUTION   ====================================================
```

```
TBLKFTR1
4840*0.00 /

TBLKFTR2
4840*0.00 /

TBLKFTR3
4840*0.00 /

TBLKFTR4
4840*0.00 /

PRESSURE
4840*100 /

swat
484*0.752388
484*0.740974
484*0.708338
484*0.681914
484*0.674995
484*0.726825
484*0.783535
484*0.798976
484*0.79431
484*0.752388
/

RPTSOL
'FIP'  'SWAT' /

RPTRST    --  Controls restart file
  'BASIC=2' -- keep all restarts, output every FREQth reporting period
  'FREQ=10'
--   'NORST=0' -- 0=full restart, 1=graphics only, 2= no well arrays
  /

summary    ============================================================

fwit
foip
fwip
fopt
fwpt
fwir
fwct
fwpr
fopr
ftptTR1
ftitTR1
ftpcTR1
ftptTR2
ftpcTR2
ftitTR2
ftptTR3
ftpcTR3
ftitTR3
ftptTR4
ftpcTR4
ftitTR4
WOPR
'Rght-1'
'Rght-2'
'Rght-3'
'Rght-4'
'Rght-5'
'Rght-6'
'Rght-7'
'Rght-8'
'Rght-9'
'Rght-10'
'Rght'
/
WWPR
'Rght-1'
'Rght-2'
'Rght-3'
'Rght-4'
'Rght-5'
'Rght-6'
'Rght-7'
'Rght-8'
'Rght-9'
'Rght-10'
'Rght'
/
WTPCTR1
'Rght-1'
'Rght-2'
'Rght-3'
'Rght-4'
'Rght-5'
'Rght-6'
'Rght-7'
'Rght-8'
'Rght-9'
'Rght-10'
'Rght'
/
WTPCTR2
'Rght-1'
'Rght-2'
'Rght-3'
'Rght-4'
'Rght-5'
'Rght-6'
```

```
'Rght-7'
'Rght-8'
'Rght-9'
'Rght-10'
'Rght'
/
WTPCTR3
'Rght-1'
'Rght-2'
'Rght-3'
'Rght-4'
'Rght-5'
'Rght-6'
'Rght-7'
'Rght-8'
'Rght-9'
'Rght-10'
'Rght'
/
WTPCTR4
'Rght-1'
'Rght-2'
'Rght-3'
'Rght-4'
'Rght-5'
'Rght-6'
'Rght-7'
'Rght-8'
'Rght-9'
'Rght-10'
'Rght'
/
RUNSUM
EXCEL

-- monitor -- Output data for run-time graphical monitor

SCHEDULE  ============================================================


RPTSCHED
  'wells'
  'summary=2'
  'welspecs'
  'SOIL'
  /

RPTRST      --  Controls restart file
  'BASIC=2' -- keep all restarts, output every FREQth reporting period
  'FREQ=10'
--   'NORST=1' -- 0=full restart, 1=graphics only, 2= no well arrays
  /

-- NOWARN

WELSPECS  -- Name     Group   I     J     Datum     Phase
      -- -------- -------- ---   ---   --------- -----
        'Left'   'L'       1     1       0       'OIL'  /
        'Rght-1'   'R'                    22                  22                  0                   'WAT'             /
                   'Rght-2'        'R'                    22                  22                  0                   'WAT'             /
                   'Rght-3'        'R'                    22                  22                  0                   'WAT'             /
                   'Rght-4'        'R'                    22                  22                  0                   'WAT'             /
                   'Rght-5'        'R'                    22                  22                  0                   'WAT'             /
                   'Rght-6'        'R'                    22                  22                  0                   'WAT'             /
                   'Rght-7'        'R'                    22                  22                  0                   'WAT'             /
                   'Rght-8'        'R'                    22                  22                  0                   'WAT'             /
                   'Rght-9'        'R'                    22                  22                  0                   'WAT'             /
                   'Rght-10'       'R'                    22                  22                  0                   'WAT'             /
                   'Rght'          'R'                    22                  22                  0                   'WAT'             /


        /

COMPDAT   -- Name      I    J   K1   K2  Status   SatTab   Tfac     Dia    Kh
        'Left'    1    1    1   10  'OPEN'     0      1*   0.25   0.0 /
        'Rght-1'  22    22    1   1  'OPEN'     0     1*   0.25   0.0 /
        'Rght-2'  22    22    2   2  'OPEN'     0     1*   0.25   0.0 /
        'Rght-3'  22    22    3   3  'OPEN'     0     1*   0.25   0.0 /
        'Rght-4'  22    22    4   4  'OPEN'     0     1*   0.25   0.0 /
        'Rght-5'  22    22    5   5  'OPEN'     0     1*   0.25   0.0 /
        'Rght-6'  22    22    6   6  'OPEN'     0     1*   0.25   0.0 /
        'Rght-7'  22    22    7   7  'OPEN'     0     1*   0.25   0.0 /
        'Rght-8'  22    22    8   8  'OPEN'     0     1*   0.25   0.0 /
        'Rght-9'  22    22    9   9  'OPEN'     0     1*   0.25   0.0 /
        'Rght-10'  22    22   10   10  'OPEN'     0     1*   0.25   0.0 /
        'Rght'       22    22   1   10  'OPEN'     0     1*   0.25   0.0 /
         /

WCONINJE  -- Name   Phase     Status      Mode   Qsurf  Qres  BHP    THP  VFP  VOL
      -- ----  -----     ------      ----   ----------------------------------
        'Left' 'WATER'   'OPEN'      'RATE'  6000      1*   1*    1*   1*   1* /
        /


WCONPROD  -- NAME   Status      Mode      Qo  Qe  Qg  Ql  Qr  BHP
      -- ----  ------      ----    ----------------------
        'Rght-1'   'OPEN'            'RESV'              1*                  1*                  1*                  1*                  0.001               1*                  /
                   'Rght-2'         'OPEN'              'RESV'              1*                  1*                  1*                  1*                  0.001               1*                  /
                   'Rght-3'         'OPEN'              'RESV'              1*                  1*                  1*                  1*                  0.001               1*                  /
                   'Rght-4'         'OPEN'              'RESV'              1*                  1*                  1*                  1*                  0.001               1*                  /
                   'Rght-5'         'OPEN'              'RESV'              1*                  1*                  1*                  1*                  0.001               1*                  /
                   'Rght-6'         'OPEN'              'RESV'              1*                  1*                  1*                  1*                  0.001               1*                  /
                   'Rght-7'         'OPEN'              'RESV'              1*                  1*                  1*                  1*                  0.001               1*                  /
                   'Rght-8'         'OPEN'              'RESV'              1*                  1*                  1*                  1*                  0.001               1*                  /
                   'Rght-9'         'OPEN'              'RESV'              1*                  1*                  1*                  1*                  0.001               1*                  /
                   'Rght-10'        'OPEN'              'RESV'              1*                  1*                  1*                  1*                  0.001               1*                  /
                   'Rght'           'open'              'bhp'               1*                  1*                  1*                  1*                  1*                  14.7                /
```

```
        /

tuning  -- Numerical controls

--    Time stepping controls

--      tsinit   tsmax    tsmin    tsmchp   tsfmax
        0.001    10       0.001    0.0015   1.5

--      tsfmin   tsfconv  tfdiff   thrupt
        1*       1*       1*       1*
  /

--    Time Truncation and convergence controls

--      trgtte   trgcnv   trgmbe   trglcv   xxxtte   xxxcnv
        1*       1*       1*       1*       1*       1*

--      xxxmbe   xxxlcv   xxwfl    trgfip   trgsft
        1*       1*       1*       1*       1*
  /

--    Newton and linear solver controls

--      newtmx   newtmn   litmax   litmin   mxwsit   mxpwit
        50       1*       100      1*       100      1*

--      ddplim   ddslim   trgdpr   xxxdpr
        1*       1*       1*       1*
  /


WTRACER   -- Well      Tracer  Conc
          'Left'  'TR1'   1.0   /
          'Left'   'TR2'   1.0   /
          'Left'  'TR3'   1.0   /
          'Left'   'TR4'   1.0   /
          /


TSTEP
1*12 /

WTRACER   -- Well      Tracer  Conc
          'Left'  'TR1'   0.0   /
          'Left'   'TR2'   0.0   /
          'Left'  'TR3'   0.0   /
          'Left'   'TR4'   0.0   /

          /


-- NOWARN
tstep
50*20 /
tstep
50*19.84/


MESSAGES    -- Message  Comment  Warning  Problem  Error  Bug -- Message Type
            1*         1*       1*       1*       1*     1*  -- Print limits
            1*         1*       1*       5        1*     1*  -- Stop limits
  /


END
```

B.2 INVERSE MODEL FORWARD RUN ECLIPSE INPUT FILE FOR TWO PHASE FLOW

```
-- 2D cross-sectional field.
-- Tracer test simulation with for the inverse model forward run
-- Eclipse input file
--    * regular grid
--    * tracer simulation
--    single phase flow, confined
-- ***************************************************************************
-- ***************************************************************************

NOECHO
RUNSPEC
TITLE
2D, layered, 66x1x2, cross-sectional, tracer injection, single-phase, 10000 days of simulation 11-11-2004
oil
water
field
start    --   start date
1 'JAN' 2000 /
dimens   --   nx   ny   nz
              66    1    2  /
eqldims  --  ntequl  ndprvd  ndrxvd  nttrvd  nstrvd
               1     100      10       1      20 /

endscale --  directional  reversible  tables  nodes
           'NODIR'      'REVERS'         2      5  /
tabdims  --  ntsfun  ntpvt  nssfun  nppvt  ntfip  nrpvt
               1      1     101     12      1     12   /
welldims --  wells  connect per well  groups  wells per group
               85                75       2               49 /
nstack   --  linear solver stack size
             200 /

TRACERS   --    oil   water   gas  environ  diffusion
                0     6    0     0     'DIFF'/
PARTTRAC
 6  6   2/
FMTOUT
IMPLICIT
--UNIFIN
--  ***********************************************************
--  ******  End    RUNSPEC section    ******************
--  ******                          ******************
--  ******  Begin  GRID section       ******************
--  ***********************************************************

GRID
-- PSEUDOS    -- Write binary files for input to Pseudo

-- RPTGRID
--   'TRANX' 'TRANZ'  'NNC' 'PORV' /
DX
 132*10 /
DY
 132*330 /
DZ
 132*25 /
TOPS
 66*13000/
--ENDBOX
PORO
 132*0.2/
permx
132*100./
COPY
PERMX PERMY /
PERMX PERMZ /

MULTIPLY
PERMZ 0.001  1 66  1 1  1 2/

GRIDFILE
   2 /

INIT
--  ***********************************************************
--  ******  End    GRID             ******************
--  ******                          ******************
--  ******  Begin  PROPS            ******************
--  ***********************************************************

PROPS
swof     --   sw   krw   kro   pcow
0.3                 0                   1                   0
0.344               0.11                0.89                0
0.389               0.2225              0.7775              0
0.433               0.3325              0.6675              0
0.478               0.445               0.555               0
0.522               0.555               0.445               0
0.567               0.6675              0.3325              0
0.611               0.7775              0.2225              0
0.656               0.89                0.11                0
0.7                 1                   0                   0
/
--swl      -- connate water end point saturations
--163840*0.3 /
--swcr     -- crtical water end point saturations
--163840*0.3 /

--swu
```

```
--163840*0.75/
--sowcr
--163840*0.25/
pvtw     --  pref  fvf  compressibility  viscosity  viscosibility
          1000  1.0            0.0        0.7          0.0 /
rock     --  reference pressure (psia)   compressibility (1/psi)
          1000                  10e-6 /
density  --   oil   water    gas  (lb/ft^3)
          52.8480   62.352  1e-4  /
pvdo     --   poil   fvfo     viso
           100   1.0001   20
          10000   1.0      20 /
TRACER
                    'TC0'                                  'WAT'  ''   'OIL'  1   /
                    'TP1'                                  'WAT'  ''   'OIL'  1   /
                    'TP2'                                  'WAT'  ''   'OIL'  1   /
                    'TP3'                                  'WAT'  ''   'OIL'  1   /
                    'TP4'                                  'WAT'  ''   'OIL'  1   /
                    'TP5'                                  'WAT'  ''   'OIL'  1   /
                    /
TRACERKP
0.0001    0
1000000   0/

0.0001    0.5
1000000   0.5/

0.0001    1
1000000   1/

0.0001    2
1000000   2/

0.0001    5
1000000   5/

0.0001    10
1000000   10/

/
TRACTVD
/
rptprops
'swfn' 'pvtw' 'pvdo' 'rock' /

REGIONS    ===========================================================

TRKPFTC0
132*1/
TRKPFTP1
132*2/
TRKPFTP2
132*3/
TRKPFTP3
132*4/
TRKPFTP4
132*5/
TRKPFTP5
132*6/

SOLUTION   ===========================================================

TBLKFTC0
132*0.00/
TBLKFTP1
132*0.00/
TBLKFTP2
132*0.00/
TBLKFTP3
132*0.00/
TBLKFTP4
132*0.00/
TBLKFTP5
132*0.00/
PRESSURE
132*5000 /

swat
66*0.6
66*0.4 /


RPTSOL
'FIP'  'SWAT' /

RPTRST    --  Controls restart file
  'BASIC=2' -- keep all restarts, output every FREQth reporting period
  'FREQ=10'
--   'NORST=0' -- 0=full restart, 1=graphics only, 2= no well arrays
  /

summary    ===========================================================

wtpctp3
'prod1'
'prod2' /

RUNSUM
EXCEL
-- monitor -- Output data for run-time graphical monitor

SCHEDULE   ===========================================================

RPTSCHED
  'wells'
  'summary=2'
  'welspecs'
  'SOIL'
```

```
  /

RPTRST       --  Controls restart file
  'BASIC=2' -- keep all restarts, output every FREQth reporting period
  'FREQ=10'
--   'NORST=1' -- 0=full restart, 1=graphics only, 2= no well arrays
  /
-- NOWARN

WELSPECS  -- Name     Group   I     J     Datum     Phase
        -- --------  -------  ---   ---   --------  -----
          'Inj'       'I'   1     1    13000 'OIL'/
          'Prod1'     'P'                 66                  1                 13000             'WAT'/
          'Prod2'     'P'                 66                  1                 13000             'WAT'/


          /
COMPDAT   -- Name     I    J  K1   K2  Status   SatTab   Tfac     Dia   Kh
'Inj'               1                   1                   1                   2                 'OPEN'            0                 1*                0.5               1000              /
'Prod1'             66                  1                   1                   1                 'OPEN'            0                 1*                0.5               1000              /
'Prod2'             66                  1                   2                   2                 'OPEN'            0                 1*                0.5               1000              /

          /
WCONINJE  -- Name   Phase     Status      Mode    Qsurf  Qres  BHP     THP  VFP  VOL
          -- ----   -----   --------      ----   ------------------------------------
'Inj'               'WATER'           'OPEN'            'RESV'            1*                1000              1*                1*                1*                1*                /
          /
WCONPROD  -- NAME   Status      Mode      Qo  Qe  Qg  Ql  Qr  BHP
          -- ----   ------      ----      ------------------------
'Prod1'             'OPEN'            'bhp'             1*                1*                1*                1*                1*                2000              /
'Prod2'             'OPEN'            'bhp'             1*                1*                1*                1*                1*                2000              /
                              /

tuning  -- Numerical controls

--    Time stepping controls

--       tsinit   tsmax    tsmin    tsmchp   tsfmax
         0.0001    10    0.0001    0.0015   1.5
--       tsfmin   tsfconv  tfdiff   thrupt
         1*       1*       1*       1*   /
--    Time Truncation and convergence controls
--       trgtte   trgcnv   trgmbe   trglcv   xxxtte   xxxcnv
         1*       1*       1*       1*       1*       1*
--       xxxmbe   xxxlcv   xxwfl    trgfip   trgsft
         1*       1*       1*       1*       1*   /
--    Newton and linear solver controls
--       newtmx   newtmn   litmax   litmin   mxwsit   mxpwit
         50       1*       150      1*       100      1*
--       ddplim   ddslim   trgdpr   xxxdpr
         1*       1*       1*       1*   /
WTRACER   -- Well     Tracer  Conc

                      'Inj'               'TC0'             1                 /
                      'Inj'               'TP1'             1                 /
                      'Inj'               'TP2'             1                 /
                      'Inj'               'TP3'             1                 /
                      'Inj'               'TP4'             1                 /
                      'Inj'               'TP5'             1                 /
                                                                              /

TSTEP
1*50/
WTRACER   -- Well     Tracer  Conc
                      'Inj'               'TC0'             0                 /
                      'Inj'               'TP1'             0                 /
                      'Inj'               'TP2'             0                 /
                      'Inj'               'TP3'             0                 /
                      'Inj'               'TP4'             0                 /
                      'Inj'               'TP5'             0                 /
/

-- NOWARN
tstep
9*50/

-- NOWARN
tstep
50*50/

MESSAGES    -- Message  Comment  Warning  Problem  Error  Bug -- Message Type
            1*       1*       1*       1*       1*     1*  -- Print limits
            1*       1*       1*       5        1*     1*  -- Stop limits
  /


END
```

Nomenclature

C	=	Tracer concentration
C_{io}	=	Concentration of tracer i in the oil phase
C_{it}	=	Total tracer concentrations for tracer i
C_{iw}	=	Concentration of the tracer i in water phase
C_o	=	Injected tracer concentration
f_w, F_w	=	Fractional flow of water
f_o, F_o	=	Fractional flow of oil
G	=	Sensitivity matrix or Frechet derivative of g
j_p	=	Production data misfit function
k	=	Permeability
K_i	=	Partition coefficient of tracer i
L	=	Spatial difference operator
m	=	Reservoir parameter
N_{dj}	=	Number of dynamic data observations of j^{th} well
N_w	=	Number of wells
P	=	Pressure
q	=	Flow rate
R^2	=	Coefficient of determination
s	=	Slowness
So	=	Oil saturation
$\overline{\hat{S}}_o$	=	Average oil saturation
Sw	=	Water saturation

t	=	Time
u	=	Total velocity of flowing phases
v	=	Interstitial velocity vector
$\bar{V}_i$	=	Mean residence volume of tracer i
V_s	=	Swept pore volume
V_{slug}	=	Volume of the tracer slug
w_{ij}	=	Data weights
y^{obs}	=	Observed response
$\overline{y^{obs}}$	=	Observed averaged response
y^{cal}	=	Calculated response

Greek Symbols

τ	=	Time of flight
ϕ	=	Porosity
δ	=	Dirac delta function
ψ	=	Streamline function
λ_t	=	Total mobility
ε	=	Residual vector
γ	=	Weighting factor

References

Abbaszadeh-Dehghani, M. and Brigham, W.E., "Analysis of Well-to Well Tracer Flow to Determine Reservoir Layering", Journal of Petroleum Technology, Oct. 1984, 1753-1762

Allison, S. B., "Analysis and Design of Field Tracers for Reservoir Description," Master's thesis, The University of Texas at Austin, 1988.

Allison, S. B., Pope, G. A. and Sepehrnoori, K., "Analysis of field tracers for reservoir description," Journal of Petroleum Science and Engineering, 5, 173-186, 1991.

Asakawa, K., "Numerical Modeling and Simulations of Microbial Enhanced Oil Recovery and Tracer Tests," PhD dissertation, The University of Texas at Austin, 2005.

Brigham, W.E., and Smith, D.H., "Prediction of Tracer Behavior in Five-Spot Flow," paper SPE 1130, presented at the SPE Conference on Production Research and Engineering, Tulsa, OK, May 3-4, 1965.

Brigham, W., Abbaszadeh, M., "Tracer Testing for Reservoir Description", Journal of Petroleum Technology (1987), 39, No. 5, 519- 527

Badessich et al., "The use of Tracers to Characterize Highly Heterogeneous Fluvial Reservoirs: Field Results" presented at the 2005 SPE International Symposium Oilfield Chemistry, Houston, TX, February 2-4, 2005.

Cheng, H., Datta-Gupta, A. and He, Z.: "A comparison of Travel Time and Amplitude Matching for Field-Scale Production Data Integration: Sensitivity, Non-Linearity and Practical Implications," paper SPE 84570 presented at the 2003 SPE Annual Technical Conference and Exhibition, Denver, CO, October 5-8, 2003

Cheng, H., Khargjoria, A., He, Z., Datta-Gupta, A.: "Fast History Matching of Finite-Difference Models Using Streamline-Derived Sensitivities", paper SPE 894417 presented at the 2004 SPE/DOE Fourteenth Symposium on Improved Oil Recovery held in Tulsa, Oklahoma, April 17-21, 2004

Crane, M. J. and Blunt, M. J.: "Streamline-based Simulation of Solute Transport," WaterResources Research (1999), 35, No 10, 3061-3078.

Datta-Gupta, A.: " Streamline Simulation: A Technology Update" paper SPE 65604, published in Journal of Petroleum Technology, December, 2000, Vol.52, No.12, p.68-74

Datta-Gupta, A., Yoon, S. S., Vasco, D. W. and Pope, G. A.: "Inverse Modeling of Partitioning Interwell Tracer Tests: A streamline Approach", Water Resources Research 38(6), June, 2002

Deeds, N. E., "Development and Evaluation of Partitioning Interwell Tracer Test Technology for Detection of Non-Aqueous Phase Liquids in Fractured Media," PhD dissertation, The University of Texas at Austin, 1999.

Dwarakanath, V., Deeds, N. and Pope, G. A., "Analysis of Partitioning Interwell Tracer Tests," Environmental Science and Technology, 33, 3829-3836, 1999

He, Z., Datta-Gupta, A., Yoon, S.: " Streamline-based Production Data Integration Under Changing Field Conditions," paper SPE 71333, presented 2001 SPE Annual Technical Conference and Exhibition held in New Orleans, Louisiana, September 30 –October 3, 2001

Jayanti, S., "Modeling Tracers and Contaminant Flux in Heterogeneous Reservoirs," PhD dissertation, The University of Texas at Austin, 2003.

Jin, M., "A Study of Nonaqueous Phase Liquid Characterization and Surfactant Remediation," Ph.D. dissertation, The University of Texas at Austin, August 1995.

Jin, M., Delshad, M., Dwarakanath, V., McKinney, D. C., Pope, G. A., Sepehrnoori, K., Tilburg, C. E., and Jackson, R. E., "Partitioning tracer test for detection, estimation, and remediation performance assessment of subsurface nonaqueous phase liquids," Water Resources Research 31(5), 1201-1211, May 1995.

Lliassov, P. A, Datta-Gupta, A., Vasco, D. W., "Field-Scale Characterization of Permeability and Saturation Distribution Using Partitioning Tracer Tests: The Ranger Field, Texas," paper SPE 71320, presented at the SPE Annual Technical Conference and Exhibition, New Orleans, Louisiana, September 30 –October 3, 2001

Mercado, M. and Perez, C. E., "Gas Flood-Flow Pattern Evaluation: A Successful Interwell Field Study," paper SPE 81005, presented at the SPE Latin American and Carribbean Petroleum Engineering Conference, West Indies, 2003.

Oyerinde, A., S.: "A Composite Tracer Analysis to Reservoir Characterization" MS thesis, Texas A&M University, College Station, TX, 2003.

Sinha, R., “Simulation of Natural and Partitioning Interwell Tracers to Calculate Saturation and Swept Volumes in Oil Reservoirs” Master thesis, The University of Texas at Austin, 2003.

Sinha et al., “Simulation of Natural and Partitioning Interwell Tracers to Calculate Saturation and Swept Volumes in Oil Reservoirs”, paper SPE 89458 presented at the 2004 SPE/DOE Fourteenth Symposium on Improved Oil Recovery, Tulsa, OK, April, 17-21, 2004.

Tang, J. S. and Harker, B., “Interwell Tracer Test to Determine Residual Oil Saturation in a Gas Saturated Reservoir. Part I; Theory and Design,” The Journal of Canadian Petroleum Technology, 30(4), 34, 1991a.

Tang, J. S. and Harker, B., “Interwell Tracer Test to Determine Residual Oil Saturation in a Gas Saturated Reservoir. Part II: Field Applications,” The Journal of Canadian Petroleum Technology, 30(3), 76, 1991b.

Tang, J. S., “Partitioning Tracers and In-Situ Fluid-Saturation Measurements,” SPE Formation Evaluation, 33-39, March 1995.

Tang, J. S., Zhang, P. X., “Determination of Residual Oil Saturation in a Carbonate Reservoir,” paper SPE 72111, presented at the SPE Asia Pacific Improved Oil Recovery Conference, Malaysia, 2001.

Yoon, S., Barman, I., Datta-Gupta, A., and Pope, G. A., “In-Situ Characterization of Residual NAPL Distribution Using Streamline-based Inversion of Partitioning Tracer Tests,” paper SPE 52729 presented at the 1999 SPE/EPA Exploration and Production Environmental Conference, Austin, Texas, February 28-March 3, 1999.

Yoon, S., Malallah, A.H., Datta-Gupta, A. and Vasco, D.W.: “A Multiscale Approach to Production Data Integration Using Streamline Models ”, paper SPE 56653 presented at the 1999 SPE Annual Technical Conference and Exhibition, Houston, TX, Oct. 3-6, 1999.

Yoon, S.: ”Dynamic Data Integration Into High Resolution Models Using Streamline-Based Inversion,” PhD dissertation, Texas A&M University, College Station, TX (2000).

Vasco, D.W., Yoon, S., and Datta-Gupta, A.: “Integrating Dynamic Data Into High-Resolution Reservoir Models Using Streamline-Based Analytic Sensitivity Coefficients”, SPE Journal (1999), 4, No.4, 389-399.

Wagner, O. R., “The Use of Tracers in Diagnosing Interwell Reservoir Heterogeneities-Field Results,” J. Pet. Tech., 1410-1416, Nov. 1977

Zemel, B., Tracers in the Oil Field, Developments in Petroleum Science, 43, Elsevier Science B. V., Amsterdam, 1995.

VITA

Elif Ilke Altinay was born in Antalya, Turkey on 28th July 1980, daughter of Mr. N. Altinay and Mrs. Y. Altinay. She received the degree of Bachelor of Science in petroleum and natural gas engineering from the Istanbul Technical University, Istanbul in June 2002. She entered the Graduate School at The University of Texas at Austin in January 2003.

Permanent Address: Lara Caddesi, Alpek Sitesi,
B-Blok, Daire: 19
Antalya, Turkey
7100

This thesis was typed by the author.